Dissertations, Theses, and Masters Projects   Theses, Dissertations, & Master Projects

2010

Integrating space-and time-scales of sediment-transport for Poverty Bay, New Zealand

Aaron J. Bever
College of William and Mary - Virginia Institute of Marine Science

Integrating space- and time-scales of sediment-transport for Poverty Bay, New Zealand

A Dissertation

Presented to

The Faculty of the School of Marine Science

The College of William & Mary in Virginia

In Partial Fulfillment

Of the Requirements for the Degree of

Doctor of Philosophy
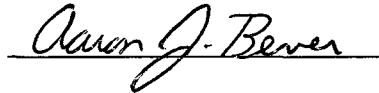
by

Aaron J. Bever

2010
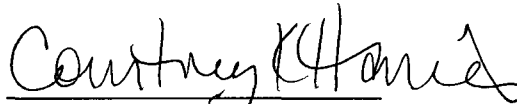
APPROVAL SHEET

This dissertation is submitted in partial fulfillment of

the requirements for the degree of

Doctor of Philosophy
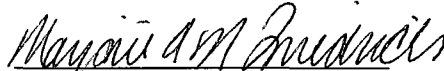
Aaron J. Bever

Aaron J. Bever
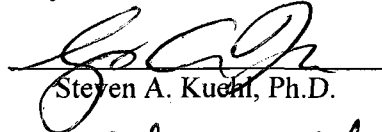
Approved, by the Committee, August 2010
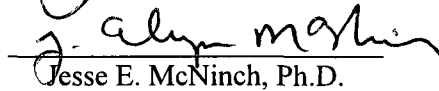
Courtney K. Harris, Ph.D.
Committee Chairman/Advisor
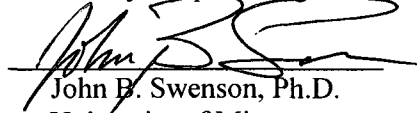
Marjorie A.M. Friedrichs, Ph.D.

Steven A. Kuehl, Ph.D.

Jesse E. McNinch, Ph.D.
U.S. Army Corps of Engineers

John P. Swenson, Ph.D.
University of Minnesota
Duluth, Minnesota

ii

TABLE OF CONTENTS

Chapter 3 - Storm and fair-weather driven sediment-transport within Poverty Bay, New Zealand, evaluated using coupled numerical models

Chapter 4 - Variations in sediment-transport and sorting between different dispersal basin geometries: A case study of Poverty Bay, New Zealand

ACKNOWLEDGEMENTS

LIST OF TABLES

LIST OF FIGURES

Chapter 3:

Appendix 3:

Chapter 4:

ABSTRACT

Poverty Bay is a small embayment located in the middle of the Waipaoa River Sedimentary Dispersal System (WSS) on the eastern coast of the north island of New Zealand. Within this dispersal system, a large multidisciplinary study was focused on determining the sediment routing from the source within the headwaters to the locations of sediment accumulation on the continental shelf and slope. Poverty Bay acts as the land to sea transition area in the WSS, and as such significantly modifies the fluvial sedimentary signal before it is exported to the continental shelf. Until this study, little hydrodynamic or sediment-transport work had been conducted in Poverty Bay, however.

This dissertation analyzed observation and numerical model results to characterize the hydrodynamics and sediment-transport within Poverty Bay. Three S4 current meters with pressure and temperature/salinity sensors, one upward looking ADCP, and one downward looking ADV were deployed in Poverty Bay for April-September, 2006. Hydrodynamics, sediment-transport, and waves were modeled using the Regional Ocean Modeling System (ROMS) fully coupled to the Simulated WAves Nearshore (SWAN) model. The 2006 winter wet season was modeled to overlap with the field observations, along with a ~40 yr recurrence interval storm that occurred from 21-23 October, 2005. For these two meteorological conditions, four different model grid and sediment load configurations were modeled; 1) the modern Poverty Bay with the modern sediment load, 2) the modern Poverty Bay with the pre-anthropogenic (PA) sediment load, 3) the 2 kya Poverty Bay with the PA sediment load, and 4) the 7 kya Poverty Bay with the PA sediment load.

Both the observation and modeling results showed significant quantities of fine sediment were ephemerally deposited within the shallow Poverty Bay during times of elevated river discharge and energetic waves and currents. The deposition of sediment within Poverty Bay during floods followed by the resuspension and export to the continental shelf during subsequent wave events created multiple pulses of sediment out of Poverty Bay. As the sediment underwent multiple resuspension episodes, the sedimentary signal initially supplied by the river, such as the timing of supply to the shelf and the grain size distribution, would be altered. Shoreward nearshore currents and a divergence in the currents seaward of the Waipaoa River mouth provided mechanisms for the segregation of the sand from the muddy sediment, with the coarse sediment preferentially moved shoreward and the fine sediment exported from Poverty Bay to deeper water. Model results also showed significant differences between the sedimentary signals supplied to the continental shelf based on the dispersal basin geometry and river mouth orientation. The model estimates showed that marine dispersal can influence the long-term trends of a slowing shoreline progradation rate and coarsening upward sequences on the continental shelf, without invoking climate change or changes to the sediment supply. This implies that the processes controlling marine and nearshore sediment dispersal must be considered when developing hypothesis based on sedimentological observations.

Integrating space- and time-scales of sediment-transport for Poverty Bay, New Zealand

Chapter 1: Introduction

The overall goal of the Source-to-Sink initiative was to increase understanding of the processes responsible for sediment routing across entire dispersal systems, from the sediment source locations on hill slopes to the ultimate locations of accumulation, including flood plains, the marine nearshore region, continental shelves, and continental slopes (Carter et al., 2010; Kuehl et al., 2003). An additional product of the initiative included increased predictive power for sediment-transport and deposition across the sedimentary system. The Waipaoa River in New Zealand, and the Fly River in Papua New Guinea, were chosen as focus sights for the MARGINS Source-to-Sink Initiative (Kuehl et al., 2006; Kuehl et al., 2003). The Waipaoa River is a prototypical small mountainous river (Milliman and Syvitski, 1992), while the Fly River is much larger in terms of freshwater discharge, at roughly 50 times the average freshwater discharge of the Waipaoa. The Waipaoa River dispersal system, sometimes called the Waipaoa Sedimentary System (WSS), was selected to represent an event-driven system within which individual, present-day, large storms and floods might produce strong signals in the sedimentary record. Additionally, the WSS was thought to be a generally closed system that trapped most sediment within offshore basins. Thirdly, sufficient background data and a strong local scientific infrastructure existed for the WSS, all of which facilitated the formulation of an integrated study (Kuehl et al., 2003). This dissertation focused on Poverty Bay, the part of the WSS that links the terrestrial and marine portions, to investigate how processes within this shallow marine setting may modulate the fluvial signal before exporting sediment to deeper parts of the system.

In this system, the Waipaoa River discharges sediment to the small, 62 km^2, Poverty Bay before sediment is exported to the continental shelf and the more distal portions of the marine dispersal system. Other studies have focused on different sections of the dispersal system, including hill slope erosion and sediment yields (Hicks et al., 2000; Hicks et al., 2004; Kettner et al., 2007; Reid and Page, 2002), fluvial processes within the Waipaoa River (Crosby and Whipple, 2006), the Waipaoa River flood plain (Marsaglia et al., 2010; Phillips et al., 2007), shoreline progradation (Brown, 1995; Smith, 1988; Wolinsky et al., 2010), hydrodynamics within Poverty Bay (Stephens et al., 2002), long- and short-term sediment deposition on the continental shelf (Gerber et al., 2010; Miller and Kuehl, 2010; Rose and Kuehl, 2010), and sediment deposition on the continental slope and within shelf-slope canyons (Alexander et al., 2010; Walsh et al., 2007).

Although extensive, these studies left gaps in the knowledge base, particularly considering the processes that modulate the fluvial sedimentary signal within Poverty Bay. Previous field experiments within Poverty Bay (Healy et al. 2002; Smith, 1988; Stephens et al., 2002) suffer from somewhat short-lived sampling strategies, did not include a storm episode, and/or did not provide time-series measurements of wave properties. For these reasons, the available observations were insufficient for characterizing sediment dispersal within the nearshore and bay setting. Furthermore, sediment transfer from the Waipaoa River through Poverty Bay to the continental shelf has not been directly studied. A working hypothesis has been invoked asserting that sediment bypasses Poverty Bay and is dispersed on the shelf through settling from a hypopycnal river plume (Foster and Carter, 1997; Kettner et al., 2009). This hypothesis

3

was inconsistent, however, with observations made offshore of similar episodic or event-driven rivers (Geyer et al., 2000; Warrick and Milliman, 2003). In fact, studies of other systems have concluded that in many settings sediment quickly settles out of river plumes and is then transported within the bottom boundary layer near the seabed (Geyer et al., 2004; Hill et al., 2007; Milligan et al., 2007).

Research within this dissertation relied on field observations and three-dimensional hydrodynamic, sediment-transport, and wave modeling to investigate the transfer of sediment from the Waipaoa River mouth to the continental shelf, and therefore addressed knowledge gaps for a critical portion of the Waipaoa Source-to-Sink system. The research focused on four main objectives; 1) Characterize the hydrodynamics and sediment-transport within the near-shore region of Poverty Bay. 2) Identify the primary transport mechanisms within Poverty Bay for sediment discharged by the Waipaoa River. 3) Develop the ability to reproduce observed hydrodynamics, sediment-transport, and depositional patterns in Poverty Bay using a numerical model that includes fluvial sediment delivery, resuspension, and transport. 4) Evaluate how the geomorphic evolution of Poverty Bay has impacted sediment dispersal and accumulation processes over the past 7,000 years.

This research is also particularly focused on investigating the timing of sediment deposition within, and export from, Poverty Bay (Chapters 2 and 3). Conclusions were drawn showing how the physical processes within the nearshore and Poverty Bay modify the fluvial sedimentary signal supplied by the Waipaoa River as it is routed through the embayment (Chapters 2 and 3). Sediment routing and the segregation of the coarse from the fine sediment was investigated for model configurations that represented the 7000

4

year ago, 2000 year ago, 650 year ago, and present-day systems to evaluate the influence of basin geometry, river mouth orientation, and anthropogenic increase in sediment load on marine dispersal (Chapter 4). The physical processes influencing sedimentary marine dispersal within the various Poverty Bay geometries were then related to observations of the shoreline progradation rate and grain size trends within sediment cores from the continental shelf (Chapter 4).

This dissertation includes three primary chapters (Chapters 2, 3, and 4), and five short appendices. Each of these main chapters was intended to stand alone and include an abstract, all necessary citations, tables, and figures. The appendices follow their respective chapters, or, if not associated with a single specific chapter they occur after Chapter 4, and if necessary, contain a reference list and figures.

Chapter Two analyzed observations collected from April through September, 2006. It includes two appendices. Results from this chapter show the nearshore of Poverty Bay (<15 m water depth) has significant sediment deposition during elevated river discharge and energetic oceanic conditions, fast currents and large waves, that is resuspended and removed within about three weeks of the elevated discharge. Appendix 2-A documents OBS turbidity data that was excluded from the manuscript because it was uncalibrated and probably influenced by dredge spoils. A second appendix (Appendix 2-B) describes the animated visualization of the data found on the supplemental DVD.

Chapter Three used three-dimensional hydrodynamic/sediment-transport and two-dimensional wave modeling to investigate sediment deposition and dispersal for two time-periods; (1) the April through September, 2006 winter wet season and (2) the 40 year recurrence interval storm that occurred from 21-23 October, 2005. The modeling

effort used the Community Sediment Transport Modeling System (CSTMS) sediment-transport routines (Warner et al., 2008) and greatly benefited from the availability of the Community Surface Dynamics Modeling System (CSDMS) High-Performance Computing Cluster. Model estimates were analyzed and compared to the observational data for April – September, 2006, showing the model accurately reproduced the sedimentological observations. The model results showed that the sediment supply to the continental shelf was dominated by moderate high-frequency elevated discharge periods and repeated episodes of wave swell, yet that extreme storms were much more likely to leave an identifiable flood layer. The appendix (Appendix 3) contains additional comparisons to the observational data and explains Taylor and target diagrams and how they can be beneficial to evaluating model skill.

Chapter Four again used the numerical models, but investigated the influence of dispersal basin geometry, river mouth orientation, and sediment load on sediment dispersal, shoreline progradation rates, and the grain size of sediment supplied to the continental shelf. This chapter showed that changes to the geometry of Poverty Bay over the last 7000 years has significantly impacted the size of the waves within Poverty Bay, current speeds, the rate of shoreline progradation, and the grain size of the sediments that were exported to the continental shelf. Here, Appendix 4-A described model visualizations included on the supplemental DVD while Appendix 4-B explained the naming conventions behind the slightly modified ROMS/SWAN source code and the input files, as archived on the supplemental DVD.

Finally, Chapter 5 summarized the overall conclusions from the dissertation, synthesizing five main results from this work. Within this chapter directions for ongoing research are suggested.

References:

Alexander, C.R., Walsh, J.P. and Orpin, A.R., 2010. Modern sediment dispersal and accumulation on the outer Poverty continental margin. Mar. Geol., 270: 213-226.

Brown, L.J., 1995. Holocene shoreline depositional processes at Poverty Bay, a tectonically active area, northeastern north island, New Zealand. Quatern. Res., 26: 21-33.

Carter, L., Orpin, A.R. and Kuehl, S.A., 2010. Landscape and sediment responses from mountain source to deep ocean sink; Waipaoa Sedimentary System, New Zealand. Mar. Geol.

Crosby, B.T. and Whipple, K.X., 2006. Knickpoint initiation and distribution within fluvial networks: 236 waterfalls in the Waipaoa River, North Island, New Zealand. Geomorphology, 82: 16-38.

Foster, G. and Carter, L., 1997. Mud sedimentation on the continental shelf at an accretionary margin - Poverty Bay, New Zealand. N. Z. J. Geol. Geophys., 40: 157-173.

Gerber, T., Pratson, L.F., Kuehl, S., Walsh, J.P., Alexander, C. and Palmer, A., 2010. The influence of sea level and tectonics on Late Pleistocene through Holocene sediment storage along the high-sediment supply Waipaoa continental shelf. Mar. Geol., 270: 139-159.

Geyer, W.R., Hill, P., Milligan, T. and Traykovski, P., 2000. The structure of the Eel River plume during floods. Cont. Shelf Res., 20: 2067-2093.

Geyer, W.R., Hill, P.S. and Kineke, G.C., 2004. The transport, transformation and dispersal of sediment by buoyant coastal flows. Cont. Shelf Res., 24: 927-949.

Hicks, D.M., Gomez, B. and Trustrum, N.A., 2000. Erosion thresholds and suspended sediment yields, Waipaoa River basin, New Zealand. Water Resour. Res., 36(4): 1129-1142.

Hicks, D.M., Gomez, B. and Trustrum, N.A., 2004. Event suspended sediment characteristics and the generation of hyperpycnal plumes and river mouths: east coast continental margin, North Island, New Zealand. J. Geol., 112(4): 471-485.

Hill, P.S., Fox, J.M., Crockett, J.S., Curran, K.J., Friedrichs, C.T., Geyer, W.R., Milligan, T.G., Ogston, A.S., Puig, P., Scully, M.E., Traykovski, P.A. and Wheatcroft, R.A., 2007. Sediment Delivery to the Seabed on Continental Margins. In: C.A. Nittrouer et al. (Editors), Continental Margin Sedimentation: Transport to Sequence. Blackwell Publishing Ltd., pp. 49-99.

Kettner, A.J., Gomez, B., Hutton, E.W. and Syvitski, J.P.M., 2009. Late holocene dispersal and accumulation of terrigenous sediment on Poverty Shelf, New Zealand. Basin Research, 21: 253-267.

Kettner, A.J., Gomez, B. and Syvitski, J.P.M., 2007. Modeling suspended sediment discharge from the Waipaoa River system, New Zealand: The last 3000 years. Water Resour. Res., 43(W07411): doi:10.1029/2006WR005570.

Kuehl, S., Alexander, C., Carter, L., Gerald, L., Gerber, T., Harris, C., McNinch, J., Orpin, A., Pratson, L., Syvitski, J., Walsh, J.P., 2006. Understanding sediment transfer from land to ocean. EOS Transactions, 87(29).

Kuehl, S., Carter, L., Gomez, B. and Trustrum, N., 2003. Holistic approach offers potential to quantify mass fluxes across continental margins. EOS Transactions, 84(38).

Marsaglia, K.M., DeVaughn, A.M., James, D.E. and Marden, M., 2010. Provenance of fluvial terrace sediments within the Waipaoa sedimentary system and their importance to New Zelanad source-to-sink studies. Mar. Geol., 270: 84-93.

Miller, A.J. and Kuehl, S.A., 2010. Shelf sedimentation on a tectonically active margin: A modern sediment budget for Poverty continental shelf, New Zealand. Mar. Geol., 270: 175-187.

Milligan, T.G., Hill, P.S. and Law, B.A., 2007. Flocculation and the loss of sediment from the Po River plume. Cont. Shelf Res., 27(3-4): 309-321.

Milliman, J.D. and Syvitski, J.P.M., 1992. Geomorphic/tectonic control of sediment transport to the ocean: The importance of small mountainous rivers. Journal of Geology, 100: 525-544.

Phillips, J.D., Marden, M. and Gomez, B., 2007. Residence time of alluvium in an aggrading fluvial system. Earth Surface Processes and Landforms, 32(2): 307-316.

Reid, L.M. and Page, M.J., 2002. Magnitude and frequency of landsliding in a large New Zealand Catchment. Geomorphology, 49: 71-88.

Rose, L.E. and Kuehl, S.A., 2010. Recent sedimentation patterns and facies distribution on the Poverty Shelf, New Zealand. Mar. Geol., 270: 160-174.

Smith, R.K., 1988. Poverty Bay, New Zealand: a case study of coastal accretion 1886-1975. N. Z. J. Mar. Freshwat. Res., 22: 135-141.

Stephens, S., Bell, R.G. and Black, K.P., 2002. Complex circulation in a coastal embayment: Shelf-current, wind and density-driven circulation in Poverty Bay, New Zealand. J. Coast. Res., 34. Special Issue. 45-59

Walsh, J.P., Alexander, C.R., Gerber, T., Orpin, A.R. and Sumners, B.W., 2007. Demise of a submarine canyon? Evidence for highstand infilling on the Waipaoa River continental margin, New Zealand. Geophys. Res. Lett., 34(L20606): doi:10.1029/2007GL031142.

Warner, J.C., Sherwood, C.R., Signell, R.P., Harris, C.K. and Arango, H.G., 2008. Development of a three-dimensional regional coupled wave-current-sediment model. Comput. Geosci., 34(10): 1284-1306.

Warrick, J.A. and Milliman, J.D., 2003. Hyperpycnal sediment discharge from semiarid southern California rivers: Implications for coastal sediment budgets. Geology, 31(9): 781-784.

Wolinsky, M.A., Swenson, J.B., Litchfield, N. and McNinch, J.E., 2010. Coastal progradation and sediment partitioning in the Holocene Waipaoa Sedimentary System, New Zealand. Mar. Geol., 270: 94-107.

Chapter 2: Hydrodynamics and sediment-transport in the nearshore of Poverty Bay, New Zealand: observations of nearshore sediment segregation and oceanic storms [1]

ABSTRACT

Nearshore regions act as an interface between the terrestrial environment and deeper waters. As such, they play important roles in the dispersal of fluvial sediment and the transport of sand to and from the shoreline. This study focused on the nearshore of Poverty Bay, New Zealand, and the processes controlling the dispersal of sediment from its main sediment source, the Waipaoa River. Hydrodynamics and sediment transport in water shallower than 15 m were observed from April through mid-September, 2006. This deployment afforded observations during 3-4 periods of elevated river discharge and 5 dry storms.

Similar wind, river discharge, wave, current, and turbidity patterns were observed during the three analyzed wet storms. At the beginning of each event, winds blew shoreward, increasing wave heights to 2 to 3 m within Poverty Bay. As the cyclonic storms moved through the system the winds reversed direction and became seaward, reducing the local wave height and orbital velocity while river discharge remained elevated. At these times,

high river discharge and relatively small waves enabled fluvially derived suspended sediment to deposit in shallow water. Altimetry measurements indicated that at least 7 cm was deposited at a 15 m deep site during a single discharge event. Turbidity and seabed observations showed this deposition to be ephemeral, however, as large swell waves from the Southern Ocean triggered resuspension of the material within three weeks of deposition. Consequently, two periods of dispersal were associated with each discharge pulse, one coinciding with fluvial delivery, and a second driven be wave resuspension a few weeks later. These observations of nearfield sediment deposition contradict current hypotheses of very limited sediment deposition in shallow water offshore of small mountainous rivers when floods and high-energy oceanic conditions coincide.

Consistently shoreward near-bed currents, observed along the 10 m isobath of Poverty Bay, were attributed to a combination of estuarine circulation, Stokes drift, and wind-driven upwelling. Velocities measured higher in the water column at the 15 m isobath, however, were directed alongshore and diverged from those at the 10 m isobath. The divergence in the currents observed at the 10 and 15 m locations seemed to facilitate segregation of coarse and fine sediment, with sand transported near-bed toward the beach, while suspended silts and clays were exported to deeper water.

1. Introduction

To understand continental margin sedimentary dispersal systems, sediment-transport processes from river headwaters to the continental slope must be identified and quantified (Carter et al., 2010; Kuehl et al., 2003). Both receiving basin bays and nearshore regions act as important interfaces between fluvial systems and the continental shelf, but have usually been seen as regions of sediment bypass during floods (Nittrouer et al., 2007; Wheatcroft, 2000). Recent studies, however, have reported the retention of river derived mud in the nearshore, and shown that nearshore processes can play an important role in dispersal system dynamics (Curran et al., 2002; Fox et al., 2004; Wadman and McNinch, 2008).

Wheatcroft (2000) used the term "oceanic storm" to describe events typical of small mountainous river systems, where flooding and therefore sediment delivery often coincides with energetic oceanic conditions such as large waves and fast currents. Guillen et al. (2006) analyzed hydrodynamic and sediment-transport observations from the inner-shelf offshore of the Tet River in the Gulf of Lions, France. They differentiated episodes of sediment dispersal into "wet storms" for which energetic oceanic conditions coincided with local precipitation and elevated river discharge; and "dry storms" which were sediment dispersal periods in the absence of significant river discharge. Offshore of the Tet River, sediment deposition occurred in the nearshore during elevated river discharge, that is during wet storms; but this material was later remobilized and transported to deeper water by subsequent wave resuspension during dry storms (Guillen et al. 2006). The amount of sediment captured in these nearshore regions, the time-scales of deposition, and their residence times are poorly understood, however, especially on

12

energetic coasts (Curran et al., 2002). This uncertainty poses difficulty for developing sediment budgets and inferring sediment-transport pathways.

This Chapter investigated fair-weather and storm-driven hydrodynamics and sediment-transport in the energetic nearshore environment of Poverty Bay, North Island, New Zealand, which serves as the interface between the fluvial and marine portions of the Waipaoa Sedimentary System (WSS; see Fig. 1). For this study, the nearshore was taken to be shallower than about 15 m water depth. The Chapter's objectives were to; 1) better understand nearshore hydrodynamics within the study area, and 2) determine sediment-transport dynamics, sediment retention within the nearshore, and the timing of sediment bypassing to deeper water. Observations from S4 and ADCP sensors were used to determine wave characteristics, current velocities, and turbidity during wet and dry storms. Observed currents were analyzed to investigate the processes that influence velocity in the nearshore. ADV altimetry data indicated time-scales of sediment deposition and remobilization within Poverty Bay. Divergence between the S4 and ADCP currents was analyzed to evaluate the degree to which this may enhance the segregation of coarse and fine sediment.

2. Background

Hydrodynamics within many nearshore environments, including Poverty Bay, are predominantly influenced by winds, local freshwater sources, and waves. Wind stress generates horizontal currents and creates setup or set down along the shoreline, potentially driving down-welling or upwelling flows (van de Meene and van Rijn, 2000). Local freshwater sources not only add momentum to the nearshore, but also introduce

baroclinic pressure gradients that can drive estuarine circulation with landward and seaward near-bed and surface flows, respectively (Chatwin, 1976; Hansen and Rattray, 1965; Hetland and Geyer, 2004). In shallow water, nonlinearities in the incident waves create radiation stress gradients and a net drift in water particles, called Stokes drift. These can cause shoreward, seaward, and shore-parallel flows (Holthuijsen, 2007; Svendsen, 2006). Underflows can occur when the sea surface height slopes up toward the beach, creating down-welling conditions (Svendsen, 2006). Waves and currents interact in the nearshore, both by contributing toward total bed shear stresses in a nonlinear fashion (Madsen, 1994; Soulsby et al., 1993; Styles and Glenn, 2000), and through interactions that can increase or decrease wave height and steepness (Svendsen, 2006).

Tectonically active continental margins, such as the east coast of New Zealand, are generally characterized by high topographic relief, short rivers that flood episodically, and steep and narrow continental shelves (Lee et al., 2007; Nittrouer et al., 2007). On these margins, many rivers are classified as "small mountainous rivers" because they are generally short and have headwaters within coastal mountain ranges (Milliman and Syvitski, 1992). The high relief and fractured rock typical of such drainage basins usually lead to large erosion rates and high sediment yields (Milliman and Syvitski, 1992). In these systems, passing weather patterns typically cause river flooding coincident with energetic oceanic conditions, and these "oceanic" or "wet" storms are responsible for much of the sediment delivery to the coastal ocean during short time-frame floods and discharge pulses (Milliman and Syvitski, 1992). For this reason, it has generally been

assumed that most sediment would be quickly carried far from the river mouth soon after entering the coastal ocean (Wheatcroft, 2000).

Very fine sediment delivered by these rivers may be transported through the nearshore within buoyant suspensions emanating from the river mouth (Hill et al., 2007). This sediment effectively bypasses the nearshore and is supplied directly to the continental shelf. Sands and fast settling flocculated fine sediment may sink to the bottom boundary layer and interact with the sediment bed, however, and persist within the nearshore long enough to be significantly influenced by processes such as nonlinearities in wave orbital velocities, underflows, rip currents, and alongshore near-bed transport (Curran et al., 2002; Geyer et al., 2004; Hill et al., 2007). Occasionally, fluvial suspended sediment concentrations are high enough that the density of the river discharge exceeds that of the surrounding seawater. In such cases a hyperpycnal plume occurs that plunges beneath the ocean water and may transport sediment along the seabed through the nearshore to deeper water (Hicks et al., 2004; Mulder et al., 2003; Warrick and Milliman, 2003).

Near-bed high-concentration suspended sediment layers can significantly stratify the water column (Glenn and Grant, 1987), which partially decouples the boundary layer from the overlying water. With high enough suspended sediment concentrations and a sloped seabed, the force of gravity acts on the near-bed water and sediment mixture to create a down-slope velocity, effectively transporting the water and sediment within the boundary layer across the shelf (Sternberg et al., 1996; Traykovski et al., 2007). This mechanism has been shown to be important for across-shelf sediment-transport on some

active margins, including the Eel (Harris et al., 2005; Scully et al., 2003; Traykovski et al., 2000) and Waiapu (Ma et al., 2008) continental shelves.

Conversely, currents caused by wave orbital asymmetries can cause shoreward transport of sediment near the seabed in the nearshore (Wright et al., 1991). In deep water, wave orbital motions are symmetric and there is negligible net movement of the water particles (Holthuijsen, 2007). As waves shoal, however, asymmetries in the shoreward and seaward velocities develop (Holthuijsen, 2007; Svendsen, 2006). Skewness in the water velocity under these shoaling waves has been shown to cause shoreward sediment fluxes, and been related to sandbar and ripple migration in water depths ranging from the beach face to about 15 m (Aagaard et al., 2002; Hsu et al., 2006; Traykovski et al., 1999; Wright et al., 1991).

During times of elevated river discharge, fine sediment such as silts and clays may be deposited in shallow water and incorporated into the sandy deposits predominantly found there. The sequestration of fines in the nearshore and inner continental shelf retains fluvial sediment closer to the river mouth than would otherwise be expected. Indeed, Crockett and Nittrouer (2004) and Wadman and McNinch (2008) found significant storage of fine sediment on the inner shelf offshore of the Eel and Waiapu Rivers, respectively. Curran et al. (2002) argued that the surf zone sequestered and then resupplied large quantities of Eel River sediment to offshore regions, thus influencing sediment budgets and hypotheses of sediment-transport. Also, Fox et al. (2004) observed fine sediment deposition in as little as 4 m of water offshore of the Po River. The role of nearshore sediment storage in overall sediment budgets and sediment-

transport pathways is poorly known for most dispersal systems, however, including that offshore of the Waipaoa River in New Zealand.

3. Study Area

Research on the Waipaoa River Sedimentary System (WSS), a focus site in the Margins Source-to-Sink initiative, spanned from erosion in the river headwaters to sediment accumulation on the continental shelf and slope (see Carter et al., 2010). Poverty Bay plays an integral role within the WSS by acting as an interface between the terrestrial and marine portions of the dispersal system. A small 62 km^2 embayment on the eastern side of the North Island of New Zealand, Poverty Bay opens to the Pacific Ocean through an 8.5 km wide mouth (Fig. 1). Active tectonics cause subsidence of the southwest and uplift of the northeast sides of the bay and coastal plain (Brown, 1995). The Waipaoa and Turanganui Rivers deliver water and sediment to the bay, although the Turanganui is generally neglected, having sediment and freshwater discharges an order of magnitude lower than those of the Waipaoa.

Buoyancy and predominantly seaward winds drive average anticyclonic circulation within the bay, with tidal currents less than 0.05 m s^{-1} (Stephens et al., 2002). Oceanic currents on the continental shelf offshore of Poverty Bay in 35 m water depth generally flowed toward the northeast near the seabed and southeast in the mid-water column over a 1.5 month period, but did not seem to strongly influence conditions within the bay (Stephens et al., 2002). Waves travel into Poverty Bay from the south and southeast, with average significant wave height and period of 1 m and 10 s, respectively (Smith, 1988).

The Waipaoa River typifies small mountainous rivers (Milliman and Syvitski, 1992), having an average freshwater discharge of 32 m^3 s^{-1} punctuated by floods that can exceed the mean by two orders of magnitude (Fig. 2A). Yearly floods of the Waipaoa River have discharges between 550 and 1,100 m^3 s^{-1}, while a discharge of about 2,400 m^3 s^{-1} has about a 10 year recurrence interval (from Reid, 1999). Most floods result from rain delivered by south or southeast traveling cyclonic storms that coincide with strong waves (Orpin et al., 2006), whose heights can reach 5-6 meters within the bay during these events (Healy et al., 2002). Winds during these storms are often shoreward at the beginning of the event, but then rotate becoming seaward as the frontal system passes (Orpin et al., 2006).

The Waipaoa River drainage basin is composed of fractured sandstones, siltstones, and mudstones. The easily erodible nature of the source rocks coupled with the steep topography and a wet maritime climate create especially high sediment yields, averaging 6750 t km^{-2} yr^{-1} (Hicks et al., 2000). About 85% of the catchment was deforested within the last 650 years, greatly increasing the rates of landsliding and gulley erosion (Reid and Page, 2002), as well as the sediment discharge of the Waipaoa River (Kettner et al., 2007). The modern Waipaoa River, on average, discharges ~15 million metric tons (MT) of suspended sediment per year to Poverty Bay (Hicks et al., 2000) (Fig. 2B). Short-lived discharge pulses caused by cyclonic storms moving through the catchment deliver most of the sediment (Hicks et al., 2004). Most of the suspended fluvial material is fine-grained, with an average grain diameter of 15 μm (6Φ); silt represents 88% of the suspended mud (Hicks et al., 2004). Sandy bedload was estimated by Orpin et al. (2006) to be about 1% of the suspended load.

The Poverty Bay shoreline has been capturing Waipaoa River sediment and actively prograding for about 7000 yr, since the last maximum marine transgression (Brown, 1995; Smith, 1988). Seabed sediment texture within Poverty Bay varies spatially. The sediment is generally sandy shallower than the 15 m isobath and fines seaward and toward the southern side of the bay (Foster and Carter, 1997; Wadman and McNinch, 2009). The processes responsible for the sand sequestration in the nearshore, the amount and timing of sediment export from Poverty Bay, and the causes of spatial heterogeneity of surface sediment within the bay are not fully understood, however. The residence time of mud within Poverty Bay seems to be much shorter than eight months, based on the appearance of fluvially derived radio-isotopes on the Poverty shelf (Rose and Kuehl, 2010). Once it leaves Poverty Bay, Waipaoa River sediment both actively infills tectonically produced accommodation space on the continental shelf and is exported to the continental slope (Gerber et al., 2010; Miller and Kuehl, 2010).

4. Methods

Section 4.1 describes the instrumentation deployed within Poverty Bay and external data sources used, such as river discharge and meteorological observations. Section 4.2 then explains the calculations used to analyze the data.

4.1 Instrumentation

Instruments were tethered to, or mounted on, stakes jetted into the seabed that provided stable platforms for data collection from 7 April to 10 September, 2006. At times the text refers to the study period as two deployments, from 7 April – 23 June, 2006;

and 12 July – 10 September, 2006, respectively. Data were not obtained from 23 June to 11 July, 2006 when instruments were serviced.

Three InterOcean S4A current meters with pressure sensors were deployed in Poverty Bay at heights of 1 meter above the bed (mab). The S4s were arrayed along the ~10 m isobath, with the central sensor located directly offshore of the Waipaoa River mouth (Fig. 1). The text refers to these instruments as the "north", "mouth", and "south" S4, reflecting each sensor's location relative to the river mouth. The S4s sampled at 2 Hz with hourly bursts lasting 8 minutes. Conductivity and temperature sensors were suspended near the water surface above each of the S4s, and recorded temperature and salinity throughout both deployments. Water depth was directly estimated from each S4 pressure sensor; post-processing corrected for changes to water density based on the S4's temperature and salinity measurements.

An upward looking RDI 600 kHz Acoustic Doppler Current Profiler (ADCP) was deployed in about 15 m water depth offshore of the Waipaoa River during the same time-period. The ADCP operated with hourly 8 minute bursts sampling at 1.3 Hz to provide measurements of current velocity within ½ m vertical bins. ADCP backscatter was not calibrated to suspended-sediment concentrations, but was corrected for beam spreading and range from the instrument. Accurate and meaningful calibrations for the ADCP backscatter would have required concurrent water sampling, which was not attempted, as calibrations would be sensitive to the sediment size distributions within the water column (Wall et al., 2006). Also, even when calibrated with great care, significant scatter remains in ADCP calibrated suspended sediment concentration data compared to measured data (Merckelbach and Ridderinkhof, 2006). For these reasons, the ADCP

backscatter was used simply to indicate periods of relatively higher or lower turbidity, which was assumed to result primarily from suspended sediment.

A downward looking Acoustic Doppler Velocimeter (Sontek ADVOcean/Hydra), collocated with the ADCP during the second deployment (11 July – 10 Sept.), used a burst duration of 8 min and a sampling frequency of 2 Hz. This provided high-frequency measurements of currents ranging from 0.7 to 0.2 mab as sediment was eroded and deposited, as well as altimetry data used to indicate changes to seabed height.

Complementing this studies data, hourly measurements of Waipaoa River freshwater discharge, collected ~48 km from the mouth (from Gisborne District Council, Fig. 2A), and hourly winds from the Gisborne Airport were available (from http://cliflo.niwa.co.nz/, Fig. 2C). During the study period, 5 winter storms occurred with peak discharges at or above 360 m^3 s^{-1}, with the largest occurring during the instrument turnaround and causing peak river discharge of about 1200 m^3 s^{-1}. The S4s captured 4 of these storms, which occurred from 28 April – 9 May, 19-20 June, 15-24 July, and 7-10 August. The ADCP was not sampling during the June event. River discharge before the deployments, January through April, 2006, was very low, rarely exceeding the yearly average value of 32 m^3 s^{-1}. Sediment discharge from the Waipaoa River was estimated using the rating curve of Hicks et al. (2000) (Fig. 2B). Seafloor sediment samples were also collected from within Poverty Bay, starting in October, 2005 and proceeding through September, 2006 (Wadman and McNinch, 2009).

4.2 Data Calculations

Here, details are given regarding the methods and calculations used to estimate wave characteristics from velocity and pressure measurements, the Stokes drift velocities, potential estuarine circulation velocities, seabed shear stress, and nearshore bedload transport.

4.2.1 Wave Characteristics

Wave spectra were calculated using instantaneous current and pressure data from the S4s and ADV with the PUV method (Pressure – current U velocity – current V velocity) using two MATLAB subroutines, the DIrectional WAve SPectra toolbox (DIWASP, Johnson, 2002) and the Wave Directional Spectra toolbox (WDS, Gordon, 2001). Both of these accounted for attenuation in the pressure and velocity signals with depth. The DIWASP toolbox was used to calculate frequency and directional spectra, while the WDS toolbox provided spectra in only frequency space. Significant wave height and Root-Mean-Squared (RMS) bottom wave orbital velocity were calculated based on Wiberg and Sherwood (2008).

4.2.2 Shoreward Directed Current Speed Calculations

Section 5.3 explores three processes that may contribute to shoreward nearshore currents observed at the S4 sites; 1) Stokes drift generated by wave motions, 2) baroclinic pressure gradients that set up estuarine circulation, and 3) upwelling caused by predominantly seaward blowing winds. The influence of Stokes drift and estuarine

circulation on near-bed velocities were quantified, for comparison with the observed shoreward velocities. Near-bed velocities due to upwelling were not quantified.

The Stokes drift velocity was used here as an approximation for the magnitude of shoreward velocity attributable to wave processes, and was calculated at each of the S4 locations using the measured wave parameters based on Mellor (2008),

$$Su = \frac{2kE}{c} \frac{\cosh(2kz)}{\sinh(2kh)};$$ (1)

where Su was the Stokes drift velocity, h was water depth (set equal to 10 m), k was wave number, z was height above the seabed, c was wave celerity, and E was wave energy. Wave energy was approximated as $E = gA^2/2$ where A was the wave amplitude and g was gravitational acceleration (9.8 m s^{-2}). Wave amplitude, A, was estimated to be one-half of the significant wave height, and z was set to 1 mab. Wave celerity was estimated using $c = \sqrt{g \tanh(kh)/k}$, from Mellor (2008).

Estuarine circulation velocities caused by baroclinic pressure gradients within Poverty Bay were estimated following Chatwin (1976);

$$U = \frac{g}{\rho A_z} \frac{\partial \rho}{\partial x} \frac{h^3}{48};$$ (2)

where U represented the velocity attributable to baroclinic pressure gradients, ρ was water density, $\partial \rho / \partial x$ was the horizontal density gradient, and A_z was the eddy viscosity. The horizontal density gradient was estimated along a transect connecting the Waipaoa River mouth to the mouth of the bay, so that x represented the along-estuary direction. The along-estuary density gradient ($\partial \rho / \partial x$) was calculated using temperatures and salinities representative of surface waters in the nearshore and at the bay mouth.

Eq. (2) was used to estimate the speed of estuarine circulation velocities during two elevated discharge events, one on 30 April through 1 May, 2006, and the other on 16 July, 2006 (see Fig. 2), as follows. The nearshore salinities were assumed to be the lowest values measured during each elevated discharge event in surface waters at the S4 offshore of the Waipaoa River mouth during the above time-frames. The nearshore salinity values for the May and July discharge pulses were 32 and 30 psu, respectively (Fig. 3A). Salinities at the bay mouth were not measured, but were assumed to be at least as high as the salinity measured by the S4s immediately before the river discharge increased. These were 35 and 34.5 psu for the discharge pulses of May and July, respectively. Water temperature was 18 and 14.5 degrees Celsius for the May and July periods, respectively (Fig. 3B). The distance from the salinity measurement to the mouth of Poverty Bay (∂x) was 4 km. Water depth, h, was assumed to be 20 m, representing the average depth within Poverty Bay (see Fig. 1). A constant A_z of 0.01 m^2 s^{-1}, consistent with energetic conditions (Peters, 1997), was used.

Inherent in Eq. (2) was the assumption that the salinity within Poverty Bay did not vary in the across-bay direction. Supporting this, salinity observations at the S4 locations were highly correlated, with correlation coefficients of 0.72 and 0.86 calculated from correlations between salinities measured offshore of the river mouth and at the northern and southern stations, respectively (Fig. 3A). The north and south S4s were also biased to less than one percent of the mean salinity near the river mouth (34.03 psu), further validating this assumption. Application of Eq. (2) also assumed that Poverty Bay behaved as a partially mixed estuary during river flooding, which seemed reasonable

given that energetic winds and currents often coincided with high discharge and would hamper the development of full stratification.

4.2.3 Shear Stress Estimates

The wave and current combined bed shear stress was calculated to evaluate the timing and duration of sediment resuspension events and to provide a means for characterizing the approximate magnitude and direction of bedload transport. Sediment characteristics, near-bed current velocities, and wave characteristics were used as input to the Wiberg et al. (1994) one-dimensional model, which calculated the bed stress. This model has been shown to work well on the inner shelf offshore of Grays Harbor, Washington (Sherwood et al., 2006), as well as several other continental shelf locations (Cacchione et al., 1999; Harris et al., 2003; Wiberg et al., 1994; Wiberg et al., 2002). Wave orbital velocity ($u_{1/10}$) and near-bed currents observed by the S4's and the ADV were used as input. The model included nonlinear interactions between waves and currents, calculating the following components of bed shear: the wave shear velocity, u_{*w}; the current shear velocity, u_{*c}; and the total shear velocity, u_{*cw}. The total bed shear stress was then calculated as $\tau_{cw} = \rho u_{*cw}^2$ where ρ was water density. The model used a continuous eddy viscosity proportional to u_{*cw} in the wave boundary layer and u_{*c} in the current boundary layer, as described in Wiberg and Smith (1983).

The model estimated bedform dimensions based on ripple geometry calculations of Wiberg and Harris (1994), as the bed contained significant quantities of sand in the nearshore (Wadman and McNinch, 2009) and likely formed ripples. Ripple dimensions were then used to estimate the hydrodynamic roughness (z_0), which ranged from a

maximum of 0.02 cm to an assumed minimum value of 0.005 cm (see Wiberg et al., 1994).

The model accounted for boundary layer stratification by sediment suspended from the seabed. Because this is a one-dimensional-vertical model, it assumed that seabed sediment properties were constant and neglected non-local sediment that might be present during times of elevated river discharge. During such times, increased sediment availability may enhance suspended sediment stratification, and model estimates of shear stress might be too high.

For comparison to the model calculations, shear stress estimates were derived from observations using the inertial dissipation method applied to each individual ADV burst, based on Stapleton and Huntley (1995) (Fig. 4A). The typical -5/3 slope was evident in most bursts, as illustrated for two bursts in Fig. 4B and C.

The u_* calculated from the inertial dissipation method, which should represent u_{*c}, fell between the u_{*c} and the u_{*cw} values calculated by the one-dimensional model (Fig. 4A). Total shear velocities estimated for the second deployment using the model were dominated by the wave component and peaked at about $u_{*cw} \sim 6$ cm s^{-1}, while current shear velocities estimated by the model were much lower (Fig. 4A). The values estimated using the inertial dissipation method were intermediate to these, peaking at about 3 cm s^{-1} and also showing a strong correlation with the waves. Lee et al. (2002) obtained similar results in a wave dominated continental shelf setting, finding that the inertial dissipation method yielded estimates of shear stress that exceeded theoretically based estimates of u_{*c} but were less than u_{*cw}. They attributed the higher than expected shear stress values to enhanced eddy viscosities caused by vortex shedding off of ripples

formed during energetic waves. Such vortices would inject turbulence much higher into the water column than would otherwise be expected based on wave boundary layer theory, and enhance turbulent velocities observed above the wave boundary layer, as those presented here were. This would explain why the estimates of u_* derived using the inertial dissipation method exceeded those expected for currents alone (u_{*c}), but remained below the wave and current combined shear velocity (u_{*cw}). Because the u_* from the inertial dissipation method fell between the modeled u_{*c} and u_{*cw}, as seen in Lee et al. (2002), and because the model has performed well at other sites (see citations above), the model calculations of total bed stress were accepted as reasonable estimates.

4.2.4 Bedload Calculations

Shoreward and alongshore bedload fluxes were calculated to determine the effectiveness of currents and waves at transporting sand observed on the seabed inshore of ~15 m water depth. The directions of bedload flux are used in Section 6.4 to investigate the segregation of coarse and fine sediment as it passes through Poverty Bay. From Soulsby (1997),

$$\Phi_{X1} = 12\theta_m^{1/2}(\theta_m - \theta_{cr}) \tag{3}$$

$$\Phi_{X2} = 12(0.95 + 0.19\cos 2\phi)\theta_w^{1/2}\theta_m \tag{4}$$

$$\Phi_X = \max(\Phi_{X1}, \Phi_{X2}) \tag{5}$$

$$\Phi_Y = \frac{12(0.19\theta_m\theta_w^2 \sin 2\phi)}{\theta_w^{3/2} + 1.5\theta_m^{3/2}}; \tag{6}$$

where Φ_X was the dimensionless bedload transport in the direction of the current, Φ_Y was the dimensionless bedload transport perpendicular to the current, $\emptyset$ was the angle

between the currents and waves. Shield's parameters θ_m, θ_w, and θ_{cr} corresponded to the mean current, wave, and critical shear stresses, respectively, based on

$$\theta = \frac{\tau}{g\rho(s-1)d};$$

(7)

where τ was the appropriate current, wave, or critical shear stress, g was acceleration due to gravity, ρ was water density, s was the ratio of the densities of sediment and water, and d was grain diameter. For both the x- and y- directions volumetric bedload fluxes were calculated using

$$q = \Phi\left[g(s-1)d^3 \right]^{1/2}.$$

(8)

Volumetric fluxes were then converted to mass flux and rotated into shoreward and alongshore axes.

In equations 3 – 8, g was 9.8 m s^{-2}, s was roughly 2.5 and calculated based on the density of the water at the S4s and a sediment density of 2650 kg m^{-3}, d was 1 mm, and τ_{cr} was 0.52 Pa. Varying these parameters did not influence the relative proportions of the shoreward and alongshore components, but did change the overall magnitude of the estimated bedload flux. Bedload was calculated using twice and one half the model estimated shear stress to evaluate how uncertainty in the shear stress estimates might impact the results. Changing the shear stress impacted the absolute value of the bedload transport, but not the directions or relative proportions of the along-shore to across-shore components, so results presented below are not overly sensitive to the estimated shear stress.

5. Results

Here, observations of water characteristics, waves, currents, and sediment-transport within Poverty Bay are presented. Also, seabed shear stresses are estimated with emphasis on periods of sediment mobilization and the direction of bedload fluxes.

5.1 Salinity and Temperature

Near surface salinity and temperature fluctuated in response to freshwater discharge pulses, wind-induced upwelling, and seasonal changes. Salinity showed marked decreases during periods of elevated river discharge and also gradually decreased throughout each deployment, presumably due to increased freshwater discharge during the rainy winter months of the field experiment relative to the dryer conditions that occurred before the deployments (Fig. 3A). Temperature responded slightly to pulses of river discharge, but cooled significantly throughout the winter deployment (Fig. 3B). The marked decrease in temperature observed between 14 and 28 May could have resulted from the upwelling of colder waters from the continental shelf into Poverty Bay, as hourly air temperature observations from the Gisborne airport (not shown) do not show significant cooling at this time.

5.2 Waves

Significant wave heights during calm conditions were about 0.5 m, while the average values observed were 1.2, 1.1, and 1.0 m at the north, mouth, and south S4 stations, respectively (Fig. 5A). Average orbital velocities were similar between the northern and southern S4, yet still showed a decrease from north to south similar to the

significant wave height, with values of 0.27 m s^{-1} and 0.24 m s^{-1}, respectively. Wave orbital velocity did differ by as much as 0.1 – 0.2 m s^{-1} at times, however (Fig. 5B). Wave orbital velocities exceeded 0.14 m s^{-1}, a conservative estimate of that needed to suspend fine sediment (Sherwood et al., 1994), about 75% of the time at these three locations. During storms, waves were moderately energetic within Poverty Bay, with wave heights reaching 2 to 3 m in only 10 m of water (Fig. 5). The largest waves coincided with shoreward winds that occurred at the beginning of locally driven wet storms, with wave height and orbital velocity then decreasing as the storms progressed. For example, at the northern S4, the wave height and orbital velocity during the middle of the discharge pulse occurring from 28 April to 9 May, 2006 were 2/3 and 1/2 that experienced at the beginning of the event, respectively. This decrease in wave height and orbital velocity can be explained by the reversal in the direction of the winds as the storms passed the study area.

A shift in wave frequency illustrated the fundamental difference in wave spectra seen in Poverty Bay during wet and dry storms. Wave spectra tended toward higher frequencies (~0.1 Hz, period ~10 s) during local wet storms, and shifted to lower frequencies (~0.06-0.08 Hz, period ~15 s) during dry storm conditions, as exemplified in the data from the northern S4 (Fig. 6). During periods of enhanced discharge, wave spectra contained significant energy in the high-frequency end, indicating the presence of short period waves (time-periods labeled W in Fig. 6A and B). Spectra observed during dry storms indicated that these events were triggered by longer period oceanic swell propagating into the bay from the Southern Ocean, and as such these spectra had significant energy in the lower frequencies (times labeled D in Fig. 6A and B). To

directly compare the wet and dry storm wave spectra, Fig. 6C demonstrated that wave energy during three wet storms exceeded that of the swell seen during three dry storms; in addition to containing more wave energy in the higher frequencies.

Directional and frequency dependent spectra calculated using the S4 data indicated that waves entered Poverty Bay from the southeast to east-southeast, and were subjected to refraction and wave sheltering. Wave energy along the 10 m isobath decreased from the north to the south S4 locations (Fig. 7). Wave directions also shifted; waves observed at the south S4 came from a more easterly direction than those seen offshore of the river mouth and at the north S4.

5.3 Currents

The current results are presented in three subsections. The first overviews the S4 currents observed in 10 m of water. The second explores possible explanations for the net shoreward current observed at each of the S4 locations. Finally, Section 5.3.3 focuses on currents observed in 15 m of water, and the divergence between these currents and those along the 10 m isobath.

5.3.1 Near-Bed Currents Along the 10 m Isobath

Near-bed currents measured by the S4s 1 mab were shoreward at all three locations, turning progressively from westward to more southward along the 10 m isobath from the northern – to – southern S4s (Fig. 8). The orientation of the along-shore component of these currents, toward Young Nicks Head, combined with the direction of the ADCP currents (Section 5.3.3) showed that the overall pattern of circulation was

31

counterclockwise within Poverty Bay (Fig. 8), consistent with previous studies (Stephens et al., 2002). The bearing of the S4 currents (Fig. 8) was also similar to near-bed shoreward flow seen during a lone ADP transect made by Stephens et al. (2002) in about 10 m of water. They attributed the shoreward component of the flow to an upwelling event caused by strong seaward winds that preceded their survey. Mean current speeds during the study period were about 0.17 m s^{-1}, with maximum speeds exceeding 0.5 m s^{-1} (Fig. 9). Current speeds increased during river discharge pulses, periods of larger waves, and increased winds, but their directions remained generally shoreward and alongshore toward Young Nick's Head during these episodes (Fig. 9).

5.3.2 Mechanisms Causing Shoreward Nearshore Currents

Shoreward current speeds measured by the S4s exceeded 0.2 - 0.4 m s^{-1} at times (Fig. 10A). Using Eq. (1), time-series estimates of Stokes drift velocities were made that reached 0.15 m s^{-1} during energetic waves (Fig. 10B). On average, the calculated Stokes drift velocity accounted for 5 – 7.5% of the total observed shoreward current speeds at the three S4 locations (Fig. 10C). The degree to which the shoreward current speed was attributable to the calculated Stokes drift velocity increased during times of energetic waves such as 15-18 May, 2006, when the calculated Stokes drift velocity accounted for 15 to 80% of the observed shoreward current speeds.

While Stokes velocities explained a significant portion (15 – 80%) of the observed shoreward velocities during energetic waves, other processes must also be important. The calculated estuarine circulation velocities explained some of the discrepancy between Stokes drift velocities and the observed shoreward current speeds.

32

Using Eq. (2), estuarine circulation velocities of 0.09 and 0.14 m s^{-1} were estimated for the S4 offshore of the river mouth for 30 April and 16 July, 2006, respectively. The fraction of the observed shoreward velocities accounted for by estuarine circulation was therefore 50-100% for the May event, and ~50% for the July event (Fig. 10A). Upwelling has also been inferred to cause shoreward currents along the ~10 m isobath (Stephens et al., 2002), but was not quantified here.

5.3.3 Currents at the 15 m Isobath

The ADCP and ADV measured currents in ~15 m water depth were oriented in a counterclockwise direction when compared to the 10 m currents, as expected based on previous studies by Stevens et al. (2001), with currents being toward the south in this location (Figs. 8 and 11). Interestingly, the currents observed at the S4 locations along the 10 m isobath diverged sharply from those seen at the ADCP site. Based on shipboard ADCP transects, Stephens et al. (2002) also reported that currents turned sharply southward offshore of the Waipaoa River mouth, which corroborates the observations seen in Fig. 8. ADCP measured current velocities, and those at the south S4, both had a stronger westward component during the 2nd deployment than during the first, possibly because the river discharge was more often elevated, which may have altered the baroclinic pressure gradients and thus the current flow.

Current speeds were not especially high at the ADCP, rarely exceeding 0.3 m s^{-1} (Fig. 11). Low-frequency, greater than 25 hr period, currents were slightly modulated the higher-frequency currents, modifying them by a RMS value of ~ 0.03 m s^{-1}, which is consistent with the value of 0.05 m s^{-1} given in Stephens et al. (2002) for the tidal current

speed in Poverty Bay. Peak speeds were associated with wet storms, and were observed just before and during periods of elevated discharge. The across-shore component of the current velocity behaved consistently for the three discharge pulses identified in Fig. 11. Each wet storm began with a period of shoreward flow, approaching 0.15 m s^{-1}, that coincided with strong shoreward winds and elevated river discharge, for example on 30 April. During this phase, river discharge was increasing as the storms had caused rain within the Waipaoa catchment. Shortly after these pulses of shoreward currents, however, wind direction reversed to be seaward, creating seaward velocities as high as 0.25 m s^{-1} that coincided with elevated river discharge (for example 6-8 May).

Generally, little vertical shear was seen within the ADCP record, which excluded the upper and lower few meters of the water column. Velocities in the upper bin (~12 mab) were slightly faster (average of 0.05 m s^{-1}) and directed ~30 degrees counterclockwise from those measured ~2.5 mab (Fig. 8), which had an average speed of 0.04 m s^{-1}. The ADV, sampling at ~0.2 to 0.7 mab observed currents to be slower (average of 0.02 m s^{-1}), and aligned with currents measured simultaneously by the bottom ADCP bin.

5.4 Seabed Shear Stress

Bed shear stresses (τ_{cw}) at the S4 locations along the 10 m isobath, calculated using the one-dimensional model, averaged about 1 Pa and reached as high as 5.8 Pa (Fig. 4D). Wave induced stress dominated over that caused by the currents, with u_{*w} generally more than four times larger than u_{*c}. Elevated shear stresses coincided with resuspension events seen in the altimetry and backscatter data (discussed in Section 5.5), specifically

around 15 May and 16 August, 2006. At the S4 located offshore of the river mouth, shear stresses (τ_{cw}) exceeded 0.038 Pa, the estimated critical shear stress of the mean grain diameter discharged by the Waipaoa River, throughout the deployment. Bed shear stresses exceeded 0.5 Pa, the critical shear stress of the coarser sand observed in grab samples, about 64% of the time at this site. These critical shear stresses were generally exceeded during both local wet storms and distinct periods of large swell waves, dry storms. As mentioned previously, these bed stresses may be slightly overestimated during discharge pulses of the Waipaoa River because they neglected the addition of fluvial fine grained material and may therefore underestimate the effect of suspended sediment stratification at such times (Wiberg and Smith, 1983). However, even if the model overestimated bed stress at times, the general result remains that the nearshore offshore of the Waipaoa River was wave-dominated, with sufficient seabed shear stress to mobilize fine sand and mud much of the time during typical winter conditions.

Both wave orbital velocities and currents were slower at the 15 m site than along the 10 m isobath, so shear stresses at the 15 m deep ADV location were reduced compared to the S4 locations, although the wave contribution still dominated the total stress. The highest shear stresses, 4 Pa, at the 15 m location were estimated for the period of high river discharge (13-20 July, Fig. 4E). Stress during later swell events was lower, not exceeding 1 Pa. Bed shear stress at the 15 m site still exceeded the critical stress needed to resuspend finer sediments 95% of the time. The bed stress estimates indicated that sand could be transported about 30% of the time for this location, half as frequently as estimated for the 10 m isobath.

5.5 Sediment

Backscatter from the ADCP and seabed altimetry from the ADV were used to identify periods of high turbidity and sediment deposition. Backscatter intensity peaked during river discharge pulses and also during large waves that followed periods of high discharge, both times when suspended sediment concentrations would likely be elevated (Fig. 12). This supported the use of backscatter for identifying periods of relatively high turbidity, although, as discussed earlier, no attempt was made to estimate suspended sediment concentration from backscatter. Backscatter was highest during elevated river discharge, responding directly to the input of sediment from the Waipaoa River, such as the discharge pulses from 28 April through 9 May, 20 to 24 July, and 7 to 10 August (Fig. 12). High backscatter also occurred during wave events that followed the delivery of fresh fluvial sediment, indicating resuspension of freshly deposited material, for example around 15-18 May (Fig. 12). After a period of about two to three weeks following discharge pulses, however, backscatter returned to average background values, as seen during the large waves around 29 May and 1 September (Fig. 12).

Altimetry data collected during the second deployment at the same location as the ADCP backscatter showed the seabed to be very dynamic, with significant sediment deposition and erosion (Fig. 13). The first two weeks of the altimetry record was removed and not included in Fig. 13, to ignore any potential scour or infilling around the instrument after its emplacement, as has been reported for other sites (see Cacchione et al., 1995, for example).

The elevated Waipaoa River discharge that started on 7 August, 2006 led to the apparent deposition of 7 to 25 cm of sediment at this location (Fig. 13). Immediately

36

following deposition, seabed elevation slowly decreased between 9 – 12 August, 2006

(Fig. 13), probably due to dewatering and consolidation of the initial deposit, leaving

about 7 cm of net deposition. This was similar to observations made in a coastal lagoon

where a rapidly formed fluid-mud consolidated over the course of about 4 days

(Anderson et al., 2006). The Poverty Bay deposit subsequently eroded within two weeks

of deposition, with much of the sediment removed quickly during a time of large waves

on 16 August (Fig. 13). These waves produced strong shear stresses (~1 Pa, Fig. 4E) that

exceeded the estimated critical shear stress of the average Waipaoa River sediment

(~0.04 Pa) by a factor of 25. The potential for large waves to influence the seabed was

seen in other erosion and deposition pulses, for example 2 cm of sediment was initially

resuspended on 10 September when wave heights reached 1.5 m, followed within three

days by 4 cm of deposition as waves waned and the river discharged sediment (Fig. 13).

Estimated bedload fluxes (Eqs. 3 – 8) along the 10 m isobath indicated that

sediment moved primarily toward shore with a southward alongshore component (Fig.

14). The magnitude of the shoreward and alongshore fluxes were similar, and they

peaked during periods of combined large waves and fast currents. The southward

alongshore bedload transport was consistent with the formation of a spit that extends

from the north to the south across the mouth of the Waipaoa River during periods of low

discharge. Although its presence was somewhat hidden by the application of a nine hour

running-mean in Fig. 14, limited seaward bedload transport was estimated to occur

during a few select times. Seaward currents at the S4s were slow and generally observed

during periods of weak waves, also resulting in small seaward bedload fluxes.

6. Discussion

This section extends interpretations of storm-driven sediment-transport in the nearshore of Poverty Bay, based on the observational data and model estimates presented above. It covers the roughly 3 week depositional time-frame seen within Poverty Bay, and demonstrates the consistency of the interpretations from this study with results of other research. Sediment-transport dynamics observed within Poverty Bay are put in the context of emerging paradigms of dispersal offshore of small mountainous rivers, showing that in such systems sediment can be deposited in shallow water during energetic oceanic conditions. Finally, the segregation of coarse and fine sediment that occurs in the nearshore and promotes progradation of the Poverty Bay shoreline is discussed.

6.1. Wet and Dry Storm-Driven Hydrodynamics and Sediment-Transport

Three wet storms were sampled by the S4s and the ADCP during the field experiments; one from 28 April through 9 May, another from 15 to 24 July, and the third from 7-10 August. Each included three distinct phases; (1) an initial period when winds blew landward and discharge increased, (2) a phase when winds reversed to be seaward as discharge peaked, and (3) a final phase when the freshwater plume flowed directly toward the bay mouth. This section uses the storm that occurred from 28 April through 9 May to illustrate hydrodynamic and sediment-transport patterns during a wet storm (Fig. 15). The overall patterns of winds, waves, and circulation were similar for these three events, although the April-May storm differed by having three distinct discharge pulses, one of which occurred during each phase of the storm (Fig. 15A). Current, wave, and

38

turbidity patterns for this discharge pulse are illustrated in the visualization of the data from the first deployment, contained on the supplemental DVD.

During the first phase of this cyclonic storm (29 to 30 April), winds blew shoreward (Fig. 15A and B) pushing water into Poverty Bay, as seen in the reversal of the ADCP currents from seaward to shoreward (29 April, Fig. 15C and D). The 2 to 10 cm increase in sea surface height observed along the 10 m isobath preceding and during this phase provided evidence of storm-driven surge (Fig. 15E). At this time, freshwater discharged by the Waipaoa River was retained within Poverty Bay, and the freshwater plume was trapped along the coastline in the inner bay. Indeed, the salinity observations at the S4s showed the plume to be directed toward the north S4 along the 10 m isobath (Fig. 15F). The shoreward winds enhanced wave heights, which reached their peak for the event of 2.75 m during the first phase (Fig. 15G). These waves combined with strong currents (Fig. 15C and D) and created bed stresses estimated to be as high as 5 Pa along the 10 m isobath (Fig. 4D). Elevated backscatter levels during this phase indicated that the water column had high levels of suspended sediment (Fig. 12A). This sediment would likely have been retained within Poverty Bay as the water was forced toward the north along the coastline.

During the second phase of the storm, beginning around 1 May, winds slowed slightly, and turned to become seaward (Fig. 15B). This reduced wave height (Fig. 15G) and it is speculated that this facilitated deposition of thick muddy layers within Poverty Bay, as bed shear stresses were less than one-half of what they were in phase 1 (Fig. 4D). Although altimetry observations were unavailable for this event, during the second phase of a similar wet storm (6 to 8 August), the ADV recorded deposition of a 7 to 25 cm thick

layer at the 15 m location (Fig. 13). ADCP backscatter initially decreased, and then increased again as the second discharge pulse added more suspended sediment to the system (Fig. 12).

Toward the end of the storm, during phase 3 which began around 6 May, currents apparently flowed directly from the Waipaoa River mouth toward the mouth of the Bay (Fig. 15C) and the ADCP observed the highest velocities (0.35 m s^{-1}) seen at this location during the deployment. Although bed shear stresses were still lower at this time than during phase 1 (~2 to 3 Pa at the 10 m isobath; Fig. 4D), backscatter indicated that some sediment remained in the water column, most likely supplied by the third discharge pulse that peaked on 5 May (Fig. 12). The strong seaward currents would have efficiently and quickly exported freshwater and this suspended sediment toward the mouth of Poverty Bay.

During the study period, winds during the wet storms followed this pattern, described in detail for the April-May, 2006 storm. For example, the largest discharge pulse of the study period (19 June), although it occurred during the instrument turnaround, had shoreward winds at the beginning of the event, which then relaxed and turned seaward. Also, a 40 year recurrence interval storm that occurred in October, 2005, and the largest storm on record, Cyclone Bola in March, 1988, followed the same pattern. That is, winds were nearly always shoreward during the initial phase of a wet storm, but then relaxed and reversed to be seaward around the time of peak discharge. Additionally, 30 years (1972-2002) of concurrent Gisborne airport wind and Waipaoa River discharge data were analyzed. This data indicated that winds during elevated discharge (>250 m^3 s$^-$^{1}) more often came from a south to southeast direction, while at all other times the winds

generally came from a northwest direction. The patterns summarized in Fig. 15 therefore seem representative of the majority of the events that would deliver sediment to Poverty Bay.

Contrary to the wet storms, the observed dry storms did not produce consistent current patterns at the 15 m site. For example, the ADCP currents flowed seaward during the dry storm occurring 15-18 May. During another dry storm (16 – 17 August), however, currents were both seaward and shoreward (Fig. 16). Peak current speeds were slower during these two dry storms than the wet storm, at 0.19 and 0.14 m s^{-1} for the May and August dry storms, respectively, compared to 0.35 m s^{-1} for the April-May wet storm. These dry storms generated bed stresses as high as the wet storm, however, from 3 to 6 Pa (Fig. 4), with sediment resuspension during the May dry storm causing a large spike in the ADCP backscatter (Fig. 12). The lack of a consistent pattern in the currents during dry storms indicated that, at least near the 15 m isobath, transport of resuspended sediment at these times may be related to "average" currents and not storm driven ones. In shallower water, however, shoreward flux near the seabed is likely enhanced during dry storms as the 1 mab shoreward currents increase under high wave conditions (Fig. 10A).

6.2. Depositional Time-frame

The ADV altimetry for the 7-10 August discharge pulse indicated that at least some fluvial sediment resided within the nearshore of Poverty Bay for time-scales of about two to three weeks before being exported to the continental shelf. Flood sedimentation initially created thick (7 – 25 cm) unconsolidated layers of fine sediment

41

for this event (7 August, Fig. 13). The altimetry record then showed a gradual decrease in bed elevation indicating consolidation and dewatering of the flood sediment within about 3 days of deposition (9 to 12 August). Following the deposition of sediment during a wet storm, dry storms periodically created bed shear stresses large enough to resuspend previously deposited sediment (Fig. 4). Large waves that persisted for more than twenty-four hours and had orbital velocities exceeding 0.28 m s^{-1} occurred, on average, weekly during the observational periods at the 10 m and 15 m isobaths (Fig. 5). Such waves would easily have generated sediment resuspension, being twice the threshold of 0.14 m s^{-1} to suspend fine sediment identified by Sherwood et al. (1994). Indeed, the altimetry record from 16 August, about 6 days after the 7 to 10 August discharge pulse, showed a rapid decrease, indicating erosion, which corresponded to a time of large waves and increased bed stress (Figs. 4 and 13). This indicated that a typical pattern for Poverty Bay following a discharge pulse would be deposition during the wet storm, some period of consolidation and dewatering, followed by rapid erosion driven by dry storm wave resuspension.

Analysis of ADCP backscatter supports this. In the weeks following discharge pulses, turbidity was enhanced as easily erodible sediment was resuspended, but then over the course of about three weeks, the elevated water column turbidity returned to background values, even in the presence of large waves. For example, following the 28 April to 9 May discharge pulse, ADCP backscatter remained elevated throughout the first half of May, with a peak when wave heights reached 1.5 m around 15 to 18 May (Fig. 12). Two weeks later near 29 May, however, even higher waves of about 1.8 m created a much more modest signal in the ADCP backscatter (Fig. 12). Based on this and the ADV

record from August, the decrease in backscatter signal seen at the end of May is speculated to have resulted from the winnowing of mud from the nearshore and subsequent export to deeper water.

The conclusion that fine grained sediment had a short, about a few weeks, residence time within the nearshore and did not appreciably accumulate there was consistent with observations of [7]Be within Poverty Bay and on the adjacent continental shelf. [7]Be adsorbs to sediment in rivers, being input from rain water (Olsen et al., 1986). Observed [7]Be activities have been lower within Poverty Bay compared to observations from the adjacent continental shelf in water depths from about 25 -100 m (Rose and Kuehl, 2010; Wadman and McNinch, 2009). Data indicated that fine sediment, with high [7]Be activity, was exported from the nearshore, and presumably the bay, within a few weeks of delivery by the river. With export, [7]Be inventory within the bay decreased, and deposition of this sediment within shelf depocenters increased [7]Be activity there.

6.3 Flood Sediment Supply Dominated Behavior

The large sediment supply from the Waipaoa River, even during the modest discharge events observed here, overwhelmed the sedimentary dispersal mechanisms in an environment that might be considered too energetic for fine sediment deposition, with estimated bed stresses sufficient to suspend fine sediment 100% and 95% of the time in 10 and 15 m water depth, respectively. When the total sediment supply exceeded the capacity for dispersal, sediment fluxes converged, causing deposition and seabed accretion. This occurred even during times of large waves and fast currents. For example, during the depositional event of 7 August, 2006, waves and currents were

sufficiently strong to suspend the sediment supplied by the Waipaoa River. The estimated maximum seabed shear stress of about 0.5 to 2 Pa (Fig. 4) exceeded the critical shear stress of the discharged Waipaoa River suspended sediment, about 0.04 Pa to 0.1 Pa. Similar behavior during floods might also occur offshore of other small mountainous rivers, such as the Eel (Curran et al., 2002), Santa Clara (Warrick and Milliman, 2003), and Waiapu Rivers (Wadman and McNinch, 2008), where very large amounts of sediment are discharged to the coastal ocean over short time-periods.

The easily erodible nature of these deposits implies that they were unconsolidated and not unlike deposits seen underneath areas of sediment convergence and turbidity maximum in the York (Lin and Kuo, 2001; Romine, 2004) and Hudson (Woodruff et al., 2001) estuarine systems. The formation of fluid-mud has also been documented at similar regions of sediment convergence (Chen et al., 1999; Kineke and Sternberg, 1995; Ogston et al., 2008), and offshore of the Eel (Ogston et al., 2000) and Amazon (Cacchione et al., 1995) Rivers. From 7 -9 August, 2006 the ADV recorded an elevated seabed, although the measurements contained high temporal variability in the vertical location of the seabed (Fig. 13). This noisy ADV return signal may be explained by a near-bed high-concentration fluid-mud layer that remained suspended by turbulent shear in the wave boundary layer, a high concentration layer near the seabed due to hindered sediment settling, or a combination of the two (Mehta, 1986; Traykovski et al., 2000).

6.4. Wet Storm Dynamics

Wheatcroft (2000) explored the idea of oceanic floods, here referred to as wet storms, with regard to short mountainous river dispersal systems. The compact drainage

44

basins of these systems imply a strong coupling between the elevated river discharge and energetic storm-driven oceanic conditions. A single storm system simultaneously increases river runoff, winds, waves, and currents. Presumably, this reduces nearfield sediment deposition offshore of the river mouth and increases transport length-scales during the flood, by enhancing the dispersal mechanisms of plume transport, near-bed suspended load, and gravity driven flows. This acts to deliver sediment directly to deeper water on the middle continental shelf during the flood itself.

The Waipaoa River, a prototypical small mountainous river, was expected to follow this conceptual model, however, observations from Poverty Bay indicated that this dispersal system deviated from this expectation. System behavior during flooding actually led to fine sediment deposition in the nearshore, where bed stresses exceed the suspension threshold for fine sediment near the river mouth where deposition occurred. This fine sediment was subsequently winnowed from the seabed and transported toward deeper water during periods of remotely generated swell that may occur days to weeks after the initial emplacement of flood material. Transport during these dry storms may follow different pathways than material exported during flooding and wet storm conditions, potentially influencing depocenters on the continental shelf.

The shape of the discharge basin also helped explain the deviation of the Waipaoa River dispersal system from the conceptual model of small mountainous rivers. The presence of an embayment encouraged the development of potentially strong estuarine circulation enhancing shoreward near-bed currents. Due to the sheltering effect of the headlands, the size of the waves impacting the nearshore is reduced, compared to those on the open coastline outside of Poverty Bay. Additionally, although the waves are

subject to refraction and sheltering (Fig. 7), the crescent shape allows waves of sufficient size to reach the nearshore to drive shoreward directed currents. All of these mechanisms helped trap sediment close to the river mouth, reduced flood dispersal distances, and promoted short-term retention of sediment in the nearshore.

6.5. Sediment Segregation

The current velocities observed along the 10 m isobath by the S4s diverged sharply from those measured by the ADCP in 15 m of water (Fig. 8), which likely impacted the segregation of sand from finer sediment. Located in deeper water than the S4s, the ADCP site was less influenced by waves so that Stokes drift velocity was roughly 2.5 times less there than along the 10 m isobath. With its bottom bin at about 2.5 mab, the ADCP also sampled higher in the water column than the 1 mab S4s, so that the ADCP currents were less likely to be influenced by upwelling or be within shoreward near-bed estuarine flows. These factors helped explain why currents measured at the ADCP location were generally more seaward or parallel to shore than those measured by the S4s, which were shoreward with an along-shelf component toward Young Nick's Head (Fig. 8).

Sand delivered by the Waipaoa River or resuspended from the bed would remain near the seabed, traveling either as bedload or near-bed suspended load. This sand would preferentially be transported toward shore, as its flux would be highest in shallow locations where shear stresses were higher and near-bed flows were shoreward. Indeed, bedload estimated for the S4 locations indicated that the net flux of sand would be shoreward and alongshore toward Young Nick's Head (Fig. 14). Finer sediment would

be entrained throughout the water column and be effectively transported as suspended load counterclockwise around the bay and to deeper water, following the direction of the ADCP currents. These conclusions were consistent with observed grain-size distributions that showed sand percentages to increase in water depths shallower than ~15 m, while mud content increased on the southern side of Poverty Bay (Foster and Carter, 1997; Wadman and McNinch, 2009). The estimated differential transport directions between the bedload and suspended load is also consistent with observations offshore of the United State east coast (Traykovski et al., 1999).

The conclusion that estuarine circulation, Stokes drift, and upwelling enhance segregation of coarse and fine sediment, preferentially moving sand shoreward to accumulate in the nearshore and on the beach face while exporting mud, was consistent with seismic data and published shoreline volumetric change rates. Seismic data showed large amounts of sand in the nearshore (Wadman and McNinch, 2009), indicating sand delivered by the Waipaoa River has contributed to observed shoreline progradation. Smith (1988) calculated that $~4x10^6$ m^3 of sediment accumulated on the shoreline from 1880 to 1975, a rate of $7x10^7$ kg yr^{-1}, using a porosity of 60%. This 95 year average rate included the anthropogenic increase in Waipaoa River sediment discharge (Smith, 1988). Bedload from the Waipaoa River was estimated by Orpin et al. (2006) to be about $15x10^7$ kg yr^{-1}, or 1% of the suspended discharge. Retention of only half of this sand would account for the observed shoreline progradation. Some of the missing sand delivered by the river likely escaped the nearshore during periods of high discharge and large waves and fast currents. Because the sand fraction alone accounted for shoreline progradation,

this further implies that over the 100 year time-scale, nearly all of the suspended load of the Waipaoa River bypassed the nearshore region and was exported from Poverty Bay.

7. Conclusions

Cyclones episodically impact the Waipaoa Sedimentary System, bringing precipitation that elevates river discharge. Typical wind patterns during these storms initially drive shoreward currents during the first phase of flooding when discharge is increasing. Around the time of peak discharge, winds typically rotate to become seaward creating seaward currents offshore of the river mouth during the second and third phases of the storm. Sediment discharged during the first phase of discharge pulses is likely retained within the bay by shoreward directed currents and a coastally trapped plume. As the winds weaken and rotate to a seaward direction during phase two, wave height and orbital velocity decrease facilitating shallow water sediment deposition. During phase three, a strong seaward flow occurs that carries some suspended sediment from the river mouth directly toward the mouth of Poverty Bay. While the freshwater plume may export some material during the discharge event, a significant portion of the fine sediment discharged by the Waipaoa River seems to be ephemerally deposited as thick layers in the nearshore. Within a few weeks, this sediment seems to be winnowed from the seabed by swell waves and transported toward the continental shelf by ambient currents. Observations from this study could not quantify the amount of sediment exported within flood or swell driven episodes, however. Application of a three-dimensional numerical model could improve estimates of the timing and direction of sediment export from Poverty Bay, and is explored in Chapters 3 and 4.

Near-bed currents observed along the 10 m isobath were consistently shoreward with a counterclockwise orientation, while at the 15 m isobath, currents were directed primarily toward Young Nick's Head with a more seaward component. Three physical processes strengthened these shoreward directed nearshore currents observed along the 10 m isobath; estuarine circulation, wind induced upwelling, and wave processes such as Stokes drift. Estimates of estuarine circulation and wave processes indicated that they could each produce shoreward velocities on the order of up to ~15 cm s^{-1}, with each accounting for approximately 50% of the observed shoreward speed during the two periods of elevated discharge.

Across-shelf current divergence, as evidenced by the S4 and ADCP observations, provided a mechanism for transporting coarser material shoreward, while carrying fines toward deeper water, effectively segregating the sand from the mud. Sand retained in the nearshore contributed to shoreline progradation, while the silt and clay were exported toward the continental shelf, likely contributing to observed depocenters there.

The Waipaoa River dispersal system differed from a paradigm developed for small mountainous rivers because significant sediment deposition occurred in the nearfield during wet storm conditions, even though elevated discharge coincided with oceanic storms. When resuspended, this sediment may follow a different transport pathway than the sediment exported during the discharge pulse. This implied that the characteristics of flood deposits on the Waipaoa shelf may be as sensitive to the climatology of swell waves and ambient currents as to the conditions present during discharge pulses themselves.

Acknowledgements

References

Aagaard, T., Black, K.P. and Greenwood, B., 2002. Cross-shore suspended sediment transport in the surf zone: a field-based parameterization. Mar. Geol., 185: 283-302.

Anderson, T.J., Pejrup, M. and Nielsen, A.A., 2006. Long-term and high-resolution measurements of bed level changes in a temperate, microtidal coastal lagoon. Mar. Geol., 226: 115-125.

Brown, L.J., 1995. Holocene shoreline depositional processes at Poverty Bay, a tectonically active area, northeastern north island, New Zealand. Quatern. Res., 26: 21-33.

Cacchione, D.A. et al., 1995. Measurements in the bottom boundary layer on the Amazon subaqueous delta. Mar. Geol., 125: 235-257.

Cacchione, D.A., Wiberg, P.l., Lynch, J., Irish, J. and Traykovski, P., 1999. Estimates of suspended-sediment flux and bedform activity on the inner portion of the Eel continental shelf. Mar. Geol., 154: 83-97.

Carter, L., Orpin, A.R. and Kuehl, S.A., 2010. Landscape and sediment responses from mountain source to deep ocean sink; Waipaoa Sedimentary System, New Zealand. Mar. Geol.

Chatwin, P.C., 1976. Some remarks on the maintenance of the salinity distribution in estuaries. Estuar. Coast. Shelf Sci., 4: 555-566.

Chen, J. Li, D., Chen, B., Hu, F., Zhu, H. and Liu, C., 1999. The processes of dynamic sedimentation in the Changjiang Estuary. J. Sea Res., 41: 129-140.

Crockett, J.S. and Nittrouer, C.A., 2004. The sandy inner shelf as a repository for muddy sediment: An example from Northern California. Cont. Shelf Res., 24: 55-73.

Curran, K.J., Hill, P.S. and Milligan, T.G., 2002. Fine-grained suspended sediment dynamics in the Eel River flood plume. Cont. Shelf Res., 22: 2537-2550.

Foster, G. and Carter, L., 1997. Mud sedimentation on the continental shelf at an accretionary margin - Poverty Bay, New Zealand. N. Z. J. Geol. Geophys., 40: 157-173.

Fox, J.M., Hill, P.S., Milligan, T.G. and Boldrin, A., 2004. Flocculation and sedimentation on the Po River Delta. Mar. Geol., 203: 95-107.

Gerber, T., Pratson, L.F., Kuehl, S., Walsh, J.P., Alexander, C. and Palmer, A., 2010. The influence of sea level and tectonics on Late Pleistocene through Holocene sediment storage along the high-sediment supply Waipaoa continental shelf. Mar. Geol., 270: 139-159.

Geyer, W.R., Hill, P.S. and Kineke, G.C., 2004. The transport, transformation and dispersal of sediment by buoyant coastal flows. Cont. Shelf Res., 24: 927-949.

Glenn, S.M. and Grant, W.D., 1987. A suspended sediment stratification correction for combined wave and current flows. J. Geophys. Res., 92: 8244-8264.

Gordon, L., 2001. http://current-meter.com/principles/Waves.html#PUV. NortekUSA LLC.

Guillen, J., Bourrin, F., Palanques, A., Durrieu de Madron, X., Puig, P. and Buscail, R., 2006. Sediment dynamics during wet and dry storms events on the Tet inner shelf (SW Gulf of Lions). Mar. Geol., 234: 129-142.

Hansen, D.V. and Rattray, M., 1965. Gravitational circulation in straits and estuaries. J. Mar. Res., 23: 104-122.

Harris, C.K., Butman, B. and Traykovski, P., 2003. Winter-time circulation and sediment transport in the Hudson Shelf Valley. Cont. Shelf Res., 23: 801-820.

Harris, C.K., Traykovski, P.A. and Geyer, W.R., 2005. Flood dispersal and deposition by near-bed gravitational sediment flows and oceanographic transport: A numerical modeling study of the Eel River shelf, northern California. J. Geophys. Res., 110(C09025, doi10.1029/2004JC002727).

Healy, T., Stephens, S., Black, K., Gorman, R., Cole, R. and Beamsley, B., 2002. Port redesign and planned beach renourishment in a high wave energy sandy-muddy coastal environment, Port Gisborne, New Zealand. Geomorphology, 48: 163-177.

Hetland, R.D. and Geyer, W.R., 2004. An idealized study of the structure of long, partially mixed estuaries. J. Phys. Oceanogr., 34(12): 2677-2691.

Hicks, D.M., Gomez, B. and Trustrum, N.A., 2000. Erosion thresholds and suspended sediment yields, Waipaoa River basin, New Zealand. Water Resour. Res., 36(4): 1129-1142.

Hicks, D.M., Gomez, B. and Trustrum, N.A., 2004. Event suspended sediment characteristics and the generation of hyperpycnal plumes and river mouths: east coast continental margin, North Island, New Zealand. J. Geol., 112(4): 471-485.

Hill, P.S., Fox, J.M., Crockett, J.S., Curran, K.J., Friedrichs, C.T., Geyer, W.R., Milligan, T.G., Ogston, A.S., Puig, P., Scully, M.E., Traykovski, P.A. and Wheatcroft, R.A., 2007. Sediment Delivery to the Seabed on Continental Margins. In: C.A. Nittrouer et al. (Editors), Continental Margin Sedimentation: Transport to Sequence. Blackwell Publishing Ltd., pp. 49-99.

Holthuijsen, L.H., 2007. Waves in oceanic and coastal waters. University Press, Cambridge.

Hsu, T., Elgar, S. and Guza, R.T., 2006. Wave-induced sediment transport and onshore sandbar migration. Coastal Engineering, 53: 817-824.

Johnson, D., 2002. DIWASP, a directional wave spectra toolbox for MATLAB: User manual, Center for Water Research, University of Western Australia.

Kettner, A.J., Gomez, B. and Syvitski, J.P.M., 2007. Modeling suspended sediment discharge from the Waipaoa River system, New Zealand: The last 3000 years. Water Resour. Res., 43(W07411): doi:10.1029/2006WR005570.

Kineke, G.C. and Sternberg, R.W., 1995. Distribution of fluid muds on the Amazon continental shelf. Mar. Geol., 125: 193-233.

Kuehl, S., Carter, L., Gomez, B. and Trustrum, N., 2003. Holistic approach offers potential to quantify mass fluxes across continental margins. EOS Transactions, 84(38).

Lee, G., Friedrichs, C.T. and Vincent, C.E., 2002. Examination of diffusion versus advection dominated sediment suspension on the inner shelf under storm and swell conditions, Duck, North Carolina. J. Geophys. Res., 107(C7): DOI:10.1029/2001JC000918.

Lee, H.J., Locat, J., Desgagnes, J.D., McAdoo, B.G., Orange, D.L., Puig, P., Wong, F.L., Dartnell, P. and Boulanger, E., 2007. Submarine mass movements on continental margins. In: C.A. Nittrouer et al. (Editors), Nittrouer, C.A. et al., 2007. Writing a Rosetta stone: insights into continental-margin sedimentary processes and strata.

In: C.A. Nittrouer et al. (Editors), Continental-Margin Sedimentation: From Sediment Transport to Sequence Stratigraphy. Blackwell Publishing Ltd., pp. 213-274.

Lin, J. and Kuo, A.Y., 2001. Secondary turbidity maximum in a partially mixed microtidal estuary. Estuaries, 24(5): 707-720.

Ma, Y., Wright, L.D. and Friedrichs, C.T., 2008. Observations of sediment transport on the continental shelf off the mouth of the Waiapu River, New Zealand: Evidence for current-supported gravity flows. Cont. Shelf Res., 28(4-5): 516-532.

Madsen, O.S., 1994. Spectral wave-current bottom boundary layer flows. Coastal Engineering 1994. Proceedings, 24th International Conference Coastal Engineering Research Council: 384-398.

Mehta, A.J., 1986. Characterization of cohesive sediment properties and transport processes in estuaries. In: A.J. Mehta (Editor), Estuarine Cohesive Sediment Dynamics. Springer, Berlin, pp. 290-325.

Mellor, G., 2008. The depth-dependent current and wave interaction equations: A revision. J. Phys. Oceanogr., 38: 2587-2596.

Merckelbach, L.M. and Ridderinkhof, H., 2006. Estimating suspended sediment concentration using backscatter from an acoustic Doppler profiling current meter at a site with strong tidal currents. Ocean Dynamics, 56: 153-168.

Miller, A.J. and Kuehl, S.A., 2010. Shelf sedimentation on a tectonically active margin: A modern sediment budget for Poverty continental shelf, New Zealand. Mar. Geol., 270: 175-187.

Milliman, J.D. and Syvitski, J.P.M., 1992. Geomorphic/tectonic control of sediment transport to the ocean: The importance of small mountainous rivers. J. Geol., 100: 525-544.

Mulder, T., Syvitski, J.P.M., Migeon, S., Faugeres, J. and Savoye, B., 2003. Marine hyperpycnal flows: initiation, behavior and related deposits. A review. Mar. Pet. Geol., 20: 861-882.

Nittrouer, C.A., Austin, J.A., Field, M.E., Kravitz, J.H., Syvistki, J.P.M. and Wiberg, P.L., 2007. Writing a Rosetta stone: insights into continental-margin sedimentary processes and strata. In: C.A. Nittrouer et al. (Editors), Continental-Margin Sedimentation: From Sediment Transport to Sequence Stratigraphy. Blackwell Publishing Ltd., pp. 1-48.

Ogston, A.S., Cacchione, D.A., Sternberg, R.W. and Kineke, G.C., 2000. Observations of storm and river flood-driven sediment transport on the northern California continental shelf. Cont. Shelf Res., 20: 2141-2162.

Ogston, A.S., Sternberg, R.W., Nittrouer, C.A., Martin, D.P., Goni, M.A. and Crockett, J.S., 2008. Sediment delivery from the Fly River tidally dominated delta to the nearshore marine environment and the impact of El Nino. J. Geophys. Res., 113(F01S11): doi:10.1029/2006JF000669.

Olsen, C.R., Larsen, I.L., Lowry, P.D., Cutshall, N.H. and Nichols, M.M., 1986. Geochemistry and deposition of [7]Be in river-estuarine and coastal waters. J. Geophys. Res., 91(C1): 896-908.

Orpin, A.R., Alexander, C., Carter, L., Kuehl, S. and Walsh, J.P., 2006. Temporal and spatial complexity in post-glacial sedimentation on the tectonically active, Poverty Bay continental margin of New Zealand. Cont. Shelf Res., 26: 2205-2224.

Peters, H., 1997. Observations of stratified turbulent mixing in an estuary: Neap-to-spring variations during high river flow. Estuar. Coast. Shelf Sci., 45: 69-88.

Reid, C.J., 1999. Waipaoa River at Kanakanaia: a review of flood data, Unpublished report to the Gisborne District Council, New Zealand.

Reid, L.M. and Page, M.J., 2002. Magnitude and frequency of landsliding in a large New Zealand Catchment. Geomorphology, 49: 71-88.

Romine, H.M., 2004. Documenting the suspended and bottom sediment dynamics of a two estuarine turbidity maximum system using 7Be and 234Th. Thesis, College of William and Mary, Virginia Institute of Marine Science, Gloucester Point, 100 pp.

Rose, L.E. and Kuehl, S.A., 2010. Recent sedimentation patterns and facies distribution on the Poverty Shelf, New Zealand. Mar. Geol., 270: 160-174.

Scully, M.E., Friedrichs, C.T. and Wright, L.D., 2003. Numerical modelling of gravity-driven sediment transport and deposition on an energetic continental shelf: Eel River, northern California. J. Geophys. Res., 108(C4): 17-1:17-14.

Sherwood, C.R., Butman, B., Cacchione, D.A., Drake, D.E., Gross, T.F., Sternberg, R.W. and Williams, A.J., 1994. Sediment-transport events on the northern California Continental Shelf during the 1990-1991 STRESS experiment. Cont. Shelf Res., 14(10/11): 1063-1099.

Sherwood, C.R., Lacy, J.R. and Voulgaris, G., 2006. Shear velocity estimates on the inner shelf off Grays Harbor, Washington, USA. Cont. Shelf Res., 26: 1995-2018.

Smith, R.K., 1988. Poverty Bay, New Zealand: a case study of coastal accretion 1886-1975. N. Z. J. Mar. Freshwat. Res., 22: 135-141.

Soulsby, R.L., 1997. Dynamics of marine sands: a manual for practical applications. Telford, London, 249 pp.

Soulsby, R.L., Hamm, L., Klopman, G., Myrhaug, D., Simons, R.R. and Thomas, G.P., 1993. Wave-current interaction within and outside the bottom boundary layer. Coastal Engineering, 21: 41-69.

Stapleton, K.R. and Huntley, D.A., 1995. Seabed stress determinations using the inertial dissipation method and the turbulent kinetic energy method. Earth Surface Processes and Landforms, 10: 807-815.

Stephens, S., Bell, R.G. and Black, K.P., 2002. Complex circulation in a coastal embayment: Shelf -current, wind and density-driven circulation in Poverty Bay, New Zealand. J. Coast. Res., 34. Special Issue. 45-59

Sternberg, R.W., Cacchione, D.A., Paulson, B., Kineke, G.C. and Drake, D.E., 1996. Observations of sediment transport on the Amazon subaqueous delta. Cont. Shelf Res., 19: 697-715.

Styles, R. and Glenn, S.M., 2000. Modelling stratified wave and current bottom boundary layers on the continental shelf. J. Geophys. Res., 105(C10): 24119-2439.

Svendsen, I.A., 2006. Introduction to nearshore hydrodynamics. Advanced Series on Ocean Engineering, 24. World Scientific Publishing Co. Pte. Ltd., Singapore, 722 pp.

Traykovski, P., Geyer, W.R., Irish, J.D. and Lynch, J.F., 2000. The role of wave-induced density-driven fluid mud flows for cross-shelf transport on the Eel River continental shelf. Cont. Shelf Res., 20: 2113-2140.

Traykovski, P., Hay, A.E., Irish, J.D. and Lynch, J.F., 1999. Geometry, migration, and evolution of wave orbital ripples at LEO-15. J. Geophys. Res., 104(C1): 1505-1524.

Traykovski, P., Wiberg, P.L. and Geyer, W.R., 2007. Observations and modeling of wave-supported sediment gravity flows on the Po prodelta and comparison to prior observations from the Eel shelf. Cont. Shelf Res., 27(4-3): 375-399.

van de Meene, J.W.H. and van Rijn, L.C., 2000. The shoreface-connected ridges along the central Dutch coast - part 1: field observations. Cont. Shelf Res., 20: 2295-2323.

Wadman, H.M. and McNinch, J.E., 2008. Stratigraphic spatial variation on the inner shelf of a high-yield river, Waiapu River, New Zealand: Implications for fine sediment dispersal and preservation. Cont. Shelf Res., 28(7): 865-886.

Wadman, H.M. and McNinch, J.E., 2009. Sediment segregation and dispersal across the land-sea interface: Waipaoa sedimentary system, New Zealand, Integration and Synthesis of MARGINS Sediment Source-to-Sink Research Workshop, Gisborne, New Zealand.

Wall, G.R., Nystrom, E.A. and Litten, S., 2006. Use of an ADCP to compute suspended-sediment discharge in the tidal Hudson River, New York, U.S. Geological Survey Scientific Investigations Report 2006-5055.

Warrick, J.A. and Milliman, J.D., 2003. Hyperpycnal sediment discharge from semiarid southern California rivers: Implications for coastal sediment budgets. Geology, 31(9): 781-784.

Wheatcroft, R.A., 2000. Oceanic flood sedimentation: a new perspective. Cont. Shelf Res., 20: 2059-2066.

Wiberg, P. and Smith, J.D., 1983. A comparison of field data and theoretical models for wave-current interactions at the bed on the continental shelf. Cont. Shelf Res., 2(2-3): 147-162.

Wiberg, P.L., Drake, D.E. and Cacchione, D.A., 1994. Sediment resuspension and bed armoring during high bottom stress events on the northern California inner continental shelf: measurements and predictions. Cont. Shelf Res., 14: 1191-1219.

Wiberg, P.L., Drake, D.E., Harris, C.K. and Noble, M., 2002. Sediment transport on the Palos Verdes shelf over seasonal to decadal time scales. Cont. Shelf Res., 22: 987-1004.

Wiberg, P.L. and Harris, C.K., 1994. Ripple geometry in wave-dominated environments. J. Geophys. Res., 99(C1): 775-789.

Wiberg, P.L. and Sherwood, C.R., 2008. Calculating wave-generated bottom orbital velocities from surface-wave parameters. Comput. Geosci., 34(10): 1243-1262.

Woodruff, J.D., W.R., G., Sommerfield, C.K. and Driscoll, N.W., 2001. Seasonal variation of sediment deposition in the Hudson River estuary. Mar. Geol., 179: 105-119.

Wright, L.D., Boon, J.D., Kim, S.C. and List, J.H., 1991. Modes of cross-shore sediment transport on the shoreface of the Middle Atlantic Bight. Mar. Geol., 96: 19-51.

Figure 1. Location and smoothed bathymetry of Poverty Bay showing locations of the instruments, Gisborne, the Gisborne airport (A in right panel), the Waipaoa River mouth (WR), Young Nick's Head, and Tuaheni Point.
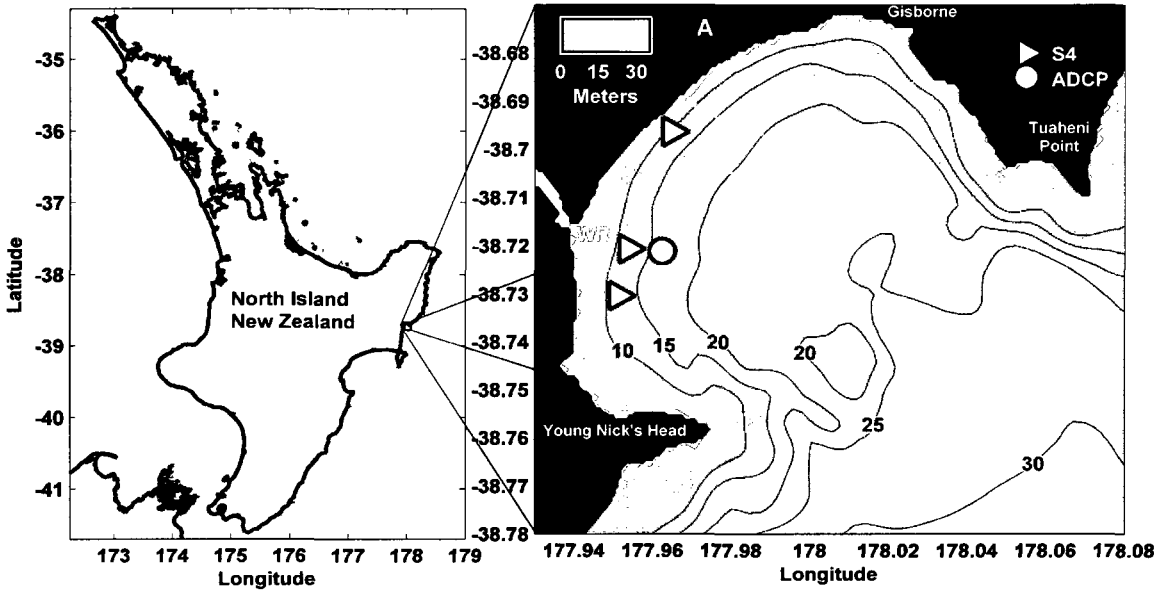
Figure 2. (A) Freshwater discharge and (B) estimated sediment discharge from the
Waipaoa River. Cumulative sediment discharge shown as the continuously increasing line
(see right axis). (C) Wind speed (line); wind velocity (vectors) were lowpass filtered
using a 33 hr cutoff frequency and point in the direction toward which the winds blew,
with straight up being northward. The grey area identifies time between deployments
when instruments were out of the water.
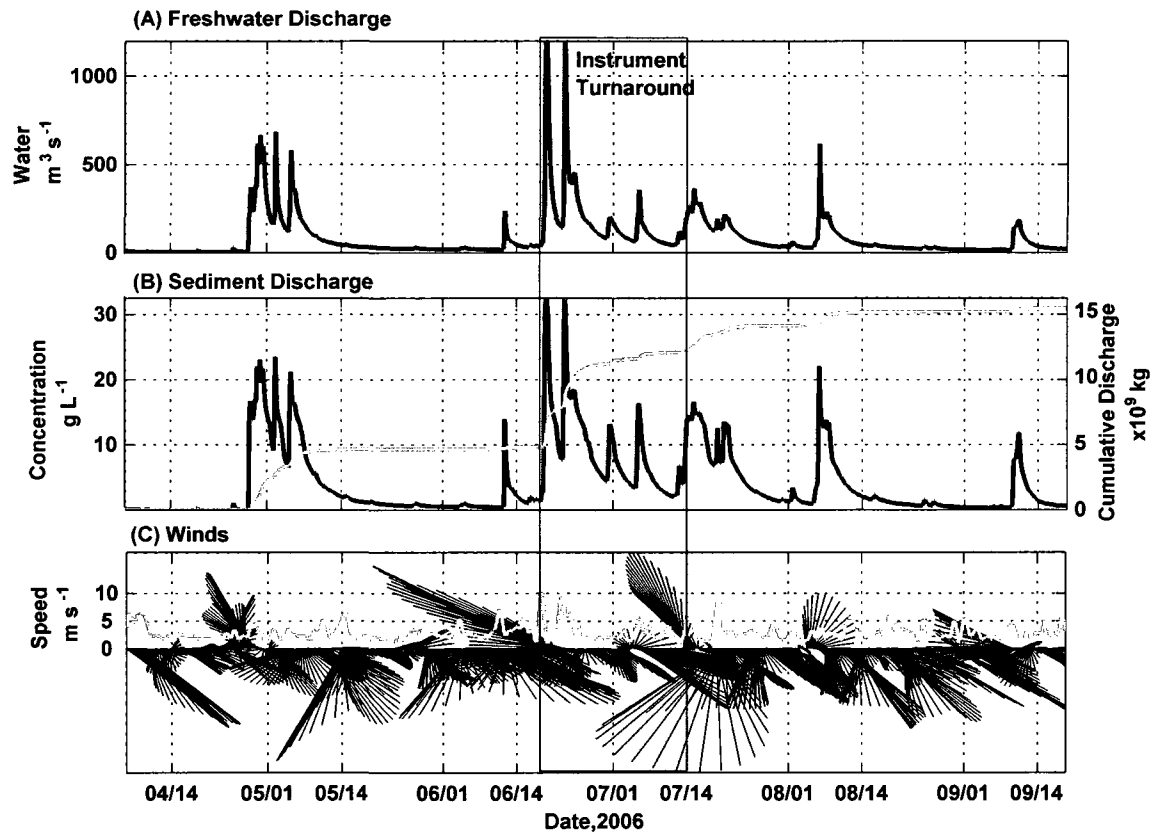
Figure 3. Nine hour running-means of near-surface (A) salinity and (B) temperature measured at the S4 locations. Data unavailable during the instrument turnaround (22 June – 12 July). Inset shows approximate locations of the north, mouth, and south S4 locations, with bathymetry contoured in meters.
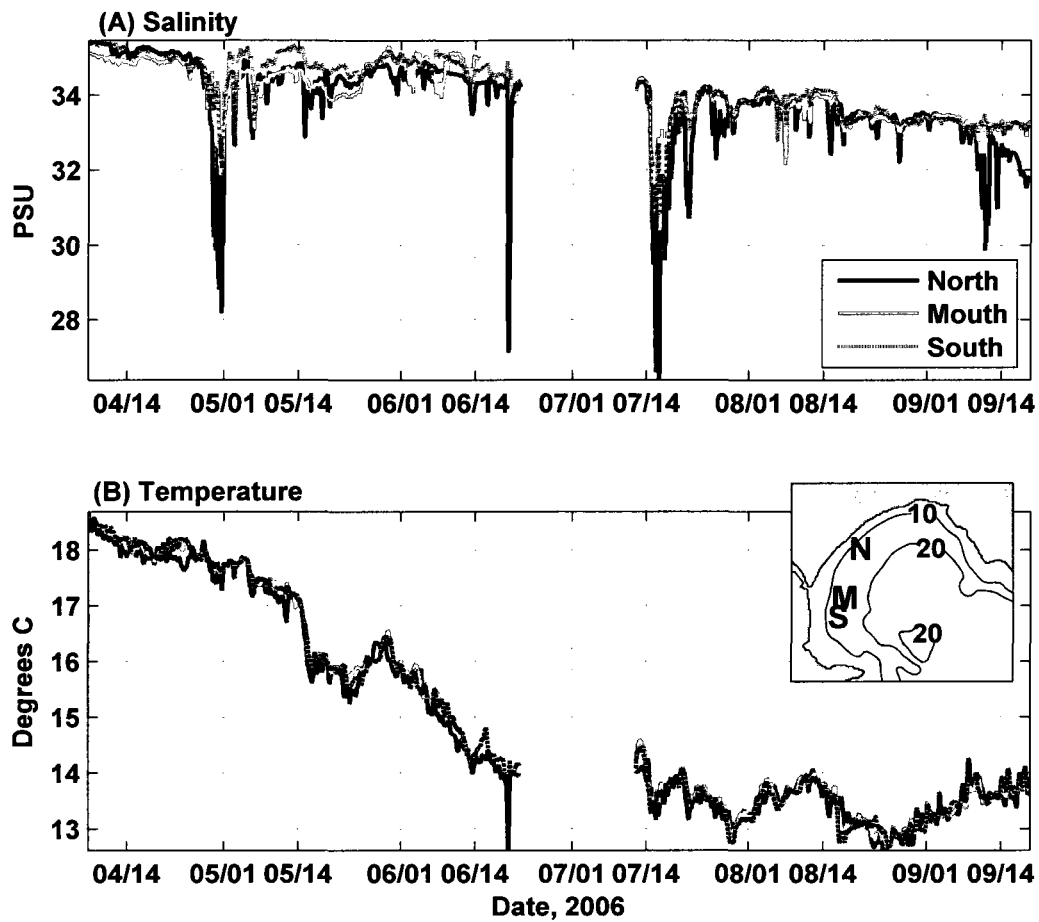
Figure 4. (A) Shear velocities (u_{*c} and u_{*cw}) estimated with the one-dimensional model of Wiberg et al. (1994), labeled 1D u_{*c} and 1D u_{*cw}. These used the ADV measured currents and waves as input. Shear velocity calculated from ADV observations with the inertial dissipation method labeled I.D. u_*. (B and C) Spectra for vertical velocity component (w) of two ADV bursts. The thick grey line shows a -5/3 slope. (D) Shear stresses (τ_{cw}) calculated with Wiberg's one-dimensional model using currents and waves measured by the S4s as input (see legend) and (E) using currents and waves observed by the ADV, which was deployed in mid-July, 2006. Panels (A), (D), and (E) show nine hour running-means. Note difference in dates between panel A and panels D and E.

Figure is on the next page.

(A) Estimated Shear Velocity

Legend: 1D u_{*c}, 1D u_{*cw}, I.D. u_*

y-axis: u_* cm s^{-1}

x-axis: 07/14, 08/01, 08/14, 09/01, 09/14

(B) 16 July, 2006

y-axis: m^2 s^{-2} Hz^{-1}

x-axis: Frequency, Hz

(C) 30 July, 2006

x-axis: Frequency, Hz

(D) 10 m Water Depth, τ_{cw}

Legend: North, Mouth, South

y-axis: Pascals

x-axis: 04/14, 05/01, 05/14, 06/01, 06/14, 07/01, 07/14, 08/01, 08/14, 09/01, 09/14

(E) 15 m Water Depth, τ_{cw}

Legend: 1D Estimation

y-axis: Pascals

x-axis: 04/14, 05/01, 05/14, 06/01, 06/14, 07/01, 07/14, 08/01, 08/14, 09/01, 09/14

Date, 2006

60

Figure 5. Three hour running-means of (A) significant wave height and (B) RMS orbital velocity measured at the S4 locations. Periods of wet storms labeled with a "W" and dry storms with a "D". Inset shows approximate locations of the north, mouth, and south S4 locations, with bathymetry contoured in meters.
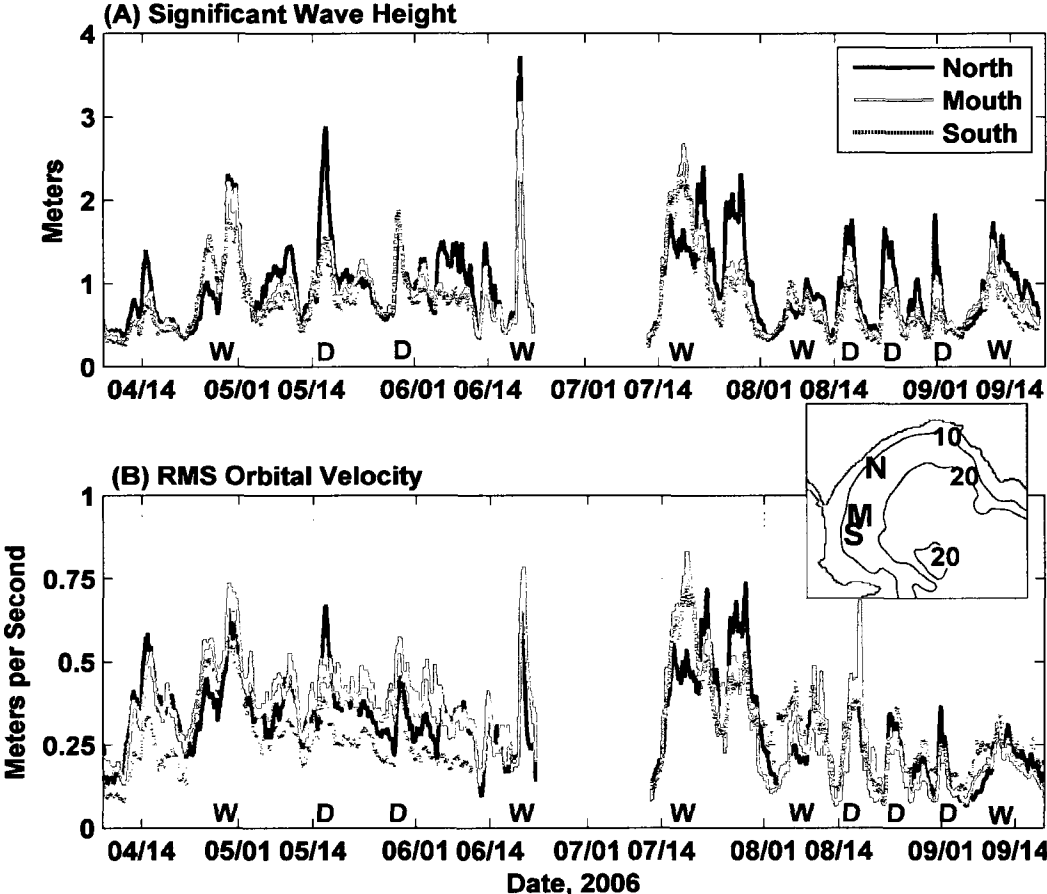
Figure 6. (A and B) Time-series of wave frequency spectra from the north S4. Labels mark times of wet storms (W), and dry storms characterized by remotely driven swell (D). (C) Spectra averaged over the three labeled wet storms and three labeled dry storms. W and D labels are above their respective storms, except the wet storm in the 2nd deployment, whose label is just to the right of the event and under the 2nd panel title. Wet storms correspond to 28 April – 3 May, 19-20 June, and 15-17 July, 2006. Dry storms correspond to 15-18 May, 16-17 August, and 10-13 September, 2006.
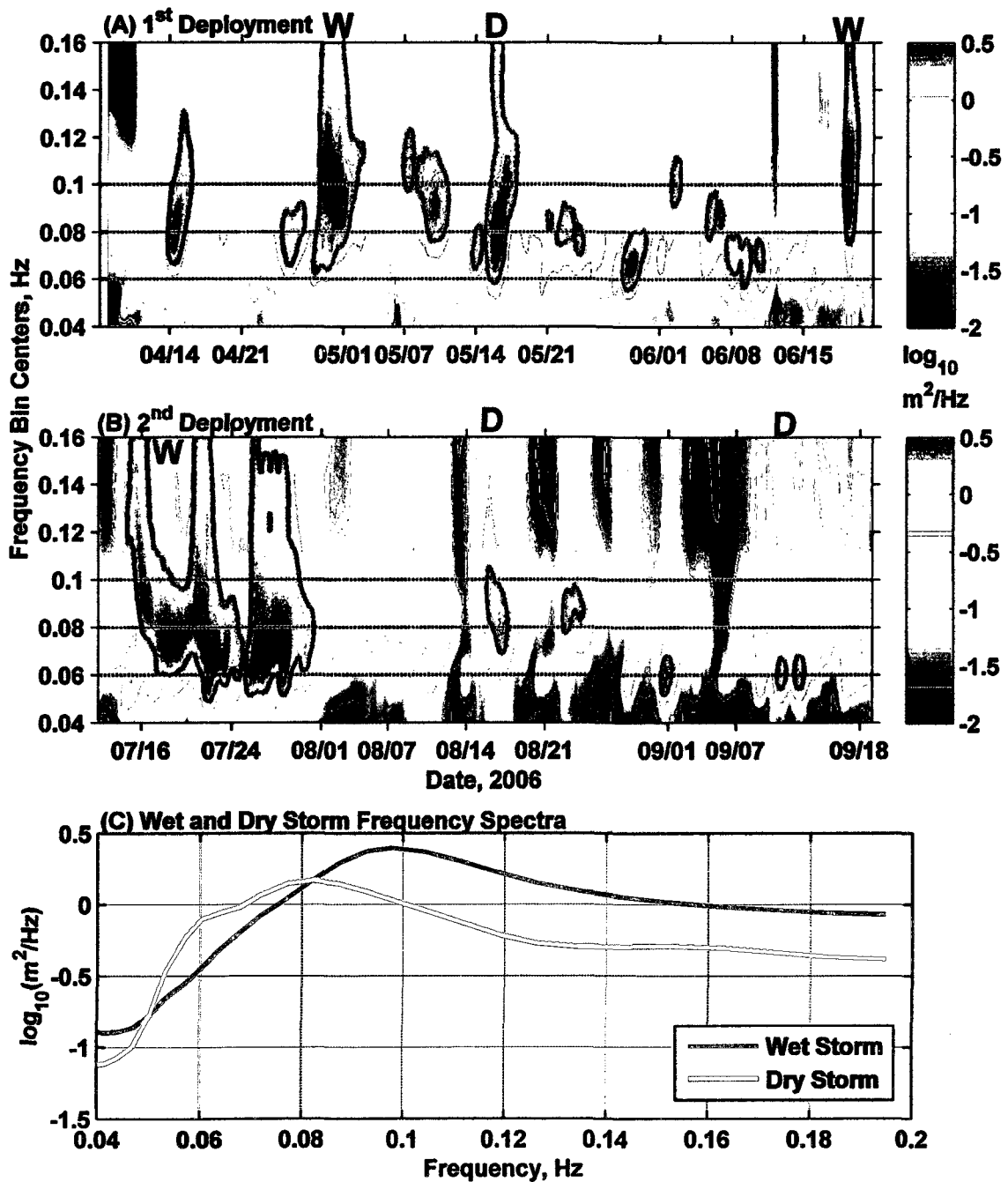
Figure 7. Wave frequency and directional spectra observed by the S4's, time-averaged over the deployments. Direction is the angle from which the waves came. Arrows identify the direction of wave propagation that had the most energy.
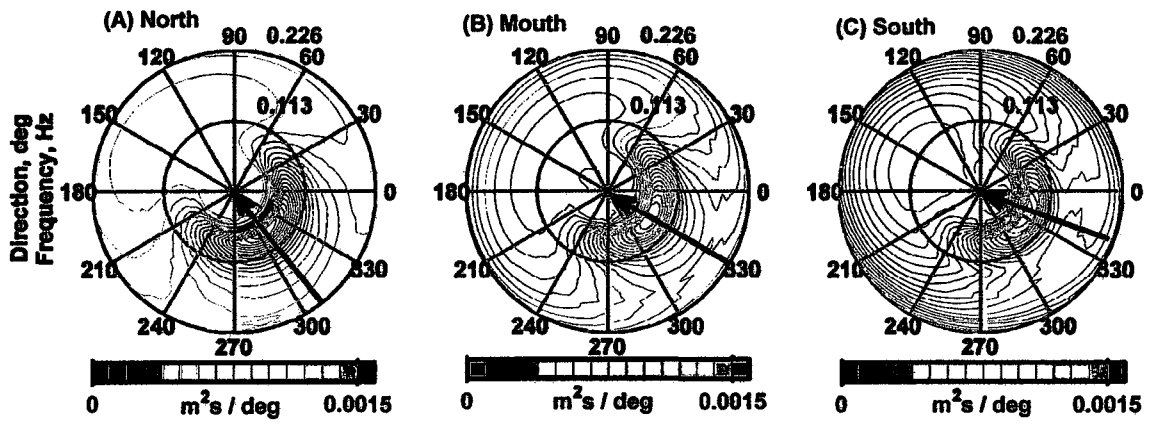
Figure 8. Progressive current velocity vectors calculated using observed velocities. Large triangles represent S4 locations, the open circle represents the ADCP location, and small triangles mark the gap in data during instrument redeployment. Progressive vectors are shown from the bottom-most ADCP bin (~2.5 mab, black line) and the upper-most ADCP bin (grey line). The progressive vector from the ADV deployed in mid-July is shown as a grey line beginning near the end of the ADCP near-bed progressive vector. Progressive vectors were not drawn to scale with the map, but the same scale was used for each instrument. "WR" identifies the Waipaoa River mouth.
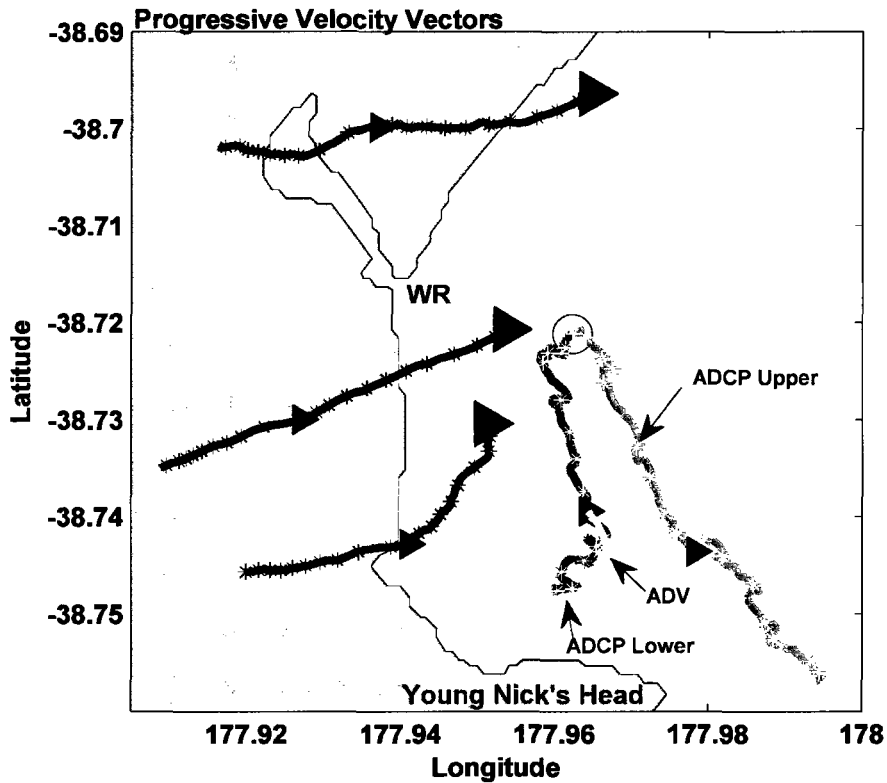
Figure 9. Current velocity (vectors) and speed (line) observed by the (A) north, (B) mouth, and (C) south S4s. Velocity vectors rotated to alongshore and seaward axes, with straight up being alongshore away from Young Nicks Head. Arrows in panel B show orientation of alongshore (A) and seaward (S) vectors. Shading identifies periods of increased river discharge (wet storms, W), wave events (dry storms, D), and wind events (WI) that are discussed in the text.
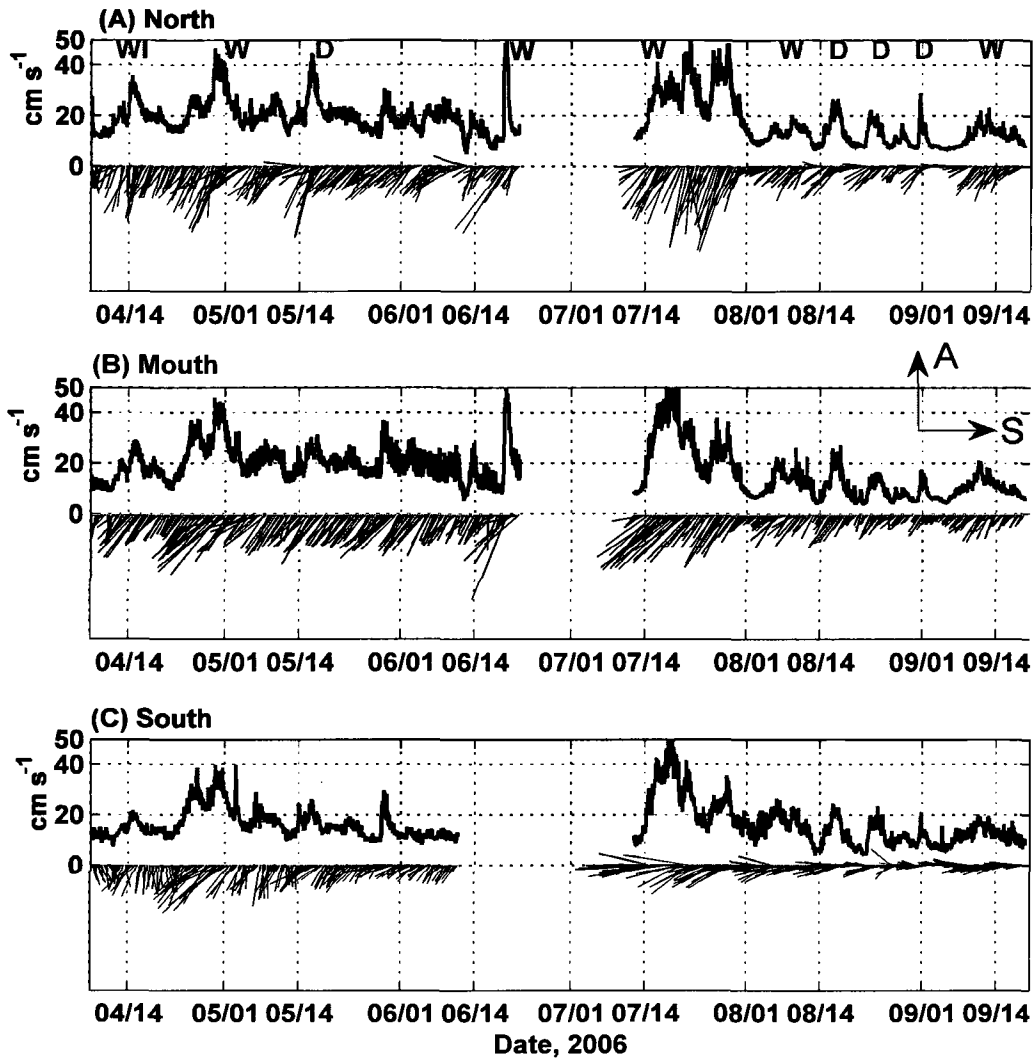
Figure 10. (A) Shoreward current speed measured by each S4. (B) Calculated Stokes drift velocity at each S4. (C) The fraction of the shoreward current speed measured by each S4 that is attributable to the calculated Stokes drift velocity. (D) Significant wave height.
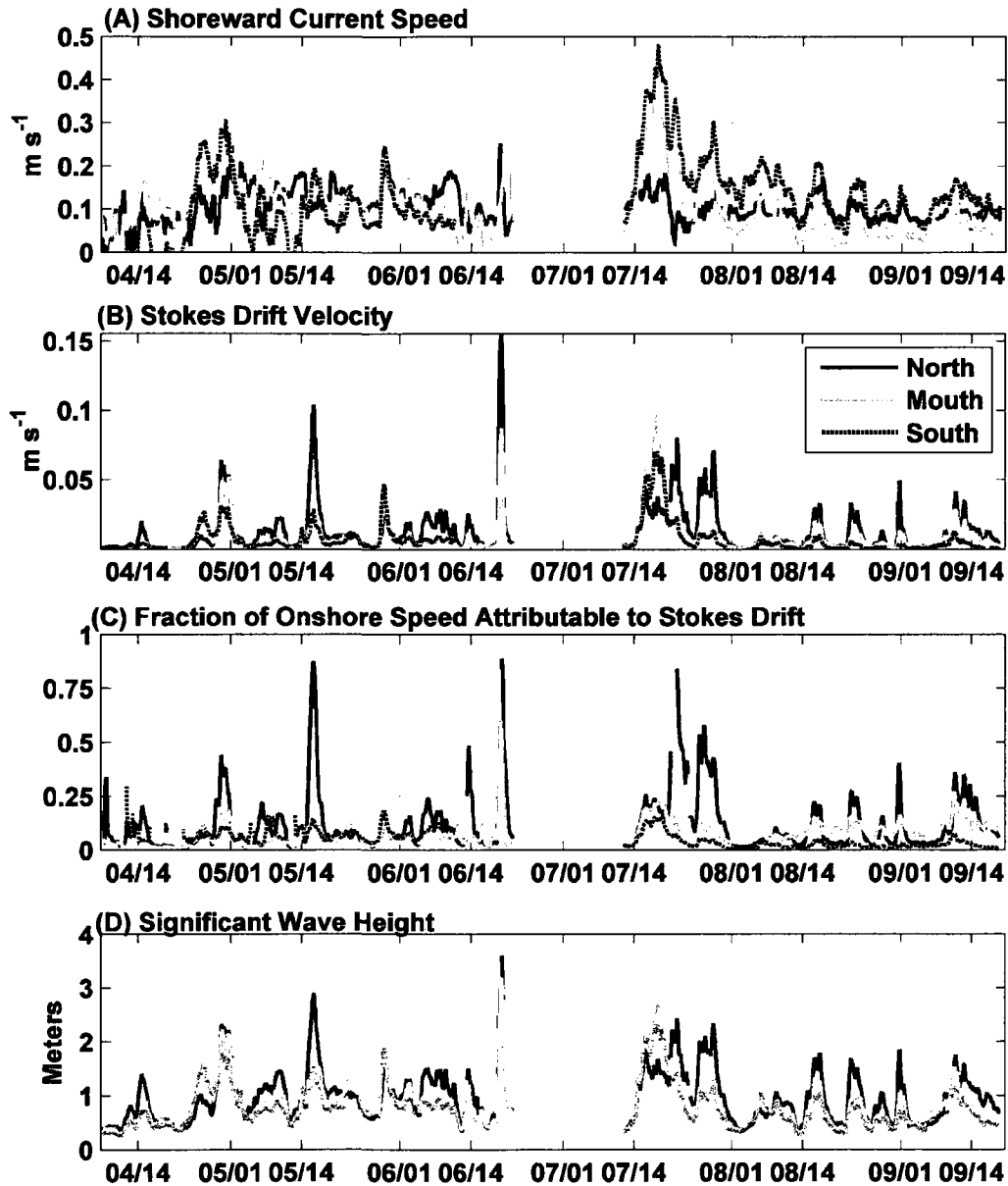
Figure 11. ADCP current velocity for the first (panels A and B) and second (panels C and D) deployments. Zero velocity is contoured in black. Seaward velocity (panels A and C) is positive toward the bay mouth. Alongshore velocity (panels B and D) is positive toward Tuaheni Point. Currents were lowpass filtered with a 25 hr cutoff frequency. Dark lines on the bottom of each plot identify times of elevated river discharge.
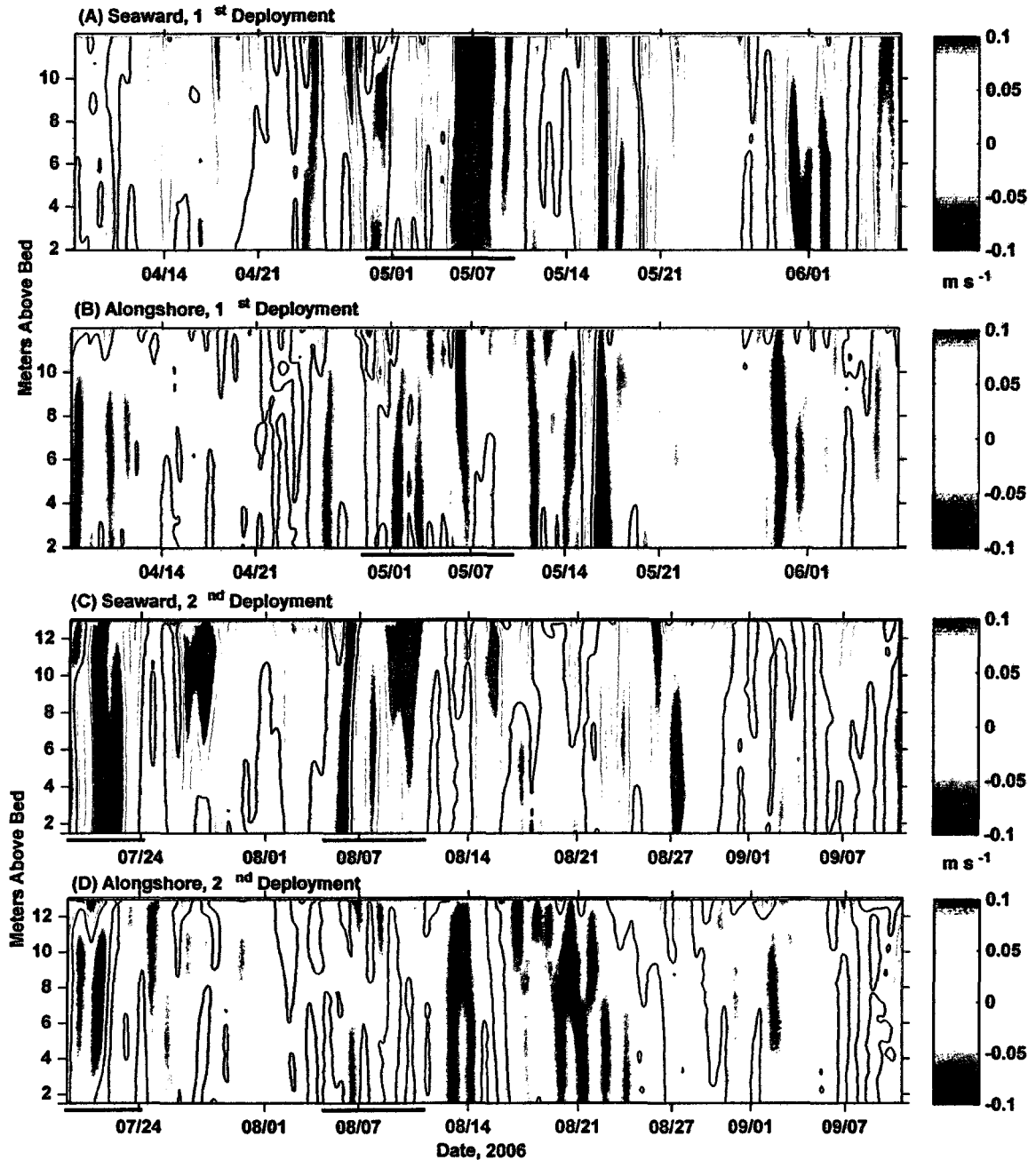
Figure 12. (A) Depth–averaged ADCP backscatter intensity, (B) Waipaoa River discharge, and (C) wave height measured by the S4 offshore of the river mouth. Gaps in (A) and (C) represent the time of instrument turnaround when data was unavailable.
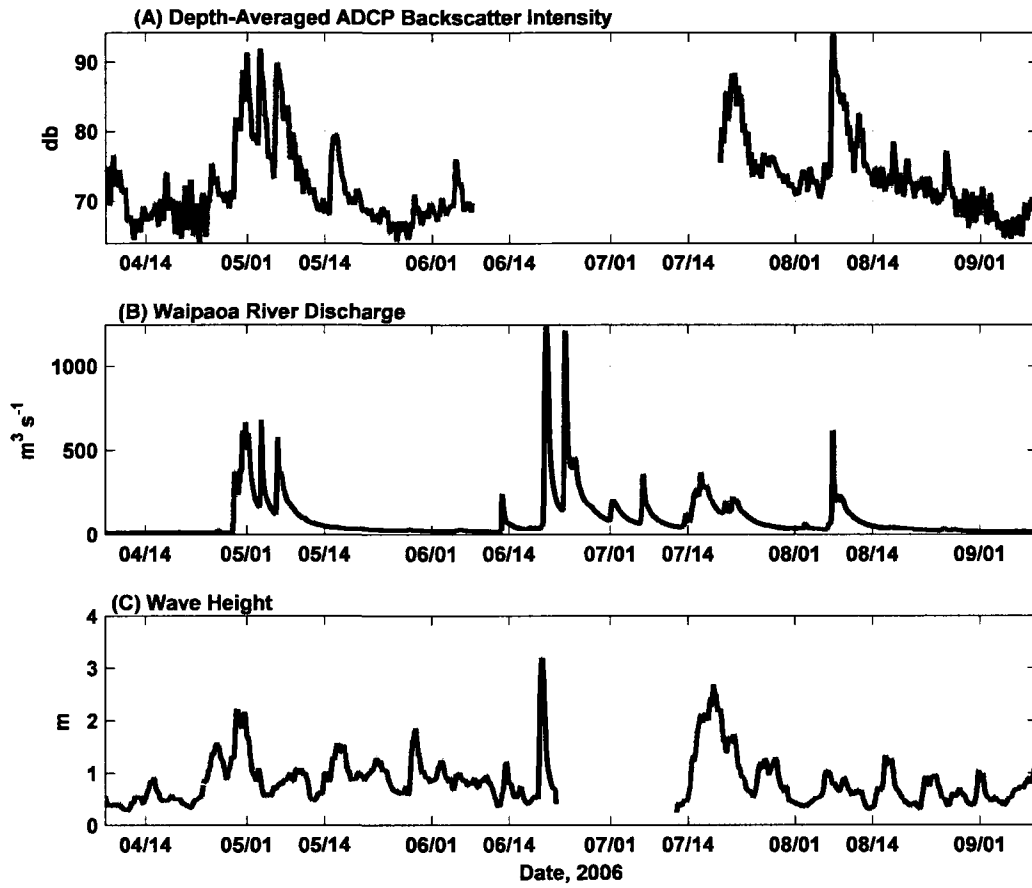
Figure 13. (A) Bed elevation measured by ADV altimetry (black) and wave height at the S4 offshore of the river mouth (grey). (B) Freshwater (black) and cumulative sediment (grey) discharges from the Waipaoa River.
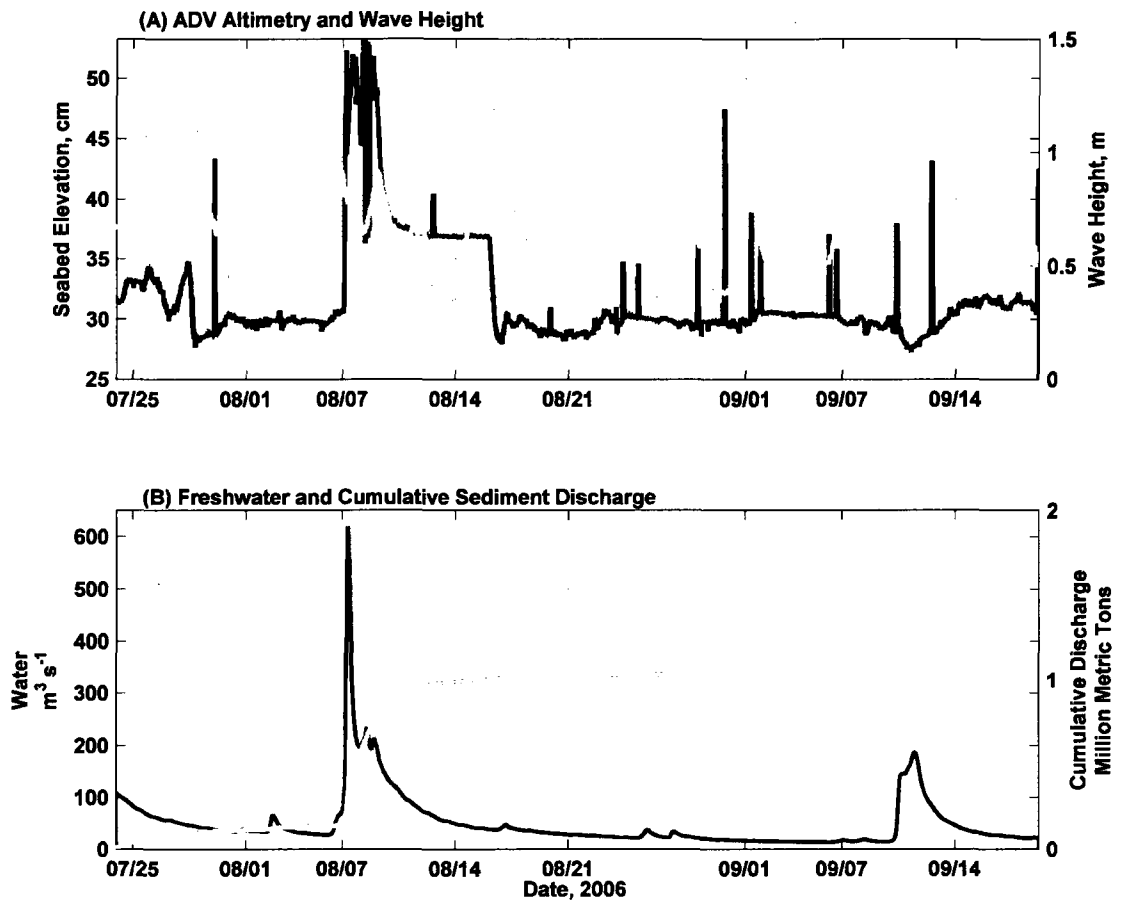
Figure 14. Nine hour running-means of estimated bedload flux for each of the S4 locations. Negative values represent shoreward values and alongshore flux toward Young Nick's Head.
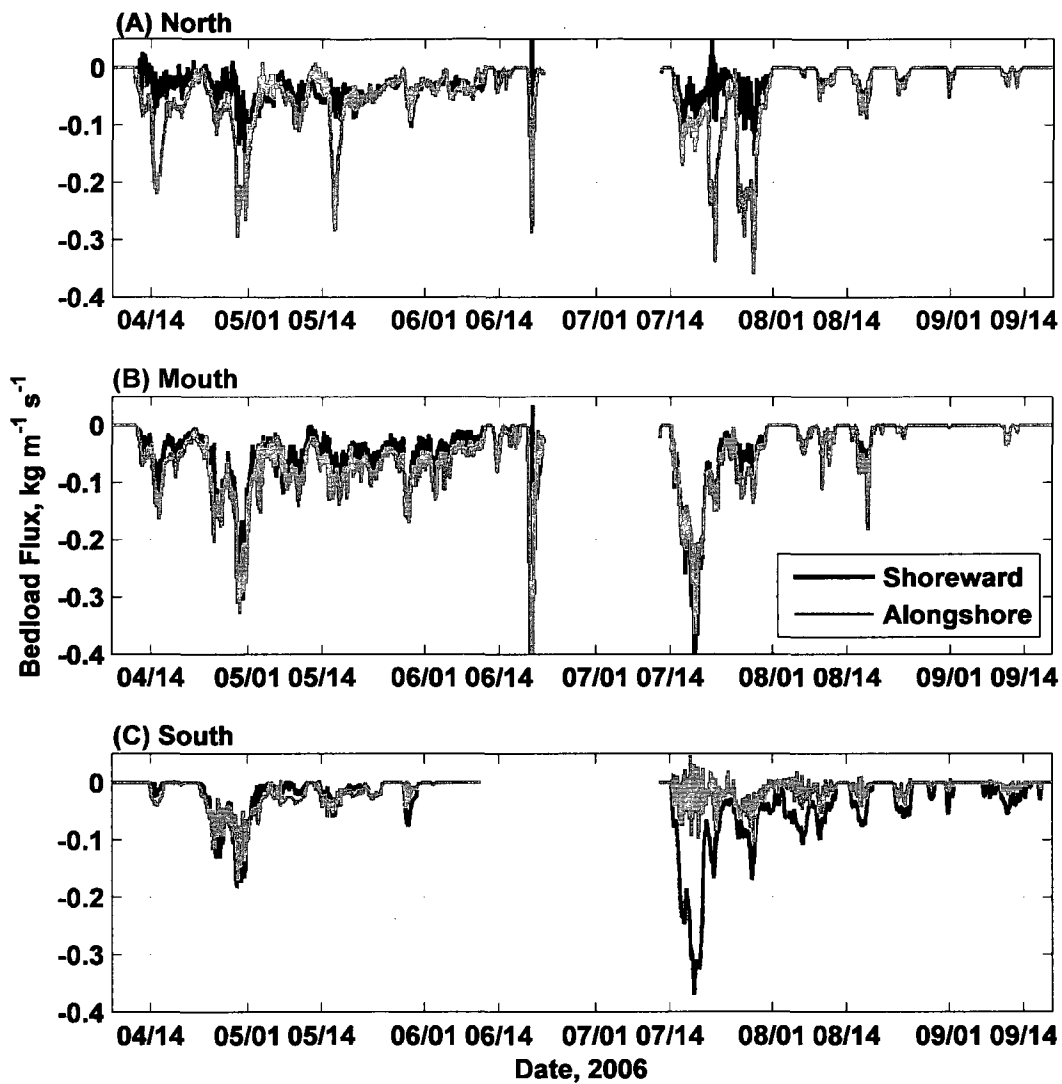
Figure 15. Data for the May discharge event. (A) Freshwater (black line) and cumulative sediment (grey line) discharge. Time of likely sediment deposition identified. (B) Wind speed (line, m s^{-1}) and velocity (vectors). Velocities were low-pass filtered using a 33 hour cutoff frequency and point in the direction toward which the winds were blowing with straight up being north. (C and D) Velocity measured by the ADCP. Positive values represent seaward currents (seaward component), and velocity away from Young Nicks Head (alongshore component). Currents were lowpass filtered using a 25 hr cutoff frequency and zero velocity is contoured in black. (E) Low-pass filtered sea surface height at each S4 using a 33 hour cutoff frequency, where zero represents the overall average for the deployment. (F) Surface salinity measured at each S4. (G) Nine hour running-mean of wave height measured at each S4.

Figure is on the next page.

(A) River Discharge

Freshwater m³ s⁻¹ / Sediment Discharge x10⁹ kg

Ephemeral Deposition Likely

(B) Wind

Speed, m s⁻¹ / Direction

Shoreward winds   Seaward Winds

(C) ADCP Seaward Velocity

Meters Above Bed

Strong Shoreward Currents   Strong Seaward Currents

(D) ADCP Alongshore Velocity

0.1

0

-0.1

m s⁻¹

(E) Sea Surface Height

Setup m

North

Mouth

South

(F) Surface Salinity

PSU

(G) Wave Height

Wave Height m

Wave Reduction

04/28   05/01   05/04   05/07

Date, 2006

Figure 16. Data for two dry storms. (A,D) Significant wave height, (B,E) seaward velocity measured by the ADCP, and (C,F) alongshore velocity measured by the ADCP. Positive alongshore velocity is away from Young Nick's Head toward the northeast. Currents were lowpass filtered with a 25 hr cutoff frequency and zero velocity is countered in black.
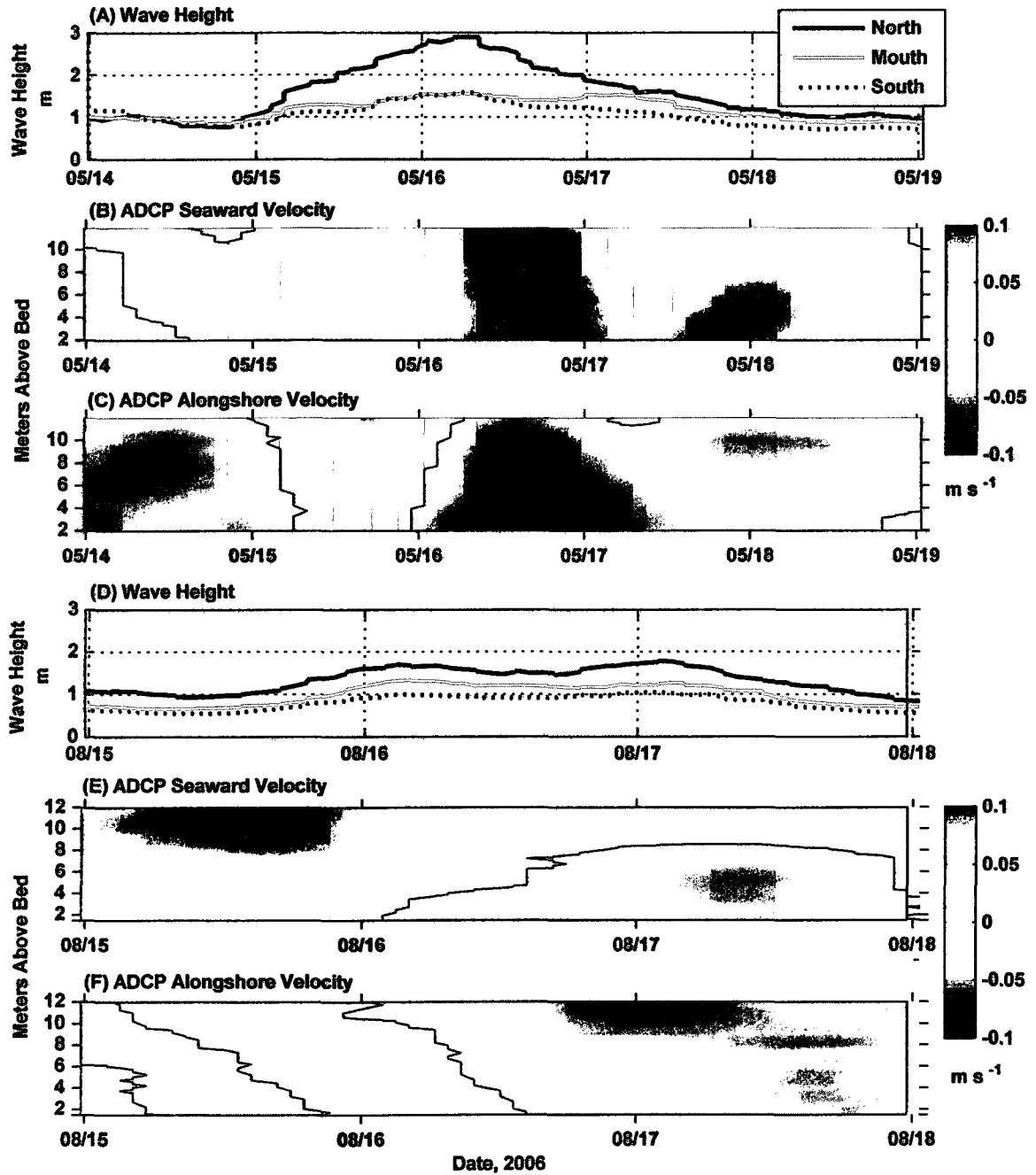
Appendix 2-A: OBS Turbidity

Each S4 was equipped with an Optical Backscatter Sensor (OBS). Data from much of the first deployment was discarded because the backscatter exceeded the instrumentation's capacity to measure it. Calibration of the OBS was not attempted because of the questionable nature of the data, and because during the second deployment the readings seemed dominated by non-local sediment, making choice of calibration material difficult. The backscatter records did clearly show, however, an increased turbidity event from elevated river discharge on 14-21 July before the readings lost resolution (Fig. A1).

During the second deployment, at each of the sensors, the measured backscatter rapidly increased about midway through the deployment when readings were saturated. This occurred progressively in a counter-clockwise direction, with the northern instrument's data increasing on 3 August, then the mouth OBS increasing nine days later on 12 August, and finally the southern OBS increasing on 17 August (Fig. A1). These signals were not attributed to due to fouling of the instruments, because both the mouth and southern S4s returned to measurable levels near the end of the deployment. Based on an online article, dredging began in Gisborne Harbor around 1 August (http://www.sandandgravel.com/news/article.asp?v1=9453), with the spoils dumped on the northeastern side of Poverty Bay (see Fig. A2). Fine dredge spoils may have traveled counterclockwise around Poverty Bay with the ambient currents and overloaded the sensors in a progression from the closest to the farthest sensor.

The signal did not appear in the ADCP backscatter. Acoustic backscatter is less sensitive to fine material than optical backscatter (Wall et al., 2006), so the lack of a

response in the ADCP record may indicate that the dredge spoils were very fine grained. Alternatively, the turbidity may have been confined to a more near-bed layer, as the bottom ADCP bin sampled about one meter higher than the OBS did. Alternatively, the dredge material may have been trapped within the shallower portion of the system, since the OBS were located in 9 m of water, while the ADCP was deployed in 15 m of water.

Using the time progression of the rapid peak in the OBS records, an alongshore drift velocity of ~3 mm s^{-1} along the 10 m isobath between the north and mouth S4s, and between the mouth and south S4s, was obtained. This is significantly lower than the averaged alongshore current speeds at the S4s of 7 to 13 cm s^{-1}, although the southwestward directions are consistent between the OBS drift estimates and the averaged S4 currents.

Reference

Wall, G.R., Nystrom, E.A. and Litten, S., 2006. Use of an ADCP to compute suspended-sediment discharge in the tidal Hudson River, New York, U.S. Geological Survey Scientific Investigations Report 2006-5055.

Figure A1. OBS Backscatter from the S4 locations during the second deployment. Data is plotted as a 3 hour running-mean.
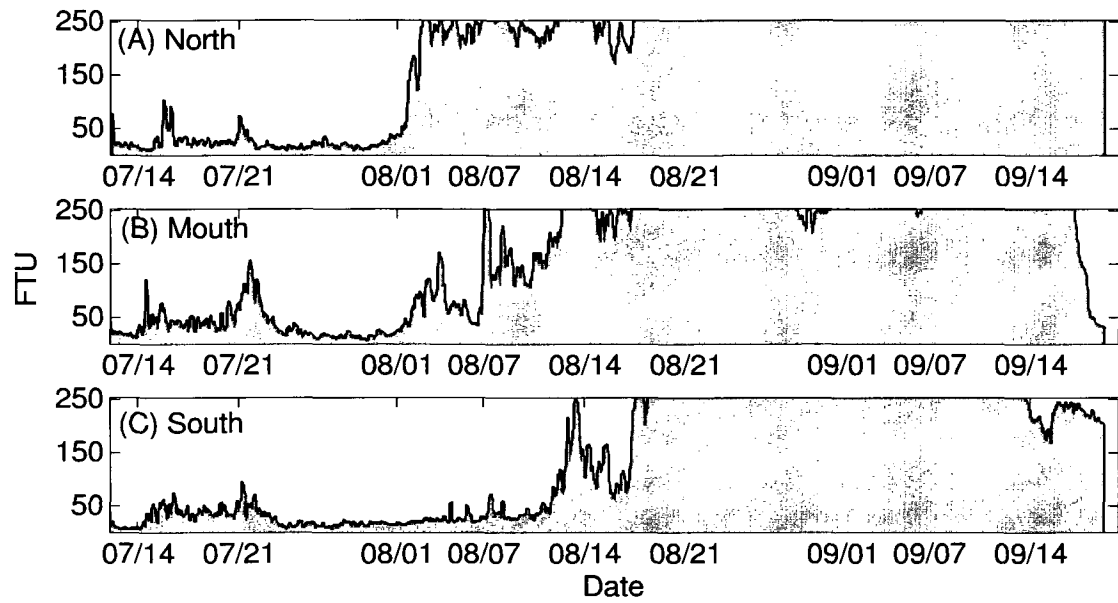
Figure A2. Location and smoothed bathymetry of Poverty Bay showing locations of the instruments, Gisborne, the Gisborne airport (A in right panel), approximate location of dredge spoil disposal (D in right panel), the Waipaoa River mouth (WR), Young Nick's Head, and Tuaheni Point.
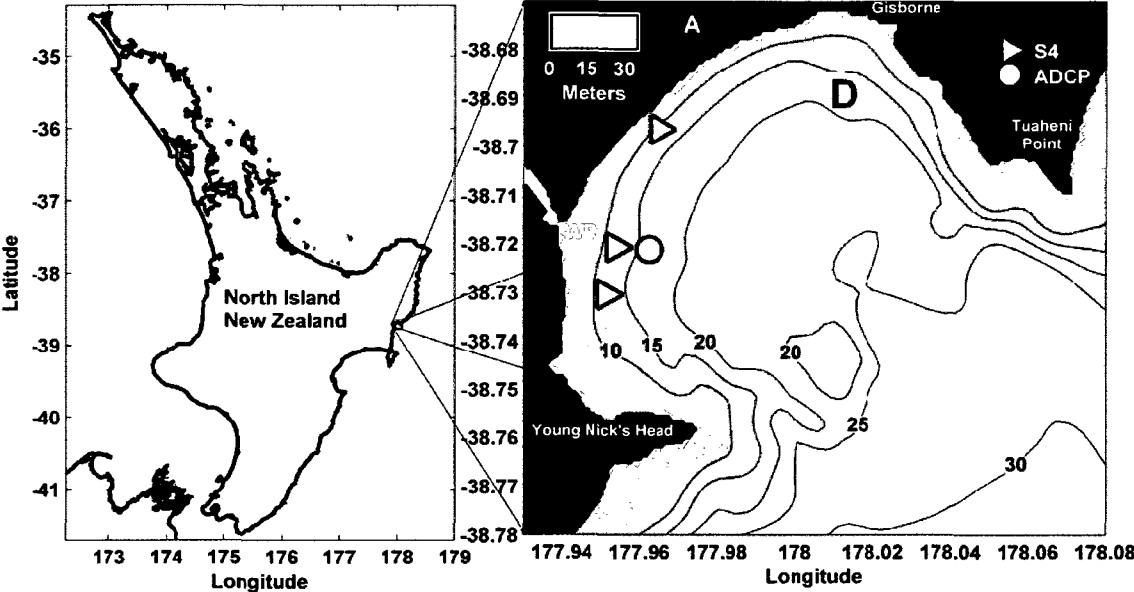
Appendix 2-B: Animated Visualization of Data

An animated visualization of the data (visualization_of_data.mpg) contained on the supplemental DVD illustrated the measured time-series of water column data and meteorological conditions collected during the first deployment, covering the dates 18 April through 30 May, 2006. Throughout much of the visualization, the average counterclockwise circulation and shoreward current flow is evident. Two portions of the visualization are particularly interesting. The discharge pulse that occurred from 28 April through 9 May, 2006 and was emphasized in Section 6.1 of Chapter 2 occurs about 30 seconds into the visualization. The resuspension event that followed on 15-18 May, 2006 and was driven by Southern Ocean swell can also be seen starting about ~1 min 19 s into the visualization. The list below describes how each component of the visualization was generated and illustrated.

- The **satellite photograph** in the background was taken of Poverty Bay, and shows the Waipaoa River, Gisborne, the Gisborne airport, and some of the flood plain (here covered by farmland). The satellite photograph was provided by World Wind®. Much of the data shown was located overtop the photograph in approximately the location where it was collected. Labels "E" and "D" were used to mark the approximate location of sewage effluent discharge and dredge spoil disposal from the town of Gisborne, respectively.

- **Time-stamp:** The date and time are provided in the upper right corner

- **River discharge:** A time-series of the freshwater discharge was provided in the top left corner of the visualization. A red star on this progresses with time. Discharge data was from the Kanakanaia Bridge about 48 km from the river mouth. River

discharge was also represented overtop of the Waipaoa River mouth by two arrows, one (brown) representing the maximum river discharge during the deployment, and another (blue) that scales with the river discharge for the specific time-stamp.

- **Winds:** Wind speed and direction were shown overtop the Gisborne airport by the green circle and arrow. The arrow points in the direction toward which the wind blew and scales with the wind speed, which is also provided in the text above the circle.

- **Instrument locations:** S4 currents, wave characteristics, ADCP currents, ADCP turbidity, instantaneous sea surface height, and low-pass filtered sea surface height were visualized. Red dots represent the S4 locations. The vertical profile of currents marked the ADCP location.

- **Currents:** Velocity measurements from the S4s and ADCP are provided. All currents on the visualization point in the direction the currents are flowing toward and scale with the current speed. Longer arrows are relatively faster currents, with the arrows comparable within each set of instruments (S4s and the ADCP), but the absolute lengths are not comparable between the two instruments. Red lines were used to represent the S4 measured currents. The light blue set of arrows represented a vertical profile of the ADCP currents, which were low-pass filtered with a 25 hour filter, removing some of the tidal signal to emphasize the dominant patterns.

- **Turbidity:** Turbidity from the ADCP was represented by the vertical color-scale to the right of the ADCP current profile, with red being high turbidity and dark blue low turbidity.

- **Waves:** Wave properties from the S4s shown included height and length calculated from the S4 data at each of the instruments, progressing from the southern to the

northern instrument as you go from the lower left to the upper right on the figure. The southern, mouth, and northern S4 instruments were represented by the green, blue, and red lines, respectively. The waves also lengthened with the calculated wave length.

- In the **sea surface height** panel, the larger set of markers represented instantaneous sea surface height, while the smaller ones showed the 33 hr low-pass filtered values. The marker color identified the S4 location in the same manner as the waves. Sea surface heights were plotted relative to a zero datum that represented the average water level for each sensor during the deployment.

Chapter 3: Storm and fair-weather driven sediment-transport within Poverty Bay, New Zealand, evaluated using coupled numerical models

ABSTRACT

The Waipaoa River Sedimentary System in New Zealand, encompassing both the terrestrial and marine components, was chosen as a focus site of the MARGINS Source-to-Sink program. Here, Poverty Bay acts as a filter between the fluvial and oceanic dispersal systems. This study used a three-dimensional hydrodynamic and sediment-transport numerical model, the Regional Ocean Modeling System (ROMS), coupled to the Simulated WAves Nearshore (SWAN) wave model to investigate the sediment-transport dynamics within Poverty Bay and the conduits for sediment routing from the Waipaoa River to the continental shelf.

Model calculations representing January-September, 2006 and a ~40 year recurrence interval storm from 21-23 October, 2005 showed that hydrodynamics and sediment-transport pathways within Poverty Bay differed during wet storms that included precipitation compared to dry storms driven by oceanic swell. The model accurately captured the average counterclockwise circulation seen in previous observational studies, and indicated that this circulation persisted during energetic storm conditions. During wet storms that included river runoff and locally driven waves, the model estimated significant sediment deposition within Poverty Bay, although around 75% of the discharged sediment was exported from the bay during the discharge pulse. Later

resuspension events generated by Southern Ocean swell reworked and modified the initial deposit, providing subsequent pulses of sediment delivery to the continental shelf. In this manner, the input fluvial signal was at times greatly modified as it transited the bay, so that the sediment characteristics and timing of export to the continental shelf differed from that supplied by the Waipaoa River.

Feedback mechanisms between sediment-transport, currents, and waves were important within the model calculations. For the October, 2005 flood, the model indicated that extremely high suspended-sediment concentrations influenced water density, creating gravity-driven transport and impacting current velocities. The modeled hydrodynamics were therefore sensitive to sediment characteristics, such as settling velocity and erosion rate parameter, for this event. Inclusion of wave-current coupling, such as radiation stresses and Stokes drift velocities, was also needed to accurately estimate current speeds.

1. Introduction

In coastal environments, many different physical processes and regional geologic features influence hydrodynamics, sediment-transport, and depositional patterns (Nittrouer et al., 2007 and references therein). Chapter 2 and Stephens et al. (2002) used limited observations to infer how interactions between freshwater discharge, winds, waves, tides, and shelf flows impacted hydrodynamics and sediment-transport within Poverty Bay, New Zealand. The spatial and temporal coverage of their instruments was, however, somewhat limited. To gain a more holistic understanding of sedimentary dispersal systems it is important to extend these physical observations in space and time (Kuehl et al., 2006). Detailed three-dimensional numerical modeling studies, such as those offshore of the Eel (Harris et al., 2005) and Po Rivers (Bever et al., 2009; Harris et al., 2008; Sherwood et al., 2004) and within Massachusetts Bay (Warner et al., 2008a) allow for a more spatially and temporally complete understanding of dispersal systems.

This study investigated the primary transport mechanisms within Poverty Bay for sediment discharged by the Waipaoa River using numerical models validated against field observations, to represent hydrodynamics and sediment-transport within Poverty Bay. The model calculations represented two periods; the winter season of 2006, and a 40 year recurrence interval flood that occurred in October, 2005. For these two time-periods, estimated waves, currents, and sediment-transport were analyzed for high river discharge events, and subsequent periods of energetic waves. Comparison between model estimates and available field data (from Chapter 2) shed light on the necessity for including wave driven currents in the hydrodynamic model. Model sensitivity to sediment characteristics and hyperpycnal discharges was also considered. To place the

study into a larger context, the Chapter also discusses how transit through Poverty Bay modifies the sedimentary signal from the Waipaoa River before it reaches the continental shelf, and compares this portion of the Waipaoa Sedimentary System (WSS) to other systems.

2. Background

This section introduces the processes that cause sediment-transport in continental shelf environments and within estuarine systems. Section 2.2 describes the study site, while Section 2.3 provides technical overviews of the numerical models used.

2.1 Sediment-Transport in Coastal Environments

On open continental shelves, waves, currents, and high-density gravity flows are the dominant mechanisms causing sediment resuspension and transport. The waves and currents interact to cause stresses on the seabed (see e.g. Madsen, 1994), with the wave induced stress generally dominating over those caused by the currents during times of sediment transport on many continental shelves (Drake and Cacchione, 1985). Resuspension occurs when the seabed shear stress exceeds that needed to suspend the sediment (Miller and Komar, 1973; Wiberg and Smith, 1987). Once suspended in the water column, sediment travels with the ambient currents, and is mixed upward by turbulence (Hill and McCave, 2001).

At times, suspended-sediment concentrations within near-bed bottom boundary layers can become high enough to impart significant density to the water (Wright and Friedrichs, 2006). This layer may then move down-slope under the force of gravity as a

high-density flow (Ogston et al., 2000; Sternberg et al., 1996; Traykovski et al., 2007). These high-density layers can be formed as sediment settles out of river plumes, or is resuspended, in regions of current convergence, or where waves or currents are strong and there is a large supply of easily erodible fine sediment. Seaward of the Amazon River, sediment is trapped in regions of current convergence, leading to hindered settling and the formation of thick fluid mud layers (Kineke and Sternberg, 1995). Suspended sediment concentration can exceed $10 \ g \ L^{-1}$ within 10 cm scale wave boundary layers offshore of the Eel (Ogston et al., 2000; Traykovski et al. 2000) and Po Rivers (Traykovski et al., 2007). Also, seaward of the Waiapu (Ma et al., 2010) and Huanghe (Wright et al., 1990) Rivers, periods of increased current speeds were shown to produce meter-thick high suspended sediment concentration layers.

Sediment discharged from rivers to the continental shelf can initially be supplied in one of two ways. In hypopycnal plumes, the discharged water and sediment mixture is less dense than the ambient ocean water and sediment is transported within the water column until it settles to the seabed (Wright, 1985). Even though satellite images often show large surface plumes, the particulate matter in the plume is usually a small fraction of the total sediment load (Milligan et al., 2007). Rather, most of the sediment discharged under hypopycnal conditions seems to quickly settle from the surface plume and is predominantly transported in the middle to lower water column (Geyer et al., 2000; Geyer et al., 2004; Milligan et al., 2007). In the second mode of sediment supply, hyperpycnal plumes, the density of the fluvial discharge exceeds that of the receiving ocean water and the river plunges below the oceanic water, carrying sediment with it along the seabed in a high-density layer (Hicks et al., 2004; Mulder et al., 2003).

In small river systems, such as the Waipaoa, sediment is generally supplied during elevated river discharge that coincides with storm conditions in the receiving basin, termed wet or oceanic storms (Wheatcroft, 2000). Subsequent periods of dry storms, periods of strong oceanic waves and/or currents but negligible river discharge, may resuspend sediment and transport it along the dispersal system (Guillen et al., 2006). Both these storm conditions have the ability to create high rates of sediment-transport, but freshwater and sediment is only directly supplied to the system during wet storms, potentially causing different system dynamics between the two types of storms.

The mixing of freshwater and saltwater within estuaries stratifies the water column, and baroclinic pressure gradients drive water flow into the estuary near the seabed while surface waters flow toward the mouth (Chatwin, 1976; Hetland and Geyer, 2004). Turbidity maxima often form at the landward extent of salt intrusion, where currents converge creating a sediment trap (Geyer, 1993; Lin and Kuo, 2001). Some of this material then settles to the seabed, leading to deposits on the seabed composed of unconsolidated fine sediment that is relatively easy to erode (Dickhudt et al., 2009; Woodruff et al., 2001).

2.2 Study Area: Poverty Bay

Poverty Bay is a small and open coastal embayment, located on the eastern coast of the North Island of New Zealand (Fig. 1). The 6 km long bay opens to the southern Pacific Ocean through a mouth that is ~8.5 km wide. Tectonics cause subsidence of the southwest and uplift of the northeast sides of the bay and coastal plain (Brown, 1995). The surrounding mountainous terrain is composed of easily erodible siltstone and

mudstone, leading to landsliding and gully erosion, and the consequently extremely high sediment yield, averaged to 6750 tonnes km^2 yr (Hicks et al., 2000; Reid and Page, 2002). As discussed below, the high sediment yield also reflects the anthropogenic deforestation that started about 650 years ago and significantly increased erosion rates (Reid and Page, 2002).

Averaged currents within Poverty Bay flow in a counterclockwise direction throughout the bay, and are predominantly driven by freshwater discharge from the Waipaoa River and local winds (Stephens et al., 2002). Observations indicate that a shoreward flow, enhanced by nonlinear wave effects, also occurs in the nearshore (Chapter 2). Poverty Bay is a microtidal environment, with peak tidal currents estimated to be around only 0.05 m s^{-1} (Stephens et al., 2002). Waves within Poverty Bay come from the southeast with average heights of 0.6 - 1 m (Smith, 1988), although they can reach upwards of 6 m during energetic storms (Healy et al., 2002). Elevated waves within Poverty Bay are caused by both local storms and Southern Ocean swell propagating into the bay. Observed during a typical winter (2006), waves during local wet storms were of shorter period and generally larger wave heights than those that propagated into the bay during dry storms (Chapter 2).

The local wet storms are generally driven by clockwise rotating atmospheric low pressure systems. These cyclones tend to originate to the northwest of New Zealand and travel southward or southeastward over the study site (Orpin et al., 2010). Storm winds, therefore, usually blow shoreward early in the storm, during which time wave height increases. Winds then rotate and become seaward as the storm passes, reducing wave heights (Chapter 2; Orpin et al., 2006).

The Waipaoa and Turanganui Rivers discharge water and sediment into Poverty Bay (see Fig. 1). Because the Waipaoa River delivers an order of magnitude more freshwater and sediment, the Turanganui River is generally neglected. The average freshwater discharge of the Waipaoa River is only 32 m^3 s^{-1}, with a background base flow of ~9 m^3 s^{-1}. Most of the freshwater and sediment is supplied to Poverty Bay during episodic periods of strong rains, caused by cyclonic storms moving through the drainage basin (Hicks et al., 2000; Orpin et al., 2006) (Fig. 2A-D). During storms, freshwater discharge can exceed the mean by two orders of magnitude; for example it was estimated to exceed 4000 m^3 s^{-1} for both Cyclone Bola in 1988 and the New Zealand Labor Day flood that occurred from 21-23 October, 2005.

Deforestation of New Zealand started with the colonization by Polynesians roughly 650 years before the present, and was greatly accelerated after the arrival of Europeans around 1870 (Reid and Page, 2002). Removal of nearly 85% of the indigenous forest after the arrival of European settlers increased sediment input to Poverty Bay by ~6.6 times (Kettner et al., 2007). The Waipaoa River now discharges about 15 million metric tonnes (15×10^9 kg, 15 MT) of sediment per year (Hicks et al., 2000). Suspended-sediment concentrations in the river may be high enough to generate hyperpycnal river flows, roughly 40 g L^{-1}, once every 40 years (Hicks et al., 2004; Kettner et al., 2007). The effective discharge, defined as the freshwater discharge at which the most sediment is discharged by the river, is 360 m^3 s^{-1}, an order of magnitude below the extreme event needed to initiate hyperpycnal flow and 0.26 times the yearly flood (1346 m^3 s^{-1}) (Hicks et al., 2000). The average grain diameter of sediment discharged by the Waipaoa River is 15 μm (6Φ), with silt representing 88% of the

suspended-sediment discharge (Hicks et al., 2004). Bedload is estimated at about 1% of the suspended load (Orpin et al., 2006).

Chapter 2 analyzed a time-series of water column and seabed measurements within Poverty Bay that covered a typical winter period. Seven to 25 cm of deposition occurred in 15 m water depth during a single moderate-sized elevated river discharge pulse. Following deposition, the newly deposited sediment was resuspended by swell waves propagating from the Southern Ocean, and then presumably removed from the nearshore as suspended load. Current and wave patterns within the bay were inferred to strongly influence observed seabed grain-size distributions. Sediment was generally sandier toward the northern part of the bay and landward of the ~10 m isobath, while the southern section of the bay was muddy (Foster and Carter, 1997), possibly because the Waipaoa River empties into the southern side of the bay, delivering mud that is then transported by predominantly counterclockwise currents. Previous observational studies failed to captured a large event, however, and lack sufficient spatial resolution to determine the sediment-transport pathways from the Waipaoa River mouth to the continental shelf. The numerical modeling study presented below addresses these knowledge gaps.

2.3 Coupled Hydrodynamic – Wave Models

Two numerical models, the Regional Ocean Modeling System (ROMS) and the Simulated WAves Nearshore (SWAN) model, were implemented to represent the Poverty Bay dispersal system. The ROMS is a hydrodynamic community model that offers many modules, including sediment-transport, biology, and sea ice components (see

www.myroms.org). The ROMS is a three-dimensional (3D), free-surface, hydrostatic, and finite-difference numerical model that uses orthogonal curvilinear horizontal grids and a stretched terrain following vertical grid (Haidvogel et al., 2008; Shchepetkin and McWilliams, 2005). The model solves the Reynolds averaged Navier Stokes equations, and provides a selection of several formulations for turbulence closure (Warner et al., 2005b), with the Generic Length Scale (GLS, Umlauf and Burchard, 2003) method being used previously in several hydrodynamic and sediment-transport modeling studies (e.g. Bever et al., 2009; Haas and Warner, 2009; Warner et al., 2005b).

Here, the ROMS routine used to numerically model sediment-transport within Poverty Bay is briefly described. See Warner et al. (2008c) for a more detailed explanation of the sediment-transport routines, which included calculations for sediment settling, resuspension by waves and currents, transport via currents, discharge from rivers, and incorporation of suspended-sediment concentration in the water density calculations. Multiple sediment grain classes were used, each with different hydrodynamic properties, such as settling velocity and critical shear stress. The ROMS accounted for armoring of the seabed with coarse sediment by keeping track of varying seabed sediment layers, each with different fractions of the sediment classes. An active layer thickness was imposed that scales with excess shear stress and the grain diameter of the sediment on the seabed, to limit erosion over a single time-step (Harris and Wiberg, 1997). Only sediment within this thin surface active layer, generally less than 5 mm thick, was available for resuspension during any one time-step. Sediment erosion rates from the surface active layer were calculated using the Partheniades equation (Partheniades, 1965). Sediment

deposition rates were calculated using the product of the suspended-sediment concentration in the bottom water column grid cell and the sediment settling velocity.

The SWAN model provided two-dimensional and time-dependent estimates of surface gravity waves, which were critical for calculating spatially and temporally varying bed stress and accounting for wave driven currents. SWAN is a third-generation wave model, formulated for use in regional applications and shallow water, that solves for the two-dimensional wave action density spectrum (Booij et al., 1999). Calculations account for the generation of waves by winds, nonlinear wave-wave interactions, wave refraction, wave dissipation by bottom friction, white capping, and depth-induced wave breaking. Coupling to a hydrodynamic model to include the influence of local currents on wave characteristics can also be performed (Delft University of Technology, 2007).

The ROMS and SWAN models were fully coupled using the Model Coupling Toolkit (MCT, Warner et al., 2008b), both to include nonlinear wave effects on current velocities within the ROMS and to improve the wave estimates in the presence of currents (Svendsen, 2006; Warner et al., 2008c). The SWAN model ran concurrently with the ROMS, and at specified time intervals provided to the hydrodynamic model these estimates: wave direction, wave height, wave length, surface and bottom wave period, wave dissipation, and the bottom orbital velocity. The ROMS then updated its wave characteristics, and used them to calculate radiation stress, Stokes drift velocity, and seabed shear stress. In return, the SWAN model received the bathymetry, sea surface height, depth-averaged horizontal currents, and bed roughness (z_0) from the hydrodynamic model. SWAN then updated the received variables and used them in the wave calculations.

3. Numerical Modeling Methods

This section details how the ROMS and SWAN models were applied to Poverty Bay and the adjacent continental shelf. It also explains the metric from Wilmott (1981) used for model skill assessment.

3.1 Numerical Model Implementation

ROMS version 3.2 was used to estimate hydrodynamic fields and sediment-transport for the Poverty Bay dispersal system. The model grid used 20 vertical layers and had a horizontal resolution of ~200 m within Poverty Bay, increasing to ~1000 m resolution at the grid cells farthest from Poverty Bay. The grid extended onto the continental shelf, to better represent tidal flows and wind-driven upwelling or down-welling in the embayment, and to limit the influence of the open boundaries on results within the bay (Fig. 1B). High resolution multibeam surveys provided bathymetry within Poverty Bay (Wadman and McNinch, 2009). Bathymetry on the continental shelf was provided by S. Stephens (National Institute of Water and Atmospheric research, NIWA).

Tides were specified based on the Oregon State Tidal Prediction Software (OTPS) TPXO7.1 global solution (Egbert et al., 1994; Egbert and Erofeeva, 2002), and included 11 constituents, specifically the m2, s2, n2, k2, k1, o1, p1, q1, mf, mm, and m4. Because tides were included, the open boundaries used Flather and Proctor (1983) and Chapman (1985) conditions for the two-dimensional momentum and free surface, respectively. The tracer and the 3D velocity open boundaries were specified using no-gradient and radiation conditions, respectively. The model was initialized with uniform temperature,

salinity, and current fields of 18.5°C, 35 PSU, and 0 m s^{-1}, respectively. The model

evolved from the initialization conditions using a 30 s time-step.

Two different meteorological conditions were modeled, the first representing

January through September, 2006, a period that overlapped with the field sampling

described in Chapter 2 and in Wadman and McNinch (2009). The Results section

examines the winter wet season of this nine month model run, roughly 15 April through 9

September, 2006, using January through mid-April as model spinup. A second model run

represented the 40 year recurrence interval flood that occurred from 21-23 October, 2005.

The simulation of the large flood began 1.5 months before the elevated discharge, to

allow the temperature, salinity, and current fields to equilibrate with the model forcing.

Hourly wind velocities, air temperature, air pressure, relative humidity, and rainfall rate,

recorded at the Gisborne Airport (see Fig. 1C) and archived by NIWA, were applied

uniformly across the entire model domain during both simulations

(http://cliflo.niwa.co.nz). Cloud cover and short wave radiation were specified as

monthly means from NIWA.

Freshwater from the Waipaoa River was specified based on hourly measurements

from the Kanakanaia Bridge, about 48 km upstream from the river mouth (Fig. 2A and B).

Suspended-sediment concentration of the river discharge was based on the rating curve of

Hicks et al. (2000) (Fig. 2C and D). The model run representing the winter season of

2006 included six events where discharge exceeded 360 m^3 s^{-1}. Swell wave events

occurred about once a week during this time-period (see section 4.1 and Fig. 3).

Four sediment size classes were used to represent fluvial sediment. Three were

near the mean grain diameter of the suspended sediment discharge of the Waipaoa River

(15 μm, Hicks et al. 2004), with each sediment class assumed to account for nearly equal proportions of the sediment discharge (Table 1). The finest size class had a higher discharge fraction, based on sensitivity tests comparing the model results to field observations. The fourth sediment class represented coarser sand, and accounted for about 1% of the suspended discharge, consistent with estimates from Orpin et al. (2006). Calculations within the model were much more sensitive to the hydrodynamic properties of the sediment classes than grain diameter. These were selected after sensitivity tests that compared model estimates to available observations. Based on the sensitivity tests, sediment settling velocity for each class was chosen to equal the Stokes settling velocity, while critical shear stress was based on Shields diagram (Shields, 1936) (Table 1).

Three additional sediment classes were used to specify a realistic initial sediment bed, based on grain size distributions from seabed samples within Poverty Bay by Wadman and McNinch (2009) and on the continental shelf by Rose (2008) (Table 1). Characteristics of the seabed sediment were specified to represent consolidated and flocculated fines (class 5), sand (class 6), and a coarse material (class 7). This coarse material was needed to account for regions of bedrock outcrops, and to armor the seabed in regions of significant wave induced sediment resuspension. This study focused on the dispersal of fluvial sediment, as such the Results and Discussion sections do not discuss this seabed sediment.

For the Partheniades equation (Partheniades, 1965), an erosion rate parameter of 5×10^{-4} kg m^{-2} s^{-1} for all sediment classes was set based on a comparison of the model estimates to the observations. This value was consistent with published literature

(Dickhudt, 2008; Stevens et al., 2007). Sediment density and porosity for all sediment classes were set to 2650 kg m^{-3} and 0.6, respectively.

The SWAN model, version 40.41AB, was run in non-stationary two-dimensional mode with a 10 minute time-step. The SWAN model was coupled to the ROMS every 20 minutes, as explained in section 2.3, using the same model grid, bathymetry, and wind forcing as the hydrodynamic model. Wave frequencies in the calculations were limited to being between 0.04 and 1 Hz. Boundary conditions from the Wave Watch 3 global model (Tolman et al., 2002) were used to specify the open-ocean swell wave height, period, and direction propagating into the bay. SWAN then converted these to wave spectra assuming a Jonswap spectrum with 20 degrees of spreading.

To better match Poverty Bay observations during calm times, the SWAN model estimates of significant wave height and bottom orbital velocity were modified. While SWAN estimated nearly zero meters significant wave height at times, the observations never showed completely calm conditions. During the same calm periods, the SWAN model also underestimated the bottom orbital velocity. These discrepancies could have been caused by the open boundary conditions not capturing small incoming waves during extremely calm periods, and/or by the limited fetch of the finite model domain. To improve model agreement during calm periods, a minimum significant wave height of 0.4 m was imposed. Likewise, a minimum value of 0.15 m s^{-1} was imposed for the orbital velocity for water depths equal to or shallower than 10 m. Linear wave theory was then used to project this orbital velocity to deeper water.

3.2 Model Skill Metric

Model skill was calculated using a skill metric presented by Wilmott (1981) that has been used previously to evaluate ROMS' skill at reproducing field observations by Warner et al. (2005a) and Haidvogel et al. (2008). This metric is calculated using:

$$S_W = 1 - \frac{\sum_{i=1}^{N} |X_{Mi} - X_{Oi}|^2}{\sum_{i=1}^{N} \left(|X_{Mi} - \overline{X_M}| + |X_{Oi} - \overline{X_O}| \right)^2} ; \tag{1}$$

where S_W is the model skill, X is the variable being compared, and $\overline{X}$ is its time-averaged value. Subscripts M and O represent modeled and observed values, respectively. Perfect agreement between the model and the observations yields a skill of one, and it decreases toward zero as the model diverges from the observations. Model skill at estimating wave height and orbital velocity, sea surface height, and current speeds were evaluated.

4. Results

The model results presented here show a very dynamic wave climate, counterclockwise circulation within Poverty Bay, sediment deposition within the bay during elevated discharge followed by resuspension and removal, and multiple sediment-transport pathways to the continental shelf. Section 4.1 covers the results of the wave modeling and shows the SWAN model accurately represented the observed wave properties. Sections 4.2, 4.3, and 4.4 present the results on temperature and salinity trends, hydrodynamics, and sediment-transport, respectively. Each section starts with a comparison of model results to observations, which, unless otherwise noted, are from

April through September, 2006 from Chapter 2. The Results and Discussion sections highlight the elevated discharge that occurred from 28 April through 9 May, 2006, and the subsequent swell driven resuspension event from 15-18 May, 2006, for both of which observational data was available. The April-May elevated discharge period was also near the effective discharge of the Waipaoa River. The 40 year recurrence interval storm that occurred from 21-23 October, 2005 is also discussed when results differed from those of the winter, 2006, simulation.

4.1 Wave Properties

The SWAN model with the specified formulation (Sections 2.3 and 3.1), produced values that skillfully matched the observed significant wave height and Root-Mean-Square (RMS) orbital velocity at three locations within Poverty Bay (Fig. 3, Table 2). The timing, duration, and magnitude of large waves were well represented by the model. The modeled waves accurately captured the spatial sheltering within the bay, estimating generally larger waves at the station in the middle of the bay with the smallest waves at the southwest location.

Complex bathymetry and wind forcing combined to produce temporally- and spatially-varying wave properties within Poverty Bay, as indicated by the SWAN model calculations. Time-averaged wave heights during fair-weather and storms showed similar spatial patterns, although, naturally, the storm waves were more energetic (Fig. 4). Wave sheltering caused by local bathymetry, headlands, and curvature of the bay reduced wave heights in the north and south of the bay compared to the center of the bay. Directly offshore of the Waipaoa River mouth, currents flowed in the opposite direction

of wave propagation, steepening and increasing wave heights there. During the October, 2005 flood, wave heights were moderate within Poverty Bay, reaching 2 to 3 m, and showed the same spatial pattern with the central bay having the largest waves.

Wave orbital velocity estimates followed the same pattern in Poverty Bay as the wave height, with the largest orbital velocities in the central bay. During the winter, 2006 simulation, wave orbital velocities exceeded a conservative estimate of that needed to resuspend fine sediment, 0.14 cm s^{-1} (see Sherwood et al., 1994), about 60% of the time at 30 m water depth seaward of Poverty Bay. This implied that, within Poverty Bay, waves during the winter of 2006 were frequently energetic enough to suspend muddy sediment.

4.2 Temperature and Salinity Trends

The model reproduced the timing and magnitude of seasonal trends in temperature and salinity within Poverty Bay. Water temperature showed a marked seasonal cooling as the study period spanned the southern hemisphere fall – to - winter transition (Fig. 5A). The model was about 2°C too warm at the beginning of the deployment, but then cooled to match the observations nearly exactly, with a correlation coefficient and bias of 0.84 and -0.07°C, respectively, for the second observational deployment (11 July - 9 September, 2006). The model also represented the water cooling between 12-28 May seen in the data. Salinity slowly decreased through the study period in both the observations and the model estimates, as the amount of freshwater discharge increased (Fig. 5B). Pulses of freshwater seen at the 10 m isobath were related to periods

of high river discharge, for example from 28 April through 9 May (Chapter 2), and at this location the model estimated similar decreases in salinity during these times (Fig. 5B).

4.3 Hydrodynamics

The model accurately represented sea surface elevation within Poverty Bay, with model skill (S_w, Eq. (1)) exceeding 0.96 at all three observed S4 locations (Table 3). Correlation coefficients at these sites exceeded 0.94, and the bias was negligible. The model represented well the tidal amplitude and phase based on pressure sensor measurements at the northern S4 (Fig. 6). The model performed as well as shown in Fig. 6 for all time-periods, as evidenced by Table 3. The lowpass filtered elevations were of much lower amplitude than the tidal motions, and the model did not represent them well. This is possibly because the finite size of the model domain precluded the inclusion of remote forcing that likely influence subtidal fluctuations in sea surface elevation.

The model reproduced the overall counterclockwise circulation along the 10 m isobath within Poverty Bay, consistent with previous observations including Stephens et al. (2002) and Chapter 2 (Fig. 7). The model skill (Sw) at representing the current speed improved from the northern to the southern 10 m location (Table 3). The modeled current speeds were weaker than those observed at the S4 locations, with a negative bias ranging from -0.05 to -0.11 m s^{-1} (Fig. 8, Table 3). Explanations for the underestimation of nearshore velocities include inaccuracies in both the turbulent mixing and the mixing of fresh and salt water, which may affect the baroclinic pressure gradients. These were difficult to evaluate with available data. Also, some inaccuracies in the model's nearshore velocities because of difficulties representing this area within a regional-scale

finite difference model were also anticipated. The model grid poorly reproduced the bathymetric gradients within the nearshore, because the 200 m horizontal resolution did not provide many grid points within the nearshore and because bathymetry was smoothed to improve model stability, as is frequently necessary within ocean models. The grid point sampled for this model-data comparison was actually in deeper water than the S4 instruments.

The average counterclockwise circulation within Poverty Bay was seen in model estimated surface currents for the study period (Fig. 7A). That is, nearshore currents were alongshore toward Young Nick's Head, while in deeper water they were directed toward the northern half of the bay or the bay mouth. During the river discharge pulses, this pattern intensified, with surface currents maintaining their counterclockwise recirculation within the inner half of Poverty Bay, and strong seaward flows through the bay mouth (Fig. 7 B and D). Depth-averaged currents, although not illustrated here, were oriented in a counterclockwise direction similar to the surface currents seen in Fig. 7A, B, and D. An exception to the counterclockwise circulation was seen during the 15-18 May resuspension event (Fig. 7C). At this time surface currents were weaker and less organized due to low river flow and weak winds, but generally flowed seaward. Generally, current speeds were highest near the river mouth and in the nearshore, due to the input of freshwater and the wave driven currents, respectively.

Near-bed velocities (Fig. 7 E, F, and G) did not show the counterclockwise circulation seen in the surface and depth-averaged currents, but flowed into Poverty Bay on the southern side while flowing seaward on the northern side of the bay.

The model estimated similar temporal and spatial patterns for the currents during each of the six wet storms that traveled through the system during the winter simulation. Fig. 9 uses the 28 April – 9 May, 2006 storm to illustrate system behavior during a typical wet storm. As the storms approached the study site, the winds blew shoreward. These shoreward winds forced the surface currents into the bay, creating a coastal trapped plume (Fig. 9A) and effectively retaining much of the freshwater and sediment within the bay. Near the time of peak discharge, the wind reversed direction, so that the plume was no longer trapped at the coast (Fig. 9B). Seaward winds then helped form a direct current transporting water and sediment from the Waipaoa River through the mouth of Poverty Bay to the continental shelf (Fig. 9C). This seaward current flow began within days of the beginning of elevated discharge for the modest discharge pulses observed in 2006.

The near-bed currents during the extreme October, 2005 storm were coherent with the surface currents. Both were strong and directed from the river mouth toward the deepest portion of Poverty Bay and onward to the continental shelf (Fig. 7 D and H). Model estimates indicated that gravity-driven forcing, enhanced by the extremely high suspended-sediment concentrations, was an important term in the momentum equation during this extremely large wet storm, as is explored in more detail in Section 5.2. The time progression of the currents during the extreme storm differed from that of the smaller events. The large freshwater input and sediment gravity-driven current overwhelmed the wind's ability to trap the river plume at the coast. Instead, a strong current flowed directly toward the mouth of Poverty Bay within hours of peak discharge. These patterns can be seen in the model visualizations on the supplementary DVD.

4.4 Sediment

The model reproduced the patterns in water column turbidity observed at the ADCP located in Poverty Bay at 15 m of water (see Fig. 10). Periods of high turbidity, in both the model results and the observations, coincided with times of elevated river discharge on 28 April through 9 May, 20-24 July, and 7-10 August. Following discharge, turbidity in the model results and the observations decreased. Turbidity was again elevated during periods of energetic waves that followed elevated discharge, such as those on 15-18 May and 16 August. Both the model and the data indicated that turbidity within the water column decreased to near a low background value within about three weeks following a discharge pulse (roughly 9-28 May and 10 August through 5 September).

The model also reproduced the timing and the approximate depositional and erosional thicknesses seen in 15 m water depth offshore of the Waipaoa River during elevated discharge and wave resuspension events (see Fig. 11). In the model and the observations, elevated river discharges from 20-24 July and 7-10 August both caused between 10 and 15 cm of sediment deposition at this location. Subsequent wave resuspension events on 26-29 June and 16 August completely removed these modeled and observed deposits. Over the course of the 1.5 months of deposition and erosion shown on Fig. 11, both the model results and the observations converged to a net deposition of about 2 cm. The model may not be capturing all the necessary processes to completely represent the data, however. This is highlighted from roughly 7-10 August, when a fluid-mud type layer occurred near the seabed in the data but was not reproduced within the model. The model lacks the vertical resolution to capture this small-scale (~15

cm) process. Because the model is not capturing the fluid-mud layer, it shows no sediment deposition until the currents and waves subside during 10 August. The reduction in current and wave strength allows sediment to now be deposited on the seabed, corresponding to a time when the observed fluid mud was consolidating into a more solid seabed.

Model results indicated that fluvial sediment was initially deposited during elevated discharge and then resuspended by subsequent wave events. At the end of both model runs, which represented the winter of 2006 and the extreme flood of October, 2005, little sediment accumulated shallower than the 10 meter isobath, and overall sediment deposits were thin, on the order of 1-10 cm (Fig. 12 A and D).

During elevated discharges in the model run representing the winter of 2006, sediment was generally deposited within the inner half of Poverty Bay, especially offshore of the Waipaoa River mouth. As an example, the thickest deposits during the April-May, 2006 discharge pulse were estimated to be 10-15 cm (Fig. 12B), with thickness increasing toward the southwest side of the bay and near the river mouth. Thick sediment deposits created during elevated discharge later underwent resuspension and export to the continental shelf during swell waves, with erosion of up to 7 cm from a single moderate swell event on 15-18 May (Fig. 12C). The cumulative deposition resulting from all of the discharge and resuspension events represented in the winter of 2006 model run showed that fluvial sediment was retained in water deeper than about 20 m, unlike what was seen directly after the April-May discharge pulse when fluvial deposits were seen in shallower water (Fig. 12 A and B). The largest two discharge events during the model run occurred in June, 2006. Both of these generated similar

depositional patterns and sediment thicknesses as shown in Fig. 12B for the April-May, 2006 event. In this manner the numerous wave resuspension events modified fluvial deposits and significantly influenced net deposition.

The model indicated that much of the sediment discharged by the Waipaoa River would be transported out of the bay over the event to seasonal time-scale, either within energetic flood currents (Fig. 7) or during subsequent swell wave resuspension events (Fig. 12C). Only 15% of the total 15.5 MT of discharged sediment was estimated to be retained within Poverty Bay at the end of the winter of 2006 model run (Fig. 13A), and only 19% was retained within 10 km of the river mouth. Furthermore, 57% of the discharged sediment exited the model domain during this seasonal time-frame, indicating dispersal beyond the proximal continental shelf.

Again, using the April-May, 2006 discharge pulse as an example, the model estimated that 73% of the 4.4 MT of sediment delivered by the river was exported to the continental shelf by the end of the event on May 9th. Another 13% of the sediment load was resuspended and removed from Poverty Bay during the wave swell event occurring on 15-18 May. These fractions of estimated deposition and remobilization are a significant part of the sediment budget, with only ~25% of the discharged sediment load accumulating on the continental shelf over roughly 100 year time-scales. The 4 consecutive swell events beginning in August exported a total of 0.25 MT of sediment from Poverty Bay, but each had a diminished impact on sediment export as the seabed grain size distributions coarsened due to the fluvially supplied fine sediment being winnowed by the energetic waves and currents.

Calculations of the fraction of each sediment class exported from Poverty Bay demonstrated that the grain size distributions of sediment exported from Poverty Bay differed during flooding, low-energy conditions (relatively small waves and weak currents), and times of swell resuspension. During the 28 April – 9 May discharge pulse the model estimated that size classes 1 and 2 accounted for 92% of the discharged sediment, while size class 3 contributed ~8%. Only trace amounts of size class 4 were exported from Poverty Bay during any time-period, so the focus is on classes 1 through 3. The exported sediment slightly coarsened during the small wave period between the discharge pulse and the 15-18 May resuspension event, and consisted of 53, 32, and 15% of size classes 1, 2, and 3, respectively, yet represented a minimal amount of sediment export. The exported sediment significantly coarsened during the 15-18 May resuspension event, with 16, 19, and 65% size classes 1, 2, and 3, respectively. The overall coarsening of the sediment exported from Poverty Bay following the discharge pulse occurred as the model removed the finer sediment classes from Poverty Bay, leaving the coarser sediment classes, which gradually began to dominate the sediment transport.

The depositional pattern estimated for the extreme October, 2005 flood differed from the April-May, 2006 event, with the sediment deposit aligned across the isobaths, not along the isobaths (Fig. 12D). During the extreme flood, 20-26 October, 2005, 87% of the 12 MT of discharged sediment was directly transported to the continental shelf during the storm and 41% was lost from the model domain. The extreme flood supplied sediment to the continental shelf much faster than the April-May discharge pulse, at average rates of .073 and .012 million MT hr^{-1}, respectively. During this storm the

fractions of each sediment class exported from Poverty Bay closely matched those

discharged by the river, at 42%, 32% and 26% size classes 1, 2, and 3, respectively.

Model estimates allowed us to distinguish sediment-transport pathways and

export from Poverty Bay during the three types of events studied: 1) moderate elevated

discharges having a recurrence interval of less than 1 year, 2) subsequent, post-

depositional reworking events triggered by wave resuspension, and 3) an extreme flood.

During the modest discharge pulses, some sediment exited Poverty Bay in the surface

water with the river plume, while a near-bed population was exported that had settled

from the plume but remained suspended (Fig. 14A). During this time, depth-integrated

sediment-transport showed an imprint of both the surface and the near-bed currents, with

sediment generally exiting Poverty Bay toward its northern side (Figs. 7A and F and

14A). The second type of event occurred during periods of remotely generated energetic

waves that caused sediment resuspension. These had enhanced near-bed sediment-

transport with minimal flux at the surface (Fig. 14B). During the wave resuspension

events, depth-integrated sediment-transport rates were more uniform throughout the bay

than during wet storms, with sediment generally exiting Poverty Bay toward the northern

side of the bay where the bottom waters flowed seaward to the continental shelf (Figs.

14B and 15B). Gravity-driven transport influenced the sediment-transport pathway

during the extreme flood of October, 2005. Instead of forming distinct surface and

benthic plumes sediment exited Poverty Bay in a rather vertically mixed water column

(Fig. 14C). At this time, large amounts of sediment followed a relatively a straight path

to the continental shelf (Fig. 15C).

5.0 Discussion

In this section, model results were interpreted to examine the role of Poverty Bay within the WSS. Sections 5.1 and 5.2 explore model sensitivity to sediment characteristics, and evaluate the need to include suspended sediment in the model's calculation of water density. Section 5.3 demonstrates the need to fully couple the hydrodynamic and wave models within Poverty Bay. Lagrangian tracers in the model were used to infer general transport patterns within Poverty Bay in Section 5.4. Modification of the terrestrial sedimentary signal during passage through Poverty Bay is examined in Section 5.5. Finally, sediment deposition within Poverty Bay is compared to dispersal offshore of other small mountainous river systems.

5.1 Model Sensitivity to the Erosion Rate Parameter

The choice of sediment characteristics, such as the erosion rate parameter, settling velocity, and critical shear stress, influenced model estimates of the relative importance of sediment transport during elevated discharge compared to during later resuspension. Uncertainties in these sediment parameters propagate into model estimates of the timing and nature of sediment export from the bay. For example, measured values for the erosion rate parameter of sediment vary over roughly three orders of magnitude, from about 1×10^{-6} to 1×10^{-3} kg m^{-2} s^{-1} (Dickhudt, 2008; Sanford, 2006; Stevens et al., 2007). Within the numerical modeling literature, erosion rate parameters also cover a wide range; 5×10^{-5} kg m^{-2} s^{-1} in Bever et al. (2009) and Harris et al. (2008), 1×10^{-4} kg m^{-2} s^{-1} in Wang and Pinardi (2002) and on the order of 1×10^{-3} kg m^{-2} s^{-1} in Rinehimer et al. (2008). Here, sediment parameters were chosen to provide estimates that agreed with the observations

of sediment deposition and erosion within Poverty Bay, with an erosion rate parameter of 5×10^{-4} kg m^{-2} s^{-1} used (Fig. 11). Using a smaller erosion rate parameter of 5×10^{-5} kg m^{-2} s^{-1} increased the modeled sediment retention within Poverty Bay, resulting in a depositional thickness at 15 m water depth offshore of the Waipaoa River of 24 cm, compared to the 2 cm shown on Fig. 11. It also enhanced the relative proportion of flood driven export compared to swell driven export, because sediment could not be resuspended as vigorously during swell events. This sensitivity to a single sediment parameter indicates the need for accurate sediment-transport data for model calibration.

5.2 Hyperpycnal Forcing

Under conditions of hyperpycnal river discharge, high suspended-sediment concentrations increase fluid density, thereby impacting the density structure of the water column and the current velocities. The net effect of the increased water density due to the suspended sediments was to more quickly export sediment to the continental shelf. Suspended-sediment concentrations exceeding 1 g L^{-1}, were estimated throughout Poverty Bay during the ~1 year recurrence interval discharge pulses that occurred in the winter of 2006, while water column concentrations exceeded 10 g L^{-1} during the extreme storm of October, 2005. Under such high suspended-sediment concentrations the density imparted to the water-sediment mixture by suspended sediment should be included in the equation of state.

To investigate the importance of gravity-driven transport within Poverty Bay, the large October, 2005 event was modeled again, this time neglecting the suspended-

sediment contribution to water density. Results from these calculations were compared to the baseline model that included sediment within the equation of state.

Neglect of sediment density caused large changes in the estimated near-bed currents, sediment deposition, and sediment-transport pathways (Fig. 16). Sediment deposition within Poverty Bay during the extreme flood of October, 2005 increased by 17% of the river discharge, 2.2 MT, compared to the baseline run in which sediment concentration influenced water density. Neglecting sediment from the equation of state decreased estimated near-bed current speeds by factors of 2 to 15. Comparison of model results indicated that the coherent current from the river mouth to the deepest portion of Poverty Bay estimated for the baseline model run (Fig. 7H) was strengthened by gravity driven flow, because it was not apparent when the model neglected the sediment contribution to density (Fig. 16).

5.3 Importance of Hydrodynamic and Wave Model Coupling

To evaluate the importance of coupling between the waves and currents, a baseline model run where ROMS and SWAN were fully coupled was compared to a second run where SWAN derived wave properties were used as input to ROMS, but nonlinear wave effects and the currents influence on the wave fields were neglected.

When currents and waves oppose each other the waves are steepened, increasing the significant wave height compared to slack current conditions. Within Poverty Bay, including the model coupling and the currents influence on the waves did not significantly alter the model estimates of wave characteristics or seabed shear stress. Results indicated that wave height time-averaged over the winter simulation only

increased by about 8 cm throughout Poverty Bay in the fully coupled framework, compared to the model run that neglected wave-current interactions. Wave characteristics were most sensitive to the coupling offshore of the Waipaoa River mouth, where currents and waves nearly always opposed one another. Offshore of the Waipaoa River mouth, time-averaged wave heights increased by about 20 cm in the fully coupled model run, compared to the uncoupled run.

When waves shoal they can generate currents due to Stokes drift and radiation stress gradients, as was seen in Chapter 2. Because of these wave driven currents, the model estimated current speeds were significantly different in the coupled compared to the uncoupled model runs, with model skill in the fully coupled system generally higher than when the models were run independently (Fig. 8, Table 3). When the waves and hydrodynamics were calculated independently of one another, the model underestimated current speed along the 10 m isobath of Poverty Bay by a factor of about 2 to 8 (Fig. 8), and the bias in the model results was greater (Table 3). That is, modeled current speeds that neglected wave effects were much slower than the observed values. This highlighted the importance of including the physics behind wave driven currents in three-dimensional models of shallow water systems with significant wave action.

5.4 Averaged Dispersal Patterns within Poverty Bay

Lagrangian tracers were added to the surface and bottom layers of the model every two days at five locations within Poverty Bay. These tracers allowed for the examination of dispersal from locations such as Gisborne Harbor and to estimate the residence time of water in Poverty Bay for both the winter, 2006 and October, 2005

110

model runs. Once initialized, diffusion was neglected and the neutrally buoyant tracers followed the current velocities, travelling horizontally and vertically throughout the model domain. As such, the tracers were not confined to the surface and bottom layers in which they were introduced. The tracers followed distinct paths during fair-weather and stormy conditions, indicating the sensitivity of dispersal within Poverty Bay to meteorological conditions.

Trajectories of floats released from 3 January through 18 April, 2006 were analyzed, a time-period generally characterized as fair-weather. During this time, the surface and bottom tracers traveled, on average ~5 and ~3 km, respectively, from their initialization locations within two days, with directions trending out of Poverty Bay and away from Gisborne (Fig. 17A). The surface floats traveled further and more quickly compared to those initialized in the bottom grid cell, being advected by the faster surface water velocities that were more influenced by winds and less by bed friction than the bottom currents.

Trajectories of the floats during storm periods fluctuated in response to the evolving wind fields seen during a typical storm. As seen for the example during 28-30 April, 2006, the beginning of an elevated discharge event, when the winds blew shoreward and river discharge increased, the surface and bottom floats were ~5 and ~5.5 km away from their initialization locations after 2 days, respectively. During shoreward directed winds at the beginning of elevated discharge, the surface floats moved shoreward with the currents (see Fig. 9A) and spent much of their time in the nearshore (Fig. 17B). Meanwhile, the bottom floats followed near-bed currents in the northern Poverty Bay toward the bay mouth (Fig. 7), and were generally exported to the

continental shelf on the northern side of the bay (Fig. 17B). During the extreme event of October, 2005, the floats exited Poverty Bay and traveled farther than during the other meteorological conditions, but followed much more erratic paths.

Based on the seaward direction of bottom current flow in the northeast of Poverty Bay (Fig. 7) and the paths taken by Lagrangian floats within the bay (Fig. 17), a residence time of about 2 days was estimated for bottom waters originating in this area. This estimate was influenced by the model calculations of near-bed currents in the inner Poverty Bay, but, based on comparison to field data the model underestimated these. Residence times of bottom water were therefore also likely underestimated, although the general conclusion that the trajectory was of alongshore toward the southwest away from Gisborne remains valid.

5.5 Fluvial Sedimentary Signal Modification

Here, the term sedimentary signal encompasses the timing of sediment flux to different portions of the dispersal system, the magnitude of that flux, and sediment characteristics such as grain size or geochemical signature. Transit through the relatively small Poverty Bay modified the sedimentary signal as it traveled from the Waipaoa River to sedimentary sinks in the marine environment. Model results indicated that elevated river discharges lasting only a few days created deposits that remained within Poverty Bay for three to four weeks (Figs. 10, 11, and 12), an interpretation supported by observations from Chapter 2. The model also indicated that grain size distributions supplied to the shelf evolved with repeated wave remobilization following elevated river discharge, and responded to the oceanographic conditions present. As such, the

sedimentary signal supplied to the shelf differed from the fluvial source signal and varied over space and time. Orpin et al. (2010, Fig. 11) also showed the modification of sedimentary signals progressing from a confined lake out to the lower continental slope on the east coast of the north island of New Zealand, through an examination of down core magnetic susceptibility measurements dating from the present to ~7000 years ago.

During elevated discharges relatively poorly sorted fluvial sediment was supplied to the continental shelf; for example, the model estimated that approximately equal proportions of sediment classes 1-3 were exported from Poverty Bay during the large storm. During low wave energy periods that followed elevated discharge, the grain size supplied to the continental shelf was modified because the waves and currents were generally weaker and the bay became winnowed of the finest sediment class. Swell waves created seabed shear stresses sufficient to mobilize the relatively coarser sediment, creating a supply of this coarse sediment to the continental shelf. The sediment export to the continental shelf then evolved through repeated swell events that occurred in the absence of river discharge, such as those occurring in late August and Early September, 2006. As each event winnowed the seabed of available muddy sediment, subsequent events carried decreasing sediment loads to the continental shelf (Fig. 13B).

The magnitude of the discharge pulse also had implications for the degree to which transit through the bay modified the sedimentary signal. For example, the October, 2005 storm not only supplied 2.75 times more sediment to the system than the 28 April – 9 May, 2006 discharge event, 12 MT compared to 4.4 MT, but also immediately exported a larger percentage of that sediment to the continental shelf, 87% compared to 73%. Also, the model estimates indicated that the average rate of sediment export to the continental

shelf during the October, 2005 flood exceeded the export rate of the smaller April–May, 2006 discharge pulse by about a factor of six (0.073 MT hr^{-1} compared to 0.012 MT hr^{-1}, respectively). As such, there was a much larger coherent pulse of sediment through Poverty Bay from the river mouth to the continental shelf during the extreme flood than during the ~1 year recurrence interval discharge pulses. The speed of sediment export to the shelf under this extreme event may limit the amount of time other mechanisms, such as swell wave resuspension or biological reworking, can operate on the sediment before it is incorporated into shelf deposits. The lack of transformation of the sedimentary signal within Poverty Bay during the large event was evidenced by the fractions of modeled sediment classes exported to the continental shelf being nearly equal to that supplied by the Waipaoa River.

Within each of the winter and extreme storm model scenarios, the Waipaoa River discharged a similar amount of sediment, 12 MT for the extreme October, 2005 event and 15.5 MT for the winter of 2006 simulation, but the mode of delivery influenced the sedimentary signals to the continental shelf. The sediment input from the yearly simulation occurred over about a five month time-frame, and was strongly influenced by repeated sediment deposition followed by wave resuspension and suspended transport (Figs. 11,12, and 13). The time spent in the shallow marine environment and repeated episodes of resuspension and transport imprinted a marine signature on fluvial sediment delivered during low magnitude discharge pulses. In contrast, the model indicated that 10.8 MT of sediment was directly supplied to the continental shelf within a few days during the extreme 2005 flood. The sedimentary characteristics of this material likely retained their fluvial signature. It therefore seems more likely that the extreme October,

2005 storm created a distinct and identifiable flood layer on the shelf than the discharge pulses that occurred from April-September, 2006, even though both scenarios discharged about the same amount of sediment.

The greater sediment discharge from numerous smaller events than the one large storm is a similar scenario to the decade-long average, where the most sediment is supplied to the marine system during relatively small (~360 m^3 s^{-1}) high-frequency discharge pulses (Hicks et al., 2000). This implies that the sediment on the adjacent continental shelf is likely to be composed of material supplied during small to moderate discharge pulses, and subject to repeated episodes of wave resuspension and redistribution.

Because the currents and sediment-transport differed during wet and dry storms (Figs. 7 and 15), sediment export during them could contribute to different depocenters and may deliver sediment with different characteristics to the shelf. Pulses of sediment during large floods may be identifiable on the shelf, with a more homogenous grain size distribution than the background material, and should possess a distinct terrestrial carbon isotopic signature. Sediment supplied by wave remobilization should have a more uniform grain size distribution, due to the sorting effect of numerous resuspension events. Wave reworking will also mix the fluvial and marine sediments, potentially reducing the terrestrial carbon isotopic signature before the remobilized sediment reaches the depocenters. The modification of the terrestrial sedimentary signal through Poverty Bay and the inner-shelf is a function of distance from the river mouth, as a proxy for sediment sorting and mixing, not a function of absolute time elapsed after elevated discharge, because remobilized sediment may be supplied to the continental shelf within weeks or

months of discharge, yet having undergone significant wave reworking (Chapter 2 and Figs. 11 and 12). As such, terrestrial metrics based on radioisotope decay, such as ^{7}Be, may not be an effective tool for determining if sediment was flood or "marine dispersal" derived.

5.6 Comparison to Other Small Mountainous River Systems

Rapid sediment delivery to the middle continental shelf has been identified offshore of the Waiapu River in New Zealand and the small rivers in northern California, such as the Eel and Santa Clara (Harris et al., 2005; Kniskern et al., 2010; Traykovski et al., 2000; Warrick and Milliman, 2003). These rivers lose upward of 70% of the discharged sediment to offshore canyons, the continental slope, or far distal portions of the continental shelf (Kniskern et al., 2010; Sommerfield and Nittrouer, 1999). In a similar manner, about 70% of the Waipaoa Rivers discharged sediment is lost to the continental slope, or transported laterally along the shelf out of the range of observations (Carter et al., 2010).

A major difference between these systems is that the Waipaoa River discharges to a small embayment, whereas the Waiapu, Eel, and Santa Clara Rivers discharge directly to the open coast. Modeling results indicated that the presence of the embayment, in general, increased the average transit time of the sediment from the river mouth to deeper water. Within Poverty Bay estuarine circulation created an inflow of water near the seabed offshore of the river mouth and an outflow at the surface. Evidence of this was shown in Fig. 7, where the surface waters flowed out of Poverty Bay and portions of the bottom waters flowed into Poverty Bay, and in observations analyzed in Chapter 2. The

shoreward near-bed flows may lead to regions of sediment trapping in Poverty Bay, similar to turbidity maximum in classical estuarine systems. Indeed, the model estimated thicker deposition (Fig. 12B) in the region where near-bed currents converged in the vicinity of the river mouth (Figs. 7F and 12). The embayment also acted to reduce wave energy close to the river mouth, potentially increasing initial deposition and residence time of sediment within the bay. Deposition within Poverty Bay was also favored by the relatively lower seabed slope within the bay (<0.005 in the middle of the bay), compared to that found offshore of the Eel and Waiapu Rivers (0.005 to >0.01, Friedrichs and Wright, 2004), for example. The gentler slope likely limited the importance of high density gravity flow transport, further increasing residence time within Poverty Bay.

In spite of typically rapid sediment transport to the continental shelf, the nearshore and inner shelf significantly influence continental shelf deposition here and on other systems, including the Waiapu (Ma et al., 2008; Wadman and McNinch, 2008) and Eel (Crockett and Nittrouer, 2004; Curran et al., 2002). In all three systems, the nearshore and inner shelf either sequesters sediment or experiences deposition with later remobilization and supply to the shelf during large waves and/or fast currents. Along with observations analyzed in Chapter 2, the model results presented here provided evidence that there was significant sediment deposition within 5 or 10 km of the river mouth, which in turn modified the sedimentary signal passed to down-stream portions of the dispersal system (section 5.5), as was seen by Curran et al. (2002), Guillen et al. (2006) and Ma et al. (2008) offshore of the Eel, Tet, and Waiapu Rivers, respectively.

Sediment deposition in the nearshore during elevated discharge may be transferable throughout these systems due to consistent meteorological forcing. Driven by

the wind, the Waipaoa (This Study), Eel (Geyer et al., 2000), and Waiapu (Wadman and McNinch, 2008) Rivers have all been shown to hug the coastline during elevated discharge. This consistency of a shoreward forced/trapped plume and nearshore sediment deposition between multiple river systems and both the southern and northern hemispheres implies that it may be generalizable to many other small mountainous river systems. The pattern of shoreward winds transitioning to seaward winds presented here has also been seen on passive margin systems, when investigating nearshore sediment-transport in the absence of a large fluvial sediment supply (Wren and Leonard, 2005; Wright et al. 1986). The shoreward to seaward pattern may locally reverse if the weather system is sufficiently large compared to the body of land it is approaching, however. For example, clockwise rotating weather systems approach New Zealand from the north. If the weather system is large enough and significant orographic effects are neglected, winds may blow towards the west over the entire east-to-west extent of the island, creating shoreward winds on the eastern and seaward winds on the western sides. This shows that the wind pattern detailed above to have significant influence on sediment dispersal can occur throughout the world, as localized storms move toward the coastline or through a dispersal system, but should be evaluated locally to determine applicability.

6. Conclusions

Fully coupling the hydrodynamic and wave models improved the accuracy of estimated current speeds in the inner Poverty Bay. When calculations neglected radiation stresses and Stokes drift velocities, modeled current speeds in the nearshore were 2 to 8 times slower than the observed values. Also, inclusion of suspended sediment in the

calculations of water density significantly impacted estimates of sediment flux and velocities within Poverty Bay. Calculated suspended-sediment concentrations exceeded 10 g L^{-1} throughout the water column during the extreme October, 2005 flood. This imparted density to the sediment-water mixture, significantly modifying bottom boundary layer currents and deflecting them toward the deepest portion of Poverty Bay.

Model results for the winter of 2006 indicated that even moderate discharge pulses having less than 1 year recurrence interval created centimeters of sediment deposition throughout Poverty Bay. Most of this sediment was subsequently resuspended and removed from Poverty Bay by swell waves that occurred within three weeks of elevated river discharge. Elevated discharges thereby set the stage for two or more pulses of sediment to the continental shelf, with an initial pulse during elevated river discharge where around 75% of the discharged sediment was directly exported to the continental shelf. Subsequent periods of export were then triggered by resuspension of deposited material. Differences in sediment characteristics supplied to deeper water by each export pulse may influence the sedimentary signal recorded in offshore strata.

The flood-driven sediment export pulse should provide to the shelf a less well sorted sediment with a more distinct terrestrial signature. The export of terrestrial sediment to the shelf was accentuated during the extreme October, 2005 storm. Model estimates indicated that the October, 2005 storm supplied massive quantities of sediment (10.8 MT at 0.073 MT/hr) to the continental shelf within a six day period. This extreme event had a much higher gravity-driven component to the sediment-transport than the yearly discharge pulses, which accelerated sediment export from Poverty Bay.

The redistribution of sediment by wave swell events during the winter simulation was important to the sediment depositional patterns within Poverty Bay and in the export of sediment to the continental shelf. Additionally, cycles of deposition and resuspension that were typical for sediment delivered by these moderate events would impart a marine signature on the fluvial sediment before they arrive at their depositional sink.

For the time-period studied, the combined sediment input of the moderate flood events during the winter of 2006 surpassed that delivered during the extreme October, 2005 storm, consistent with decade-long averages by Hicks et al (2000). The model estimated a larger fraction of the extreme storm's discharged sediment to be directly supplied to the continental shelf during the flood compared to the yearly discharge pulses, however. Large storms such as the October, 2005 event should create sedimentary layers having a higher potential of being preserved in the sedimentary record compared to the higher-frequency events. The model therefore indicated that while much of the sediment delivery to the Waipaoa shelf is dominated by moderate discharge events and swell resuspension, only extremely large floods have the potential to create identifiable flood layers in the strata.

Acknowledgements

References:

Bever, A.J., Harris, C.K., Sherwood, C.R. and Signell, R.P., 2009. Deposition and flux of sediment from the Po River, Italy: An idealized and wintertime numerical modeling study. Mar. Geol., 260(1-4): 69-80. doi:10.1016/j.margeo.2009.01.007.

Booij, N., Ris, R.C. and Holthuijsen, L.H., 1999. A third-generation wave model for coastal regions 1. Model description and validation. J. Geophys. Res., 104(C4): 7649-7666.

Brown, L.J., 1995. Holocene shoreline depositional processes at Poverty Bay, a tectonically active area, northeastern north island, New Zealand. Quatern. Res., 26: 21-33.

Carter, L., Orpin, A.R. and Kuehl, S.A., 2010. Landscape and sediment responses from mountain source to deep ocean sink; Waipaoa Sedimentary System, New Zealand. Mar. Geol.

Chapman, D.C., 1985. Numerical treatment of cross-shelf open boundaries in a barotropic coastal ocean model. J. Phys. Oceanogr., 15: 1060-1075.

Chatwin, P.C., 1976. Some remarks on the maintenance of the salinity distribution in estuaries. Estuar. Coast. Shelf Sci., 4: 555-566.

Crockett, J.S. and Nittrouer, C.A., 2004. The sandy inner shelf as a repository for muddy sediment: An example from Northern California. Cont. Shelf Res., 24: 55-73.

Curran, K.J., Hill, P.S. and Milligan, T.G., 2002. Fine-grained suspended sediment dynamics in the Eel River flood plume. Cont. Shelf Res., 22: 2537-2550.

Delft_University_of_Technology, 2007. SWAN user manual, SWAN cycle III version 40.51A, Delft University of Technology, The Netherlands.

Dickhudt, P.J., 2008. Controls on Erodibility in a Partially Mixed Estuary: York River, Virginia. M.S. Thesis, Virginia Institute of Marine Science, College of William and Mary, Gloucester Point, 230 pp.

Dickhudt, P.J., Friedrichs, C.T., Schaffner, L.C. and Sanford, L.P., 2009. Spatial and temporal variation in cohesive sediment erodibility in the York River estuary, eastern USA: A biologically influenced equilibrium modified by seasonal deposition. Mar. Geol., 267: 128-140.

Drake, D.E. and Cacchione, D.A., 1985. Seasonal variation in sediment transport on the Russian River shelf, California. Cont. Shelf Res., 4(5): 495-514.

Egbert, G., Bennett, A. and Foreman, M., 1994. TOPEX/Poseidon tides estimated using a global inverse model. J. Geophys. Res., 99(C12): 24821-24852.

Egbert, G.D. and Erofeeva, S.Y., 2002. Efficient inverse modeling of barotropic ocean tides. Journal of Oceanic Technology, 19(2): 183-204.

Flather, R.A. and Proctor, R., 1983. Prediction of North Sea storm surges using numerical models: recent developments in the U.K. In: J. Sundermann and W. Lenz (Editors), North Sea Dynamics. Springer-Verlag, New York.

Foster, G. and Carter, L., 1997. Mud sedimentation on the continental shelf at an accretionary margin - Poverty Bay, New Zealand. N. Z. J. Geol. Geophys., 40: 157-173.

Friedrichs, C.T. and Wright, L.D., 2004. Gravity-driven sediment transport on the continental shelf: Implications for equilibrium profiles near river mouths. Coastal Engineering, 51(8-9): 795-811.

Geyer, W.R., 1993. The importance of suppression of turbulence by stratification on the estuarine turbidity maximum. Estuaries, 16(1): 113-125.

Geyer, W.R., Hill, P., Milligan, T. and Traykovski, P., 2000. The structure of the Eel River plume during floods. Cont. Shelf Res., 20: 2067-2093.

Geyer, W.R., Hill, P.S. and Kineke, G.C., 2004. The transport, transformation and dispersal of sediment by buoyant coastal flows. Cont. Shelf Res., 24: 927-949.

Guillen, J. et al., 2006. Sediment dynamics during wet and dry storms events on the Tet inner shelf (SW Gulf of Lions). Mar. Geol., 234: 129-142.

Haas, K.A. and Warner, J.C., 2009. Comparing a quasi-3D to a full 3D nearshore circulation model: SHORECIRC and ROMS. Ocean Model. Online, 26: 91-103.

Haidvogel, D.B., Arango, H., Budgell, W.P., Coruelle, B.D., Curshitser, E., Lorenzo, E.D., K.Fennel, Geyer, W.R., Hermann, A.J., Lanerolle, L., Levin, J., McWilliams, J.C., Miller, A.J., Moore, A.M., Powell, T.M., Schepetkin, A.F., Sherwood, C.R., Signell, R.P., Warner, J.C., Wilkin, J., 2008. Regional ocean forecasting in terrain-following coordinates: Model formulation and skill assessment. Journal of Computational Physics, 227: 3595-3624.

Harris, C.K., Sherwood, C.R., Signell, R., Bever, A.J. and Warner, J., 2008. Sediment dispersal in the northwestern Adriatic Sea. J. Geophys. Res., 113(C11S03): doi:10.1029/2006JC003868.

Harris, C.K., Traykovski, P.A. and Geyer, W.R., 2005. Flood dispersal and deposition by near-bed gravitational sediment flows and oceanographic transport: A numerical modeling study of the Eel River shelf, northern California. J. Geophys. Res., 110(C09025, doi10.1029/2004JC002727).

Harris, C.K. and Wiberg, P.L., 1997. Approaches to quantifying long-term continental shelf sediment transport with an example from the Northern California STRESS mid-shelf site. Cont. Shelf Res., 17(11): 1389-1418.

Healy, T., Stephens, S., Black, K., Gorman, R., Cole, R., Beamsley, B., 2002. Port redesign and planned beach renourishment in a high wave energy sandy-muddy coastal environment, Port Gisborne, New Zealand. Geomorphology, 48: 163-177.

Hetland, R.D. and Geyer, W.R., 2004. An idealized study of the structure of long, partially mixed estuaries. J. Phys. Oceanogr., 34(12): 2677-2691.

Hicks, D.M., Gomez, B. and Trustrum, N.A., 2000. Erosion thresholds and suspended sediment yields, Waipaoa River basin, New Zealand. Water Resour. Res., 36(4): 1129-1142.

Hicks, D.M., Gomez, B. and Trustrum, N.A., 2004. Event suspended sediment characteristics and the generation of hyperpycnal plumes at river mouths: east coast continental margin, North Island, New Zealand. J. Geol., 112(4): 471-485.

Hill, P.S. and McCave, I.N., 2001. Suspended particle transport in benthic boundary layers. In: B.P. Boudreau and B.B. Jorgensen (Editors), The Benthic Boundary Layer. Oxford University Press, pp. 78-103.

Kettner, A.J., Gomez, B. and Syvitski, J.P.M., 2007. Modeling suspended sediment discharge from the Waipaoa River system, New Zealand: The last 3000 years. Water Resour. Res., 43(W07411): doi:10.1029/2006WR005570.

Kineke, G.C. and Sternberg, R.W., 1995. Distribution of fluid muds on the Amazon continental shelf. Mar. Geol., 125: 193-233.

Kniskern, T.A., Kuehl, S.A., Harris, C.K. and Carter, L., 2010. Sediment accumulation patterns and fine-scale strata formation on the Waiapu River shelf, New Zealand. Mar. Geol., 270: 188-201.

Kuehl, S., Alexander, C., Carter, L., Gerald, L., Gerber, T., Harris, C., McNinch, J., Orpin, A., Pratson, L., Syvitski, J., Walsh, J.P., 2006. Understanding sediment transfer from land to ocean. EOS Transactions, 87(29).

Lin, J. and Kuo, A.Y., 2001. Secondary turbidity maximum in a partially mixed microtidal estuary. Estuaries, 24(5): 707-720.

Ma, Y., Wright, L.D., and Friedrichs, C.T. 2008. Observations of sediment transport on the continental shelf off the mouth of the Waiapu River, New Zealand: Evidence for current-supported gravity flows. Cont. Shelf Res. 28(4-5): 516-532.

Madsen, O.S., 1994. Spectral wave-current bottom boundary layer flows. Coastal Engineering 1994. Proceedings, 24th International Conference Coastal Engineering Research Council: 384-398.

Miller, P.D. and Komar, M.C., 1973. The threshold of sediment movement under oscillatory water waves. Journal of Sedimentary Petrology, 43(4): 1101-1110.

Milligan, T.G., Hill, P.S. and Law, B.A. 2007. Flocculation and the loss of sediment from the Po River plume. Cont. Shelf Res., 27(3-4): 309-321

Mulder, T., Syvitski, J.P.M., Migeon, S., Faugeres, J. and Savoye, B., 2003. Marine hyperpycnal flows: initiation, behavior and related deposits. A review. Mar. Pet. Geol., 20: 861-882.

Nittrouer, C.A., Austin, J.A., Field, M.E., Kravitz, J.H., Syvitski, J.P.M., Wiberg, P.L., 2007. Writing a Rosetta stone: insights into continental-margin sedimentary processes and strata. In: C.A. Nittrouer et al. (Editors), Continental-Margin Sedimentation: From Sediment Transport to Sequence Stratigraphy. Blackwell Publishing Ltd., pp. 1-48.

Ogston, A.S., Cacchione, D.A., Sternberg, R.W. and Kineke, G.C., 2000. Observations of storm and river flood-driven sediment transport on the northern California continental shelf. Cont. Shelf Res., 20: 2141-2162.

Orpin, A.R., Alexander, C., Carter, L., Kuehl, S. and Walsh, J.P., 2006. Temporal and spatial complexity in post-glacial sedimentation on the tectonically active, Poverty Bay continental margin of New Zealand. Cont. Shelf Res., 26: 2205-2224.

Orpin, A.R., Carter, L., Page, M.J., cochran, U.A., N, A., Trustrum, Gomez, B., Palmer, A.S., Midenhall, D.C., Rogers, K.M., Brackley, H.L., Northcote, L., 2010. Holocene sedimentary record from Lake Tutira: A template for upland watershed erosion proximal to the Waipaoa Sedimentary System, northeastern New Zealand. Mar. Geol., 270: 11-29.

Partheniades, E., 1965. Erosion and deposition of cohesive soils. Journal of the Hydraulic Division, 91(HY1).

Reid, C.J., 1999. Waipaoa River at Kanakanaia: a review of flood data, Unpublished report to the Gisborne District Council, New Zealand.

Reid, L.M. and Page, M.J., 2002. Magnitude and frequency of landsliding in a large New Zealand catchment. Geomorphology, 49: 71-88.

Rinehimer, J.P., Harris, C.K., Sherwood, C.R. and Sanford, L.P., 2008. Sediment consolidation in a muddy, tidally-dominated environment: Model behavior and

sensitivity. In: M. Spaulding (Editor), Estuarine and Coastal Modeling: Proceedings of the 10th International Conference, Newport, RI, pp. 819-838.

Rose, L., 2008. Recent sedimentation patterns and facies distribution on the Waipaoa River shelf, NZ. Thesis, Virginia Institute of Marine Science, College of William and Mary, Gloucester Point.

Sanford, L.P., 2006. Uncertainties in sediment erodibility estimates due to lack of standards for experimental protocols and data interpretation. Integr. Environ. Assess. Manage., 2(1): 29-34.

Shchepetkin, A.F. and McWilliams, J.C., 2005. The Regional Oceanic Modeling System (ROMS): a split-explicit, free-surface, topography-following-coordinate oceanic model. Ocean Modeling, 9: 347-404.

Sherwood, C.R., Book, J.W., Carniel, S., Cavaleri, L., Chiggiato, J., Das, H., Douyle, J., Harris, C.K., Niedoroda, A., Perkins, H., Poulain, P., Pullen, J., Reed, C., Russo, A., Sclavo, M., Signell, R., Traykovski, P., Warner, J., 2004. Sediment dynamics in the Adriatic Sea investigated with coupled models. Oceanography, 17(4): 58-69.

Sherwood, C.R., Butman, B., Cacchione, D.A., Drake, D.E., Gross, T.F., Sternberg, R.W., Williams, A.J., 1994. Sediment-transport events on the northern California Continental Shelf during the 1990-1991 STRESS experiment. Cont. Shelf Res., 14(10/11): 1063-1099.

Shields, A., 1936. Anwendung der Aehnlichkeitsmechanik und der Turbulenzforschung auf die Geschiebebewegung, Mitt. Preuss. Versuchsanst. Wasserbau Schiffbau, (English translation by W. P. Ott and J. C. van Uchelen, 36 pp., U.S. Dep. of Agric. Soil Conser. Serv. Coop. Lab., Calif., Inst. of Technol., Pasadena, 1936.).

Smith, R.K., 1988. Poverty Bay, New Zealand: a case study of coastal accretion 1886-1975. N. Z. J. Mar. Freshwat. Res., 22: 135-141.

Sommerfield, C.K. and Nittrouer, C.A., 1999. Modern accumulation rates and a sediment budget for the Eel shelf: A flood-dominated depositional environment. Mar. Geol., 154: 227-241.

Stephens, S., Bell, R.G. and Black, K.P., 2002. Complex circulation in a coastal embayment: Shelf-current, wind and density-driven circulation in Poverty Bay, New Zealand. J. Coast. Res., 34. Special Issue. 45-59

Sternberg, R.W., Cacchione, D.A., Paulson, B., Kineke, G.C. and Drake, D.E., 1996. Observations of sediment transport on the Amazon subaqueous delta. Cont. Shelf Res., 19: 697-715.

Stevens, A.W., Wheatcroft, R.A. and Wiberg, P.L., 2007. Seabed properties and sediment erodibility along the western Adriatic margin, Italy. Cont. Shelf Res., 27(3-4): 400-416.

Svendsen, I.A., 2006. Introduction to nearshore hydrodynamics. Advanced Series on Ocean Engineering, 24. World Scientific Publishing Co. Pte. Ltd., Singapore, 722 pp.

Tolman, H.L., Balasubramaniyan, B., Burrouhgs, L.D., Chalikov, D.V., Chao, Y.Y., Chen, H.S., Gerald, V.M., 2002. Development and implementation of wind-generated ocean surface wave models at NCEP. Weather and Forecasting, 17: 311-333.

Traykovski, P., Geyer, W.R., Irish, J.D., and Lynch, J.F. 2000. The role of wave-induced density-driven fluid mud flows for cross-shelf transport on the Eel River continental shelf. Cont. Shelf Res., 20: 2113-2140.

Traykovski, P., Wiberg, P.L. and Geyer, W.R., 2007. Observations and modeling of wave-supported sediment gravity flows on the Po prodelta and comparison to prior observations from the Eel shelf. Cont. Shelf Res., 27(4-3): 375-399.

Umlauf, L. and Burchard, H., 2003. A generic length-scale equation for geophysical turbulence models. J. Mar. Res., 61: 235-265.

Wadman, H.M. and McNinch, J.E., 2008. Stratigraphic spatial variation on the inner shelf of a high-yield river, Waiapu River, New Zealand: Implications for fine sediment dispersal and preservation. Cont. Shelf Res., 28(7): 865-886.

Wadman, H.M. and McNinch, J.E., 2009. Sediment segregation and dispersal across the land-sea interface: Waipaoa sedimentary system, New Zealand, Integration and Synthesis of MARGINS Sediment Source-to-Sink Research Workshop, Gisborne, New Zealand.

Wang, X.H. and Pinardi, N., 2002. Modeling the dynamics of sediment transport and resuspension in the northern Adriatic Sea. J. Geophys. Res., 107(C12): 18-1:18-23.

Warner, J.C., Butman, B. and Dalyander, P.S., 2008a. Storm-driven sediment transport in Massachusetts Bay. Cont. Shelf Res., 28: 257-282.

Warner, J.C., Geyer, W.R. and Lereczak, J.A., 2005a. Numerical modeling of an estuary: A comprehensive skill assessment. J. Geophys. Res., 11(C05001): doi:10.1029/2004JC002691.

Warner, J.C., Perlin, N. and Skyllingstad, E.D., 2008b. Using the Model Coupling Toolkit to couple earth system models. Environ. Model. Software, 23: 1240-1249.

Warner, J.C., Sherwood, C.R., Arango, H.G., Butman, B. and Signell, R.P., 2005b. Performance of four turbulence closure methods implemented using a generic length scale method. Ocean Modeling, 8: 81-113.

Warner, J.C., Sherwood, C.R., Signell, R.P., Harris, C.K. and Arango, H.G., 2008c. Development of a three-dimensional regional coupled wave-current-sediment model. Comput. Geosci., 34(10): 1284-1306.

Warrick, J.A. and Milliman, J.D., 2003. Hyperpycnal sediment discharge from semiarid southern California rivers: Implications for coastal sediment budgets. Geology, 31(9): 781-784.

Wheatcroft, R.A., 2000. Oceanic flood sedimentation: a new perspective. Cont. Shelf Res., 20: 2059-2066.

Wiberg, P.L. and Smith, J.D., 1987. Calculations of the critical shear stress for motion of uniform and heterogeneous sediments. Water Resour. Res., 23(8): 1471-1480.

Wilmott, C.J., 1981. On the validation of models. Physical Geography, 2: 184-194.

Woodruff, J.D., W.R., G., Sommerfield, C.K. and Driscoll, N.W., 2001. Seasonal variation of sediment deposition in the Hudson River estuary. Mar. Geol., 179: 105-119.

Wren, P.A. and Leonard, L.A., 2005. Sediment transport on the mid-continental shelf in Onslow Bay, North Carolina during Hurricane Isabel. Estuarine, Coastal and Shelf Science, 63: 43-56.

Wright, L.D., 1985. River deltas. In: R.A. Davies Jr. (Editor), Coastal Sedimentary
Environments. Springer-Verlag, New York, pp. 1-76.

Wright, L.D., Boon, J.D., Green, M.O. and List, J.H., 1986. Response of the mid
shoreface of the southern Mid-Atlantic bight to a "Northeaster". Geo-Marine
Letters, 6: 153-160.

Wright, L.D., Wiseman, W.J., Yang, Z.S., Bornhold, B.D., Keller, G.H., Prioi, D.B. and
Suhayda, J.N., 1990. Processes of marine dispersal and deposition of suspended
silts off the modern mouth of the Huanghe (Yellow River). Cont. Shelf Res., 10:
1-40.

Wright, L.D. and Friedrichs, C.T., 2006. Gravity driven transport on continental shelves:
A status report. Cont. Shelf Res., 26(17-18): 2092-2107.

Table 1. Sediment grain class characteristics and their source locations within the model.

Source	Class	Diameter (µm)	W_s (mm s^{-1})	τ_{cr} (N m^{-2})	Erosion Rate Parameter (kg m^{-2} s^{-1})	Fraction of Discharge
River	1	7.8	0.038	0.02		40
	2	15	0.15	0.03		30
	3	31	0.62	0.06		30
	4	125	10	0.14	5×10^{-4}	1
Seabed	5	63	2.4	0.10		
	6	125	10	0.14		NA
	7	1000	125	0.53		

Table 2. Modeled and observed wave statistics from three locations within Poverty Bay. Station locations correspond to the relative location of each S4 in relation to the Waipaoa River mouth, with the Mouth station being directly seaward of the river mouth, and are shown in Fig. 1C. Model Skill calculated as S_W in Eq. 1.

Wave Metric	Wave Station Location	Wave Source	Mean (m)	Correlation Coefficient	Bias (m)	Model Skill
Height	North	Observation	0.96	0.69	-0.03	0.82
		Modeled	0.93			
	Mouth	Observation	0.85	0.80	0.07	0.87
		Modeled	0.92			
	South	Observation	0.75	0.87	0.12	0.90
		Modeled	0.87			
Orbital Velocity	North	Observation	0.31	0.75	0.00	0.84
		Modeled	0.31			
	Mouth	Observation	0.33	0.74	-0.05	0.83
		Modeled	0.28			
	South	Observation	0.28	0.78	-0.02	0.87
		Modeled	0.26			

Table 3. Modeled and observed statistics at each S4 location for the sea surface height and the current speed for the ROMS-SWAN coupled and independent model runs. Station locations correspond to the relative location of each S4 in relation to the Waipaoa River mouth, with the Mouth station directly seaward of the river mouth, and are shown in Fig. 1C. Model Skill calculated as S_W in Eq. 1.

Variable	Station Location	Source	Standard Deviation (m, m s^{-1})	Correlation Coefficient	Bias (m, m s^{-1})	Model Skill
Sea Surface Height, Coupled	North	Observation	0.45	0.93	-0.01	0.96
		Model	0.44			
	Mouth	Observation	0.45	0.94	0.00	0.97
		Model	0.44			
	South	Observation	0.45	0.94	0.00	0.97
		Model	0.44			
Current Speed Coupled	North	Observation	0.08	-0.33	-0.05	0.25
		Model	0.06			
	Mouth	Observation	0.09	0.51	-0.11	0.53
		Model	0.05			
	South	Observation	0.07	0.67	-0.06	0.73
		Model	0.09			
Current Speed Independent	North	Observation	0.08	-0.03	-0.16	0.36
		Model	0.03			
	Mouth	Observation	0.09	0.36	-0.15	0.41
		Model	0.02			
	South	Observation	0.07	0.25	-0.15	0.39
		Model	0.01			

Figure 1. (A,B) Location of Poverty Bay and (B,C) model grid. In panel B, bathymetry is contoured every 10 m from 10-100 m, every 100 m from 200-1000 m, and every 250 m thereafter. The spatial extent of the model grid is traced in panel B. The locations of Gisborne and the Gisborne airport (AP) are shown in panel C. The Waipaoa River mouth location is at the WR in panel C, and the Turanganui River mouth corresponds to the G in Gisborne. S4 (triangles) and ADCP/ADV (square) observations from Chapter 1 and used in model validation are shown in panel C. The profile transect used in Fig. 8 is the dashed line in panel C.
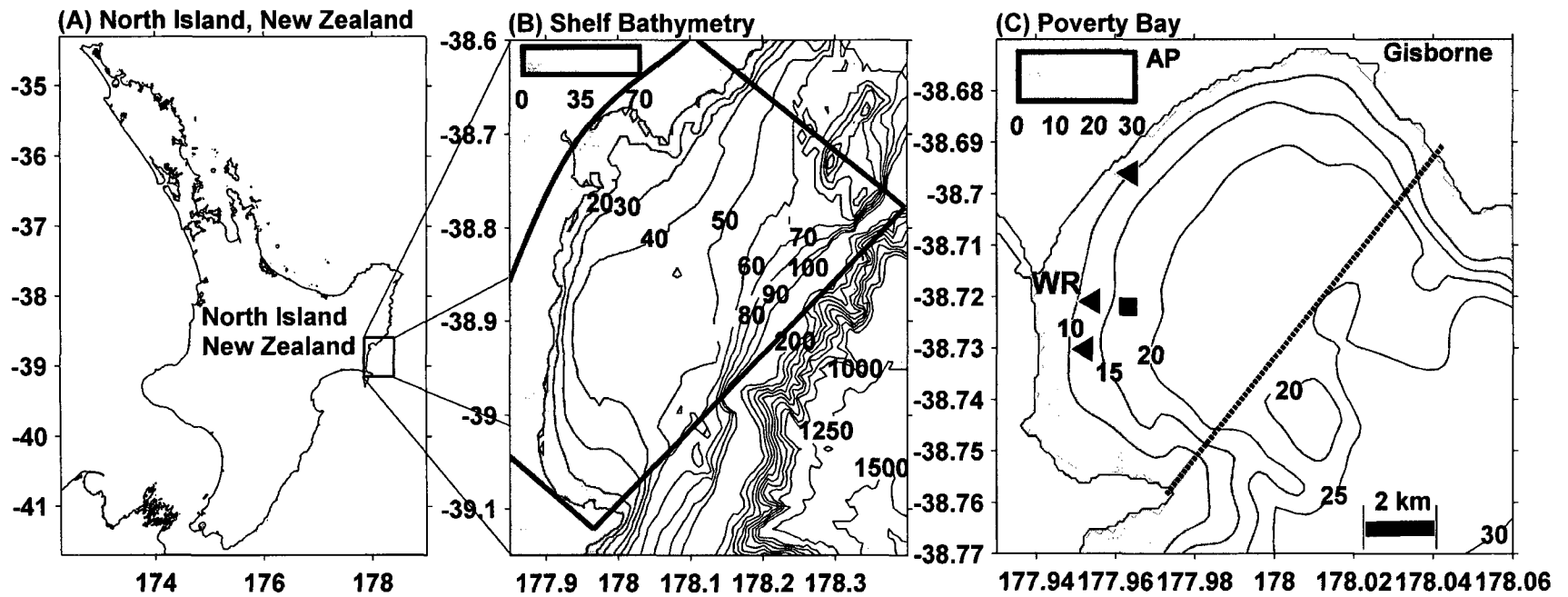
Figure 2. Waipaoa River (A,B) freshwater discharge and (C,D) suspended-sediment concentration (black) and cumulative sediment discharge (grey), and the (E,F) wind speed (line) and velocity (vectors). Wind speed and velocity underwent a 33 hr lowpass filter. The shaded portion of panel B shows when the instruments used for model validation were not in the water due to instrument turnaround. River discharge was negligible between January and mid-April, 2006, and is not shown.
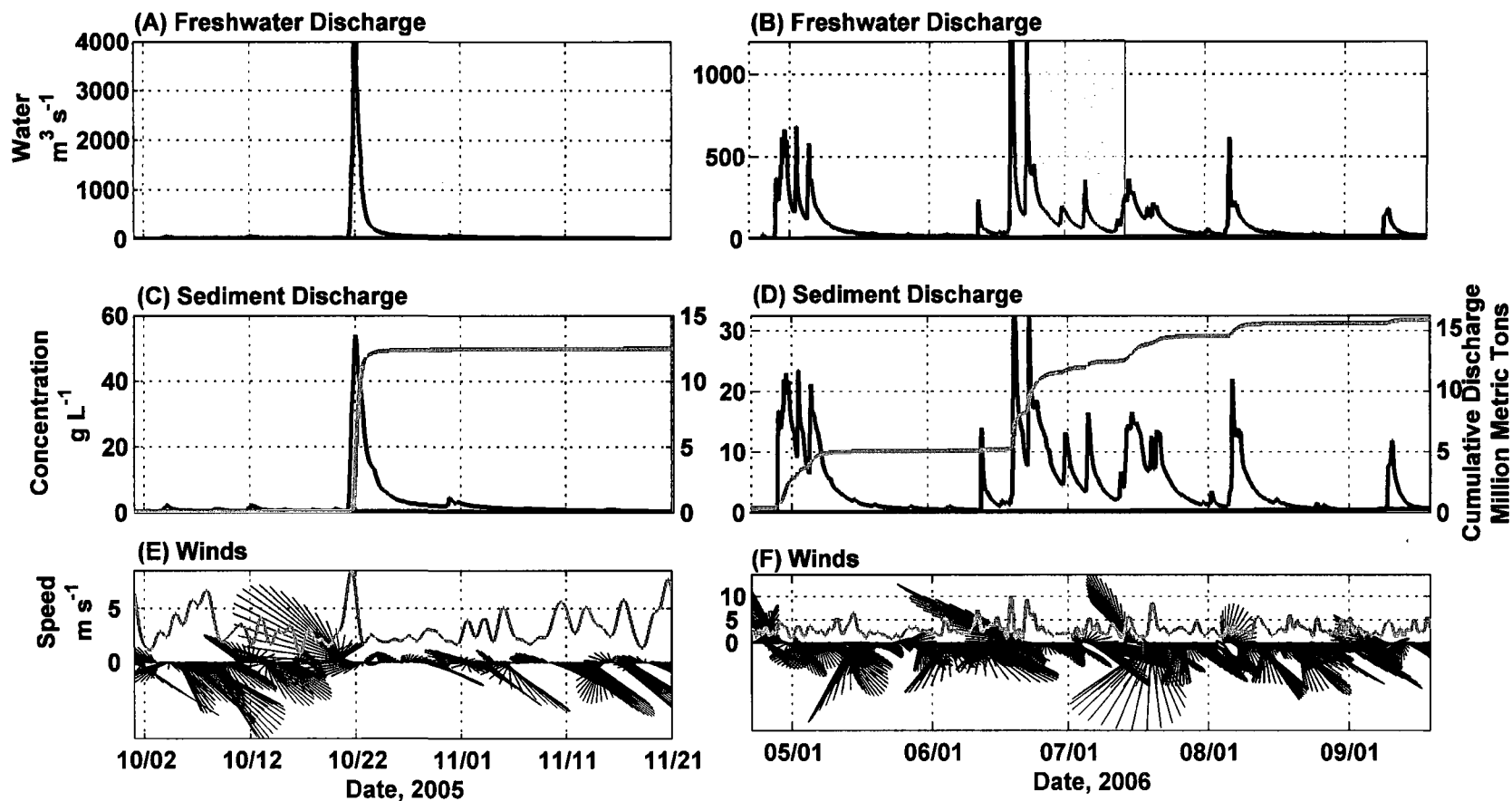
Figure 3. SWAN estimated (black) and observed (grey) wave height (A,B,C) and orbital velocity (D,E,F) at three locations within Poverty Bay. The stations represent those (A, D) to the north of the Waipaoa River, (B, E) seaward of the Waipaoa River mouth, and (C, F) to the south of the river. Locations are shown in Fig. 1C. The gap in the observations was due to an instrument turnaround period.
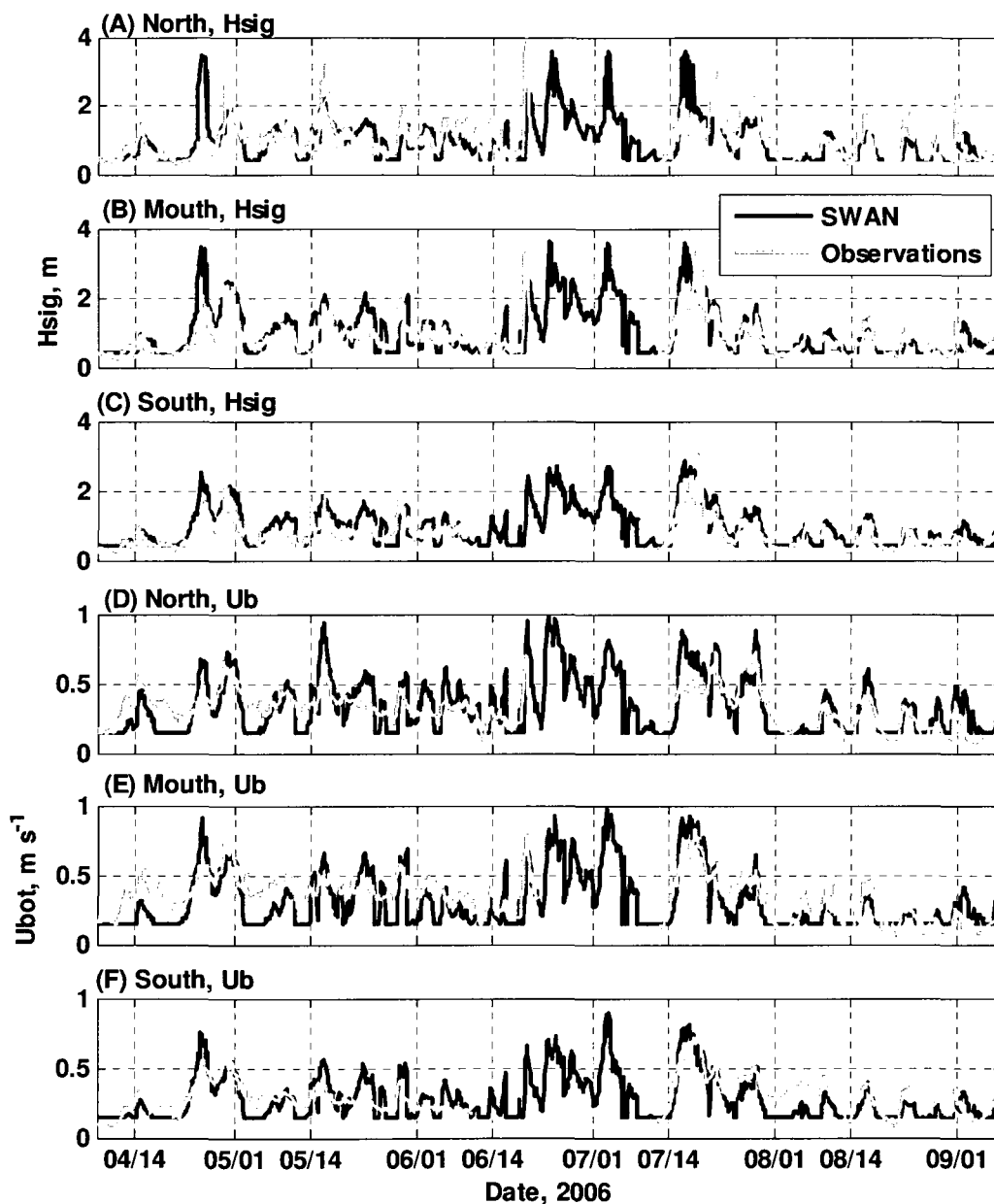
Figure 4. Time-averaged wave height (colors) and direction (arrows) estimated by the SWAN model for (A) the winter simulation, (B) the beginning of the May discharge pulse, and (C) the swell event following the May discharge pulse.
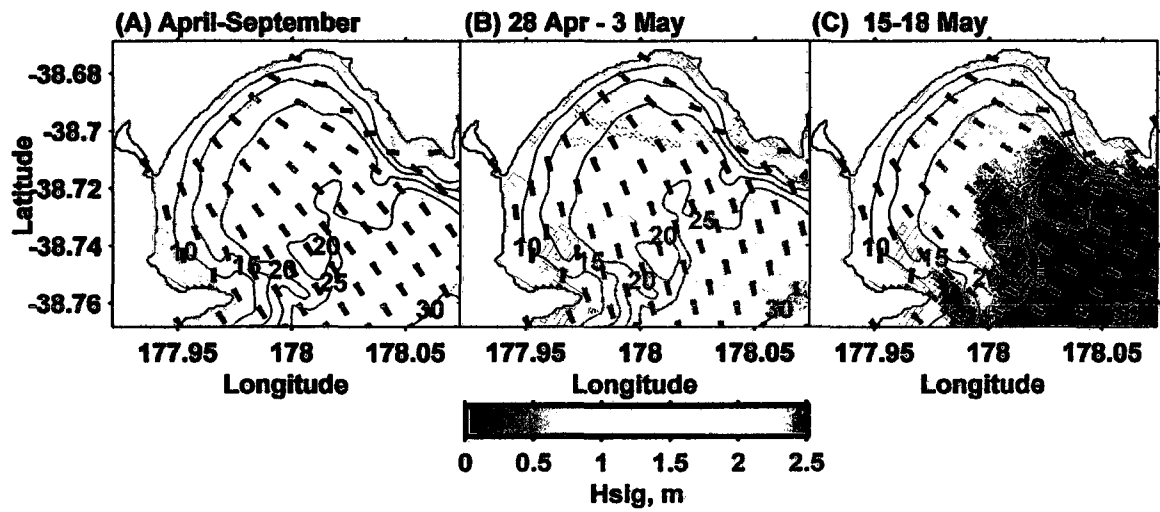
Figure 5. Modeled and observed near surface (A) water temperature and (B) salinity at the northern S4 location specified in Fig. 1.
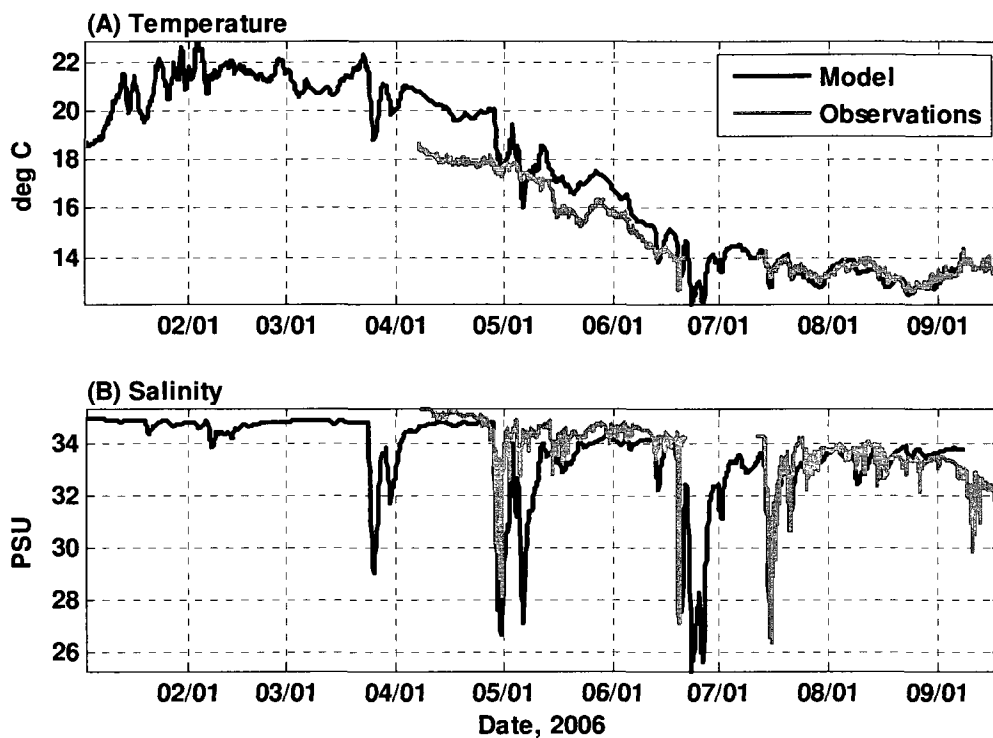
Figure 6. Sea surface height at the northern S4 location during the elevated discharge period in April-May. The data shown was truncated because the comparison becomes impossible to see with longer time-frames.

North S4, Sea Surface Height
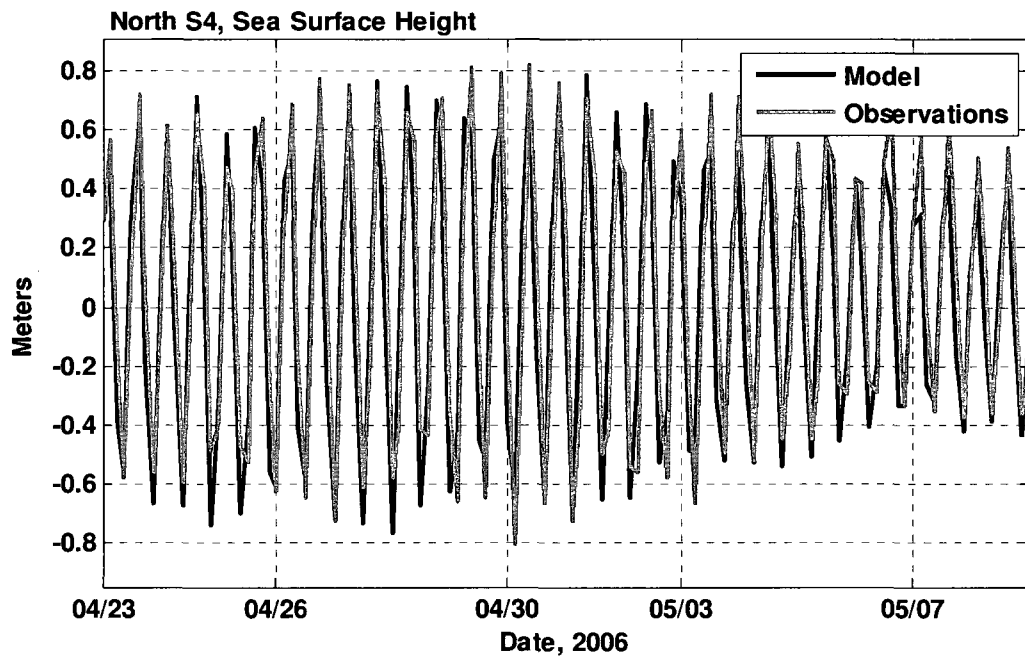
Figure 7. Time-averaged surface (left column) and one meter above the bed (right column) currents for (A,E) the winter 2006 simulation, (B,F) the April-May, 2006 discharge event, (C,G) the swell wave resuspension event following the April-May flood, and (D,H) the large flood in October, 2005. Colors represent the current speed, vectors represent the current direction where speeds exceeded 0.01 m s^{-1}. Water depth is contoured every 10 m.

The figure is on the next page.

(A) April-September, 2006

(B) 28 Apr-9 May, 2006

(C) 15-18 May, 2006

(D) 20-26 October, 2005

(E) April-September, 2006

(F) 28 Apr-9 May, 2006

(G) 15-18 May, 2006

(H) 20-26 October, 2005

137
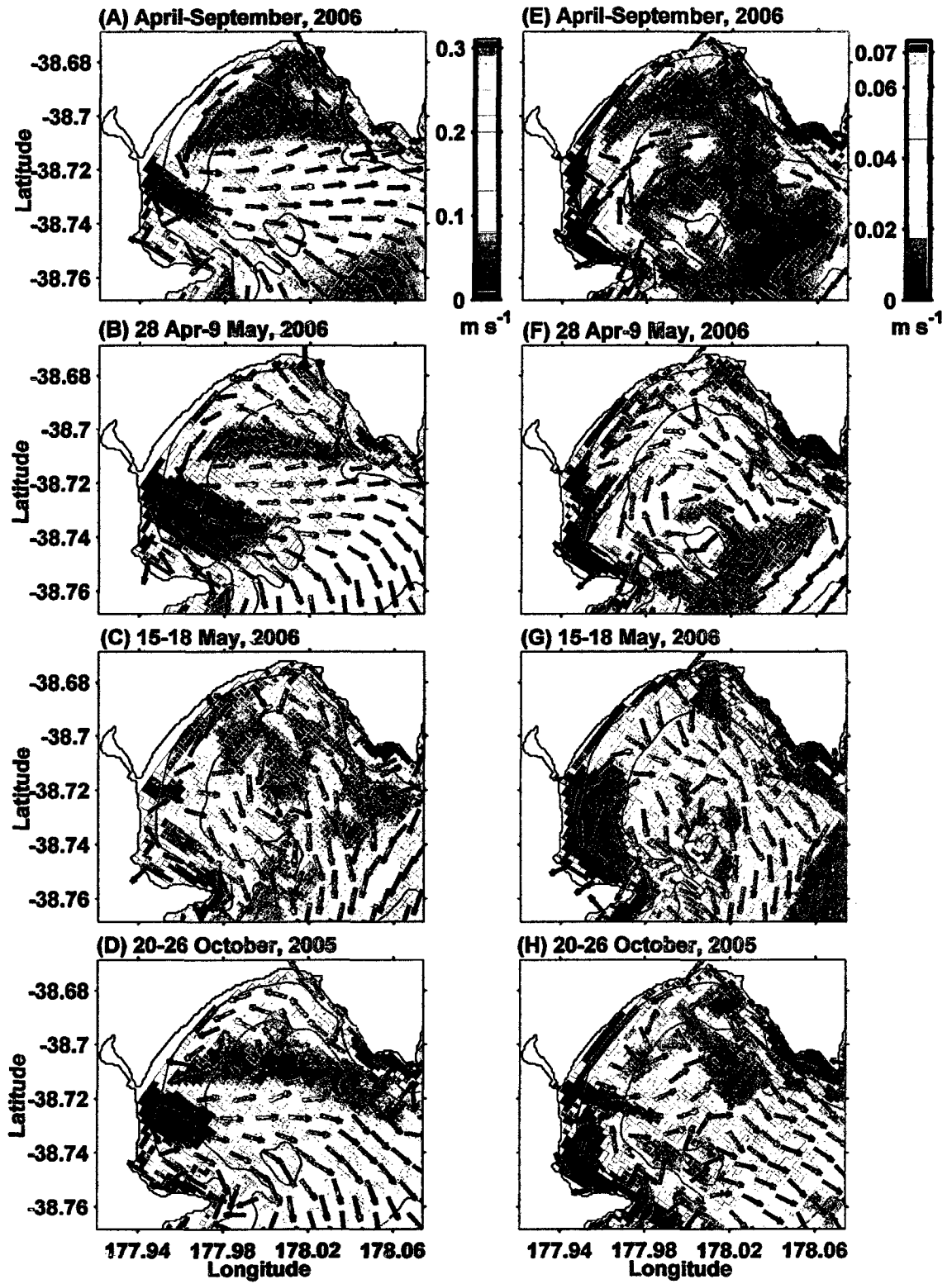
Figure 8. One meter above the bed current speed at the S4 north of the river mouth. Coupled represents the model run described herein with ROMS-SWAN two-way coupling. Independent represents an identical run, except the two models were run independently of each other. Values are plotted as 9 hour running-means.
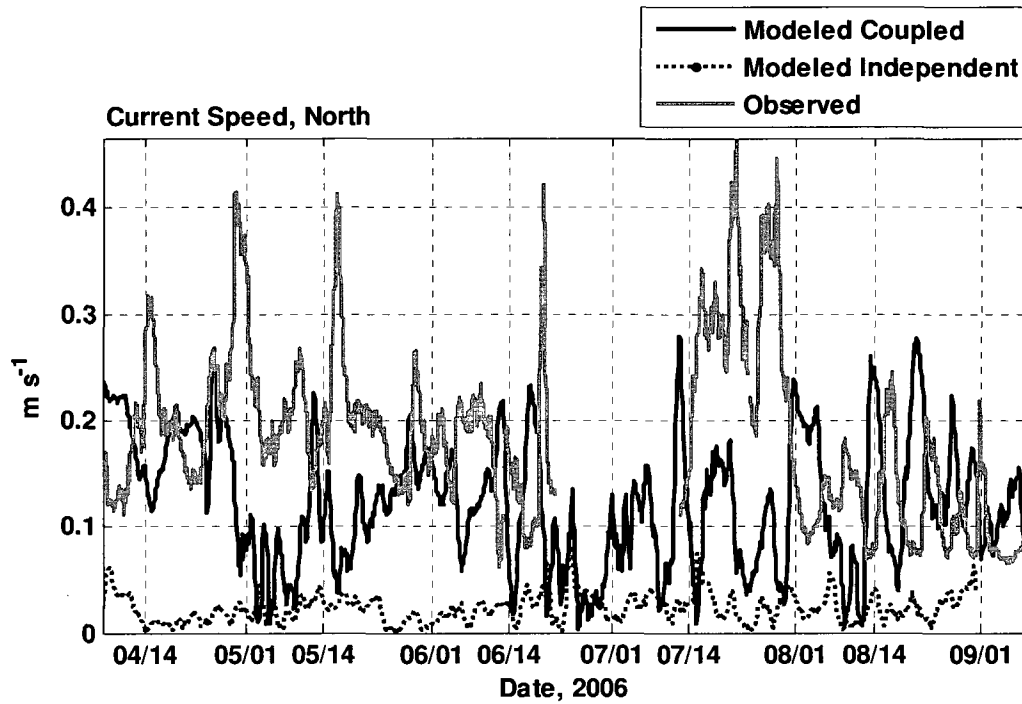
Figure 9. Surface salinity (shading) and current velocities (vectors) throughout the elevated discharge in April-May, 2006. Wind directions and relative speeds are shown by the arrow in the top right of each panel. Bathymetry is contoured every 10 m.

The figure is on the next page.

(A) 29 April, 6hrs, 2006
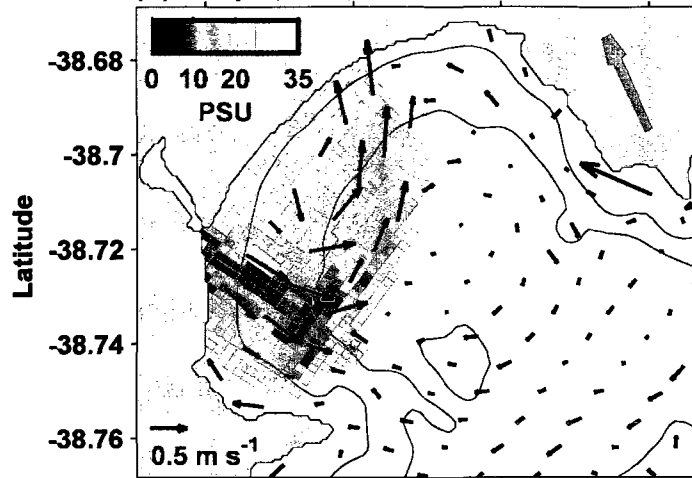
(B) 30 April, 15 hrs, 2006
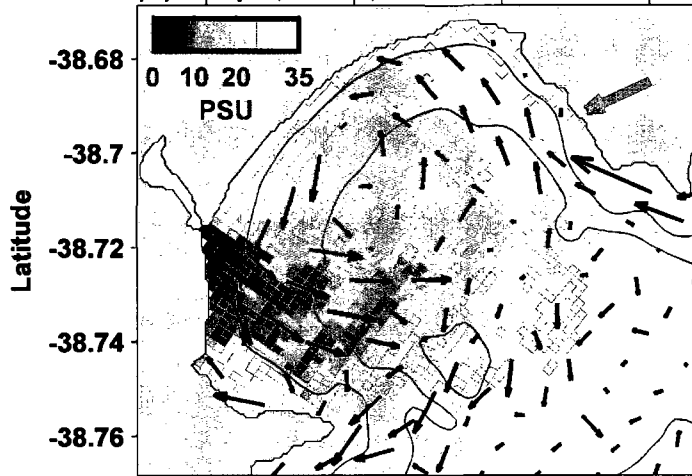
(C) 1 May, 21 hrs, 2006
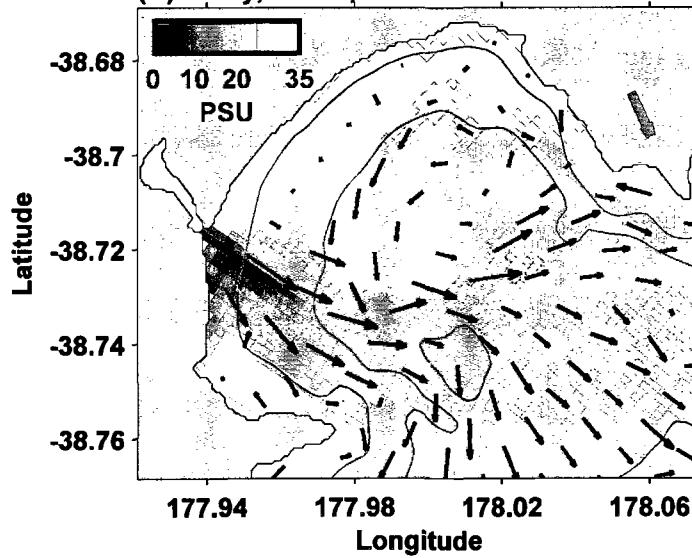
Figure 10. Modeled and observed depth-averaged turbidity at the ADCP location. Values were normalized by the maximum values of the model estimates (kg m^{-3}) and the data (decibels), and are shown as the 9 hour running-mean.
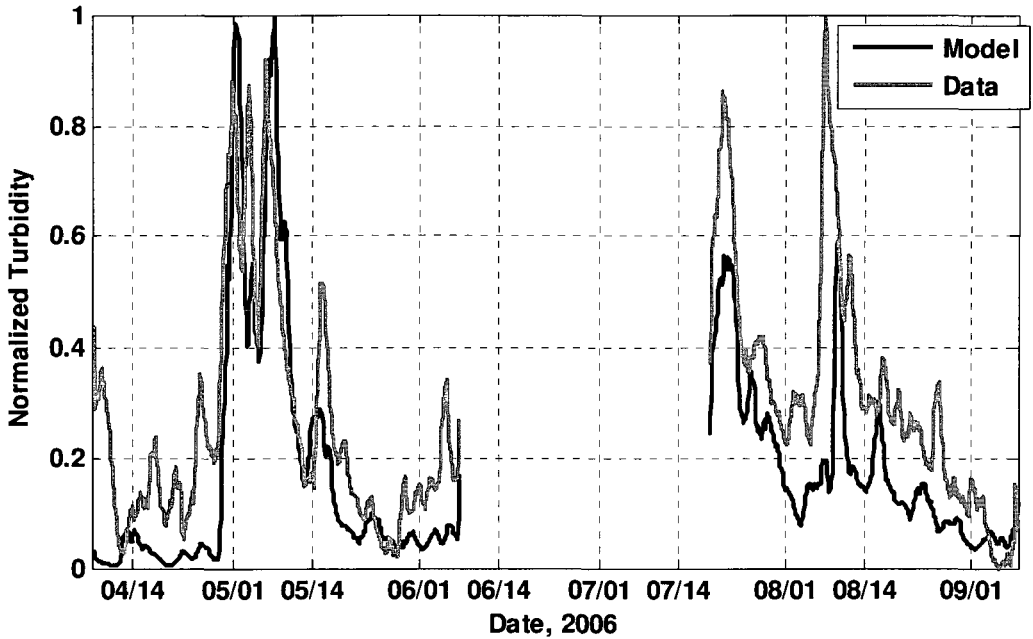
Figure 11. Modeled and observed sediment deposition at 15 m water depth offshore of the river mouth (ADCP/ADV location, Fig. 1). Modeled deposit mass was converted to thickness assuming a porosity of ~65%, causing the modeled kg m^{-2} to directly equal mm of deposition. The model and observations are shown relative to their seabed elevation on 22 July, 2006, to highlight the relative changes over the same time-period.
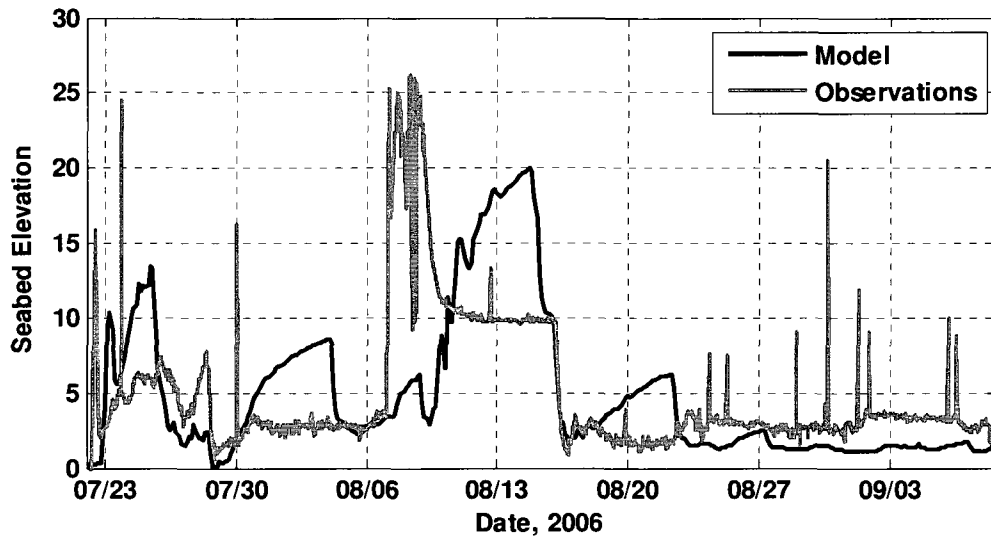
Figure 12. Sediment deposition for (A) the winter 2006 simulation, (B) the April-May, 2006 discharge event, (C) the swell wave resuspension event following the April-May discharge event, and (D) the large flood in October, 2005. Erosional areas in each panel are plotted as white. 1 and 5 cm erosion thicknesses are contoured on panel D. Modeled deposition was converted from mass per area (kg m^{-2}) to cm by assuming a porosity of ~65% and dividing by 10. Note the difference in the scale between the resuspension event and the others. Water depth is contoured every 5 m starting at 10 m.

(A) April-September, 2006

(B) 28 Apr-9 May, 2006

(C) 15-18 May, 2006

(D) 20-26 October, 2005
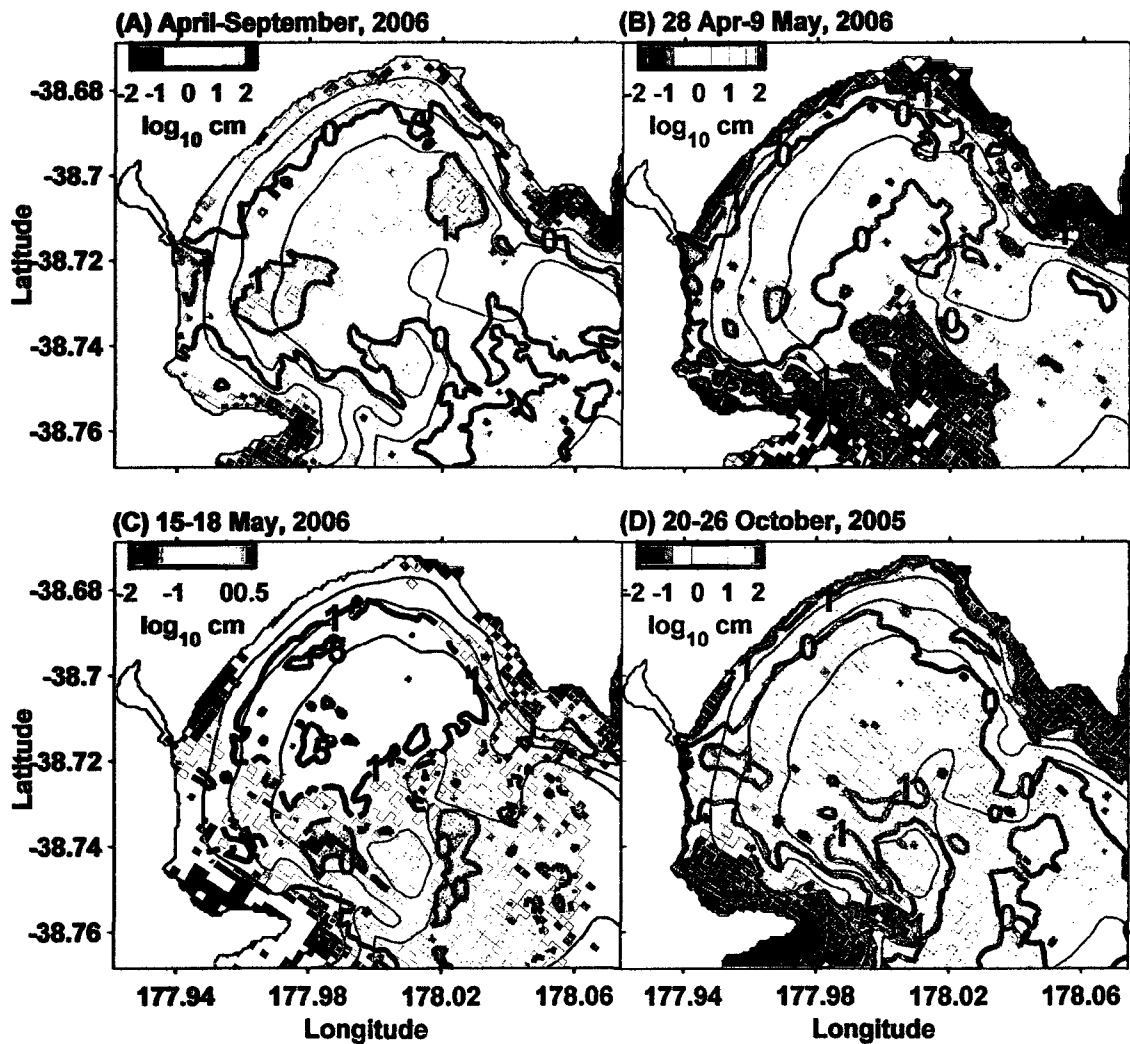
Figure 13. (A) Cumulative sediment exported from Poverty Bay (black) and the cumulative sediment discharge from the Waipaoa River (grey). (B) The rate of sediment export from Poverty Bay.
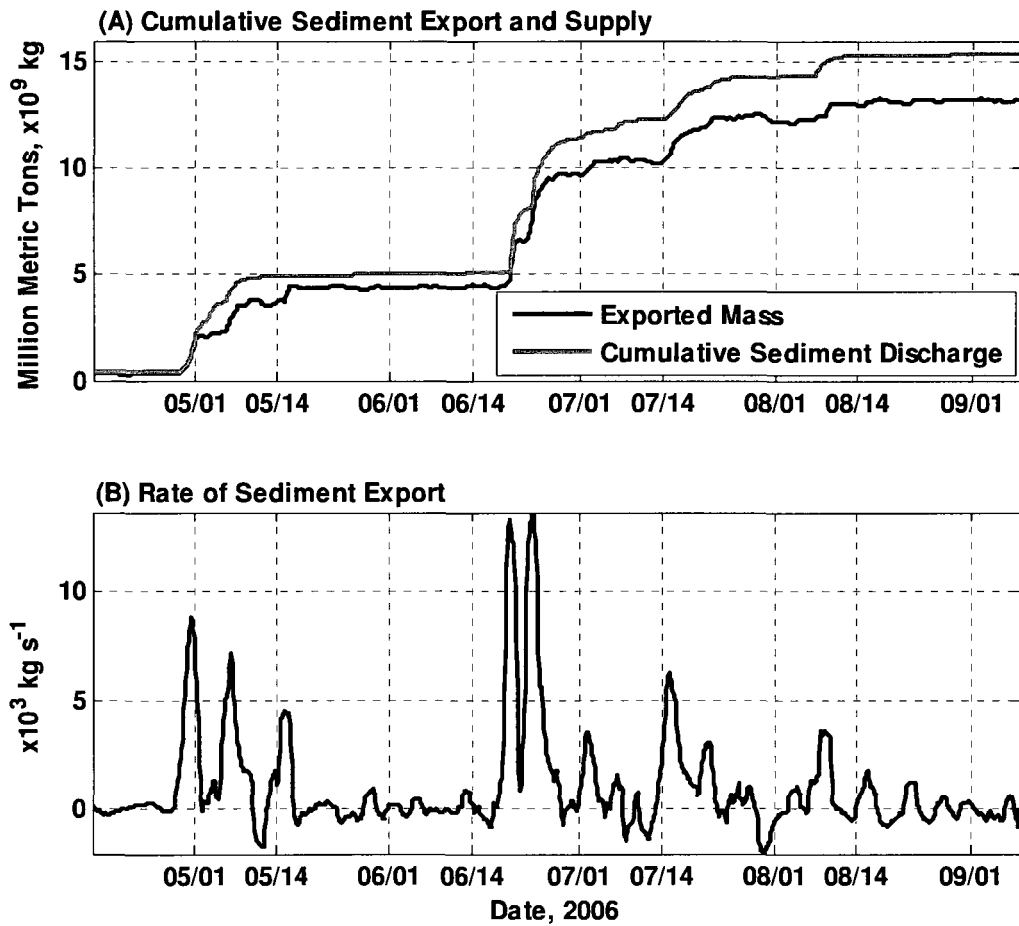
Figure 14. Time-averaged sediment flux directed through the mouth of Poverty Bay along the transect shown in Fig. 1. Values are in kg m^{-2} s^{-1}, with positive values directed toward the southeast, that is, out of Poverty Bay. Zero transport is contoured in black, and 0.1 kg m^{-2} s^{-1} is contoured in grey.
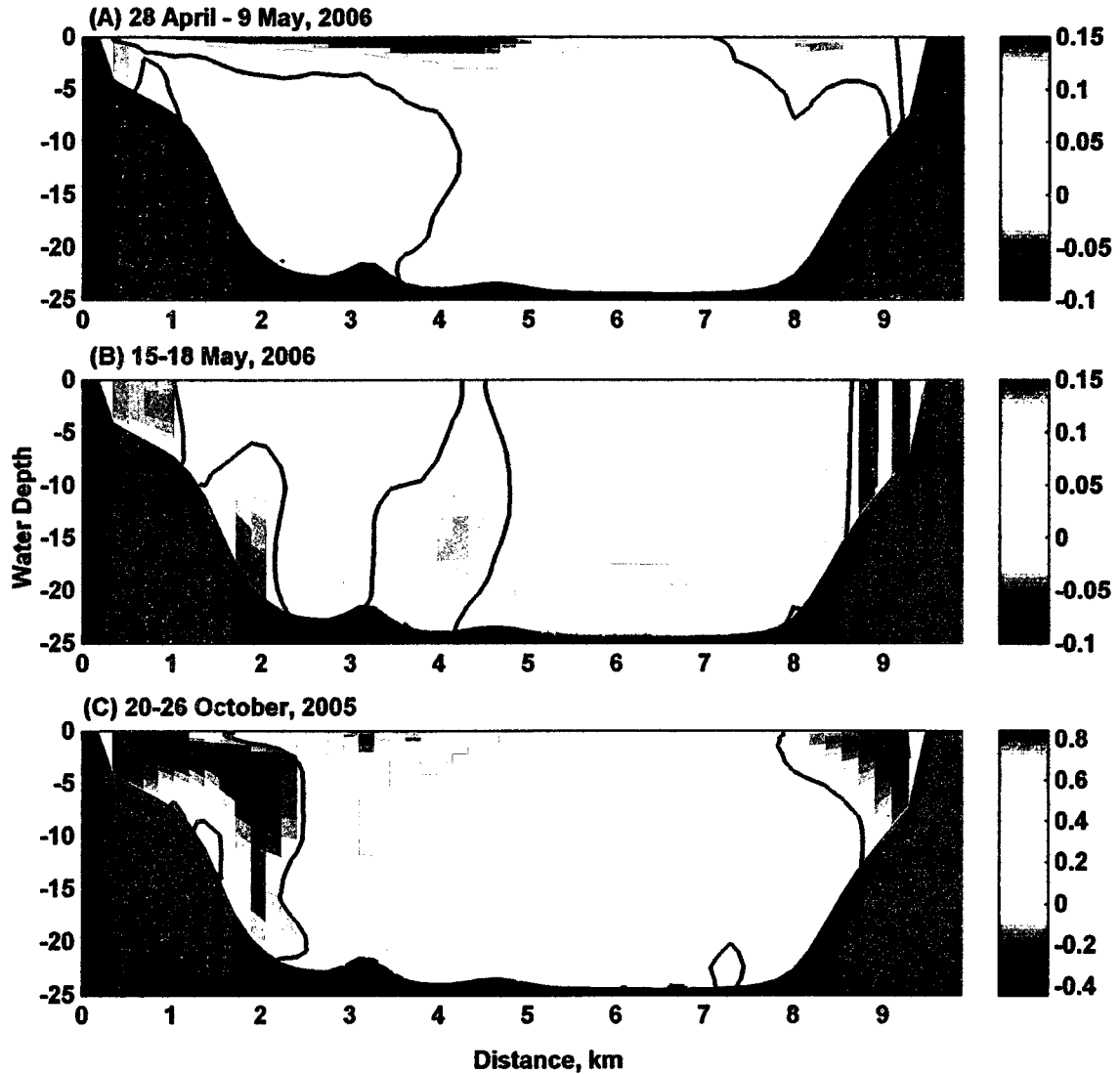
Figure 15. Depth-integrated and then time-averaged sediment transport (kg m^{-1} s^{-1}) magnitude (colors, on a log$_{10}$ scale) and direction (arrows) over (A) the April-May flood, (B) the subsequent swell resuspension event, and (C) the October flood. Note the different scales between panels A, B and C. Water depth is contoured in meters.

The figure is on the next page.

(A) 28 April-9 May, 2006
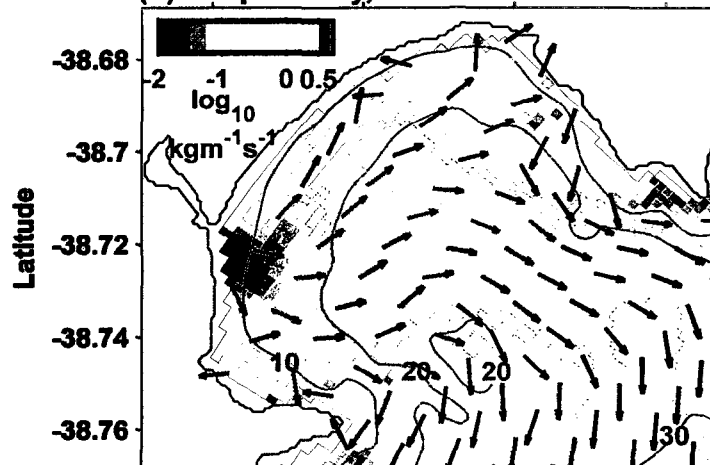
(B) 15-18 May, 2006
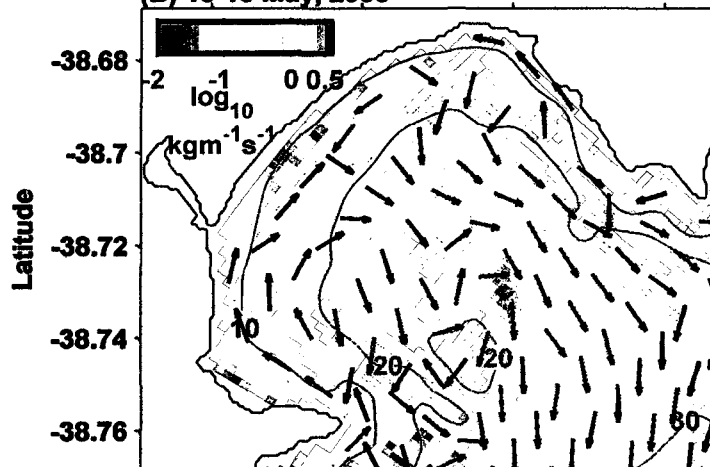
(C) 20-26 October, 2005

Longitude
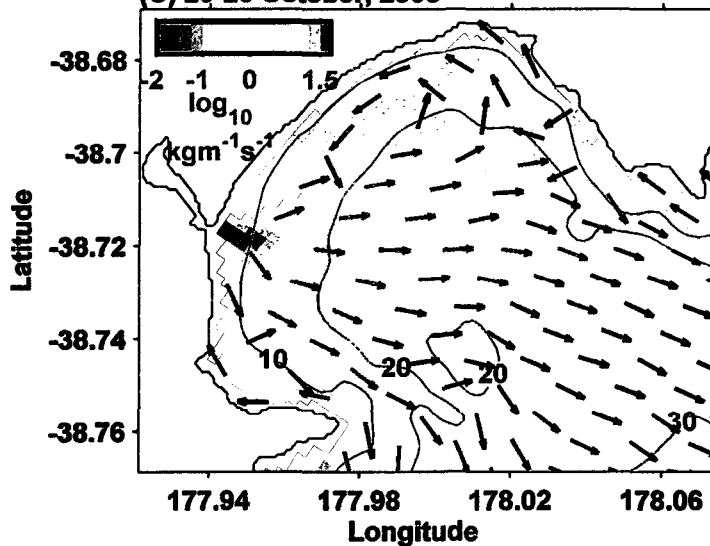
Figure 16. (A) Surface and (B) 1 mab current speed (colors) and velocity (arrows) and (C) sediment deposition for the October, 2005 storm with suspended sediment concentration not used in the water density calculations.
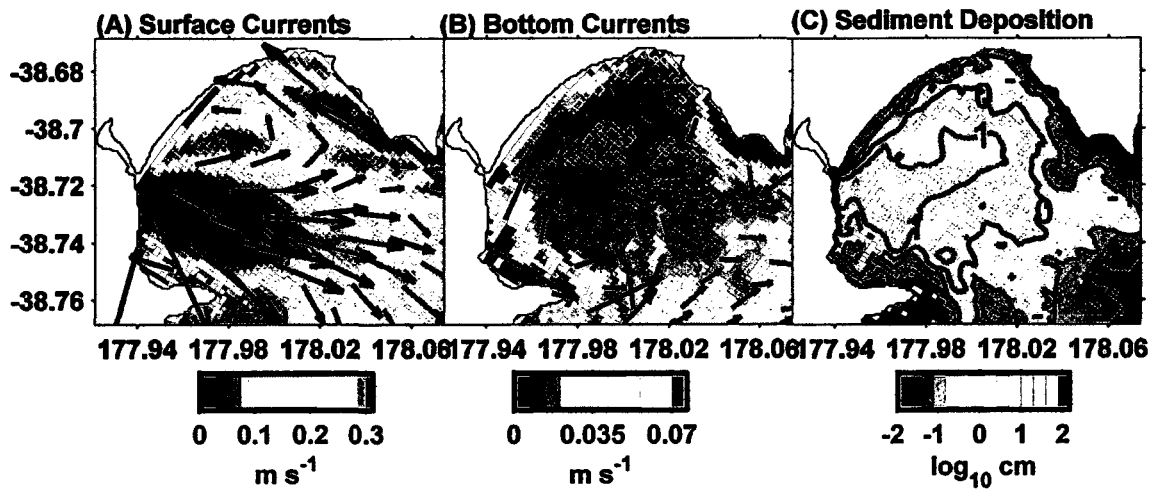
Figure 17. Travel paths of surface introduced (black) and bottom introduced (grey) floats.
(A) Float paths are the average of the first 2 days after the floats were introduced. Panel
A averages 53 floats from each initialization location, spanning the period of 5 January
through 20 April when river discharge was minimal. (B) Float travel paths starting on 28
April, 2006, and progressing through 2 days. Floats were introduced at the black circles.

149
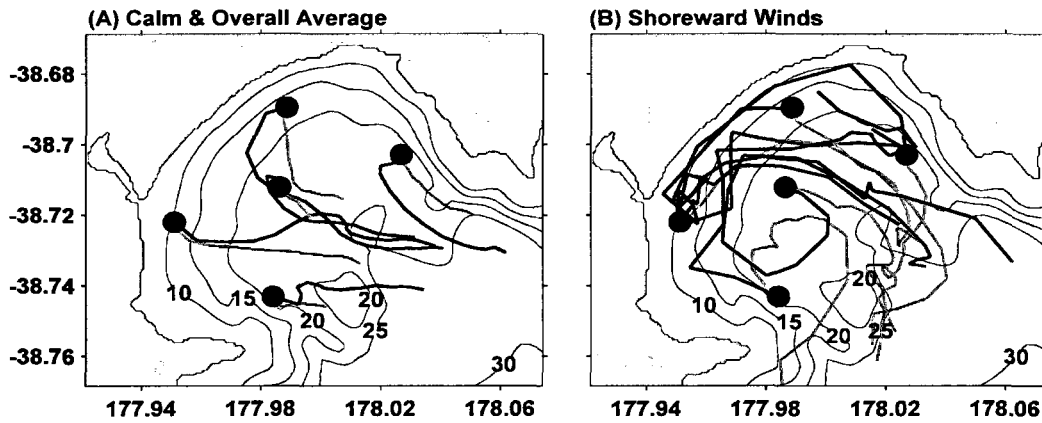
Appendix 3: Extended Model to Data Comparison

Only through comparisons of model estimates to field observations can model performance be evaluated to identify critical areas where either better data, theory, or numerical ability are needed to improve the accuracy of model calculations (special volume highlighted by Lynch et al., 2009). Many model to data comparisons have been conducted for one- and two-dimensional sediment-transport numerical models (see Davies et al., 1997; Traykovski et al., 2007; Wiberg et al., 1994). However, many published three-dimensional models provide, at best, very limited comparisons to data (see Bever et al., 2009; Blass et al., 2007; Harris et al., 2005; Wang et al., 2007), because it is very difficult for three-dimensional models to represent observations collected at single points. Here, an extended comparison of the field observations (Chapter 2) to the model results (Chapter 3) is presented, to show that with the included physical processes and grid resolution the model accurately represents temporally- and/or spatially-averaged patterns in the data, but does not reproduce the available point measurements as well. To limit repetition, this appendix is not written to be a standalone chapter, and assumes the reader has read Chapters 2 and 3, or is familiar with the study location, the observations, and the modeling work. Figures or tables from Chapter 3 pertinent to the model to data comparison are repeated, however.

This appendix is broken into 6 subsections. The first section gives background information on the model skill metrics used here, and also explains Taylor and target diagrams and how they can be used for model validation and intramodel comparisons. The next four sections step through comparisons of the modeled waves, sea surface height, hydrodynamics, and sediment-transport to the available observational data. The

final section summarizes my overall interpretation of how well the model performed within Poverty Bay, based on the available data.

A.1 Methods for Model Skill Assessment

Model skill metrics offer the benefit of being able to use a single quantified number to evaluate a models performance against different formulations of the same model, or against different models altogether (Friedrichs et al., 2009; Sutherland et al., 2004). Many different model skill metrics have been proposed to evaluate numerical models, however (Hetland, 2006; Stow et al., 2009). A consistent use of the same model skill metric is important for evaluation of model performance in different locations, with different numerical or forcing configurations, or when updating to newer model versions (Stow et al., 2009). Within ROMS specifically, Warner et al. (2005) and Haidvogel et al. (2008) used the model skill metric from Wilmott (1981) to evaluate performance. This metric is calculated using the equation,

$$S_W = 1 - \frac{\sum_{i=1}^{N}|X_{Mi} - X_{Oi}|^2}{\sum_{i=1}^{N}\left(\left|X_{Mi} - \overline{X_M}\right| + \left|X_{Oi} - \overline{X_O}\right|\right)^2} \tag{1}$$

where S_W is the model skill, X is the variable being compared, and $\overline{X}$ is the time-averaged value. Subscripts M and O represent modeled and observed values, respectively. A perfect agreement between the model and the observations yields a skill of one, and it decreases toward zero as the model diverges from the observations.

Other model skill metrics evaluate the models skill at reproducing the observations better than some set value(s), such as the mean of the observations or a

climatology value(s) (Hetland, 2006; Sutherland et al., 2004). One of these is calculated as,

$$S_C = 1 - \frac{\sum_{i=1}^{N}\left(X_{Oi} - X_{Mi}\right)^2}{\sum_{i=1}^{N}\left(X_{Mi} - C_i\right)^2} \tag{2}$$

where C is the climatology value(s) (Hetland, 2006). Skill values range from $-\infty$ to 1, with a value of zero representing the same skill as simply using the climatology value(s) and negative skill showing the model performed worse than the climatology. In this Appendix, the mean of the observations was used as the baseline climatology value, C, when calculating the skill metric. This choice of C calculates a model skill score relative to constantly using the mean of the observations. Hetland (2006) and A. Bever (unpublished work) showed this formulation of C to be a rigorous test of a models skill, with values less than zero not uncommon.

Graphical methods of evaluating model skill can make it easier than table presented skill metrics to understand how many different model formulations and even different models perform against one another, although they seem to be rarely used in the hydrological and sedimentological sciences. Two of these methods are the Taylor (Taylor, 2001) and target (Jolliff et al., 2009) diagrams. Examples of their use for oceanographic modeling can be found in a special volume on "Skill assessment for coupled biological/physical models of marine systems" in the Journal of Marine Systems (volume 76) (Lynch et al., 2009).

The Taylor diagram compares the correlation coefficient (r) of the model and observations to the standard deviations (σ) of the model and the observations (Fig. A1)

152

(Taylor, 2001). For clarity, the correlation coefficient (r) is simply the square root of the r^2 values presented on comparison plots. Using Taylor diagrams it is easy to graphically display how different models are more or less correlated to the data and how well the variance in the model estimates, here represented by the standard deviation, represents the variance in the observations. Taylor diagrams have the problem of not representing the bias between the model results and the observations, however, where the bias (B) is simply taken to be the mean of the model estimates minus the mean of the observations, $B = \overline{X_M} - \overline{X_O}$. Model estimates could be perfectly correlated to the data and have the same standard deviation, but have a non-negligible bias and be consistently higher or lower than the observations. As such, Taylor diagrams are acceptable when the bias between the model and the observations is small, but less well suited to when there is a non-negligible bias. Here, the bias is deemed small enough to use a Taylor diagram if it is less than 5% of the mean, for all the points being plotted on a single diagram.

Target diagrams make up for the non-inclusion of the bias in the Taylor diagrams, and are better suited for model estimates that are biased against the observational data (Friedrichs et al., 2009; Jolliff et al., 2009). Target diagrams utilize the bias between the model estimates and the observations, the unbiased Root Mean Square Difference (RMSD), and the total RMSD to evaluate model skill. The unbiased RMSD is:

$$unRMSD = \left(\frac{1}{N} \sum_{i=1}^{N} \left[\left(X_{Mi} - \overline{X_M} \right) - \left(X_{Oi} - \overline{X_O} \right) \right]^2 \right)^{0.5}$$

(3)

which does not take into account any bias between the model estimates and the observations. The total RMSD is a measure of the average magnitude of difference between the model estimates and the observations, and is calculated as:

$$tRMSD = \left[\frac{1}{N} \sum_{i=1}^{N} \left(X_{Mi} - X_{Oi} \right)^2 \right]^{0.5}. \tag{4}$$

In a target diagram the X axis is the unbiased RMSD, while the Y axis is the bias. Once plotted, the distance from the origin to any point on the diagram is equal to the total RMSD. Strictly speaking, the unbiased RMSD must be positive, but is multiplied by the sign of the difference in the modeled and observed standard deviation, $\sigma_d = sign(\sigma_M - \sigma_O)$. This incorporates whether the modeled standard deviation is higher or lower than the observations, thus utilizing both the positive and negative X axes. As such, the true X axis becomes:

$$unRMSD = \left(\frac{1}{N} \sum_{i=1}^{N} \left[\left(X_{Mi} - \overline{X_M} \right) - \left(X_{Oi} - \overline{X_O} \right) \right]^2 \right)^{0.5} * sign\left(\sigma_{XM} - \sigma_{XO} \right). \tag{5}$$

Here, the plotted values are all in the units of the variable being examined. To aid in any intramodel comparison of different variables, the X and Y axes can be normalized by the observed standard deviation (σ_O). After normalization, the X axis becomes unRMSD/σ_O and the Y axis becomes B/σ_O (Fig. A2). When normalized by the standard deviations, as in Fig. A2, any point plotting inside the circle of radius one performed better than simply the mean of the observations. A drawback of the target diagram is that it does not directly give information on the correlation between the model and the observations. The relative correlation between different points can be understood from knowing the bias and the total RMSD, however (see Jolliff et al., 2009).

A.2 Wave Comparison

Using Eqs. (1) and (2), the SWAN model showed good skill in reproducing the observed wave height and orbital velocity in both the coupled and uncoupled model runs (Table A1). Based on Fig. A3 and the Sc skill metric, both wave height and orbital velocity performed better than simply using the observational mean.

A.3 Sea Surface Height

The model very skillfully reproduced the sea surface height at each S4 within Poverty Bay using 11 tidal constituents (Table A2). Here, the sea surface height of the observations is the total water depth minus the mean of each deployment, to highlight the tidal and longer time-scale sea surface height excursions about the mean water depth. The modeled sea surface height is the excursion above or below a zero starting value. Fig. A4A quantifies and highlights the high correlation and nearly identical standard deviations between the model and the observations that is shown in more traditional figures (Fig. A5). Fig. A4A also highlights that the use of 11 instead of 4 tidal constituents improved the models ability to estimate the astronomic tides.

The 33 hr low-pass filtered sea surface height shows the model did not perform as well for long time-scale sea surface height excursions, such as wind induced setup or setdown, as for predominantly tidal fluctuations (Figs. 4B and 6, Table A2). Wind induced setup and setdown was not captured by the model to the magnitude that it occurred in the observations. Thus, even though both the model and the observations fluctuated from a zero sea surface height, and the model showed a very low bias, the overall magnitude of the fluctuations were much lower than observed. Some of this

mismatch is inherently due to the small size of the model domain. Other sources of error could potentially come from the observations themselves, such as fouling or other malfunctioning of the instrumentation, although this is not likely in this case due to the nearly perfect correlation of all 3 instruments throughout the deployments.

A.4 Hydrodynamics

The model reproduced the overall depth-averaged counterclockwise circulation seen within Poverty Bay by other studies (Fig. A7) (see figures in Stephens et al., 2002 for observations). The model did not reproduce the averaged shoreward current at each S4 location well (Fig. A8) (Table A3). The model did estimate shoreward currents from wave generated Stokes drift within the nearshore domain of Poverty Bay, but the resolution of the model grid did not adequately represent the bathymetric gradients in the nearshore zone, however. This made it very difficult for the model to estimate currents at specific points, such as the S4s, that were very near a closed boundary (the shoreline) and within such a dynamic environment. The model did capture the overall across-shore and alongshore toward the south flow that was observed within the observations, highlighting that the model was representing the physics driving the system, even though the horizontal resolution was not adequate to completely reproduce the observations. To better match the instantaneous current observations at the exact locations of the S4 instrumentation, a nested modeling scenario would be very beneficial. This would have allowed for the incorporation of a finer resolution nearshore model grid, and, presumably, better captured the dynamics that are driven by both the physics within the system and

the large bathymetric gradients. Nesting capability has not currently been incorporated into the Rutgers version of ROMS, however.

The model estimated currents at the S4 locations were significantly different when ROMS and SWAN were run independently and the nearshore calculations were neglected, with observed current speeds much better represented by the fully coupled system (Fig. A8). When the waves and hydrodynamics were calculated independently of one another, the model underestimated current speed along the 10 m isobath of Poverty Bay by a factor of about 2 to 8 (Fig. A8). That is, modeled current speeds that simplified nearshore processes were much slower than the observations. This highlighted the importance of including the physics behind wave driven currents in three-dimensional models of systems with significant wave action, especially when considering shallow water.

A.5 Sediment

The suspended sediment concentration within the model was well correlated to the turbidity observations at the ADCP (r = 0.78) (Fig. A9). Periods of high turbidity, in both the model results and the observations, coincided with times of elevated river discharge on 28 April through 9 May, 20-24 July, and 7-10 August. Following discharge, turbidity in the model results and the observations decreased. Turbidity was again elevated during periods of energetic waves that followed elevated discharge, such as those on 15-18 May and 16 August. Both the model and the data indicated that turbidity within the water column decreased to near a low background value within about three weeks following a discharge pulse (roughly 9-28 May and 10 August through 5

September). Model skill could not be directly evaluated because of a lack of calibration of the ADCP turbidity to suspended sediment concentration, however.

Fig. A10 shows the model also reproduced the timing and the approximate depositional and erosional thicknesses seen in 15 m water depth offshore of the Waipaoa River during elevated discharge and wave resuspension events. In the model and the observations, elevated river discharges from 20-24 July and 7-10 August both caused between 10 and 15 cm of sediment deposition at this location. Subsequent wave resuspension events on 26-29 June and 16 August completely removed these modeled and observed deposits. Over the course of the 1.5 months of deposition and erosion shown on Fig. A10, both the model results and the observations converged to a net deposition of about 2 cm.

Even though Fig. A10 shows the model captured the temporal trend in the seabed elevation, all the statistics of model skill are low (r=0.05, Sw = 0.37, Sc = -3.38). Some reasons why the skill metrics are poor are related to both the data and the model estimates; 1) The spikes in the data are not real deviations in the seabed, and as such hamper the quantitative validation of the model. 2) The model estimates are output in the units of kg m^{-2}, which were converted directly to units of mm of thickness assuming a porosity of ~65% throughout the seabed. Better estimates of porosity and a better conversion to actual depositional thickness would require a seabed consolidation and compaction sediment module within ROMS. This is not available in the ROMS source code, however. 3) A flocculation routine would allow the settling velocity of the sediments to increase or decrease dependent on the oceanographic conditions and the suspended sediment concentration. An increase in flocculation following flooding may reduce the

saw tooth shape of the modeled deposition thickness by allowing the sediment to settle to

the seabed faster. Floc breakup during wave events would then allow the dispersal of

sediment out of Poverty Bay. 4) The model may not be capturing all the necessary

processes to completely represent the data. This is highlighted from roughly 7-10 August,

when a fluid-mud type layer occurred near the seabed in the data but was not reproduced

within the model. The model lacks the vertical resolution to capture this small-scale (~15

cm) process. Because the model is not capturing the fluid-mud layer, it shows no

sediment deposition until the currents and waves subside during 10 August. The

reduction in current and wave strength allows sediment to now be deposited on the

seabed, corresponding to a time when the observed fluid mud was consolidating into a

more solid seabed.

Sediment deposition, resuspension, and redistribution over the course of the 5

month winter season created a seabed surface grain size distribution that matched with

observations collected around the same time as the observations (late 2005 through 2006)

(Fig. A11). Both the model and the observations show coarser sediment nearshore of the

about 10 m isobath, due to the higher wave induced seabed stresses in the nearshore.

Also, the relatively finer sediment is confined to primarily the southern side of the bay

near the river mouth, and the deeper middle portion near the mouth of the bay.

Disregarding the location of dredge spoil disposal, the northern corner of the bay has

relatively coarser sediment in both the model and the observations.

A.6 Overall Model Performance

The ROMS and SWAN models reproduced spatial and temporal patterns within Poverty Bay very well. The SWAN model with Wave Watch 3 open boundary conditions reproduced the spatial structure of the significant wave height and bottom orbital velocity. This fed back into the shear stress calculations and the modeled surface grain size distributions, of which Fig. A11 shows the surface grain size distribution pattern closely matched the observations. The pattern of overall counterclockwise circulation within Poverty Bay was reproduced. The model also accurately reproduced the averaged southward alongshore current flow that helps build a spit across the mouth of the Waipaoa River during low discharge periods.

Instantaneous point measurements were not represented by the model as well as the spatial patterns, although the model did capture the general trends of each variable at each measurement location. As highlighted earlier, this shows the difficulty of comparing model estimates generated on a finite grid to point measurements. The models capture of the correct trends in different variables, such as shoreward and alongshore to the south currents at the S4s and repeated deposition and erosion at the ADV, and the relatively correct magnitudes of the variables is taken here to show that the model reproduced the observations with enough skill to validate conclusions generated from the numerical model.

Overall, the model performed well with the specified physical processes and with a model grid, 180x115x20 cells, that was numerically feasible. The inclusion of the physics and/or vertical resolution needed to model a near-bed fluid mud layer may have improved the seabed elevation comparison at the beginning of the discharge pulse near 7

August. A flocculation routine may have also improved the elevation comparison. Increasing the horizontal resolution within Poverty Bay may have allowed the model to better match the bathymetric structure in the nearshore and better match the currents at each S4. The model runs presented here, however, took ~4 days to complete the January-September simulation. A decrease in the horizontal grid size by half would increase the runtime by 4 times and make this length of model runs not feasible. A nested modeling setup could reduce this extra runtime, but is not available in the ROMS source code.

References

Bever, A.J., Harris, C.K., Sherwood, C.R. and Signell, R.P., 2009. Deposition and flux of sediment from the Po River, Italy: An idealized and wintertime numerical modeling study. Mar. Geol., 260(1-4): 69-80. doi:10.1016/j.margeo.2009.01.007.

Blass, M., Dong, C., Marchesiello, P., McWilliams, J.C. and Stolzenbach, K.D., 2007. Sediment-transport modeling on Southern Californian shelves: A ROMS case study. Cont. Shelf Res., 27: 832-853.

Davies, A.G., Ribberink, J.S., Temperville, A. and Zyserman, J.A., 1997. Comparison between sediment transport models and observations made in wave and current flows above plane beds. Coastal Engineering, 31: 163-198.

Friedrichs, M.A.M., Carr, M., Barber, R.T., Scardi, M., Antoine, D., Armstrong, R.A., Asanuma, I., Behrenfeld, M.J., Buitenhuis, E.T., Chai, F., Christian, J.R., Ciotti, A.M., Doney, S.C., Dowell, M., Dunne, J., Gentili, B., Gregg, W., Hoepffner, N., Ishizaka, J., Kameda, T., Lima, I., Marra, J., Melin, F., Moore, J.K., Morel, A., O'Malley, R.T., O'Reilly, J., Saba, V.S., Schmeltz, M., Smyth, T.J., Tjiputra, J., Waters, K., Westberry, T.K., Winguth, A., 2009. Assessing the uncertainties of model estimates of primary productivity in the tropical Pacific Ocean. J. Mar. Syst., 76: 113-133.

Haidvogel, D.B., Arango, H., Budgell, W.P., Coruelle, B.D., Curshitser, E., Lorenzo, E.D., K.Fennel, Geyer, W.R., Hermann, A.J., Lanerolle, L., Levin, J., McWilliams, J.C., Miller, A.J., Moore, A.M., Powell, T.M., Schepetkin, A.F., Sherwood, C.R., Signell, R.P., Warner, J.C., Wilkin, J., 2008. Regional ocean forecasting in terrain-following coordinates: Model formulation and skill assessment. Journal of Computational Physics, 227: 3595-3624.

Harris, C.K., Traykovski, P.A. and Geyer, W.R., 2005. Flood dispersal and deposition by near-bed gravitational sediment flows and oceanographic transport: A numerical modeling study of the Eel River shelf, northern California. J. Geophys. Res., 110(C09025, doi10.1029/2004JC002727).

Hetland, R.D., 2006. Event-driven model skill assessment. Ocean Model. Online, 22: 214-223.

Jolliff, J.K., Kindle, J.C., Shulman, I., Penta, B., Friedrichs, M.A.M., Helber, R., Arnone, R.A., 2009. Summary diagrams for coupled hydrodynamic-ecosystem model skill assessment. J. Mar. Syst., 76(2009): 64-82.

Lynch, D.R., jr., D.J.M. and Werner, F.E., 2009. Skill assessment for coupled biological/physical models of marine systems. J. Mar. Syst., 76: 1-3.

Stephens, S., Bell, R.G. and Black, K.P., 2002. Complex circulation in a coastal embayment: Shelf -current, wind and density-driven circulation in Poverty Bay, New Zealand. J. Coast. Res., 34. Special Issue. 45-59

Stow, C.A., Jolliff, J., jr., D.J.M., Doney, S.C., Allen, J.I., Friedrichs, M.A.M., Rose, K.A., Wallhead, P., 2009. Skill assessment for coupled biologocal/physical models of marine systems. J. Mar. Syst., 76: 4-15.

Sutherland, J., Peet, A.H. and Soulsby, R.L., 2004. Evaluating the performance of morphological models. Coastal Engineering, 51: 917-939.

Taylor, K.E., 2001. Summarizing multiple aspects of model performance in a single diagram. J. Geophys. Res., 106(D7): 7183-7192.

Traykovski, P., Wiberg, P.L. and Geyer, W.R., 2007. Observations and modeling of wave-supported sediment gravity flows on the Po prodelta and comparison to prior observations from the Eel shelf. Cont. Shelf Res., 27(4-3): 375-399.

Wang, X.H., Pinardi, N. and Malacic, V., 2007. Sediment transport and resuspension due to combined motion of wave and current in the northern Adriatic Sea during a Bora event in January 2001: A numerical modeling study. Cont. Shelf Res., 27: 613-633.

Warner, J.C., Geyer, W.R. and Lereczak, J.A., 2005. Numerical modeling of an estuary: A comprehensive skill assessment. J. Geophys. Res., 11(C05001): doi:10.1029/2004JC002691.

Wiberg, P.L., Drake, D.E. and Cacchione, D.A., 1994. Sediment resuspension and bed armoring during high bottom stress events on the northern California inner continental shelf: measurements and predictions. Cont. Shelf Res., 14: 1191-1219.

Wilmott, C.J., 1981. On the validation of models. Physical Geography, 2: 184-194.

Table A1. Modeled and observed wave statistics from three locations within Poverty Bay. Sw stands for the skill based on that of Wilmott (1981), Eq. (1) and Sc for that of Hetland (2006), Eq. (2). See text for more information.

Wave Metric	Wave Station Location	Wave Source	Mean	Standard Deviation	Correlation Coefficient	Bias	Sw	Sc
Height	North	Observation	0.96	0.51	0.69	-0.03	0.82	0.45
		Modeled	0.93	0.60				
	Mouth	Observation	0.85	0.48	0.80	0.07	0.87	0.63
		Modeled	0.92	0.63				
	South	Observation	0.75	0.40	0.87	0.12	0.90	0.70
		Modeled	0.87	0.51				
Orbital Velocity	North	Observation	0.31	0.14	0.75	0.00	0.84	0.56
		Modeled	0.31	0.18				
	Mouth	Observation	0.33	0.15	0.74	-0.05	0.83	0.48
		Modeled	0.28	0.18				
	South	Observation	0.28	0.12	0.78	-0.02	0.87	0.59
		Modeled	0.26	0.14				

Table A2. Modeled and observed statistics at each S4 location for the sea surface height and the 33 hr low-pass filtered sea surface height. Sw stands for the skill based on that of Wilmott (1981), Eq. (1) and Sc for that of Hetland (2006), Eq. (2). See text for more information.

Variable	Station Location	Source	Standard Deviation (m, m s^{-1})	Correlation Coefficient	Bias (m, m s^{-1})	Sw	Sc
Sea Surface Height	North	Observation	0.45	0.93	-0.01	0.96	0.86
		Model	0.44				
	Mouth	Observation	0.45	0.94	0.00	0.97	0.87
		Model	0.44				
	South	Observation	0.45	0.94	0.00	0.97	0.87
		Model	0.44				
Sea Surface Height, Low-pass Filtered	North	Observation	0.08	0.20	-0.01	0.23	-28.88
		Model	0.01				
	Mouth	Observation	0.06	0.35	0.00	0.35	-14.21
		Model	0.02				
	South	Observation	0.07	0.26	0.00	0.32	-13.67
		Model	0.02				

Table A3. Modeled and observed statistics for the currents at the exact locations as the S4 instrumentation. Across-shore and alongshore are for the current speed in those directions. Current speed coupled is for the magnitude of the current speed from the ROMS/SWAN coupled model run at each S4. Sw stands for the skill based on that of Wilmott (1981), Eq. (1) and Sc for that of Hetland (2006), Eq. (2). See text for more information.

Variable	Station Location	Source	Mean (m s^{-1})	Standard Deviation (m s^{-1})	Correlation Coefficient	Bias (m s^{-1})	Sw	Sc
Across-shore	North	Observation	-0.10	0.04	-0.29	0.10	0.27	-0.18
		Model	0.00	0.04				
	Mouth	Observation	-0.11	0.07	-0.12	0.14	0.34	-0.23
		Model	0.03	0.03				
	South	Observation	-0.12	0.09	-0.15	0.14	0.38	-0.43
		Model	0.02	0.05				
Alongshore	North	Observation	-0.14	0.09	-0.41	0.02	0.16	-3.18
		Model	-0.12	0.06				
	Mouth	Observation	-0.14	0.06	-0.49	0.16	0.25	-0.28
		Model	0.02	0.07				
	South	Observation	-0.08	0.06	-0.37	0.15	0.19	-0.26
		Model	0.07	0.11				
Current Speed Coupled	North	Observation	0.18	0.08	-0.33	-0.05	0.25	-1.48
		Model	0.13	0.06				
	Mouth	Observation	0.17	0.09	0.51	-0.11	0.53	-0.21
		Model	0.06	0.05				
	South	Observation	0.17	0.07	0.67	-0.06	0.73	0.39
		Model	0.11	0.09				

Figure A1. Sample Taylor diagram. The X, lower, axis is the standard deviation of the model results normalized by the standard deviation of the observations. Lines that radiate from the center to the outer hemisphere represent the correlation coefficient of the model results and the observations, with values to the right representing a positive correlation and values to the left representing a negative correlation. Concentric circles highlight normalized standard deviation distances from the center. Naturally, the observations lie at a normalized standard deviation and a correlation coefficient of 1, and are highlighted here by the black diamond. Note the maximum of the X axis is arbitrary here, and will depend on the actual comparison of the model estimates and the observations.
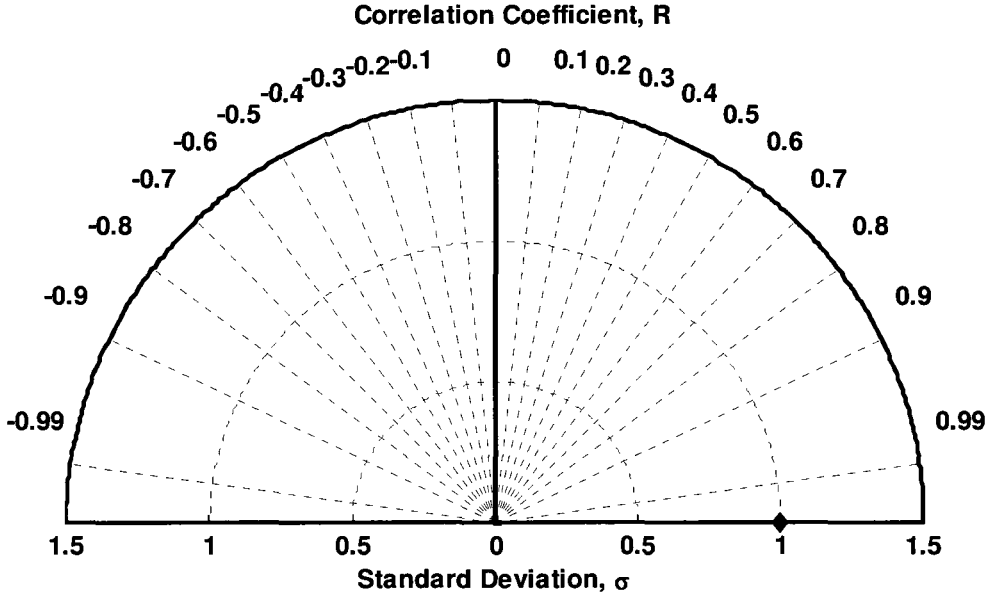
Figure A2. Sample target diagram with the axes normalized by the observed standard deviation.
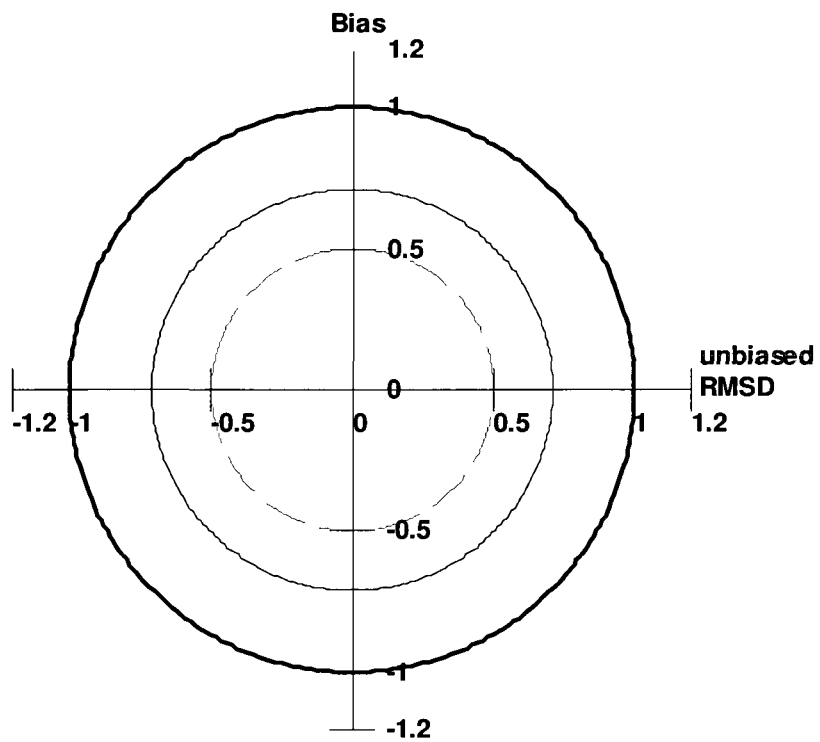
Figure A3. Target diagram showing the model skill at reproducing the observed significant wave height and orbital velocity at the three S4 locations.
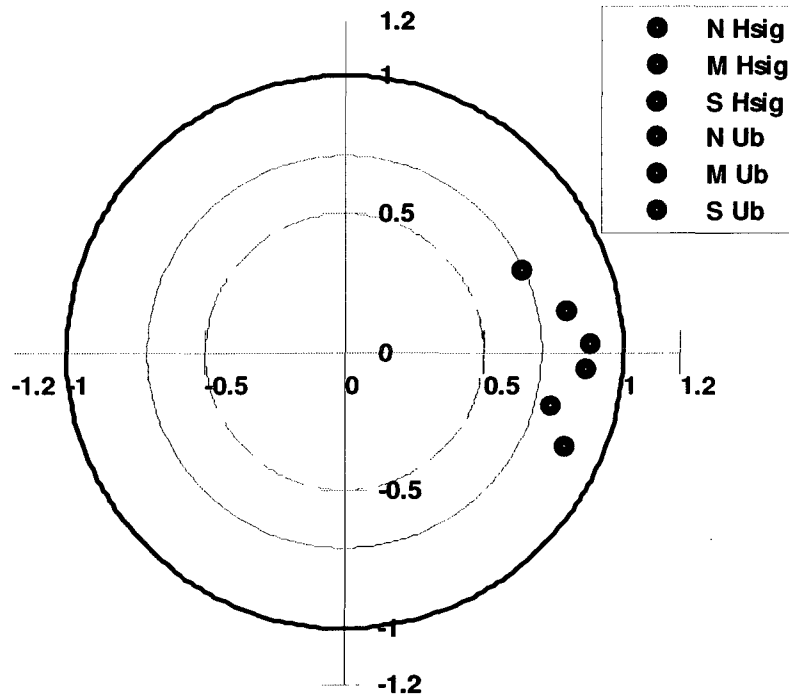
Figure A4. Taylor diagrams showing how well the (A) modeled sea surface height and
(B) low-pass filtered (33 hr) sea surface height model results matched the observations.
The station offshore of the river mouth (M ssh) is underneath the red dot in panel A. 11C
corresponds to the model run using 11 tidal constituents, 4C the run using 4 tidal
constituents.
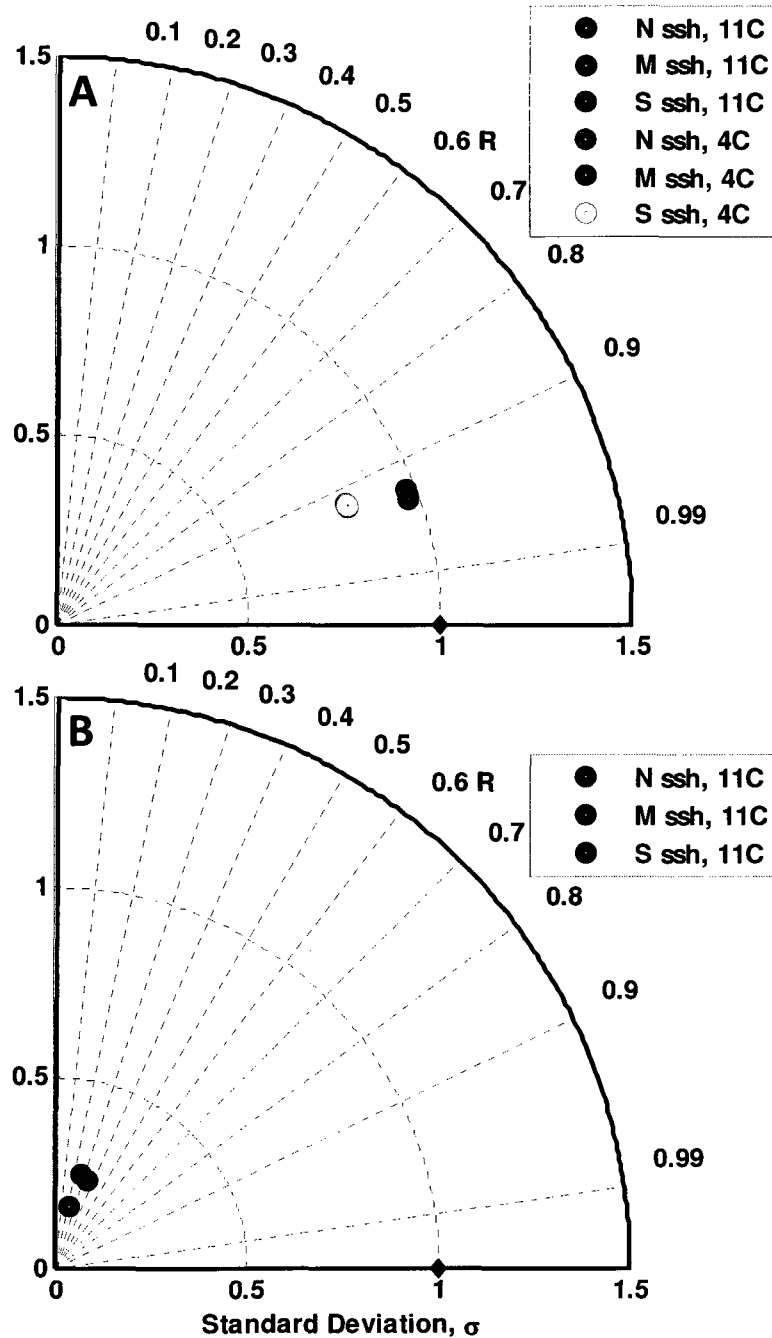
Figure A5. Sea surface height at the northern S4 location during the elevated discharge period in May. The data shown was truncated because the comparison becomes impossible to see with longer-timeframes.
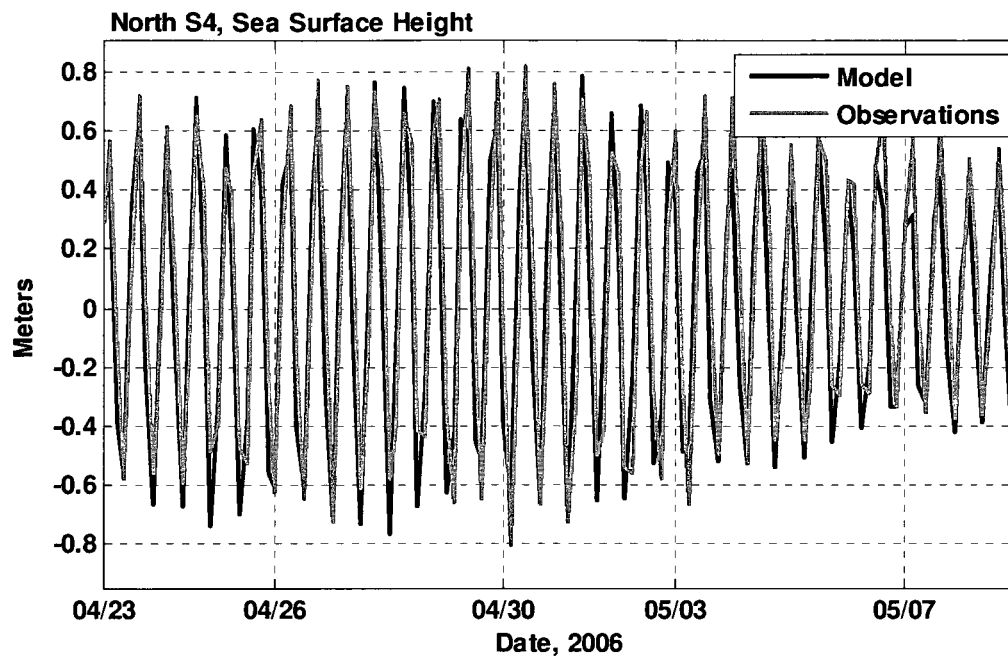
Figure A6. Lowpass filtered sea surface height. Zero represents the overall mean at that location.
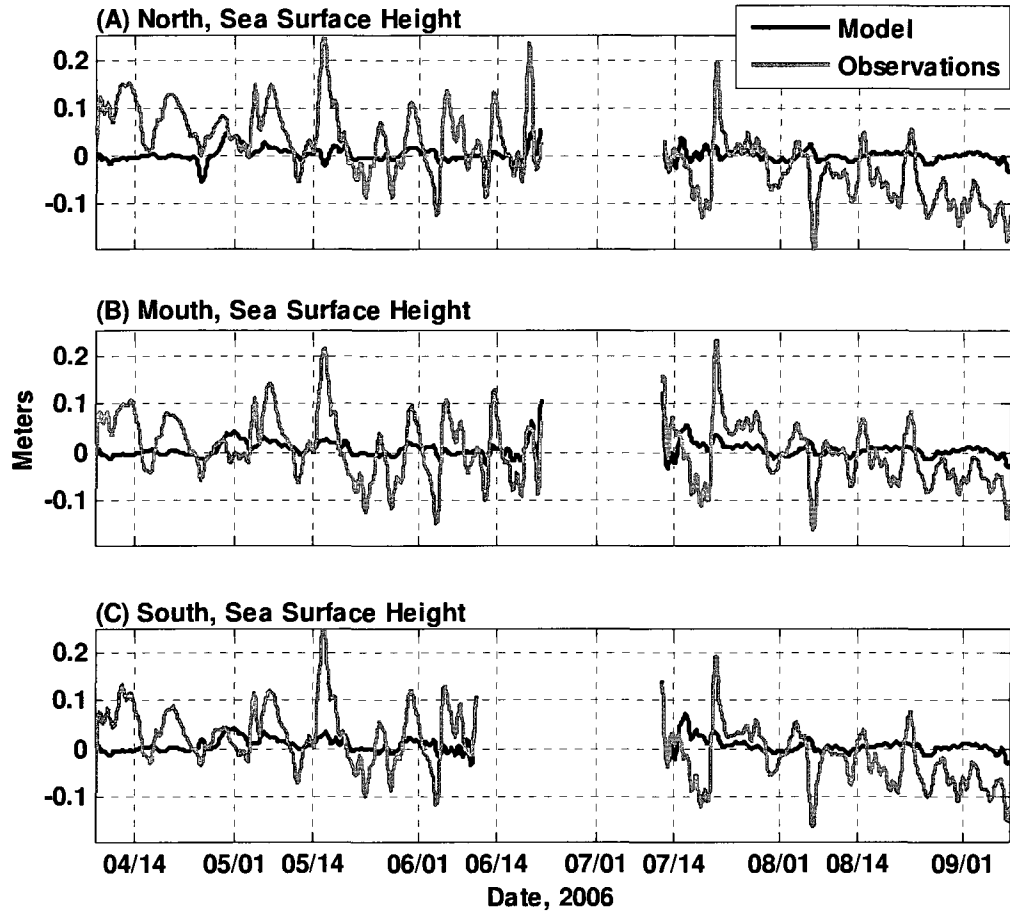
Figure A7. Time- and depth-averaged current speed (colors) and vectors (arrows) over the January through September, 2006 simulation.
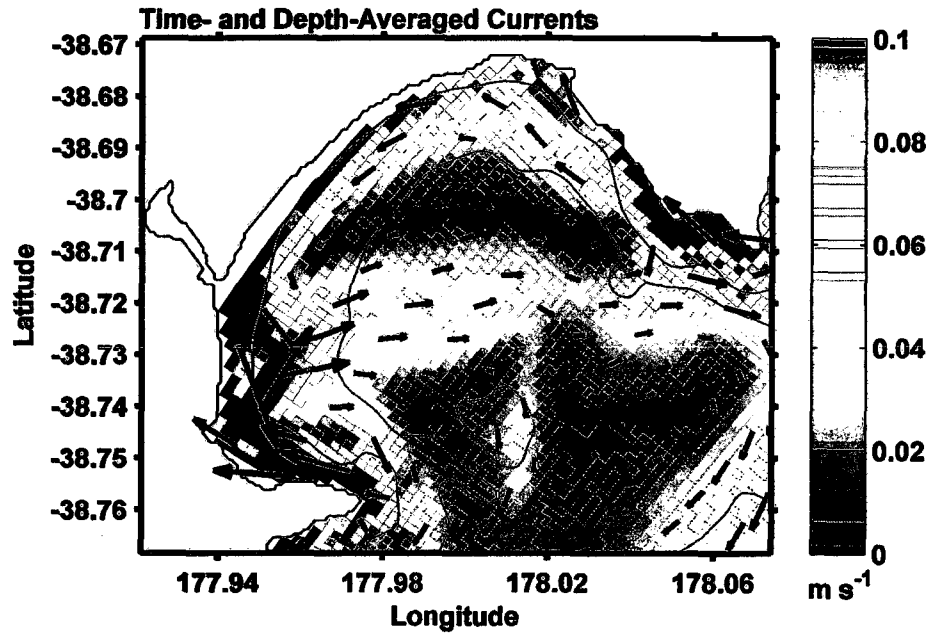
Figure A8. (A) Across-shore and (B) alongshore current speed at the northern S4 for model runs where ROMS and SWAN were run two-way coupled (black line) and independently (blue line).
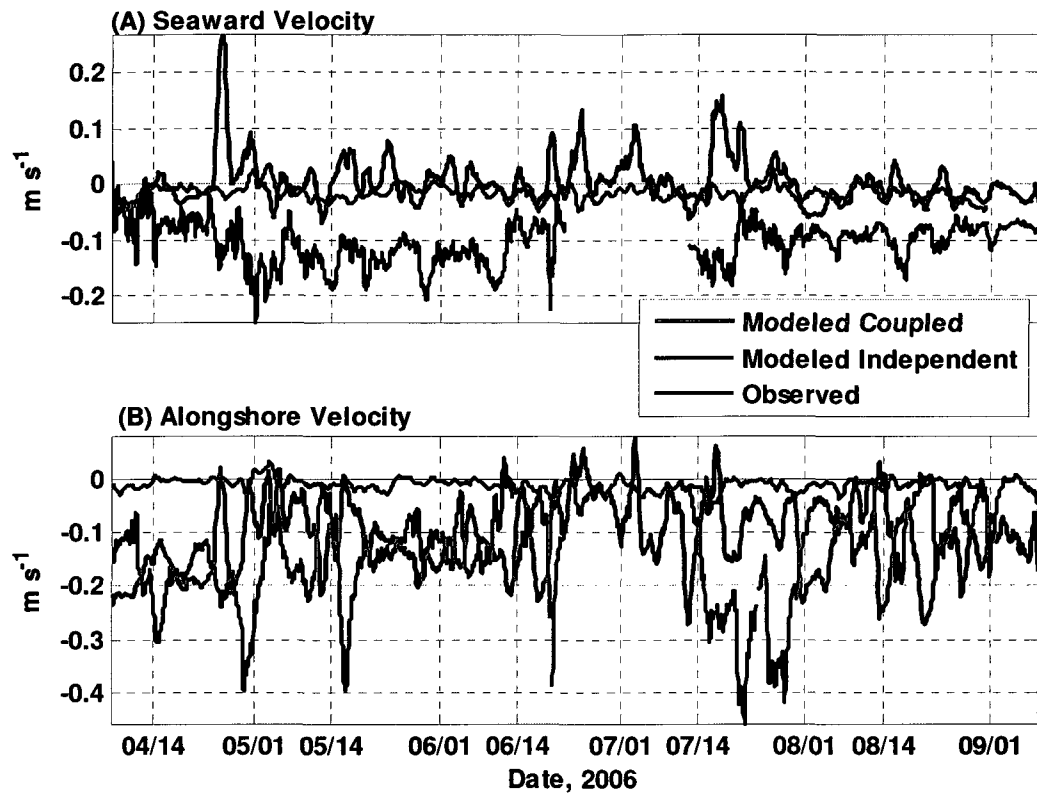
Figure A9. Modeled and observed depth-averaged turbidity at the ADCP location. Values were normalized by the maximum values of the model estimates (kg m^{-3}) and the data (decibels), and are shown as the 27 hour running-mean.
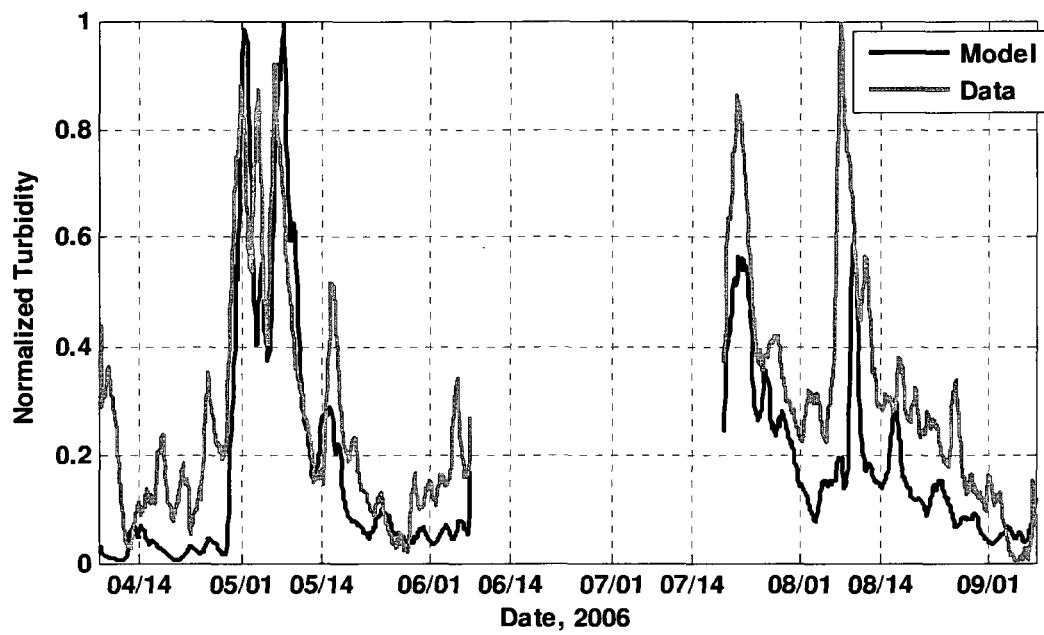
Figure A10. Modeled and observed sediment deposition in centimeters at a location offshore of the river mouth (ADCP/ADV location). Modeled deposit mass was converted to thickness assuming a porosity of ~65%, causing the modeled kg m^{-2} to directly equal mm of deposition. The model and observations are shown relative to their seabed elevation on 22 July, 2006, to highlight the relative changes over the same time-period.
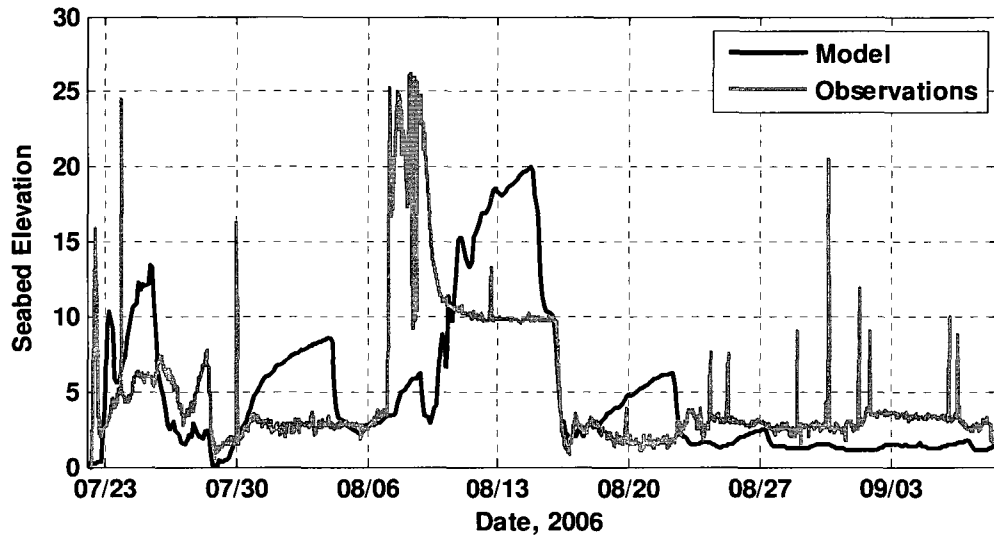
Figure A11. (A) Modeled grain size distribution, as averaged over the top 1 cm of the seabed. (B) Observed seabed surface percent sand fraction, from H. Wadman (USACE).

A. Modeled Average Surface Grain Size
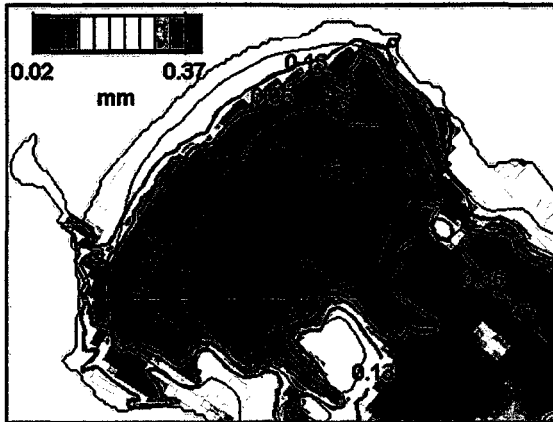
B. Observed Percent Sand
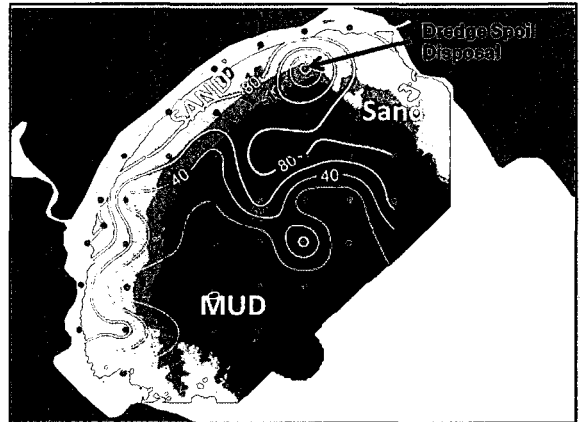
Chapter 4: Variations in sediment-transport and sorting between different dispersal basin geometries: A case study of Poverty Bay, New Zealand

ABSTRACT

Poverty Bay plays a significant role in the Waipaoa River sedimentary dispersal system. It has acted as a sediment sink over the past 7,000 years, and processes within the bay significantly modify the fluvial sedimentary signal en route to the continental shelf. In this Chapter numerical modeling experiments explore the role that basin geometry and river mouth configuration have played in sediment retention within and export from Poverty Bay. The Simulating Waves Nearshore (SWAN) model coupled to the Regional Ocean Modeling System (ROMS) numerically estimated wave characteristics, current velocities, and sediment-transport within Poverty Bay. Three different bay geometry and river mouth combinations were investigated; (1) the modern bay, (2) the modern bay circa 2 kya when the river mouth discharged at the bay's northern end, and (3) maximum marine transgression (~7 kya) when the shoreline was 12 km landward of its present position. Modeled representations of realistic yearly floods and a 40 year recurrence interval storm were conducted using present-day and pre-anthropogenic sediment loads. Model estimates were analyzed to characterize the wave energy, sediment-transport dynamics, sediment preservation, and coarse and fine sediment segregation for these configurations.

Dispersal patterns were sensitive to river mouth orientation, shoreline position, and sediment load. Model estimates indicated that changes to river mouth configuration could generate subtle changes to sediment export from the bay. Of the processes considered, however, the wave sheltering effect generated by basin geometry provided the most dominant control on sediment dispersal. Wave height on an along-bay transect of the 7 kya bay varied inversely with shoreline progradation rate along the same transect, indicating a link between wave energy, sediment retention, and shoreline progradation. Higher wave energy and proximity between the river mouth and continental shelf have led to increased export of sediment from the modern bay and coarsened sediment supply to the continental shelf, compared to the 7 kya bay. Relative to the modern bay, the 7 kya bay less effectively segregated sediment by size and retained more sediment, which likely fueled the rapid shoreline progradation occurring at that time.

1. Introduction

During the last sea level lowstand, rivers incised valleys on what are now coastal plains and the continental shelf (Blum and Tornqvist, 2000). From about 16,000 years ago (16 kya) to 7 kya sea level rose rapidly and created estuaries where a river discharged into newly flooded relict river valleys (Kennett, 1982 and references therein). As these rivers continued to supply sediment, shorelines in some of these estuaries prograded as the paleo river valleys infilled, increasing its coastline's exposure to oceanic conditions (Dalrymple et al., 1994; Roy et al., 1980). This infilling of river-incised valleys has been noted worldwide (examples in Dalrymple et al., 1994), such as the Mont-Saint-Michel Bay in northwest France (Tessier et al., 2010), southwest Australia (Roy et al., 1980), and Poverty Bay in New Zealand (Brown, 1995). As shorelines prograded, the sediment deposited on adjacent continental shelves coarsened over time, so that sediment cores offshore of these systems record coarsening upward sequences (Mountain et al., 2007 and references therein), with Rose et al. (2010) showing a consistent coarsening upward sequence in the sedimentary record seaward of Poverty Bay. This feature has been attributed to reduced sediment trapping within the estuaries and the increased proximity of the sediment sources to the locations of accumulation (Mountain et al., 2007; Wright, 1985).

Morphological models have been able to represent shoreline progradation and coarsening upward trends over fairly long time-scales (thousands of years) by simplifying the physical processes that act to redistribute sediment, using generalized model domains, and/or idealized boundary conditions (Hutton and Syvitski, 2008; Mountain et al., 2007; Paola, 2000; Syvitski et al., 2007), for example the Kura delta (Hoogendoorn et al., 2008),

the Eel River continental shelf and Knight Inlet (Morehead et al., 2001), and the Waipaoa River continental shelf (Kettner et al., 2009). This thousands of year modeling approach, however, requires the parameterization of important system drivers, such as storm frequency, river discharge, and/or wave resuspension events (Paola, 2000).

Gradations in the physical energy levels at the coastline, and within estuaries and embayments, as the shoreline prograes will influence sediment retention within and export from the estuary (Blum and Tornqvist, 2000; Sommerfield et al., 2007). As the distance from the river mouth to the open ocean increases, sheltering reduces the wave energy present within the embayment capable of mobilizing sediment (Caliskan and Valle-Levinson, 2008; Frihy, 2009; Hicks and Hume, 1996). Changes to basin geometry also modify current velocities and estuarine circulation, both of which influence sediment deposition and transport within the estuary (Chatwin, 1976; Hansen and Rattray, 1965; Lin and Kuo, 2001; Traykovski et al., 2004). While many short-term (daily to yearly) process based three-dimensional modeling studies have focused on the waves, currents, and dispersal of sediment within estuarine and bay systems (see Chen et al., 2009; Lin and Kuo, 2003; Sheng et al., 2010; Warner et al., 2005a), few of these have attempted to address longer-term (thousands of years) trends.

This study explored how basin shape and sediment-transport processes may have influenced each other as river-associated shorelines prograded since the last marine transgression. Toward this goal, sediment-transport within an embayment and estimated sediment export to the proximal continental shelf based on calculations that accounted for physical processes and marine dispersal were quantified. In doing so, this study also worked to better understand how long-term (~10 ky) trends observed in continental shelf

sediment cores relate to the short term (weeks to months) physical processes within the estuarine portion of the dispersal system. To this end, Poverty Bay, New Zealand, was used as a case study to investigate how waves, currents, and gravity-driven transport influenced sediment dispersal for differing bay geometries, river mouth orientations, and sediment loads. Specifically, this Chapter used a seasonal time-scale process-based three-dimensional numerical model to explore; 1) The degree to which sediment dispersal, basin shape, and marine energy levels explain shoreline progradation rates within Poverty Bay. 2) How sediment sorting and segregation of coarse and fine sediment within Poverty Bay have changed since the maximum marine transgression? 3) Whether changes to sediment dispersal and wave energy within Poverty Bay since the maximum transgression can explain grain size changes over the same time-period observed in sediment cores on the adjacent shelf? 4) How an increased sediment load since European colonization has impacted marine sediment dispersal in the Waipaoa Sedimentary System?

2. Background

This section presents background on sediment-transport on the continental shelf and within estuaries or drowned river valleys, followed by a description of the study area.

2.1 Sediment Dispersal

River discharges provide the largest source of sediment to the coastal ocean (Milliman and Meade, 1983; Milliman and Syvitski, 1992). Typically, fluvial plumes have a water density below that of the surrounding ocean water, in which case they are called hypopycnal plumes (Geyer et al., 2004). Studies have shown that even under

182

hypopycnal discharge conditions, however, most sediment quickly settles from the river plume and is typically transported near the seabed (Geyer et al., 2004; Hill et al., 2000; Milligan et al., 2007). Conversely, hyperpycnal river plumes occur under extremely high sediment loads when the density of the water and sediment mixture exceeds that of the surrounding ocean water and the river plunges below the saline oceanic water (Dadson et al., 2005; Hicks et al., 2004; Mulder et al., 2003). Although few observations exist, it seems that under hyperpycnal conditions the water and sediment may be transported down-slope as a gravity-driven flow near the seabed (Milliman et al., 2007; Warrick and Milliman, 2003; Warrick et al., 2008).

Wright and Coleman (1973) and Zaitlin et al. (1994) proposed that the relative magnitude of river discharge and the oceanographic energy available to transport sediment was the dominant factor influencing the character of sediment deposits seaward of river mouths. Once deposited on the seabed, sediment may be resuspended by energetic waves and currents that impart bed stress (Madsen, 1994; Soulsby et al., 1993). On many continental shelves wave induced bed stresses dominate the total seabed stress and cause the majority of sediment resuspension (Butman et al., 1979; Drake and Cacchione, 1985; Fain et al., 2007; Green et al., 2004). Because of this, sheltered locations where wave energy may be blocked or attenuated tend to experience more net deposition than exposed areas (Frihy, 2009). Sediment is mobilized when the stress on the seabed exceeds a critical value, called the critical shear stress (Wiberg and Smith, 1987). It can then move along the seabed as bedload or be completely suspended into the water column and travel in the direction of ambient currents (Meyer-Peter and Muller, 1948; Soulsby, 1997; Soulsby and Damgaard, 2005). Suspended sediment concentrations

create feedbacks for transport, both by increasing density stratification (Hill and McCave, 2001; Traykovski et al., 2007), and also at sufficiently high concentrations, by creating down-slope forces that drive gravity flows (Sternberg et al., 1996; Wright and Friedrichs, 2006). The relative importance of sediment-transport mechanisms such as plume transport, suspension, bed-load, and gravity flows depends on sediment characteristics, bed stresses, bathymetric slope, and the current shear within the water column. These often combine to create complicated dispersal patterns and non-uniform deposits on the continental shelf offshore of river mouths (Sommerfield et al., 2007).

Sediment distributions offshore of small rivers on active continental shelves, such as the Eel River in northern California and New Zealand's Waiapu River, generally become finer with distance from the river mouth as the coarser sediment settles to the seabed and is preferentially deposited (Crockett and Nittrouer, 2004; Kniskern et al., 2010; Sommerfield et al., 2007; Wright, 1985). As such, sand is deposited near the shoreline, while silt and clay travel greater distances from the river mouth and are often deposited within a mud belt on the middle continental shelf (Crockett and Nittrouer, 2004; Kniskern et al., 2010; Miller and Kuehl, 2010; Sommerfield and Nittrouer, 1999). Although recent studies have noted the non-negligible deposition of fine sediment in water as shallow as 10 to ~30 m offshore of river mouths on energetic active margins (Chapter 2; Crockett and Nittrouer, 2004; Wadman and McNinch, 2008), transport mechanisms in general act to segregate the coarser sands from the finer sediment. Depositional and dispersal patterns and the mechanisms behind sediment segregation respond to sediment supply, the geometry of the dispersal basin, and the oceanographic

forces within the sedimentary system, all of which may evolve with time (Blum and Tornqvist, 2000; Sommerfield et al., 2007).

When a river discharges to an embayment, estuarine processes influence sediment-transport and deposition. Estuaries are dynamic regions that primarily trap sediment in the bottom boundary layer where baroclinic pressure gradients typically create landward flows directed up-estuary (Festa and Hansen, 1978; Hansen and Rattray, 1965; Hetland and Geyer, 2004). Sediment is trapped in turbidity maximum within estuaries, at locations where stratification breaks down and at the landward edge of salt intrusion (Geyer, 1993; Lin and Kuo, 2001). As estuaries and embayments sequester sediment, their shorelines and river mouths prograde toward the coastal ocean (Mountain et al., 2007). The amount of sediment retained within the estuary or embayment, and by corollary, the rate of shoreline progradation, depends on the relative magnitudes of fluvial sediment supply and the processes acting to disperse the sediment, namely the waves and currents (Wright and Coleman, 1973; Zaitlin et al., 1994).

2.2 Study Area

Poverty Bay, located within the Waipaoa Sedimentary System (WSS), acts as the interface between the terrestrial and marine components of the dispersal system (Carter et al., 2010). The backbone of the terrestrial part of the WSS, the Waipaoa River, empties into Poverty Bay and is located on the eastern coast of the tectonically active North Island of New Zealand (Fig. 1). At present, the ~6 km long Poverty Bay opens to the Pacific Ocean through an ~8.5 km wide mouth. At the last maximum marine transgression (~7 kya), the embayment stretched ~20 km inland covering area that

185

evolved into Poverty Flats, the modern flood plain of the Waipaoa River (Brown, 1995) (Fig. 2). Over the past 7 ky the surface area of the embayment has decreased from about 190 km^2, to the present 62 km^2. Active tectonics have caused uplift of the northeast and subsidence of the southwest sides of the bay and coastal plain, with rates reaching about 1 and 4 m ky^{-1} for the uplift and subsidence, respectively (Brown, 1995; Wolinsky et al., 2010).

Based on the sediment and biochemical records from lacustrine sediment cores, climate change within the WSS over the last 7 ky was characterized as a gradual drying and cooling, although significant oscillations in temperature and precipitation occurred around the long-term trends (Page et al., 2010). Gomez et al. (2004b) related climate proxy data from outside New Zealand to an increase in grain size within three long (~15 m) cores near Poverty Bay. They concluded that roughly 3-4 kya the initiation of ENSO may have increased the frequency of storms within the WSS, but that the climate has remained relatively constant since that time. Orpin et al. (2010), however, analyzed storm event beds and sediment deposition within a confined lake on the North Island of New Zealand but found no correlation between the sedimentary record and any single climatic index (i.e. ENSO, SOI).

Erosion from the fractured and easily erodible siltstone and mudstone hill slopes provides the sediment to the Waipaoa River (Reid and Page, 2002). The system has an extremely high sediment yield of 6750 tonnes km^{-2} yr^{-1}, which is large by global standards (Hicks et al., 2000; Milliman and Syvitski, 1992). Most of this sediment is discharged to Poverty Bay during episodic storms whose heavy rains cause landsliding and gullying on the hill slopes (Hicks et al., 2000; Reid and Page, 2002). The

characteristic freshwater discharge that delivers the most sediment is 360 m^3 s^{-1}, over ten

times the yearly average discharge, and occurs multiple times every year (Hicks et al.,

2000). The modern Waipaoa River discharges roughly 15 million metric tonnes (MT) of

sediment to Poverty Bay each year (Hicks et al., 2000). The sediment load has been

anthropogenically increased, however, due to deforestation that began 650 years ago and

peaked during European colonization around 1920 (Reid and Page, 2002). The modern

load reflects a ~660% anthropogenic increase; before deforestation the Waipaoa River

sediment load was estimated to have been 2.3±4.5 MT; (Kettner et al., 2007). These

loads are extremely high considering that the Waipaoa River carries relatively little

freshwater discharge, averaging ~32 m^3 s^{-1} and having a base flow of ~9 m^3 s^{-1}.

The Waipaoa River mouth has migrated over the past 7 ky. For example, as the

shoreline has prograded since maximum transgression, the river mouth advanced ~12 km

seaward. Over more recent times, it migrated laterally from the northern extent of

Poverty Bay toward the south over the last ~2 ky (Fig. 1C) (Pullar and Penhale, 1970;

Wolinsky et al., 2010).

The modern Poverty Bay acts predominantly as a region of sediment bypass,

experiencing apparently negligible fine sediment accumulation within the bay Chapters 2

and 3; Wadman and McNinch, 2009). Sediment retained within Poverty Bay acts to fill

the embayment and contributes toward shoreline advance (Smith, 1988). Brown (1995)

used radiocarbon dating of samples from boreholes on the Poverty Bay flats and sand

ridges/dunes, while Pullar and Penhale (1970) used buried soils and volcanic ash layers,

to show that progradation has slowed as the shoreline advanced toward the continental

shelf. Wolinsky et al. (2010) used borehole data and regional tectonics to reconstruct the

shape and bathymetry of Poverty Bay 7 kya. Through geometric reconstructions, they attributed the deceleration of shoreline progradation to tectonic subsidence, the triangular basin shape, and sediment storage within the Poverty Bay flood plain.

Other factors, however, have possibly influenced shoreline progradation rate, including variations in fluvial sediment supply and increased exposure to marine dispersal mechanisms. Before modern deforestation, however, Kettner et al. (2007) estimated the Waipaoa River sediment discharge to be relatively constant for the past 3 ky, a time-period when the shoreline progradation rate slowed rapidly (Brown, 1995). The degree to which exposure to oceanographic energy (i.e. waves and currents) could have influenced fluvial dispersal as the shoreline advanced and the river mouth became more exposed has remained unstudied, however.

Depositional basins on the landward side of two upward rising anticlines on the continental shelf seaward of Poverty Bay have captured some of the Waipaoa River sediment, and appear to preserve a good record of the sediment exported from Poverty Bay throughout the Holocene (Gerber et al., 2010; Miller and Kuehl, 2010). Long cores (>15 m) collected within these depositional basins have been analyzed by Rose et al. (2010) and Gomez et al. (2004b) who identified three sequences; (1) from 10 to 6 kya, a fining upward sequence from 11 to 4 μm; (2) from 6 kya to 500 years ago, a coarsening upward sequence from 4 μm to 22 μm; and (3) since ~ 500 years ago an abrupt fining to roughly 4 to 7 μm attributed to anthropogenic effects. Rose et al. (2010) interpreted the older part of the sequence as the classical signature of marine transgression when the Poverty Bay shoreline retreated inland from the open coastline; while the overlying facies represented marine regression and the seaward advancement of the shoreline and river

mouth. Gomez et al. (2004b) discussed an abrupt coarsening between 3 and 4 kya, attributing it to large-scale changes in climate brought about by the initiation of ENSO. The initiation of ENSO roughly 3 kya created an overall stormier climate (McGlone et al., 1992), which would have increased the frequency of landsliding and coarsened the sediment supplied to the Waipaoa River by the hillslopes (Gomez et al., 2004b). Neither Rose et al. (2010) nor Gomez et al. (2004b), however, directly considered the manner in which oceanographic dispersal, influenced by wave resuspension and current-driven transport, may have modified the fluvial sediment source en route to continental shelf depocenters.

3. Methods

This section describes the hydrodynamic, sediment-transport, and wave models used. It explains how they were configured for Poverty Bay and the nearfield continental shelf within eight model runs, to represent conditions during the past 7 ky. Finally, the section describes the eight model runs and how they were analyzed.

3.1 Numerical Models

The Regional Ocean Modeling System (ROMS) was run fully coupled to the Simulated WAves Nearshore (SWAN) model. The ROMS (version 3.2) was used to estimate three-dimensional hydrodynamic and sediment-transport fields, while the SWAN model (version 40.41AB) calculated spatially and temporally varying wave properties. The ROMS, an open-source, three-dimensional, free-surface, hydrostatic, and finite-difference numerical model; uses a stretched terrain-following vertical grid

allowing for higher resolution near the surface and the seabed (Haidvogel et al., 2008; Shchepetkin and McWilliams, 2005). An orthogonal curvilinear horizontal grid enables the model to increase horizontal resolution in areas of interest and decrease it with distance from the focus site. The Reynolds-averaged Navier-Stokes equations are solved, with choices of multiple turbulence closure schemes available within the model (Warner et al., 2005b). A community model, the ROMS has the capability of using many different modules, such as sediment-transport, biology, and sea ice (see www.myroms.org).

This study used the Community Sediment-Transport Modeling System (CSTMS) routines that were included with the ROMS source code. These routines included the ability to account for multiple sediment classes, discharge from rivers, resuspension from the seabed, advective transport as suspended load, and the inclusion of sediment density in the equation of state (Warner et al., 2008b). Each sediment grain class could be assigned individual hydrodynamic characteristics, such as settling velocity, erosion rate parameter, and critical shear stress. The sediment-transport routines accounted for bed armoring by keeping track of varying seabed sediment layers, each with different fractions of the sediment classes, following Harris and Wiberg (1997). Sediment erosion was calculated using the Partheniades (1965) equation, and deposition rates were calculated as the product of the sediment settling velocity and the suspended sediment concentration within the bottom-most grid cell. See Warner et al. (2008b) for a more detailed description of the sediment-transport routines.

SWAN, a third-generation wave model, solves for the two-dimensional wave action density spectrum (Booij et al., 1999). It was formulated for use in regional

applications and shallow water (Booij et al., 1999). Within wave calculations SWAN can account for the influence of time-varying local current velocities, water depth, seabed roughness, and open boundary conditions. The generation of wind waves, nonlinear wave-wave interactions, wave refraction, wave dissipation by bottom friction, white capping, and depth-induced wave breaking can all be included in SWAN (Booij et al., 1999)

The ROMS and SWAN models have been fully coupled for use in wave-current-sediment-transport modeling (Warner et al., 2008a; Warner et al., 2008b). Calculations in both models proceed concurrently, and the two models use an identical model grid and bathymetry. At specified time intervals, ROMS supplies to SWAN the depth-averaged current velocities, seabed roughness (z_o), bathymetry, and sea surface height, which SWAN then updates and uses in the wave calculations. ROMS receives from SWAN the wave height, wave direction, bottom orbital velocity, and wave period, and uses these in calculations of radiation stress, Stokes drift velocity, and seabed shear stresses. The calculation of the radiation stress and Stokes drift velocity terms in the momentum balance, facilitated by this two-way coupling, has been shown to improve the ROMS estimated current speeds when compared to observational data in ~10 m of water within Poverty Bay (Chapter 3).

3.2 Overview of Model Configurations and Scenarios

Four different model configurations were used to investigate how basin geometry, river mouth orientation, and the anthropogenic increase in sediment discharge have affected sediment export from Poverty Bay and sediment retention near the river mouth.

Here, basin geometry is defined as the combination of the plan-view shape and the best estimate of bathymetry for Poverty Bay at any given time. The four model configurations used three different model grids; one representing the modern bay (Fig. 1C); another representing about 2 kya when the bay was very similar to its current state, but the Waipaoa River mouth was north of its present location (Fig. 1C); and a third representing the bay ~7 kya (Fig. 1D). Two different sediment loads were used for the modern bay geometry. The first assumed the modern anthropogenically enhanced sediment load, while the second represented the reduced pre-anthropogenic load based on Kettner et al. (2007). The following describes each of the model configurations, with their labels in italics:

1) *Modern:* This used the modern Poverty Bay model grid and the modern, anthropogenically increased sediment load. Results from this configuration were compared to observational data in Chapter 3, and are further analyzed within this Chapter through comparison to the other model runs.

2) *Modern PA:* This used the modern Poverty Bay grid with a lower sediment load assumed to be at pre-anthropogenic (PA) levels. Sediment discharge was reduced by a factor of 6.6 in an attempt to represent the system roughly 650 years ago, prior to ~1350, after which colonization increased the sediment yield of the catchment (Kettner et al., 2007; Reid and Page, 2002).

3) *2 kya:* Here, the river mouth was located to the northern side of the bay, representing Poverty Bay ~2 kya. The river mouth was also deflected to discharge toward the southwest instead of the southeast (see Fig. 1C), to

maximize the potential impact of changes to the orientation of the river. This

configuration used the PA sediment load.

4) *7 kya:* This used the 7 kya Poverty Bay grid (Fig. 1D) and PA sediment load.

As described Section 3.2.1, the model bathymetry relied on analysis by

Wolinsky et al. (2010) to account for basin changes due to sediment infilling

and tectonics.

For each model configuration, available estimates of river discharge, wind

velocity, offshore wave conditions, and atmospheric conditions for 2005 – 2006 were

used to derive the necessary model forcing. This provided model inputs that included

realistic temporal fluctuations needed to represent system behavior during seasonal time-

frames and storms. Other than reducing the sediment load to remove the anthropogenic

increase, time-series model inputs were identical for the different configurations.

Additionally, the relative fractions of different sediment grain sizes supplied by the river

were identical for the present-day and pre-anthropogenic inputs; only the total sediment

load was adjusted. No attempt was made within this study to account for climatic

variations in the weather forcing or climates effect on the sediment discharge. Although

both climatic factors and changes to discharged grain size distributions have undoubtedly

been important during the past 7 ky, the present study focused on the degree to which

basin geometry alone could influence sediment trapping and seaward dispersal within the

WSS. This modeling effort does not attempt to recreate the absolute shoreline

progradation rates or absolute observed grain size changes through time; doing so would

require extensive specification of the climatic influence on paleo weather, changes to

grain size distributions within the Waipaoa River discharge through time, and greater bathymetric precision within the numerical model grid, which are beyond the scope of this study.

Each of the four model configurations was used with two meteorological scenarios, resulting in a total of eight model runs. The first meteorological scenario represented a seasonal period, and encompassed 1 January through 9 September, 2006. The first 4.5 months were used to allow the model to equilibrate with the meteorological forcing, such that the analysis starts on 15 April, 2006 near the beginning of the "winter wet season". This April through September, 2006 time-period contained numerous elevated discharge and swell resuspension events, delivering a total of slightly over 15 MT of sediment over the 5 month period (Fig. 3 right panels). Peak discharges occurred during stormy conditions having strong winds, and also energetic waves as indicated by the SWAN model estimates. The second set of model inputs represented an "extreme storm", and used wind and discharge conditions measured during the so-called "Labor Day Storm" that occurred from 21-23 October, 2005 (Fig. 3 left panels). For the modern WSS, this event was assigned a roughly 40 year recurrence interval, based on flood data from Reid (1999). It delivered about 12 MT of sediment to the coastal ocean within a few days. Model runs of this storm were initiated in September, 2005, so that the model had over 1.5 months to equilibrate with meteorological conditions and freshwater discharge before the storm occurred. Specially, the model calculations included 9 September to 7 November, 2005. The next Sections provide details about the ROMS and SWAN model implementations.

3.2.1 ROMS Implementation Offshore of the Waipaoa River

Use of three model grids (Fig. 1C and D) allowed consideration of the role that basin geometry has played in sediment dispersal within the WSS since maximum marine transgression. All model grids extended seaward to the shelf break, but focused their resolution within Poverty Bay. The modern and 2 kya grids had a resolution of ~200 m within Poverty Bay (Fig. 1C), while the 7 kya bay had a resolution of ~325 m within the paleo Poverty Bay (Fig. 1D). Bathymetry for the modern and 2 kya Poverty Bays were developed using high-resolution multibeam data from within Poverty Bay (Wadman and McNinch, 2009). The 7 kya grid used the bathymetry within Poverty Bay developed by Wolinsky et al. (2010), to maintain a consistent Poverty Bay geometry for future comparisons between studies. Their bathymetric reconstruction was created through the interpretation of borehole data on the Poverty Bay floodplain (Litchfield, 2003) and corrected for regional tectonics (see Wolinsky et al. 2010). A previous bathymetric reconstruction performed for this dissertation generated 10-20 m deeper water depths within Poverty Bay than that from Wolinsky et al. (2010), indicating there is a large amount of uncertainty in the 7 kya bathymetry. The shelf bathymetry for all grids was based on bathymetric data provided by S. Stephens (National Institute of Water and Atmospheric Research, NIWA).

The model grids had two open boundaries (see Fig. 1B), and used boundary conditions based on Flather and Proctor (1983) and Chapman (1985) for the sea surface height and depth-averaged velocity fields, respectively. The tracer and the three-dimensional velocity open boundaries were specified using no-gradient and radiation conditions, respectively. Tides were included based on the Oregon State University

OTPS 7.1 tidal prediction software (Egbert et al., 1994; Egbert and Erofeeva, 2002), and included the m2, s2, n2, k2, k1, o1, p1, q1, mf, mm, and m4 constituents. Suspended sediment concentrations and current velocities were initialized to zero, and the initial temperature and salinity fields were uniformly set to 15°C and 35 ppt, respectively. The model evolved from this initialization with a 30 s time step.

A gauge at the Kanakanaia Bridge, located 48 km upstream of the river mouth, provided freshwater discharge for the Waipaoa River (Fig. 3A and B). Present-day suspended sediment concentrations were specified based on the rating curve of Hicks et al. (2000) (Fig. 3C and D). These were divided by 6.6 based on the long-term discharge modeling of Kettner et al. (2007) to estimate pre-anthropogenic (PA) sediment loads for the equivalent freshwater discharges (Fig. 3E and F). For both the modern and PA sediment inputs, sediment discharge was partitioned into four sediment classes, with three representing the suspended load of the Waipaoa River and one representing coarser sand (Table 1). The sizes of the three suspended classes were chosen to bracket the mean grain size discharged by the present-day Waipaoa River (6Φ, Hicks et al., 2004). They were assumed to account for nearly equal proportions of the Waipaoa River discharge, except the relative proportion of the finest size class (class 1) was increased compared to the others, based on model sensitivity tests. The coarsest type (class 4), a sand, represented one percent of the suspended load, based on Orpin et al. (2006). Sediment settling velocities and critical shear stresses were based on Stokes settling velocities and the Shields (Shields, 1936) diagrams, respectively. Sediment density and porosity for all sediment classes were set to 2650 kg m^{-3} and 0.6, respectively. A constant erosion rate parameter of 5x10^{-4} kg m^{-2} s^{-1} was assumed for all sediment classes within the

Partheniades (1965) equation, consistent with published literature that used observations to estimate this parameter (Dickhudt, 2008; Stevens et al., 2007). Earlier model runs used a range of erosion rate parameters, from 5×10^{-5} to 5×10^{-4} kg m^{-2} s^{-1}, and the value chosen produced model results that were the most consistent with observational data collected from April through September, 2006, as described in Chapter 3.

Meteorological inputs were obtained from observations made at the Gisborne airport located near the Poverty Bay shoreline (Fig. 1). These included hourly wind velocity, air temperature, air pressure, relative humidity, and rainfall rate (see http://cliflo.niwa.co.nz). Monthly mean values obtained from the same location were used for cloud cover and shortwave radiation. Time-series model input representing this meteorology was specified to be spatially uniform.

3.2.2 SWAN Implementation

The SWAN model used a 10 minute time-step in the non-stationary two-dimensional mode. The same model grids, bathymetry, and wind velocities were used for SWAN as for ROMS. Coupling between the two models occurred every 20 minutes, as explained in Section 3.1. Wave frequencies were limited to between 0.04 and 1 Hz, with calculations including those specified in Section 3.1 and Madsen bottom friction (Booij et al., 2002). Open boundaries were specified based on estimates from the Wave Watch 3 global model (Tolman et al., 2002) and assumed a Jonswap spectrum, to account for the propagation of open-ocean swell waves into the study area.

3.3 Analysis of Model Calculations

Cumulative dispersal patterns, time averages, and instantaneous behavior were analyzed for each of the eight model runs. This section describes the analysis used to synthesize the suite of model calculations.

In some cases, time-averaged values were used to represent system behavior for the winter wet season or extreme storm scenarios. The significant wave height, bottom orbital velocity, and current speed that are presented in the Results as time-averages were calculated as the mean for the winter wet season, 15 April through 9 September, 2006 and over the entire extreme storm 21 to 27 October, 2005. In some cases, the time averages for grid cells within Poverty Bay were spatially averaged to provide a single quantitative estimate, of wave strength for example, within the bay.

Sediment deposition was estimated as the sum of all four fluvially derived sediment classes on the seabed on 9 September, 2006 for the winter scenario and 5 November, 2005 for the extreme storm scenario. At these times any sediment suspended within the water column was minimal compared to that deposited on the seabed or exported from the model domain, so that the seabed deposit included nearly all of the fluvial sediment that remained in Poverty Bay and in the model domain.

Section 4 presents model estimates of cumulative sediment deposition as a function of distance from the Waipaoa River mouth. To derive these; 1) The distance from each grid cell to the Waipaoa River was calculated for each model grid (Fig. 4). 2) For each fluvial sediment class, all sediment deposited on the seabed at the end of the modeled time-period within a set distance (X km) from the Waipaoa River mouth was summed to give a total amount of sediment deposited (kg) within X km of the river

mouth. 3) The distance, X, was increased from 0 km to the maximum extent of the numerical model grid; roughly 46 km for the modern grid, and 60 km for the 7 kya model grid. 4) The resulting cumulative deposition curves were then divided by the total Waipaoa River sediment discharge for each sediment class, giving a cumulative percent of the river discharge that was deposited as a function of distance from the river mouth.

These cumulative sediment deposition curves were then used to calculate the average grain size that the model supplied to three distances from the Waipaoa River, corresponding to the mouth of Poverty Bay, the long shelf core MD972122 (~18 km seaward of the mouth of Poverty Bay), and the far edge of the model grid. These were generated as follows; 1) The total amount of sediment deposited on the seabed within each distance and for each sediment class was subtracted from the total river discharge for that sediment class. This gave the total amount (kg) of each sediment class that was dispersed to or beyond that distance from the river mouth. 2) These were normalized by their total to derive the fraction of each sediment class that was transported as far as those three distances. 3) The average grain size dispersed to that distance from the river mouth was calculated based on the weighted average of these fractions.

4. Results

This section presents results from the coupled models that show the complexity of waves, currents, and sediment-transport in the land to sea transition area. The wave results for different model configurations are discussed first. For the currents and sediment-transport, the winter scenario is first described in detail, followed by an abbreviated description of results from the extreme storm scenario.

4.1 Waves

Because wave estimates were insensitive to sediment load and placement of the river mouth, this analysis primarily focused on wave calculations for the modern and the 7 kya bay configurations. Similar results were obtained regarding the relative strength of waves within the 7 kya and modern bays during both the winter and extreme storm scenarios. For brevity, this section focused on estimates from the winter scenario. Significant differences in wave height and bottom orbital velocity were calculated for these model grids, with the modern system experiencing overall larger waves throughout Poverty Bay compared to the 7 kya bay (Fig. 5). The temporally and spatially averaged wave height within Poverty Bay was 1.03 m and 0.73 m for the modern and 7 kya bay geometries, respectively. Averaged wave orbital velocities within the bay for this time-period were 0.24 m s^{-1} and 0.16 m s^{-1} for the modern and 7 kya bay configurations, respectively.

Excluding the part of the 7 kya bay that has since filled and become Poverty Flats, wave calculations were very similar for the two model runs within what is now Poverty Bay. Along a transect through the middle of the modern Poverty Bay (Fig. 5C, A-A'), for example, estimates showed little difference between wave heights (correlation coefficient = 0.99, bias = 0.01 m) in the 7 kya bay and those calculated at the same locations for the modern bay. This implied that basin geometry explained the increased average wave heights within the modern system.

Differences in wave energy were apparent, however, within the nearshore of the two systems (Fig. 5). For example, at 10 m deep sites offshore of the river mouths (shown in Fig. 1C and D), wave orbital velocities during the winter scenario reached 1.11

m s^{-1} within the modern bay, but peaked at only 0.31 m s^{-1} for the 7 kya bay. Also, the standard deviations of the wave orbital velocities at these locations were 0.26 and 0.06 m s^{-1} for the modern and 7 kya bays, respectively. These metrics demonstrate that, with the same offshore wave energy and wind forcing, the peaks in wave energy near the river mouth during storms in the modern bay greatly exceed those experienced in a similar location 7 kya. Using the formulation of Madsen (1994), a bottom orbital velocity of 0.1 m s^{-1} produces a seabed shear stress of 0.08 Pa, which exceeds the critical shear stress to resuspend the fine sediment from the Waipaoa River yet is too low to initiate motion of the coarser sands (Table 1). For the winter scenario, the modern Poverty Bay exceeded this orbital velocity threshold 74% of the time at the location offshore of the river mouth, compared to 23% for the 7 kya Poverty Bay.

Sheltering reduced wave heights in the upper 7 kya Poverty Bay. Wave height estimates for the winter scenario steadily increased along a transect drawn from the 7 kya shoreline to the present-day shoreline (Fig. 6A; transect in Fig. 5C A'-A"). Wave orbital velocity along the same transect increased as water depth decreased near the embayment head, and again increased toward the mouth of Poverty Bay as sheltering became less effective (Fig. 6B). This trend in increasing wave height and orbital velocity toward the mouth of Poverty Bay was evident across a range of time-scales, from the winter and storm scenario averages to instantaneous snapshots, and therefore a persistent phenomenon. Barring drastic changes to offshore wave energy, the shoreline and river mouth were exposed to ever increasing wave energy as they prograded.

4.2 Model Estimates for a Winter Season

Model calculations representing the five month winter scenario indicated that the modern PA and 7 kya system responded to storm winds and waves very differently, due to differences in basin geometry. Considering the other two model configurations, river mouth location had a less pronounced effect, but recent increases to sediment load were estimated to produce large signals in terms of sediment dispersal. This section first compares the estimated current velocities within the bay for the different model configurations, and then evaluates sediment dispersal.

4.2.1 Winter Season: Currents

For all model grid configurations, the time- and depth-averaged current speeds were high at coastline locations that were exposed to waves. In such locations, both wave driven flows and wind forcing enhanced current speeds, which ranged between 0.05 and 0.40 m s^{-1} (Fig. 7). Model results indicated neither fluvial sediment load nor river mouth location significantly affected time- and depth-averaged currents for the modern Poverty Bay geometry (Fig. 7A, B, and C). Within the modern, modern PA, and 2 kya bay configurations, average currents were counterclockwise with speeds of about 0.05 m s^{-1} in the middle of the bay.

Speeds and circulation patterns estimated for the 7 kya model differed significantly from those calculated for the modern, modern PA, and 2 kya bay configurations, however, with currents slower in the 7 kya Poverty Bay (Fig. 7D). Sheltering reduced the wave influence on currents near the shoreline within much of the 7 kya bay (Fig. 7). Near-bed current speed (1 mab), analyzed at locations directly offshore

of the river mouth on the 10 m isobath (see Fig. 1C and D for locations), was on average

reduced by half in the 7 kya configuration where currents rarely exceeded 0.1 m s^{-1}

compared to the modern, modern PA, and 2 kya configurations whose peak currents

reached 0.3 m s^{-1} (Fig. 8). The bay wide temporally and spatially averaged current speed

for the 7 kya configuration (0.03 m s^{-1}) was also half that calculated for the modern

Poverty Bay (0.06 m s^{-1}). Model results also implied that the Poverty Bay gyre flowed in

a clockwise direction in the upper 7 kya bay, compared to the counterclockwise

orientation of the modern gyre (Fig. 7).

Both basin geometry and river mouth orientation influenced the currents and the

Waipaoa River plume during elevated river discharge. Focusing on the elevated

discharge period based on 28 April through 9 May, 2006, the modern and modern PA

model configurations developed a plume structure and current flow that differed from

those calculated for the 2 kya and 7 kya model configurations. Modeled plume behavior

and currents were compared for the four grid configurations at three points during this

event.

Early in the event (on 29 April) when discharge was near the peak, winds were

strongly shoreward. In the modern and modern PA configurations, seaward directed

currents emanated from the Waipaoa River mouth that then turned counterclockwise

toward the coastline at this time (Fig. 9 column 1). Conversely, within the 2 kya

configuration the currents flowed roughly along the isobaths to the southwest. In the 7

kya configuration the surface currents were forced toward the northwest, with the plume

confined near the head of the bay.

During the next phase of this event (30 April), discharge remained high but was decreasing, and the winds weakened and turned to be toward the southwest. In all model configurations the river plume spread out away from the coastline as the winds rotated (Fig. 9 column 2). Here, estimates from the modern, modern PA, and 2 kya model configurations were similar to those calculated during shoreward winds. Within the 7 kya configuration, however, currents confined the river plume to the northeast side of the bay, although the plume did spread as it progressed toward the bay mouth and was no longer trapped near the bay head.

Later in the event, discharge decreased as winds rotated to become seaward. Under seaward winds, currents within the modern, modern PA, and 2 kya configurations were directed toward the mouth of Poverty Bay, and the river plume spread onto the continental shelf (Fig. 9 column 3). During this phase, freshwater within the 7 kya Poverty Bay flowed along the northeast coast out to the continental shelf.

4.2.2 Winter Season: Sediment Depositional Patterns

Over the five month winter scenario, depositional patterns within Poverty Bay were sensitive to the location of the river mouth and especially to the bay geometry. In the modern Poverty Bay configuration, for the post- and pre-anthropogenic sediment loads, sediment deposition occurred near the river mouth on the western side of Poverty Bay and in the central portion of the bay (Fig. 10A and B). While the anthropogenically increased sediment load did not alter depositional patterns, it increased the deposit thicknesses by 5 to 20 cm. Because sediment deposited near the river mouth, depositional patterns differed in the 2 kya bay compared to the present-day configuration.

204

In the 2 kya bay, sediment deposited toward the northern side of the bay and in a thin band near the bay mouth (Fig. 10C). Depositional patterns on the shelf immediately seaward of the bay did not significantly differ between the modern, modern PA, and 2 kya bay configurations.

In the 7 kya configuration, Poverty Bay retained over twice as much sediment than it did in the other configurations (Table 2). Deposition occurred near the river mouth and stretched seaward along the northeast coastline of the bay in the direction of current flow (Fig. 10D).

4.2.3 Winter Season: Sediment Dispersal

Model results indicated that regardless of the model configuration, the bay would export higher fractions of the finer sediment classes than the sand (class 4), which was primarily retained within the bay (Fig. 11). Sediment dispersal away from the river mouth was relatively similar for the modern, modern PA, and 2 kya Poverty Bay configurations. Nearly of all the finest size class (>99.5%) was exported from Poverty Bay, and ~92% was lost from the model domain by the end of the model run. As settling velocity increased, the dispersivity of sediment size classes decreased, with progressively higher fractions of each coarser sediment class retained within Poverty Bay and in the model domain. Overall, the modern and 2 kya configurations only retained about 45% of the discharged sediment within the model domain (Table 2). The 7 kya bay geometry, being less dispersive (Table 2), retained 6% of the fine sediment discharged during the winter scenario within the bay, six times as much as the other configurations.

The sensitivity of sediment dispersal to bay geometry and settling velocity led to sediment segregation within the bay and on the shelf, implying basin geometry alone influenced grain size supplied to different locations on the model domain, because the fractions of each sediment class supplied by the Waipaoa River were held constant within the model and each configuration used the same forcing conditions. To explore basin geometries influence on sediment sorting, the calculations described in Section 3.3 were used to compare sediment sizes dispersed to locations at three distances from the Waipaoa River mouth for model configurations representing the 7 kya bay up to the present-day system. For all model configurations, the average grain size dispersed to different distances from the Waipaoa River became finer as the distance was increased (Fig. 12). Also, grain sizes supplied to these three distances were estimated to be significantly finer in the 7 kya configuration than those calculated for the modern, modern PA, and 2 kya configurations (Fig. 12). This implied that sediment size dispersed to the bay mouth and the continental shelf would have progressively coarsened through time, in response to shoreline progradation and a changing basin shape. Grain size was less sensitive to river mouth location than basin shape, but the modern PA and the 2 kya configurations did supply subtly different sediment sizes to equal distances from the river mouth.

The model calculations, which neglected changes to grain size distributions, indicated that under modern conditions when sediment load has been anthropogenically enhanced, sediment grain size delivered to the bay mouth and continental shelf would be coarsened due to increased seaward transport of the coarser sediment classes (classes 3 and 4) (Figs. 11 and 12). This finding contradicts sediment core data on the continental

shelf from Rose et al. (2010) and Gomez et al. (2004b), however, and is explored in more detail in the Discussion Section 5.3.

Although the magnitude of sediment export to the continental shelf was sensitive to model configuration, the timing of sediment export to the continental shelf was less so (Fig. 13). Sediment export from Poverty Bay occurred at the same times, and under the same conditions, i.e. elevated discharge and swell resuspension, for all four model configurations. Even though there were significant depositional thicknesses within Poverty Bay during the modern, modern PA, and 2 kya configurations, sediment export during discharge events exceeded that during wave resuspension events (Fig. 13). Sediment export from the 7 kya Poverty Bay was much more variable than estimated for the other configurations (Fig. 13B). In the 7 kya configuration, export responded strongly to the largest discharge events on 28 April to 9 May and 19 to 25 June, 2006, but was otherwise driven by wave resuspension and dispersal. The increased role of wave resuspension on sediment export was related to the length of the embayment 7 kya. Sediment had to travel about three times farther during an elevated discharge period to exit the bay 7 kya compared to today. The decreased waves in the 7 kya bay compared to the modern and 2 kya configurations also reduced the capacity for the flood pulse to transport sediment seaward during elevated discharge.

4.3 Model Estimates for the Extreme Storm Scenario

To evaluate system behavior during a large storm, currents and sedimentation estimated for the extreme storm scenario that used wind, wave, and river discharge inputs based on the October, 2005 storm were evaluated. Model results for the four model

configurations are presented, emphasizing how the extreme conditions differed from the seasonally averaged results presented previously.

4.3.1 Extreme Storm: Currents

Model results indicated that both sediment load and river mouth location influenced currents within the modern Poverty Bay during extremely large storms (Fig. 14). While the time- and depth-averaged current speeds during the storm were the same, ~0.08 m s^{-1}, for the modern, modern PA, and 2 kya bay configurations; current patterns differed between the three models.

With the present-day sediment load the river plume extended to the seabed, while with a reduced sediment load the freshwater was confined to the surface waters (Fig. 15). This demonstrates the potential for suspended sediment concentrations to influence currents and salinity structure within the modern Poverty Bay.

Using the present-day sediment load, currents from the river mouth were directed toward the deepest portion of the bay, located at the northeast side of the mouth of Poverty Bay, while speeds were relatively slow in the northern bay (Fig. 14A). At the mouth of the bay the currents then abruptly turned toward deeper water. This behavior was attributed to strong gravity-driven transport from the high suspended sediment concentrations in Chapter 3, through comparison with model runs that neglected the sediment contribution to water density.

Using the pre-anthropogenic, reduced, sediment load, the storm-driven circulation more closely matched those calculated for the moderate events in the winter scenario (Figs. 7 and 14B), albeit with higher current speeds. For these configurations, currents

from the river mouth had a more northward direction than those using the modern sediment load, and turned more gradually toward the continental shelf and at the mouth of the bay.

The location of the river mouth influenced the behavior of currents during the large flood. Calculations for the 2 kya bay configuration showed strong current speeds directed southwest from the river mouth (Fig. 14C). For this configuration, during the storm the Poverty Bay gyre encompassed the entire bay and water exited to the continental shelf toward the southern side of the bay, in contrast to the modern and modern PA configurations where the model calculated net inflow of water there.

The 7 kya Poverty Bay configuration developed a clockwise rotating gyre under flood conditions, similar to that calculated for the winter scenario (Fig. 14D), although the bay-wide averaged current speeds increased to 0.05 m s^{-1}. A strong southward flow formed near the northeast shoreline, with current speeds reaching 0.15 m s^{-1} in response to enhancement of that side of the gyre by seaward flowing freshwater.

4.3.2 Extreme Storm: Sediment Deposition

Model calculations indicated that the system's response to extreme storms has evolved as the shoreline prograded, sediment supply increased, and, to a lesser degree, in response to river mouth migrations. For all model configurations, the extreme storm produced thick fluvial sediment deposits within the bay (Fig. 16). For the modern, modern PA, and 2 kya bay configurations, deposition peaked near the river mouth (Fig. 16A, B, and C). Deposition was also significant on the continental shelf immediately adjacent to the bay when sediment load was increased to account for anthropogenic

effects (Fig. 16A). For the 7kya configuration, deposition stretched seaward from the river mouth to the bay mouth (Fig. 16D).

Depositional patterns were significantly thicker for the extreme storm case than those calculated at the end of the winter scenario (Figs. 10 and 16). With a pre-anthropogenic sediment load, similar depositional patterns were created within Poverty Bay for both the extreme storm and winter scenarios, and the deposit location remained sensitive to the river mouth location (Fig. 16B and C). The deposit for the 7 kya bay had a similar pattern to that calculated for the winter scenario, except that for the extreme storm sediment was confined even more toward the head of the bay (Fig. 16D).

4.3.3 Extreme Storm: Sediment Dispersal

Model calculations for the extreme storm indicated that both basin geometry and sediment load influenced sediment retention within Poverty Bay and export to the continental shelf (Fig. 17). Even within the short, two week, time-frame of these calculations, the WSS supplied significant amounts of sediment to the continental shelf and beyond (Table 2). River mouth location subtly modified sediment export out of the bay, changing it from 75% to 67% of the river discharge as the river mouth migrated from its northern position to the present-day location. Gravity driven currents in the modern configuration, with an anthropogenic sediment load, enhanced export of the coarser sediment classes from Poverty Bay, increasing the total percent of the river discharge exported to the continental shelf to 84%. The 7 kya model configuration exported much less sediment from the bay (25%) than did the other configurations (Fig. 17). The more sheltered nature of the 7 kya configuration reduced the wave and current

strength and thus increased sediment deposition. Also, the increased distance to the bay mouth in the 7 kya bay meant that sediment had to travel about 12 km farther to exit the bay than for the other configurations.

Comparison between sediment dispersal calculations for the two week extreme storm and the five month winter scenario showed that extreme events can deliver large amounts of sediment directly to the continental shelf. Model calculations indicated that an increased fraction of sediment would be retained in Poverty Bay within all but the modern model configuration, with the increased sediment load, for the extreme storm compared to the winter scenario, because of the shorter time-frame of the calculations (Figs. 11 and 17). Within the longer time-frame of the winter scenario, fluvial deposits were subjected to repeated periods of wave resuspension that effectively exported sediment to the continental shelf. The modern configuration lost about the same fraction of discharged sediment to the shelf during the six day extreme storm as during the much longer winter scenario, because the extreme storm scenario had more gravity driven flow that efficiently removed material from Poverty Bay. For all model configurations, the fraction of sand transported away from the river mouth was estimated to be higher for the short-lived extreme storm than was calculated for the winter scenario (Figs. 11 and 17).

Calculations of fluvial sediment size supplied to three distances away from the river mouth, described in Section 3.3, indicated the degree to which changes to the bay configuration and sediment load impacted grain sizes (Fig. 18). The grain size supplied to the mouth of Poverty Bay differed for all four model configurations; in general coarsening with time, and slightly responding to the change in river mouth location (Fig. 18). Grain sizes estimated for the continental shelf distance and the edge of the model

grid were similar to each other and also coarsened with time. This contrasted with estimates made for the winter scenario, where grain sizes estimated for the continental shelf distance were significantly coarser than those estimated for the edge of the model grid. This may indicate the importance of post-depositional reworking in creating sediment size gradation on the continental shelf; because many episodes of swell-induced resuspension occurred during the five month winter scenario, unlike the extreme storm.

5. Discussion

This section expands on the model results in a number of ways. It explores the role that increased exposure to wave energy played in the deceleration of shoreline progradation in the WSS. Because marine and nearshore processes modulate sediment dispersal, dispersal basin geometry and oceanographic processes should be considered when analyzing the sedimentary record from continental shelves. Finally, the section evaluates the manner in which the ~6.6 fold increase in sediment load over the past 650 years (see Kettner et al., 2007) may have impacted sediment deposition and dispersal within Poverty Bay and on the continental shelf.

5.1 Sediment Dispersal and Shoreline Progradation Rates

Shoreline progradation rates reflect the cumulative impact of short-term events (days to weeks) that redistribute sediment, like floods and storms, integrated over much longer times. The deceleration in shoreline advance observed for the WSS was inversely correlated with the increase in wave energy that occurred as the coastline became more exposed to oceanographic conditions. To explore this link, the SWAN model estimated

wave properties were analyzed. Fig. 6A provides wave heights along a transect from the river mouth to the bay mouth calculated for the 7 kya model configuration. SWAN estimated wave heights calculated for the modern bay configuration along this transect closely matched the values calculated for the same locations within the 7kya configuration, having a correlation coefficient of 0.99 and bias of 0.01 m, respectively, so that Fig. 6A serves as a proxy for wave exposure as the shoreline advanced. Comparing wave height along this transect to shoreline progradation rates illustrates the decrease in shoreline advance slowed as wave exposure increased (Fig. 6).

Feedbacks between shoreline progradation and factors such as basin geometry and current velocity are more difficult to analyze using this study's modeling approach than its link with wave energy. However, Section 4.2.1 showed that changes to basin geometry alone may have increased the current speeds seaward of the river mouth in the modern Poverty Bay compared to 7 kya. Speeds in the modern Poverty Bay were estimated to be about twice as fast offshore of the river mouth compared to the 7 kya bay configuration, with peak speeds being over 0.2 m s^{-1} faster in the modern Poverty Bay.

Therefore, modification to basin geometry alone seems to have increased both wave energy and current speed as the shoreline prograded. Both of these effects enhanced sediment dispersal away from the river mouth and increased export to the continental shelf, as shown in Figs. 11 and 17 and Table 2. Enhanced sediment export from Poverty Bay then decreased the amount of sediment available to advance the shoreline, slowing progradation, and creating feedbacks between basin geometry, sediment dispersal, and shoreline progradation.

This analysis linked increased sediment dispersal from the Waipaoa River mouth

to decreased shoreline progradation rate and increased oceanographic energy. This builds

on arguments presented by Wright and Coleman (1973), who analyzed the impacts of

waves, tides, and sediment supply on delta morphology and concluded that, in general,

sediment preservation near river mouths depends on the relative strengths of the

oceanographic energy and the sediment supply from the river. Zaitlin et al. (1994)

reached similar conclusions while examining infilled estuarine systems. The results for

Poverty Bay build on this theory; sediment preservation within the bay decreased as wave

energy and current speeds increased. That is, sediment export from the bay increased in

modern times in response to enhanced oceanographic forces. This conclusion, derived

using a three-dimensional process-based numerical model, focused on the degree that

basin geometry can impact wave exposure and sediment dispersal. Although the model

neglected changes to fluvial sediment grain size distributions and climate that have likely

been important over the time-scale studied, its results numerically validate and readdress

a classical theory originally developed from field observations.

Factors other than oceanographic energy impact shoreline progradation rate in the

WSS, including regional tectonics (Wolinsky et al., 2010), sediment supply (Kettner et al.,

2007; Smith, 1988), and the proximity of the river mouth to the open continental shelf.

As the shoreline progressively advanced, the Waipaoa River delivered sediment closer to

the bay mouth and open ocean, increasing export. Much (41%) of the sediment

discharged by the Waipaoa River during the winter scenario in the 7 kya model

configuration remained within ~18 kilometers of the river mouth and therefore was

contained within the bay (Figs. 10 and 11, Table 2). Sediment supplied by the modern

Waipaoa River, however, has a short transit to the open continental shelf with the river mouth located only ~5 km from the bay mouth. Model results, therefore, implied that wave energy, current velocity, and the proximity of the river mouth to the open coast impact shoreline progradation rate.

5.2 Anthropogenic Increase of Sediment Load and the Impact on Sediment Dispersal

The large increase in sediment load attributed to land-use changes since Maori and European colonization led to consummate increases in the suspended sediment concentration of the Waipaoa River (Kettner et al., 2007; Reid and Page, 2002). This implies that, compared to pre-anthropogenic conditions, present-day fluvial suspended sediment concentrations more frequently exceed ~40 g L^{-1} (Hicks et al., 2004), the value often considered sufficient to form hyperpycnal river discharge (Mulder et al., 2003) (Fig. 3C). Because sediment loads before colonization of the WSS were estimated to be ~15% of their present-day values (Kettner et al., 2007), a similar meteorological event during pre-anthropogenic times would have supplied much less sediment than in the present-day system, at lower concentrations, and would have been unlikely to exceed 40 g L^{-1}.

Under present-day sediment loads, the increased sediment supply did in fact produce gravity-driven flows for the extreme storm scenario as emphasized in Results Section 4.3. The gravity-driven flow increased the seaward dispersal of sediment out of Poverty Bay (Fig. 17A and B). Model results indicated that, with the addition of gravity forcing, even the sand fraction was transported away from the river mouth during extreme floods, whereas sand remained trapped in the nearshore under most other situations modeled (Figs. 11 and 17). A gravity-driven signal was less obvious within

model estimates for the winter scenario, but comparison of the modern and modern PA model configurations showed that the anthropogenic increase in sediment concentrations increased the fraction of sediment exported from Poverty Bay (Table 2). Although model results indicated that the anthropogenic enhancement of sediment load increased the relative proportion of fluvial material exported from Poverty Bay (Table 2), the total amount of deposition within the bay still grew with modern land-use changes. Specifically, estimated deposit thicknesses within Poverty Bay increased with the modern sediment load, based on comparing estimates of the modern and modern PA configurations for both the winter and the extreme storm scenarios (Figs. 10 and 16).

Model results indicated the anthropogenically increased sediment load has changed sediment dynamics within Poverty Bay in two ways, which in turn would impact both the marine portions of the dispersal system and shoreline progradation. First, the model estimated that sediment exported from Poverty Bay accounted for a larger fraction of the fluvial load under present-day conditions. This effectively transferred much of the increased sediment load directly to the continental shelf and slope systems. Having shorter residence in Poverty Bay, this sediment would be less impacted by nearshore and estuarine processes. Second, under present-day conditions the model also estimated an overall increase in depositional thicknesses within Poverty Bay. This implied that there would still be an increase in sediment available to further advance the shoreline and fill the bay. The anthropogenic increase in sediment effectively decreased the relative strengths of the waves and currents compared to sediment supply. Based on the ideas of Wright and Coleman (1973) and Zaitlin (1994) presented in Section 5.1, this suggested that the rate of river mouth and shoreline progradation would increase relative to the pre-

colonization rates. This conclusion was indeed confirmed by Smith (1988), who used coastal surveys and aerial photographs since 1886 to derive shoreline progradation rates of >1.5 m yr^{-1}. These greatly exceeded the rate of ~0.2 to 0.8 m yr^{-1} for the 2000 years before colonization estimated by Brown (1995) and Pullar and Penhale (1970).

5.3 Shelf Sedimentation Responds to Marine Dispersal

Marine and nearshore dispersal processes significantly impact sediment characteristics on the continental shelf, and should be especially considered when analyzing shelf cores. Model results imply that even relatively modest changes to a sedimentary system, such as river mouth migration, can modify sediment sizes supplied to the continental shelf (Figs. 12 and 18). Larger-scale changes, such as filling of an embayment, can leave an even larger imprint on sediment supply to the continental shelf. With infilling, the shoreline progrades and becomes more exposed as the overall wave and current energy within the embayment increases (Sections 4.1, 4.2.1, and 4.3.1, Fig. 6). This strengthening of the physical processes that drive sediment-transport increases dispersal of the coarser sediment, and thereby coarsens sediment supplied by the embayment to the deeper portions of the dispersal system (Figs. 12 and 18).

Such coarsening has been noted in long cores spanning the Holocene on the continental shelf seaward of Poverty Bay (Gomez et al., 2004b; Rose et al., 2010). Except for model runs that assumed an anthropogenically increased sediment load, all of the numerical experiments used an identical sediment source term at the river mouth. Model results indicated, however, that sediment exported to the continental shelf would have coarsened since last maximum transgression (Figs. 12 and 18). This implies that the

evolution of the physical geometry of the sedimentary system alone can explain, to some degree, the coarsening observed in continental shelf sediment cores. This conclusion was robust whether the model scenario covered a seasonal time-frame or an extreme storm, indicating that it was somewhat insensitive to the details of meteorological inputs.

In addition to estimating that grain size would have coarsened on the continental shelf since the last maximum transgression, model results for the winter scenario also indicated that grain sizes would become segregated and graded across the marine portion of the WSS (Fig. 12). Sediment segregation did not occur to the same degree within the shorter six day time-frame extreme storm scenario (Fig. 18), implying that size sorting depended on repeated episodes of wave resuspension and sediment redistribution that take place over seasonal time-scales. As such, progressive sorting of sands, silts, and clays away from the river mouth seemed to be controlled by climatic conditions that encompass the timing of sediment supply and the wave climate.

The model did not reproduce the dramatic sediment fining seen at the top of long continental shelf cores (Gomez, et al., 2004b; Rose et al., 2010). For example, Rose et al. (2010) saw a fining of 1 to 2 Φ in the last ~500 years in cores on the continental shelf seaward of Poverty Bay, and attributed this feature to anthropogenic effects. Anthropogenic deforestation over the last ~650 years shifted the hillslope erosional regime from one dominated by landslides to one more influenced by gulleying and overland flow, decreasing the grain size supplied to the Waipaoa River and the continental shelf (Gomez et al. 2004a; Gomez et al., 2007; Wilmshurst et al., 1999). In contrast, the model results presented here estimated that the grain size supplied to the continental shelf would have coarsened under the scenario of an anthropogenic increase

in sediment load (Figs. 12 and 18). The modeled Waipaoa River discharge neglected any changes to the grain size supplied by the river, however. Therefore, consistent with Gomez et al. (2004b), these model results suggest that an overall fining of the discharged Waipaoa River sediment since deforestation led to the dramatic fining at the top of shelf cores.

6. Conclusions

This study showed that transport processes within even relatively small bays, like Poverty Bay, can significantly modulate sediment supply to the continental shelf. Nearshore and marine dispersal processes should be considered when interpreting the sedimentary record from continental shelves offshore of river mouths. The Poverty Bay shoreline, the bay in general, and the Waipaoa River mouth are more exposed to wave energy now than 7 kya. Additionally, the river mouth is now closer to the bay mouth. The model results indicated that both of these significantly impact the sedimentary signal supplied to the continental shelf. The geometry of the bay 7 kya facilitated sediment sequestration and deposition, whereas the modern bay geometry favors sediment bypass. Shifting of the river mouth from the northern to southern sides of the bay may also have lead to more subtle signatures in the sediment signal from the bay.

Results from this work complement other studies that focused on the shoreline progradation rate within Poverty Bay and the coarsening upward sequence on the adjacent continental shelf. Specifically, it was demonstrated that the shoreline progradation rate varied inversely with available wave energy, which evolved with time as shoreline advanced and the coast become more exposed. The increase in current

speeds in the modern, modern PA, and 2 kya configurations compared to the 7 kya configuration also helped export more sediment from Poverty Bay. In full, the shoreline progradation rate will be driven by a combination of tectonics, basin geometry, sediment supply, and the physical processes that redistribute the sediment. Model results presented in this Chapter also indicated that average grain size exported to the continental shelf would have increased over the 7 ky time-scale, purely in response to changes to bay geometry, without needing to modify sediment supply, or other model inputs reflective of climatic changes. As such, along with Rose et al. (2010), this study concluded that the sediment grain size trend observed in long cores on the continental shelf represents a classical coarsening upward sequence due to shoreline regression.

Acknowledgements

References

Blum, D.M. and Tornqvist, T.E., 2000. Fluvial Response to climate and sea-level change: a review and look forward. Sedimentology, 47(S1): 2-48.

Booij, N., Ris, R.C. and Holthuijsen, L.H., 1999. A third-generation wave model for coastal regions 1. Model description and validation. J. Geophys. Res., 104(C4): 7649-7666.

Brown, L.J., 1995. Holocene shoreline depositional processes at Poverty Bay, a tectonically active area, northeastern north island, New Zealand. Quatern. Res., 26: 21-33.

Butman, B., Noble, M. and Folger, D.W., 1979. Long-term observations of bottom current and bottom sediment movement on the Mid-Atlantic continental shelf. J. Geophys. Res., 84(C3): 1187-1205.

Caliskan, H. and Valle-Levinson, A., 2008. Wind-wave transformations in an elongated bay. Cont. Shelf Res., 28: 1702-1710.

Carter, L., Orpin, A.R. and Kuehl, S.A., 2010. Landscape and sediment responses from mountain source to deep ocean sink; Waipaoa Sedimentary System, New Zealand. Mar. Geol.

Chapman, D.C., 1985. Numerical treatment of cross-shelf open boundaries in a barotropic coastal ocean model. J. Phys. Oceanogr., 15: 1060-1075.

Chatwin, P.C., 1976. Some remarks on the maintenance of the salinity distribution in estuaries. Estuar. Coast. Shelf Sci., 4: 555-566.

Chen, S., Sanford, L.P. and Ralston, D.K., 2009. Lateral circulation and sediment transport driven by axial winds in an idealized, partially mixed estuary. J. Geophys. Res., 114(C12006): doi:10.1029/2008JC005014.

Crockett, J.S. and Nittrouer, C.A., 2004. The sandy inner shelf as a repository for muddy sediment: An example from Northern California. Cont. Shelf Res., 24: 55-73.

Dadson, S., Hovius, N., Pegg, S., Dade, W.B., Horng, M.J., Chen, H., 2005. Hyperpycnal river flows from an active mountain belt. J. Geophys. Res., 110(F04016): doi:10.1029/2004JF000244.

Dalrymple, R.W., Boyd, R. and Zaitlin, B.A., 1994. History of research, types and internal organization of incised-valley systems: Introduction to the volume. In: R.W. Dalrymple, R. Boyd and B.A. Zaitlin (Editors), Incised-valley systems: Origin and sedimentary sequences. SEPM. Special Publication, No. 51, Tulsa, OK, pp. 3-10.

Dickhudt, P.J., 2008. Controls on Erodibility in a Partially Mixed Estuary: York River, Virginia. M.S. Thesis, Virginia Institute of Marine Science, College of William and Mary, Gloucester Point, 230 pp.

Drake, D.E. and Cacchione, D.A., 1985. Seasonal variation in sediment transport on the Russian River shelf, California. Cont. Shelf Res., 4(5): 495-514.

Egbert, G., Bennett, A. and Foreman, M., 1994. TOPEX/Poseidon tides estimated using a global inverse model. J. Geophys. Res., 99(C12): 24821-24852.

Egbert, G.D. and Erofeeva, S.Y., 2002. Efficient inverse modeling of barotropic ocean tides. Journal of Oceanic Technology, 19(2): 183-204.

Fain, A.M.V., Ogston, A.S. and Sternberg, R.W., 2007. Sediment transport event analysis on the western Adriatic continental shelf. Cont. Shelf Res., 27: 431-451.

Festa, J.F. and Hansen, D.V., 1978. Turbidity maxima in partially mixed estuaries: A two-dimensional numerical model. Estuarine and Coastal Marine Science, 7: 347-359.

Flather, R.A. and Proctor, R., 1983. Prediction of North Sea storm surges using numerical models: recent developments in the U.K. In: J. Sundermann and W. Lenz (Editors), North Sea Dynamics. Springer-Verlag, New York.

Frihy, O.E., 2009. Morphodynamic implications for shoreline management of the western-Mediterranean sector of Egypt. Environmental Geology, 58: 1177-1189.

Gerber, T., Pratson, L.F., Kuehl, S., Walsh, J.P., Alexander, C., Palmer, A., 2010. The influence of sea level and tectonics on Late Pleistocene through Holocene sediment storage along the high-sediment supply Waipaoa continental shelf. Mar. Geol., 270: 139-159.

Geyer, W.R., 1993. The importance of suppression of turbulence by stratification on the estuarine turbidity maximum. Estuaries, 16(1): 113-125.

Geyer, W.R., Hill, P.S. and Kineke, G.C., 2004. The transport, transformation and dispersal of sediment by buoyant coastal flows. Cont. Shelf Res., 24: 927-949.

Gomez, B., Brackley, H.L., Hicks, D.M., Neff, H. and Rogers, K.M., 2004a. Organic carbon in floodplain alluvium: Signature of historic variations in erosion processes associated with deforestation, Waipaoa River basin, New Zealand. J. Geophys. Res., 109(F04011): doi:10.1029/2004JF000154.

Gomez, B., Carter, L., Trustrum, N.A., Palmer, A.S. and Roberts, A.P., 2004b. El Nino-Southern Oscillation signal associated with middle Holocene climate change in intercorrelated terrestrial and marine sediment cores, North Island, New Zealand. Geology, 32(8): 653-656.

Gomez, B., Carter, L. and Trustrum, N.A., 2007. A 2400 yr record of natural events and anthropogenic impacts in intercorrelated terrestrial and marine sediment cores: Waipaoa sedimentary system, New Zealand. GSA Bulletin, 119(11/12): 1415-1432.

Green, M.O., Vincent, C.E. and Trembanis, A.C., 2004. Suspension of coarse and fine sand on a wave-dominated shoreface, with implications for the development of rippled scour depressions. Cont. Shelf Res., 24: 317-335.

Haidvogel, D.B., Arango, H., Budgell, W.P., Coruelle, B.D., Curshitser, E., Lorenzo, E.D., K.Fennel, Geyer, W.R., Hermann, A.J., Lanerolle, L., Levin, J., McWilliams, J.C., Miller, A.J., Moore, A.M., Powell, T.M., Schepetkin, A.F., Sherwood, C.R., Signell, R.P., Warner, J.C., Wilkin, J., 2008. Regional ocean forecasting in terrain-following coordinates: Model formulation and skill assessment. Journal of Computational Physics, 227: 3595-3624.

Hansen, D.V. and Rattray, M., 1965. Gravitational circulation in straits and estuaries. J. Mar. Res., 23: 104-122.

Harris, C.K. and Wiberg, P.L., 1997. Approaches to quantifying long-term continental shelf sediment transport with an example from the Northern California STRESS mid-shelf site. Cont. Shelf Res., 17(11): 1389-1418.

Hetland, R.D. and Geyer, W.R., 2004. An idealized study of the structure of long, partially mixed estuaries. J. Phys. Oceanogr., 34(12): 2677-2691.

Hicks, D.M., Gomez, B. and Trustrum, N.A., 2000. Erosion thresholds and suspended sediment yields, Waipaoa River basin, New Zealand. Water Resour. Res., 36(4): 1129-1142.

Hicks, D.M., Gomez, B. and Trustrum, N.A., 2004. Event suspended sediment characteristics and the generation of hyperpycnal plumes at river mouths: east coast continental margin, North Island, New Zealand. J. Geol., 112(4): 471-485.

Hicks, D.M. and Hume, T.M., 1996. Morphology and size of ebb tidal deltas at natural inlets on open-sea and pocket-bay coasts, North Island, New Zealand. J. Coast. Res., 12(1): 47-63.

Hill, P.S. and McCave, I.N., 2001. Suspended particle transport in benthic boundary layers. In: B.P. Boudreau and B.B. Jorgensen (Editors), The Benthic Boundary Layer. Oxford University Press, pp. 78-103.

Hill, P.S., Milligan, T.G. and Geyer., W.R., 2000. Controls on effective settling velocity of suspended sediment in the Eel River flood plume. Cont. Shelf Res., 20: 2095-2111.

Hoogendoorn, R.M., Overeem, I. and Storms, J.E.A., 2008. Process-response modelling of fluvio-deltaic stratigraphy. Computers and Geosciences, 34: 1394-1416.

Hutton, E.W.H. and Syvitski, J.P.M., 2008. *Sedflux 2.0*: An advanced process-response model that generates three-dimensional stratigraphy. Computers and Geosciences, 34: 1319-1337.

Kennett, J.P., 1982. Marine Geology. Prentice-Hall, Inc., Englewood Cliffs, N.J.

Kettner, A.J., Gomez, B., Hutton, E.W. and Syvitski, J.P.M., 2009. Late holocene dispersal and accumulation of terrigenous sediment on Poverty Shelf, New Zealand. Basin Research, 21: 253-267.

Kettner, A.J., Gomez, B. and Syvitski, J.P.M., 2007. Modeling suspended sediment discharge from the Waipaoa River system, New Zealand: The last 3000 years. Water Resour. Res., 43(W07411): doi:10.1029/2006WR005570.

Kniskern, T.A., Kuehl, S.A., Harris, C.K. and Carter, L., 2010. Sediment accumulation patterns and fine-scale strata formation on the Waiapu River shelf, New Zealand. Mar. Geol., 270: 188-201.

Lin, J. and Kuo, A.Y., 2001. Secondary turbidity maximum in a partially mixed microtidal estuary. Estuaries, 24(5): 707-720.

Lin, J. and Kuo, A.Y., 2003. A model study of turbidity maxima in the York River Estuary, Virginia. Estuaries, 26(5): 1269-1280.

Litchfield, N., 2003. Maps, stratigraphic logs and age control data for river terraces in the Eastern North Island, Institute of Geological and Nuclear Sciences, Wellington, New Zealand.

Madsen, O.S., 1994. Spectral wave-current bottom boundary layer flows. Coastal Engineering 1994. Proceedings, 24th International Conference Coastal Engineering Research Council: 384-398.

McGlone, M.S., Kershaw, A.P. and Markgraf, V., 1992. El Nino / Southern Oscillation climatic variability in Australasia and South American paleoenvironmental records. In: H.F. Diaz and V. Markgraf (Editors), Historical and palaeoclimatic aspects of the Southern Oscillation. Cambridge University Press, Cambridge, pp. 435-462.

Meyer-Peter, E. and Muller, R., 1948. Formulas for bedload transport, Report on the 2nd Meeting International Association Hydraulic Research, Stockholm, Sweden, pp. 39-64.

Miller, A.J. and Kuehl, S.A., 2010. Shelf sedimentation on a tectonically active margin: A modern sediment budget for Poverty continental shelf, New Zealand. Mar. Geol., 270: 175-187.

Milligan, T.G., Hill, P.S. and Law, B.A., 2007. Flocculation and the loss of sediment from the Po River plume. Cont. Shelf Res., 27(3-4): 309-321.

Milliman, J.D. et al., 2007. Short-term changes in seafloor character due to flood-derived hyperpycnal discharge: Typhoon Mindulle, Taiwan, July 2004. Geology, 35(9): 779-782.

Milliman, J.D. and Meade, R.H., 1983. World-wide delivery of river sediment to the oceans. J. Geol., 91(1): 1-21.

Milliman, J.D. and Syvitski, J.P.M., 1992. Geomorphic/tectonic control of sediment transport to the ocean: The importance of small mountainous rivers. J. Geol., 100: 525-544.

Morehead, M.D., Syvitski, J.P.M. and Hutton, E.W.H., 2001. The link between abrupt climate change and basin stratigraphy: a numerical approach. Global Planet. Change, 28: 107-127.

Mountain, G.S., Burger, R.L., Delius, H., Fulthorpe, C.S., Austin, J.A., Goldberg, D.S., Steckler, M.S., McHugh, C.M., Miller, K.G., Monteverde, D.H., Orange, D.L., Pratson, L.F., 2007. The long-term stratigraphic record on continental margins. In: C.A. Nittrouer et al. (Editors), Continental-Margin Sedimentation: From Sediment Transport to Sequence Stratigraphy. Blackwell Publishing Ltd., pp. 381-458.

Mulder, T., Syvitski, J.P.M., Migeon, S., Faugeres, J. and Savoye, B., 2003. Marine hyperpycnal flows: initiation, behavior and related deposits. A review. Mar. Pet. Geol., 20: 861-882.

Orpin, A.R., Alexander, C., Carter, L., Kuehl, S. and Walsh, J.P., 2006. Temporal and spatial complexity in post-glacial sedimentation on the tectonically active, Poverty Bay continental margin of New Zealand. Cont. Shelf Res., 26: 2205-2224.

Page, M.J., Trustrum, N.A., Orpin, A.R., Carter, L., Gomez, B., Cochran, U.A., Mildenhall, D.C., Rogers, K.M., Brackley, H.L., Palmer, A.S., Northcote, L., 2010. Storm frequency and magnitude in response to Holocene climate variability, Lake Tutira, North-Eastern New Zealand. Mar. Geol., 270: 30-44.

Paola, C., 2000. Quantitative models of sedimentary basin filling. Sedimentology, 47(S1): 121-178.

Partheniades, E., 1965. Erosion and deposition of cohesive soils. Journal of the Hydraulic Division, 91(HY1).

Pullar, W.A. and Penhale, H.R., 1970. Periods of recent infilling of the Gisborne plains basin. New Zealand Journal of Science, 13(410-434).

Reid, C.J., 1999. Waipaoa River at Kanakanaia: a review of flood data, Unpublished report to the Gisborne District Council, New Zealand.

Reid, L.M. and Page, M.J., 2002. Magnitude and frequency of landsliding in a large New Zealand Catchment. Geomorphology, 49: 71-88.

Rose, L.E., Kuehl, S., Alexander, C. and Orpin, A., 2010. Carbon isotopes provide distinctive signatures for tracking tectonic forcing and sea level changes on an active margin, AAPG 2010 Annual Convention, New Orleans, LA.

Roy, P.S., Thom, B.G. and Wright, L.D., 1980. Holocene sequences on an embayed high-energy coast: An evolutionary model. Sediment. Geol., 26: 1-19.

Shchepetkin, A.F. and McWilliams, J.C., 2005. The Regional Oceanic Modeling System (ROMS): a split-explicit, free-surface, topography-following-coordinate oceanic model. Ocean Modeling, 9: 347-404.

Sheng, Y.P., Alymov, V. and Paramygin, V.A., 2010. Simulation of storm surge, wave, currents, and inundation in the Outer Banks and Chesapeake Bay during Hurricane Isabel in 2003: The importance of waves. J. Geophys. Res., 115(C04008): DOI:10.1029/2009JC005402.

Shields, A., 1936. Anwendung der Aehnlichkeitsmechanik und der Turbulenzforschung auf die Geschiebebewegung, Mitt. Preuss. Versuchsanst. Wasserbau Schiffbau, (English translation by W. P. Ott and J. C. van Uchelen, 36 pp., U.S. Dep. of Agric. Soil Conser. Serv. Coop. Lab., Calif., Inst. of Technol., Pasadena, 1936.).

Smith, R.K., 1988. Poverty Bay, New Zealand: a case study of coastal accretion 1886-1975. N. Z. J. Mar. Freshwat. Res., 22: 135-141.

Sommerfield, C.K. and Nittrouer, C.A., 1999. Modern accumulation rates and a sediment budget for the Eel shelf: A flood-dominated depositional environment. Mar. Geol., 154: 227-241.

Sommerfield, C.K., Ogston, A.S., Mullenbach, B.L., Drake, D.E., Alexander, C.A., Nittrouer, C.A., Borgeld, J.C., Wheatcroft, R.A., Leithold, E.L., 2007. Oceanic dispersal and accumulation of river sediment. In: C.A. Nittrouer et al. (Editors), Continental-Margin Sedimentation: From Sediment Transport to Sequence Stratigraphy. Blackwell Publishing Ltd., pp. 157-212.

Soulsby, R.L., 1997. Dynamics of marine sands: a manual for practical applications. Telford, London, 249 pp.

Soulsby, R.L. and Damgaard, J.S., 2005. Bedload sediment transport in coastal waters. Coastal Engineering, 52: 673-689.

Soulsby, R.L. et al., 1993. Wave-current interaction within and outside the bottom boundary layer. Coastal Engineering, 21: 41-69.

Sternberg, R.W., Cacchione, D.A., Paulson, B., Kineke, G.C. and Drake, D.E., 1996. Observations of sediment transport on the Amazon subaqueous delta. Cont. Shelf Res., 19: 697-715.

Stevens, A.W., Wheatcroft, R.A. and Wiberg, P.L., 2007. Seabed properties and sediment erodibility along the western Adriatic margin, Italy. Cont. Shelf Res., 27(3-4): 400-416.

Syvitski, J.P.M., Pratson, L.F., Wiberg, P.L., Steckler, M.S., Garcia, M.H., Geyer, W.R., Harris, C.K., Hutton, E.W.H., Imran, J., Lee, H.J., Morehead, M.D., Parker, G., 2007. Prediction of margin stratigraphy. In: C.A. Nittrouer et al. (Editors), Continental-Margin Sedimentation: From Sediment Transport to Sequence Stratigraphy. Blackwell Publishing Ltd., pp. 460-529.

Tessier, B., Billeaud, I. and Lesuer, P., 2010. Stratigraphic organization of a composite macrotidal wedge: the Holocene sedimentary infilling of the Mont-Saint-Michel Bay (NW France). Bull. Soc. Geol. Fr., 181(2): 99-113.

Tolman, H.L. et al., 2002. Development and implementation of wind-generated ocean surface wave modelsat NCEP. Weather and Forecasting, 17: 311-333.

Traykovski, P., Geyer, R. and Sommerfield, C., 2004. Rapid sediment deposition and fine-scale strata formation in the Hudson estuary. J. Geophys. Res., 109(F022004): doi:10.1029/2003JF000096.

Traykovski, P., Wiberg, P.L. and Geyer, W.R., 2007. Observations and modeling of wave-supported sediment gravity flows on the Po prodelta and comparison to prior observations from the Eel shelf. Cont. Shelf Res., 27(4-3): 375-399.

Wadman, H.M. and McNinch, J.E., 2008. Stratigraphic spatial variation on the inner shelf of a high-yield river, Waiapu River, New Zealand: Implications for fine sediment dispersal and preservation. Cont. Shelf Res., 28(7): 865-886.

Wadman, H.M. and McNinch, J.E., 2009. Sediment segregation and dispersal across the land-sea interface: Waipaoa sedimentary system, New Zealand, Integration and Synthesis of MARGINS Sediment Source-to-Sink Research Workshop, Gisborne, New Zealand.

Warner, J.C., Geyer, W.R. and Lereczak, J.A., 2005a. Numerical modeling of an estuary: A comprehensive skill assessment. J. Geophys. Res., 11(C05001): doi:10.1029/2004JC002691.

Warner, J.C., Perlin, N. and Skyllingstad, E.D., 2008a. Using the Model Coupling toolkit to couple earth system models. Environ. Model. Software, 23: 1240-1249.

Warner, J.C., Sherwood, C.R., Arango, H.G., Butman, B. and Signell, R.P., 2005b. Performance of four turbulence closure methods implemented using a generic length scale method. Ocean Modeling, 8: 81-113.

Warner, J.C., Sherwood, C.R., Signell, R.P., Harris, C.K. and Arango, H.G., 2008b. Development of a three-dimensional regional coupled wave-current-sediment model. Comput. Geosci., 34(10): 1284-1306.

Warrick, J.A. and Milliman, J.D., 2003. Hyperpycnal sediment discharge from semiarid southern California rivers: Implications for coastal sediment budgets. Geology, 31(9): 781-784.

Warrick, J.A., Xu, J., Noble, M.A. and Lee, H.J., 2008. Rapid formation of hyperpycnal sediment gravity currents offshore of a semi-arid California river. Cont. Shelf Res., 28: 991-1009.

Wiberg, P.L. and Smith, J.D., 1987. Calculations of the critical shear stress for motion of uniform and heterogeneous sediments. Water Resour. Res., 23(8): 1471-1480.

Wilmshurst, J.M., Eden, D.N. and Froggatt, P.C., 1999. Late Holocene forest disturbance in Gisborne, New Zealand: a comparison of terrestrial and marine pollen records. New Zealand Journal of Botany, 37: 523-540.

Wolinsky, M.A., Swenson, J.B., Litchfield, N. and McNinch, J.E., 2010. Coastal progradation and sediment partitioning in the Holocene Waipaoa Sedimentary System, New Zealand. Mar. Geol., 270: 94-107.

Wright, L.D., 1985. River deltas. In: R.A. Davies Jr. (Editor), Coastal Sedimentary Environments. Springer-Verlag, New York, pp. 1-76.

Wright, L.D. and Coleman, J.M., 1973. Variations in morphology of major river deltas as functions of ocean wave and river discharge regimes. The American Association of Petroleum Geologists Bulletin, 57(2): 370-398.

Wright, L.D. and Friedrichs, C.T., 2006. Gravity driven transport on continental shelves: A status report. Cont. Shelf Res., 26(17-18): 2092-2107.

Zaitlin, B.A., Dalrymple, R.W. and Boyd, R., 1994. The stratigraphic organization of incised-valley systems associated with relative sea-level change. In: R.W. Dalrymple, R. Boyd and B.A. Zaitlin (Editors), Incised-valley systems: Origin and sedimentary sequences. SEPM. Special Publication, No. 51, Tulsa, OK, pp. 45-60.

Table 1. Modeled sediment grain class characteristics.

Class	Diameter (μm)	W_s (mm s^{-1})	τ_{cr} (N m^{-2})	Erosion Rate Parameter (kg m^{-2} s^{-1})	Fraction of Discharge
1	7.8	0.038	0.02		40
2	15	0.15	0.03	5×10^{-4}	30
3	31	0.62	0.06		30
4	125	10	0.14		1

Table 2. The percent of the total river discharge that is deposited within 3 distances from the river mouth. Extending the 22-26 October storm until 5 November allowed sediment to settle from the water column, such that these numbers are not significantly influenced by sediment suspended in the water column within the model domain.

Meteorology	Model grid	Poverty Bay Mouth	Shelf Core MD972122	Edge of Model Grid
Jan – Sept 2006	Modern	13	27	42
	Modern PA	18	34	46
	2 kya	18	33	48
	7 kya	41	44	48
22 October – 5 November 2005	Modern	14	53	59
	Modern PA	33	49	54
	2 kya	25	50	53
	7 kya	75	86	90

Figure 1. Study site and model grids. (A) Box identifies location of Poverty Bay on the North Island of New Zealand. (B) Bathymetry in meters and the marine extent of numerical model grids (thick black line). Model grid configurations and bathymetry for (C) modern and 2 kya Poverty Bay, and (D) 7 kya Poverty Bay. Bathymetry contoured in meters. 7 kya Poverty Bay bathymetry was from Wolinsky et al. (2010). The arrows in (C) and (D) represent Waipaoa River mouth locations and discharge directions. Labels on river mouths identify the arrows corresponding to the modern (m), 2 kya, and 7 kya river mouths. The star in panel C shows the location of wave estimates presented in Fig. 3 and the black diamonds in panels C and D mark the locations at 10 m water depth offshore of the Waipaoa River discussed in the text.
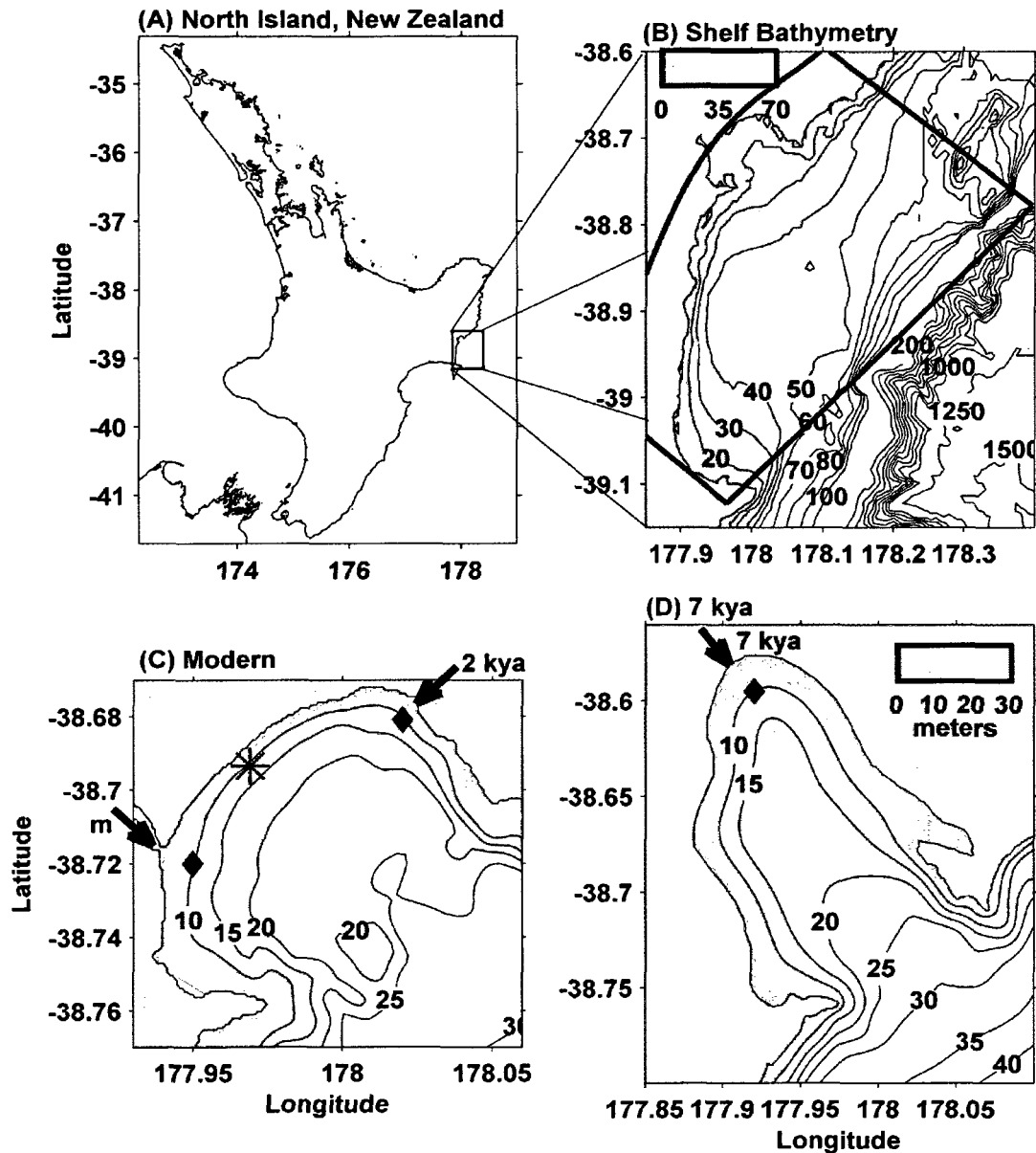
Figure 2. Estimated locations of Poverty Bay shorelines from 9 kya until the present. From Brown (1995).
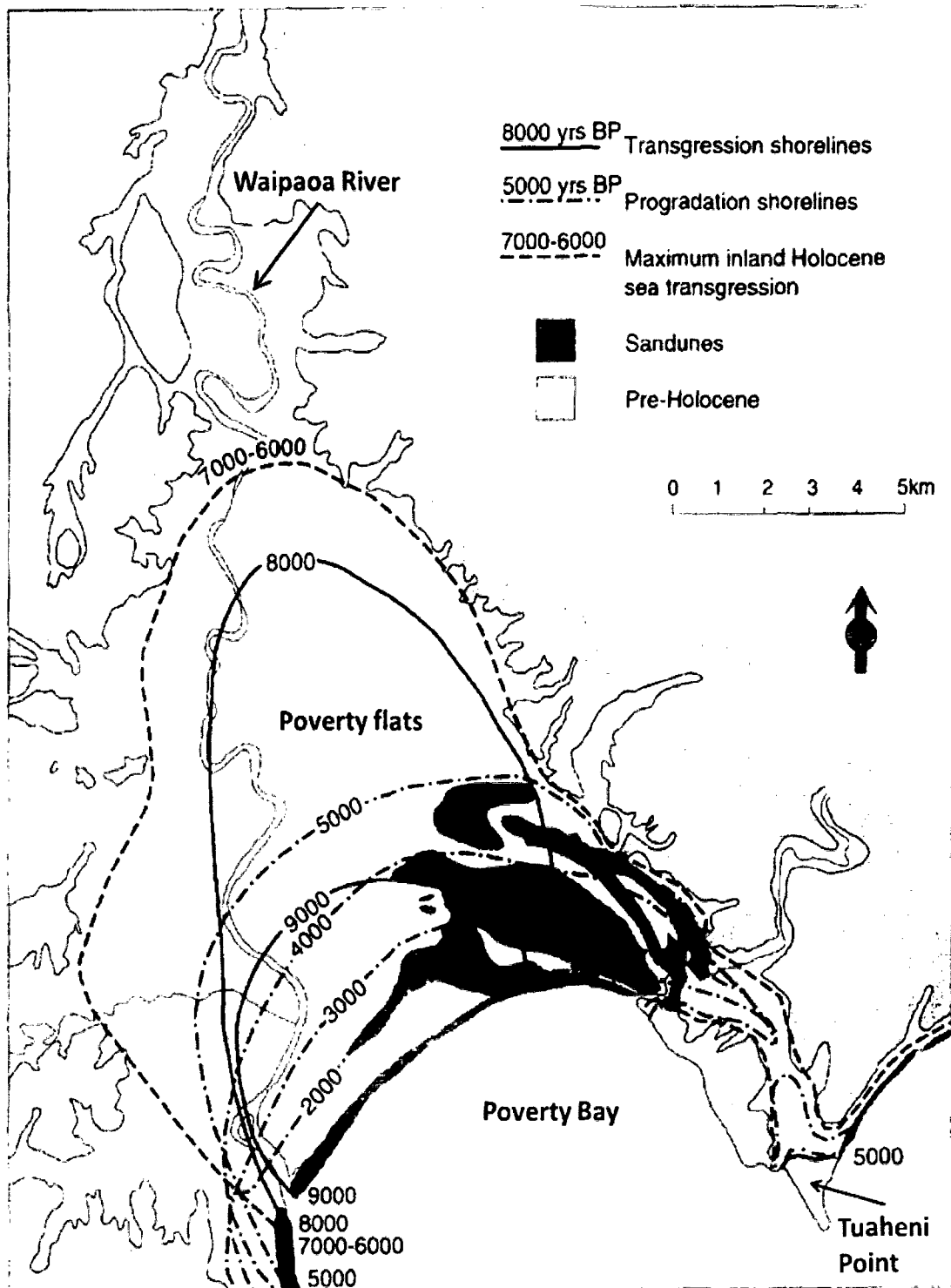
Figure 3. Waipaoa River discharge and wind velocity for the numerical model scenarios. The left column shows model input for the extreme storm scenario, based on conditions in October, 2005. The right column shows the same fields for the winter scenario, based on 25 April – September, 2006. Though used in model spinup, the period from 1 January through 25 April, 2006 was omitted from this figure to emphasize the winter wet season. Panels show (A,B) freshwater discharge, (C,D) present-day suspended sediment concentration (black line) and cumulative sediment discharge (grey line), (E,F) estimated pre-anthropogenic suspended sediment concentration (black line) and cumulative sediment discharge (grey line) for the same level of freshwater discharge, (G,H) wind velocity vectors (black lines) and speed (grey line), and (I,J) modeled significant wave height at 10 m water depth near the center of Poverty Bay (at the star in Fig. 1C).
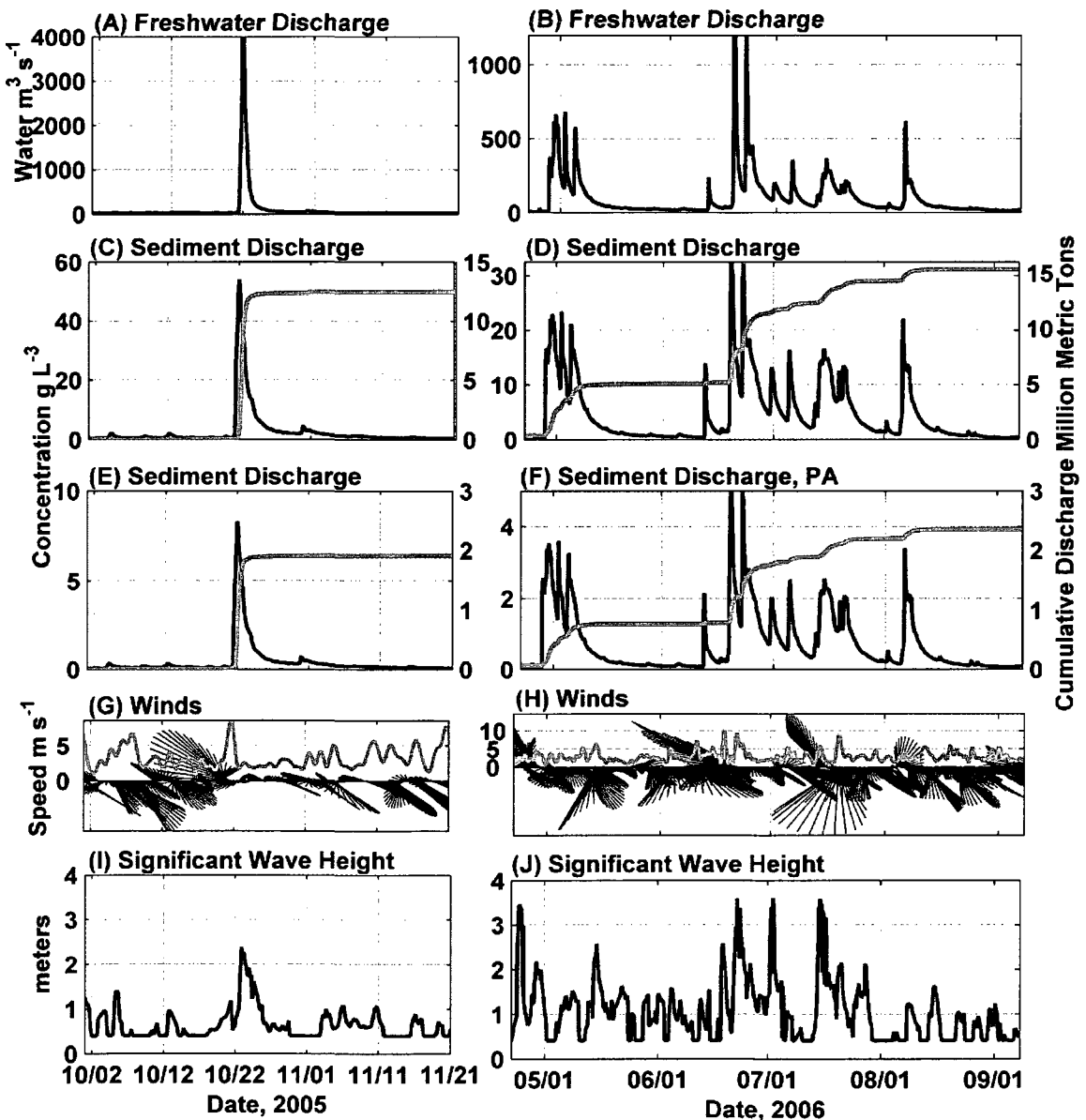
Figure 4. Radii of equal distance (km) from the modern and 7 kya Waipaoa River mouths. The radii of the 2 kya bay (not shown) differ only slightly from those for the modern bay. Thick lines mark the radii used as the mouth of Poverty Bay and the distance to the shelf core used in later Sections.
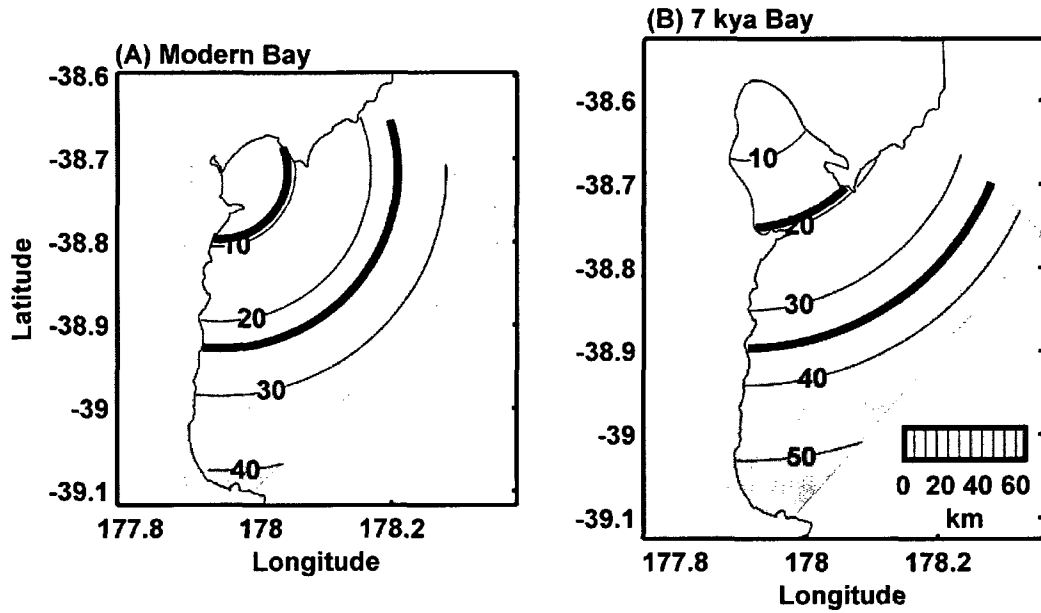
Figure 5. Significant wave height (top row, in m) and RMS of the maximum bottom orbital velocity (bottom row, in m/s) time-averaged for the winter scenario for each model configuration (see panel titles). Bathymetry contoured in meters. (C and F): Location of the modern shoreline also drawn. (C): Transects for (A-A') the comparison of the modern and 7 kya wave heights in Section 4.1 and (A'-A") analyzed for Fig. 6 also shown.
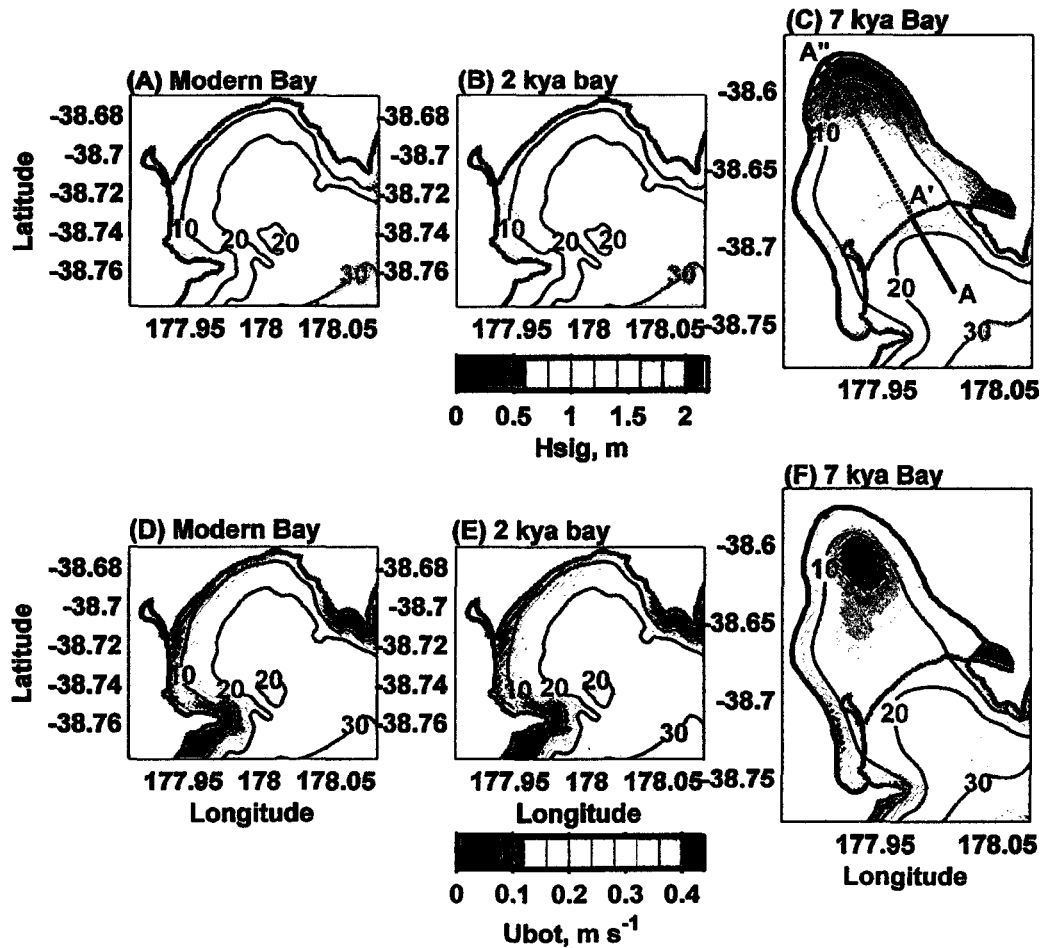
Figure 6. (A) Significant wave height and (B) RMS of the maximum bottom orbital velocity time-averaged for the winter scenario along a transect down the middle of the 7 kya Poverty Bay configuration (see A' – A" in Fig. 5C). (E) The age of the shoreline as it progressed from its 7 kya to present-day location and (D) the rate of shoreline progradation along the same transect as the waves.
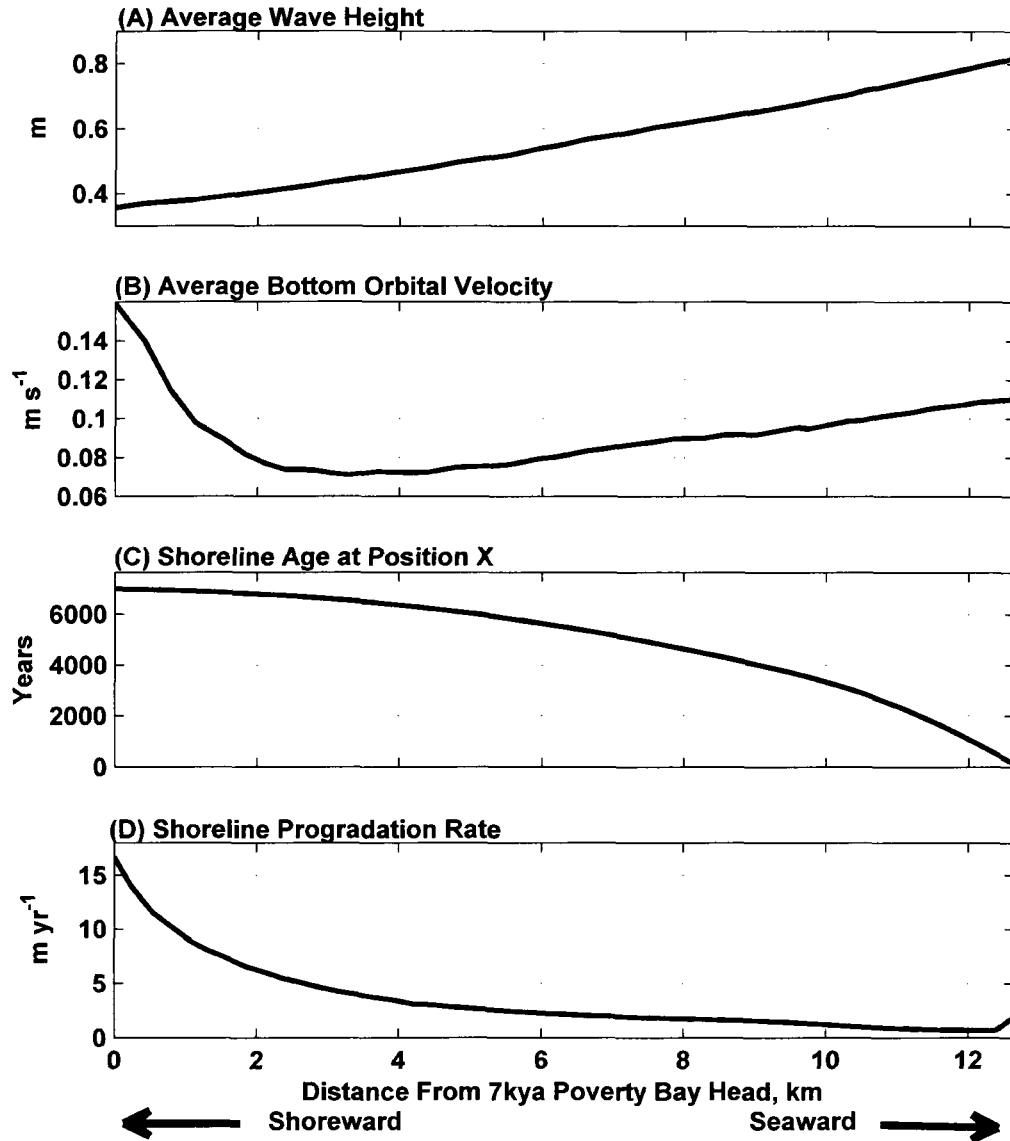
Figure 7. Time- and depth-averaged current speed (colors) and velocity vectors (arrows) for the winter scenario for each model grid and sediment load configuration (see panel titles). Bathymetry contoured in meters.
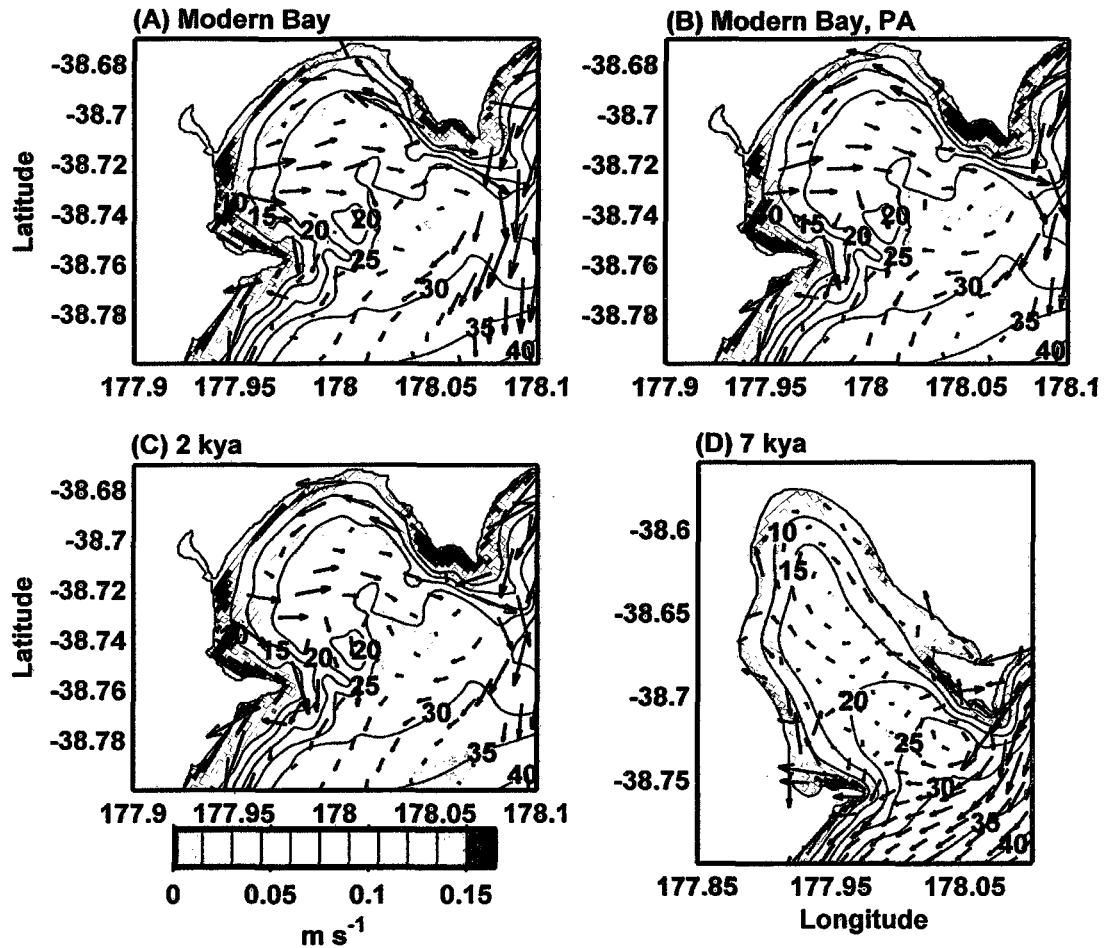
Figure 8. One meter above the bed current speeds in 10 m water depth seaward of the river mouth during the winter scenario for each configuration (see panel titles). Location of currents shown as diamonds in Fig. 1D and C.
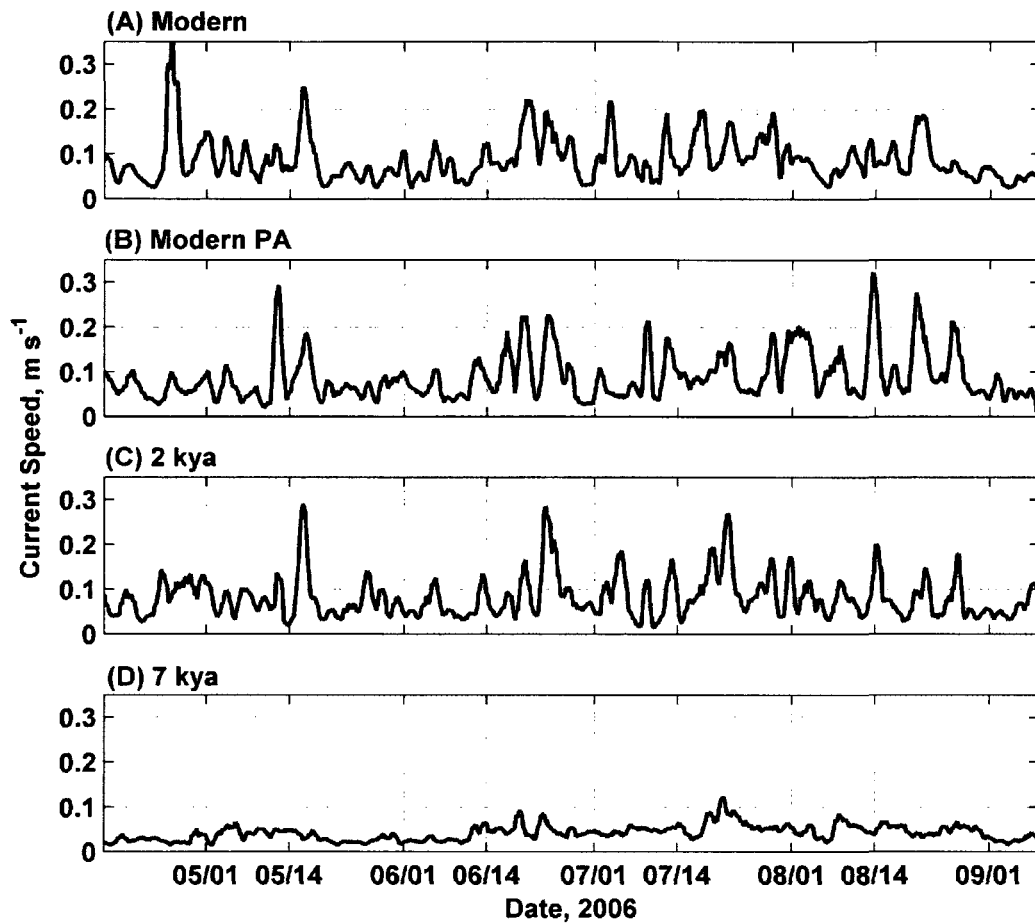
Figure 9. Surface salinity (colors) and surface current velocities (vectors) for three times during an elevated discharge from the winter scenario for each configuration (see Y axis labels). Wind directions and relative speeds shown by the arrow in the top right of each panel. Bathymetry contoured every 10 m. Current scale arrow in lower left of left column panels. Titles on columns provide the date in 2006 used to derive model inputs for that snapshot.
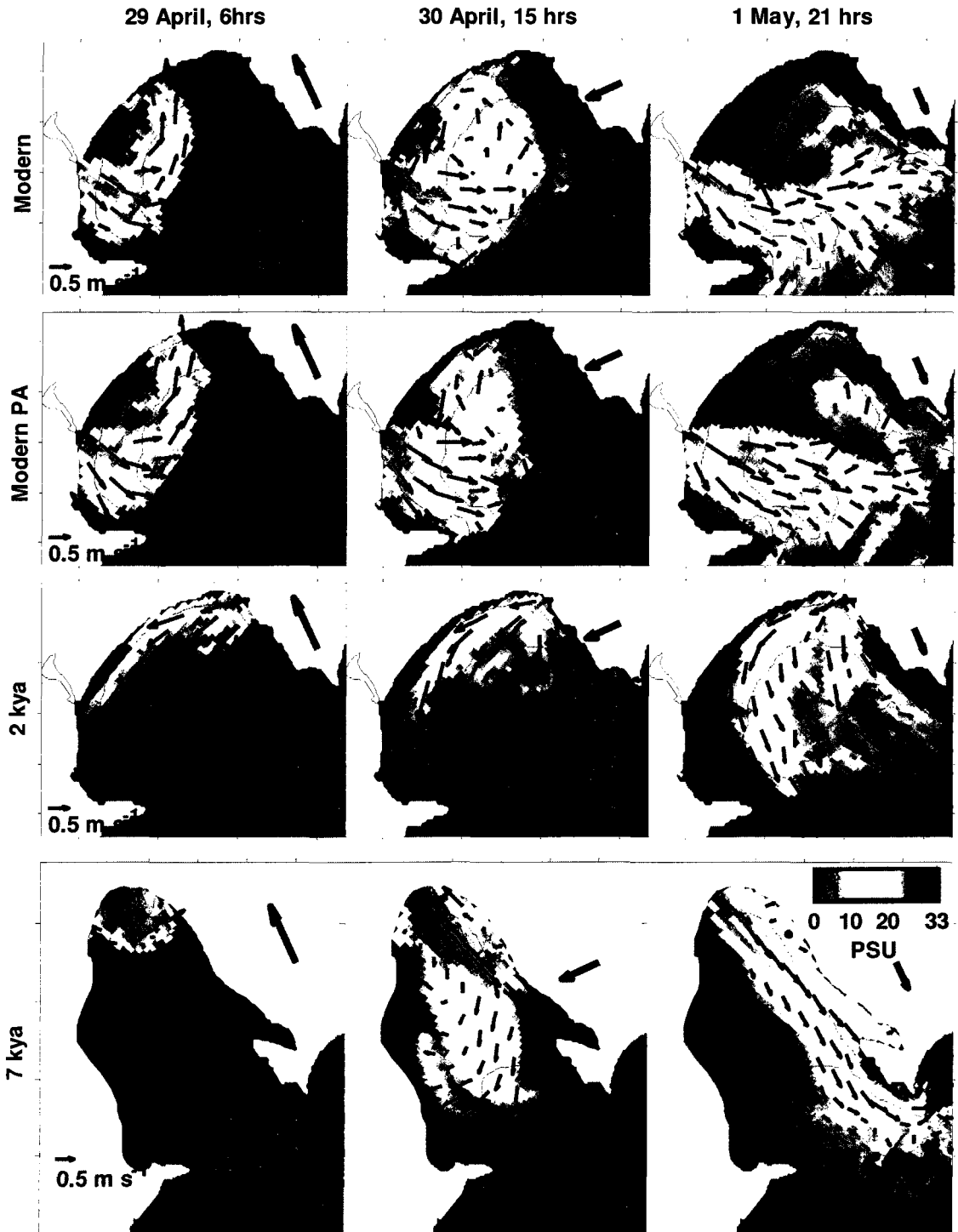
Figure 10. Sediment deposition ($\log_{10}$ scale) at the end of the winter scenario for each configuration. Assuming a porosity of about 65%, the plotted units of kg m^{-2} equate to mm of thickness. The color-scale axis labels are contoured for clarity (grey lines). Bathymetry is contoured in meters (black lines).
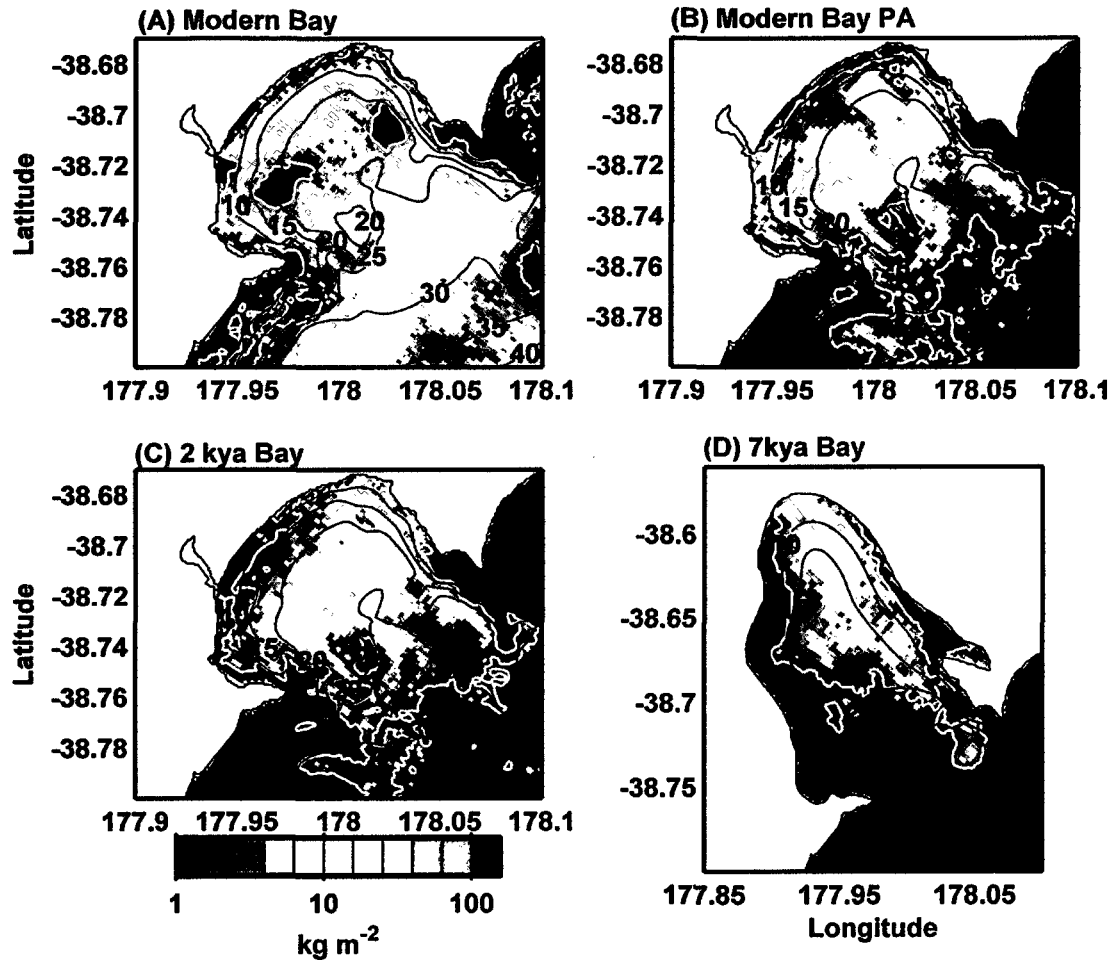
Figure 11. Sediment dispersal from the Waipaoa River mouth at the end of the winter scenario for each model configuration (see panel titles). The horizontal axis provides the distance from the Poverty Bay mouth, with the left side of the horizontal axis located at the river mouth. Zero was chosen to mark the mouth of Poverty Bay (dark vertical line). The second dark line at ~18 km marks the distance to long core MD972122. Figure 4 shows lines of equal distance radiating from the Waipaoa River mouth. The vertical axis shows the cumulative percent of each sediment class discharged by the Waipaoa River that was deposited within that distance of the river mouth. A value of 100% implies that no sediment was dispersed beyond that point, while 0 indicates that no sediment was deposited within that distance. Legend indicates the sediment class, with class 1 being the finest sediment increasing to sand at class 4.
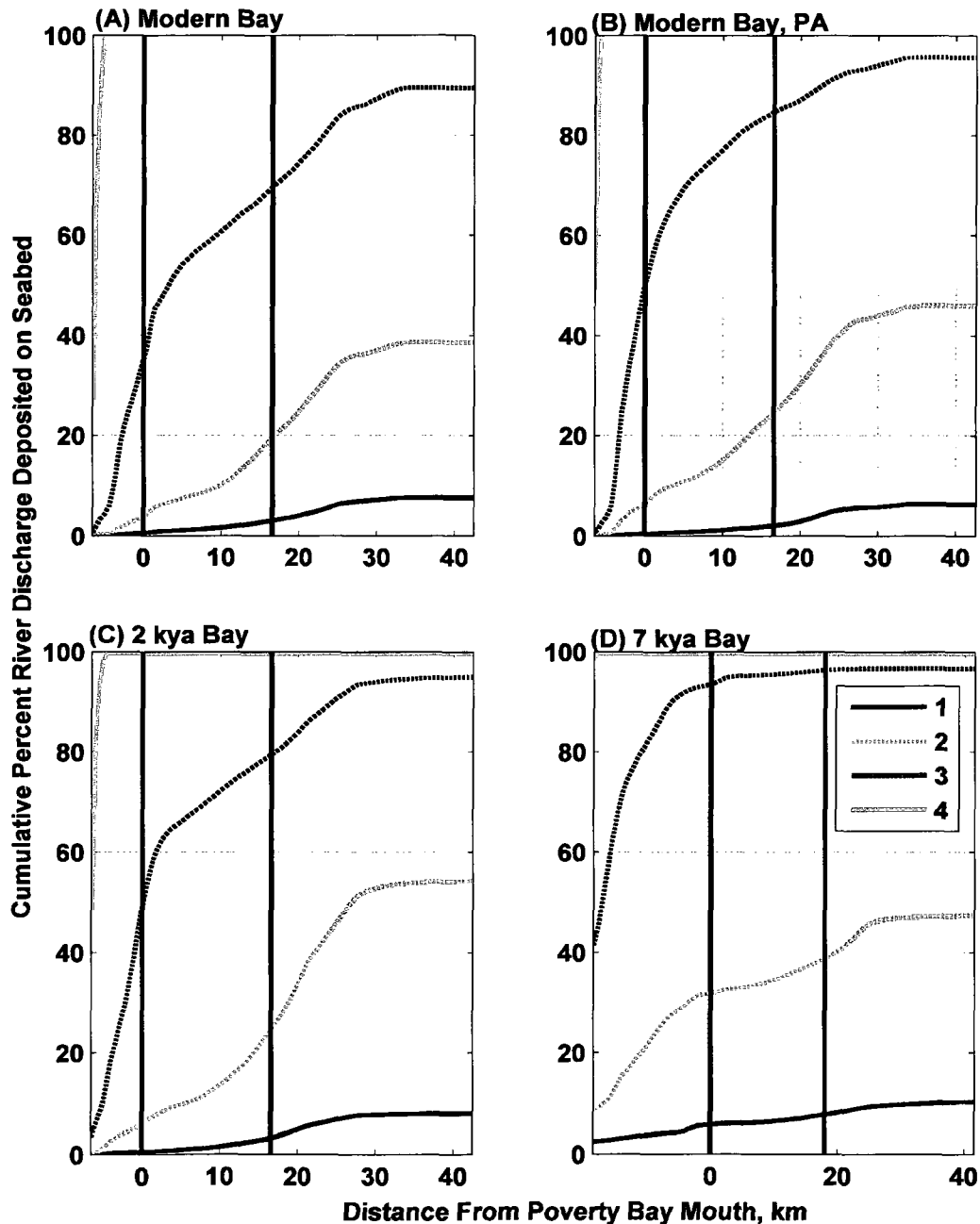
Figure 12. Average grain size dispersed to three distances from the Waipaoa River mouth at the end of the winter scenario. The distances correspond to the mouth of Poverty Bay, the shelf core MD972122, and the edge of the model domain.
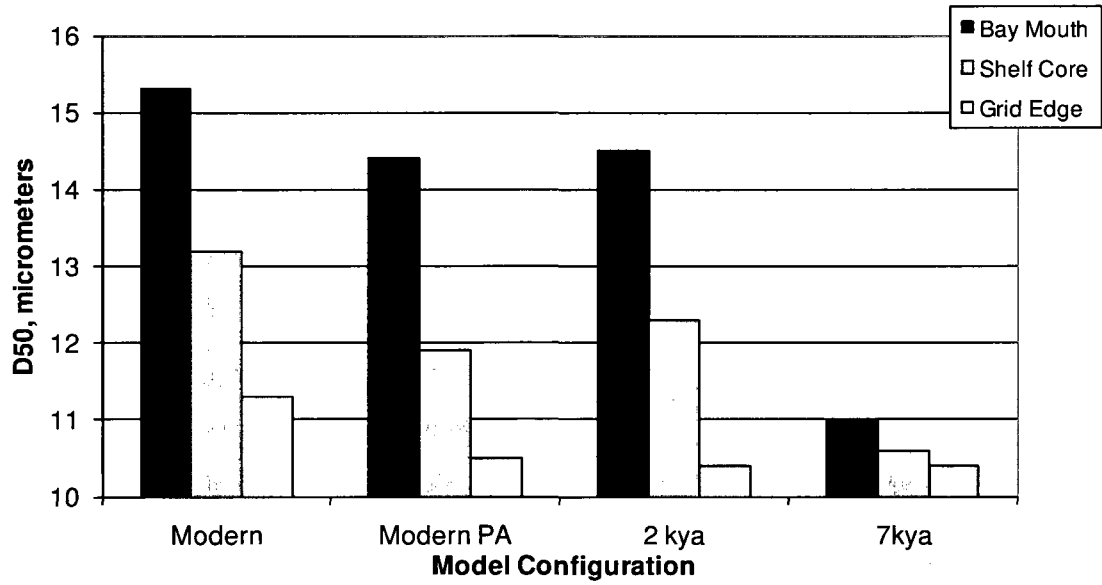
Figure 13. Cumulative sediment export from Poverty Bay during the winter scenario for each model configuration. The Modern PA and 2 kya curves fall nearly over top of each other.

(A) Present Day Sediment Load

Legend: Modern; Cumulative River Discharge

(B) Pre-Anthropogenic Sediment Load

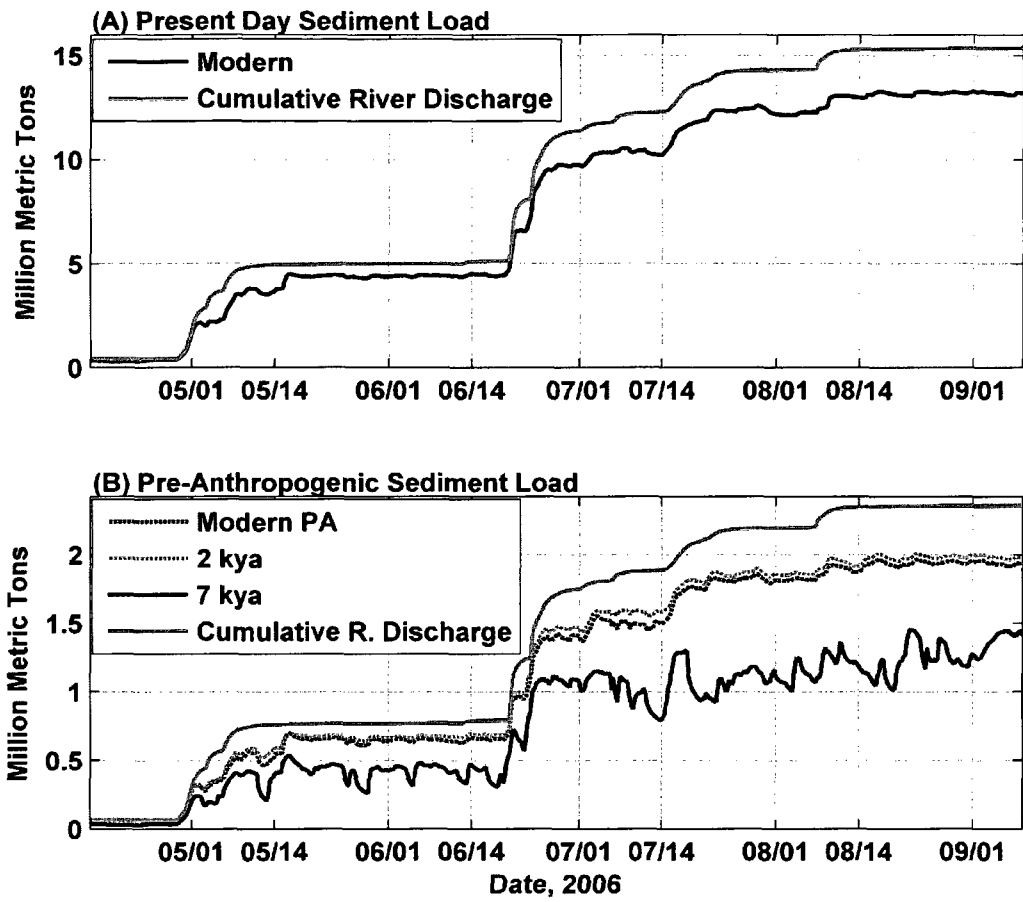Legend: Modern PA; 2 kya; 7 kya; Cumulative R. Discharge

Date, 2006

Figure 14. Time- and depth-averaged current speed (colors) and velocity vectors (arrows) for the extreme storm scenario for each model configuration (see panel titles). Bathymetry contoured in meters.
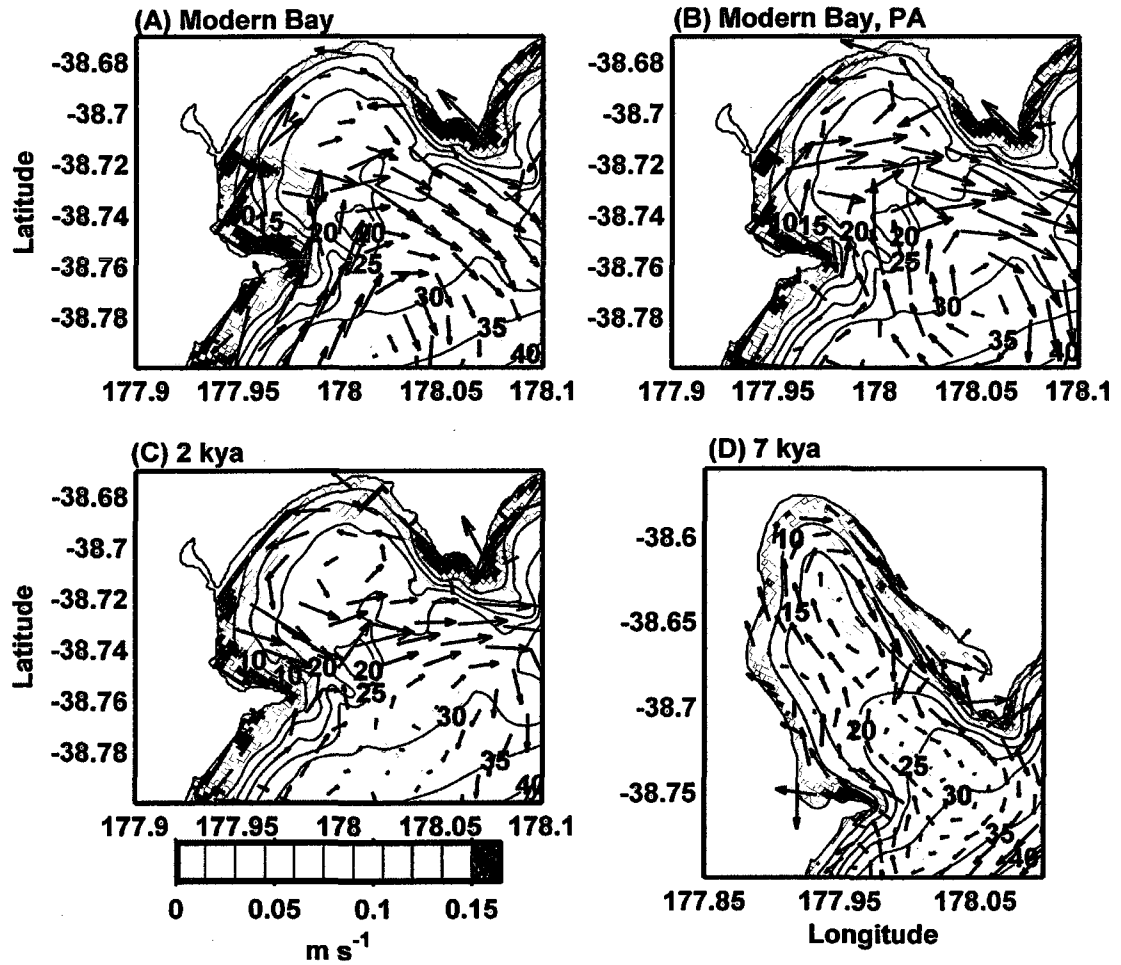
Figure 15. (A, B) Surface and (C, D) bottom salinity at the peak of the extreme storm
scenario for the modern and modern PA model configurations Model inputs during these
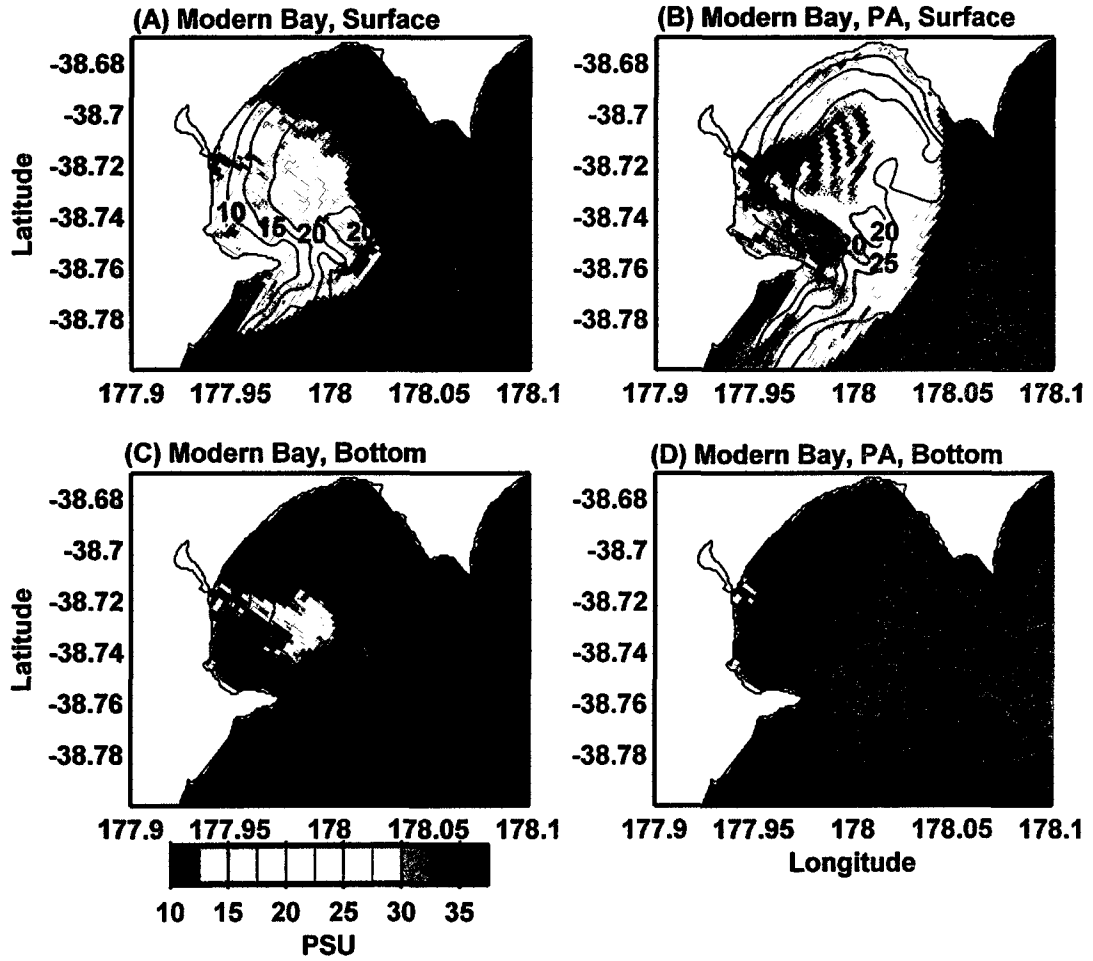snapshots based on 22 October, 2005. Bathymetry contoured in meters.

Figure 16. Sediment deposition ($\log_{10}$ scale) at the end of the extreme storm scenario for each model configuration (see panel titles). Assuming a porosity of 65%, the plotted units of kg m^{-2} equate to mm of thickness. The color-scale axis labels are contoured for clarity. Bathymetry contoured in meters.
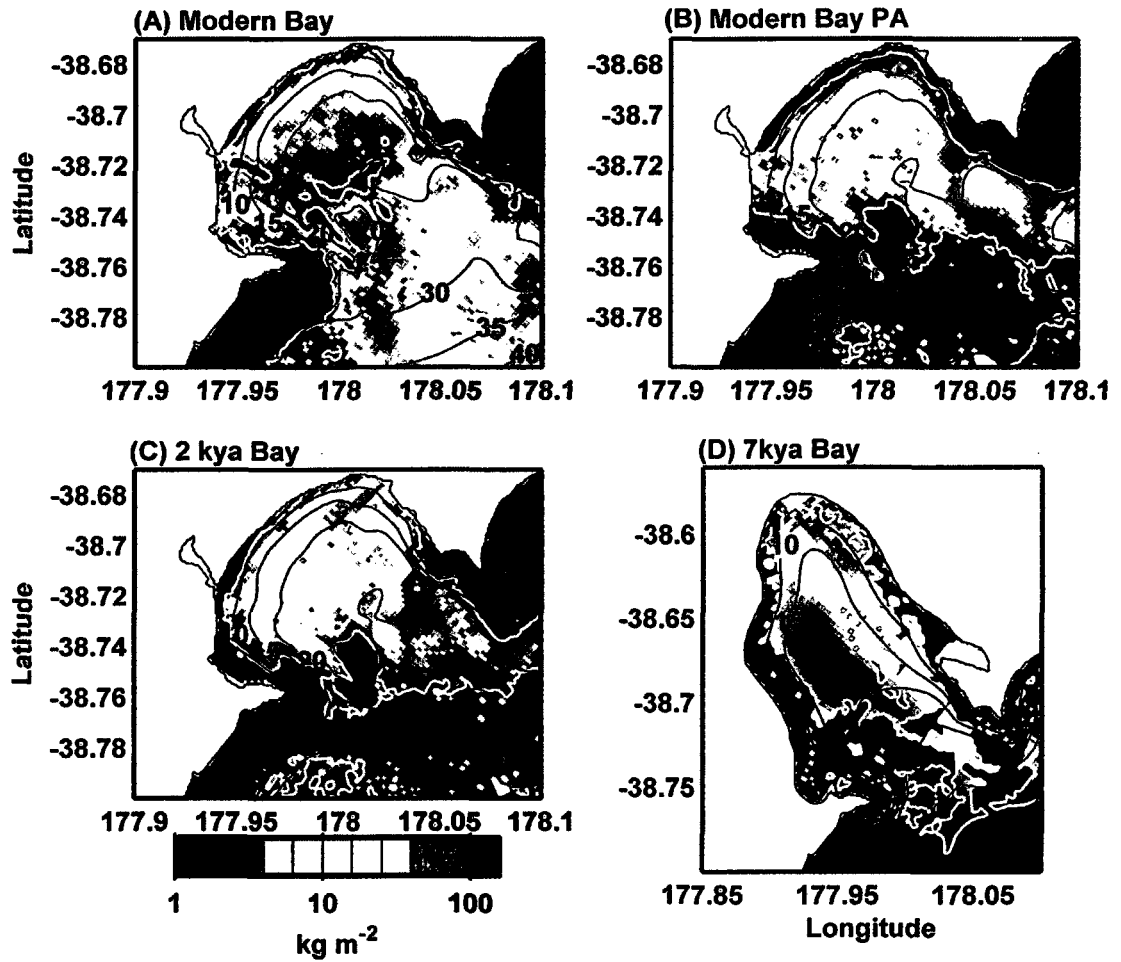
Figure 17. Sediment dispersal from the Waipaoa River mouth at the end of the extreme storm scenario for each model configuration (see panel titles). The horizontal axis provides the distance from the Poverty Bay mouth, with the left side of the horizontal axis located at the river mouth. Zero was chosen to mark the mouth of Poverty Bay (dark vertical line). The second dark line at ~18 km marks the distance to long core MD972122. Figure 4 shows radii radiating from the Waipaoa River mouth. The vertical axis shows the cumulative percent of each sediment class discharged by the Waipaoa River that was deposited within that distance of the river mouth. A value of 100% implies that no sediment was dispersed beyond that point, while 0 indicates that no sediment was deposited within that distance. Legend indicates the sediment class, with class 1 being the finest sediment increasing to sand at class 4.
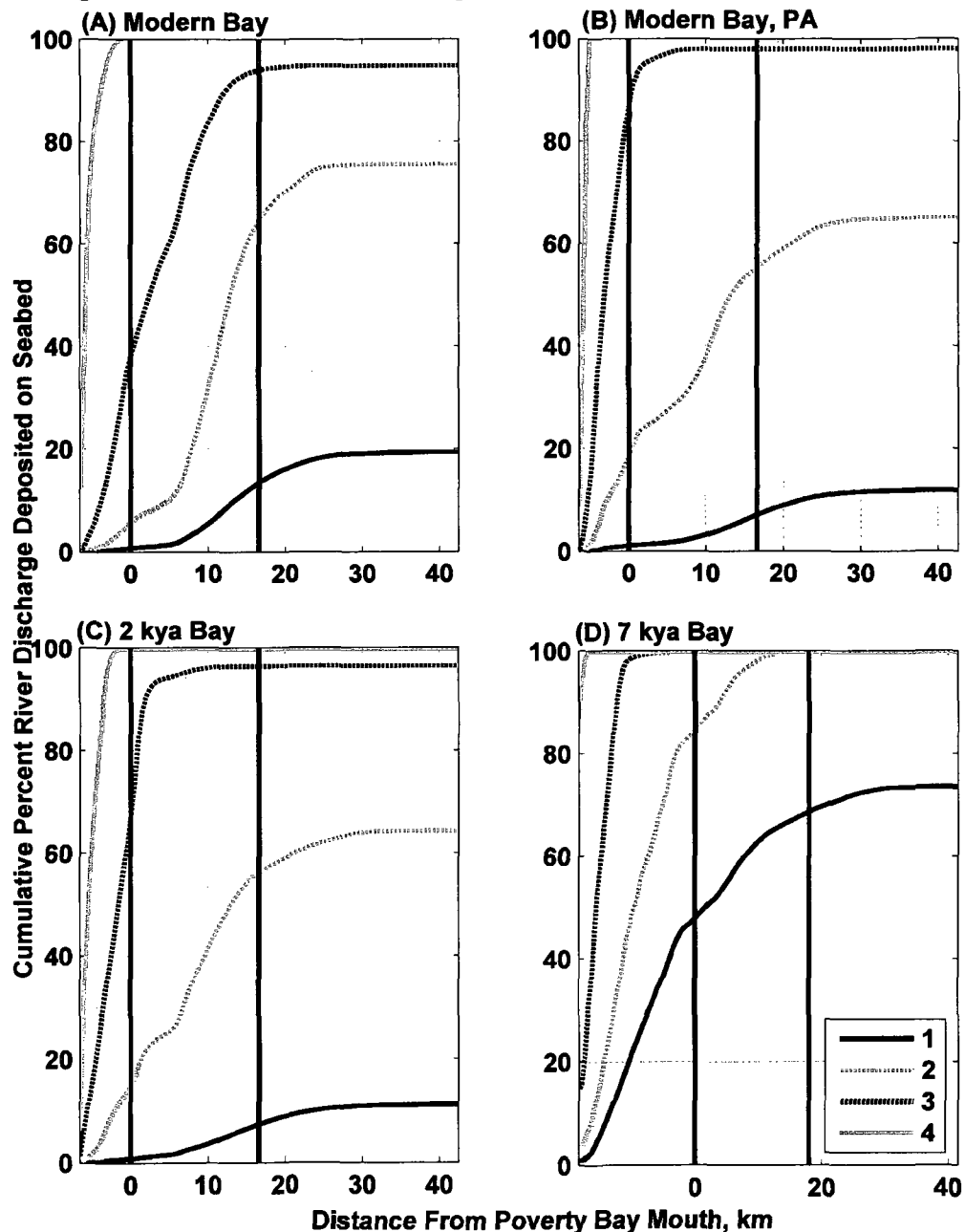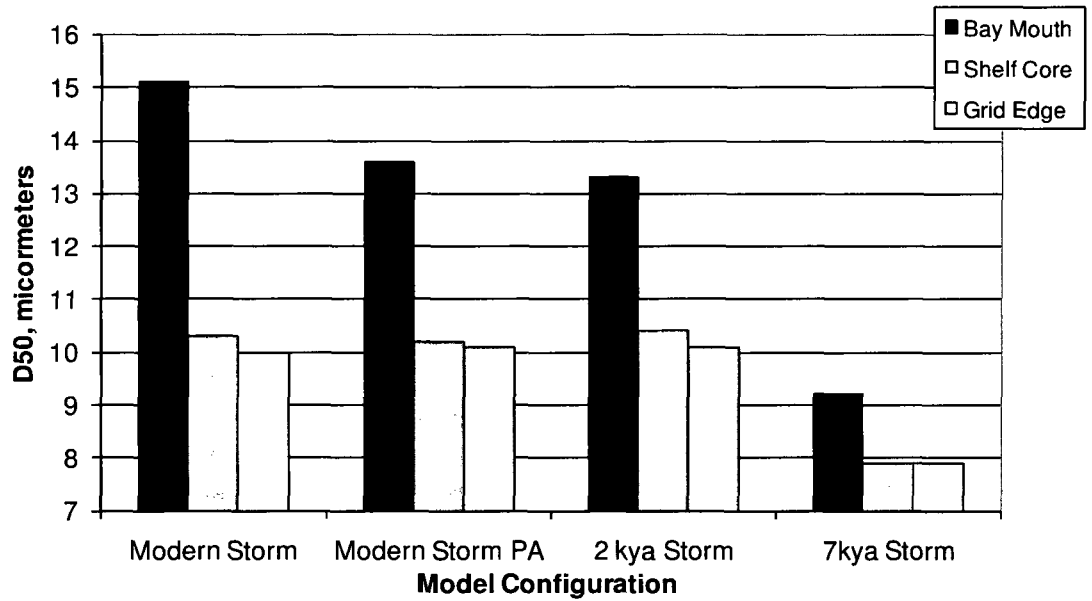
Figure 18. Average grain size dispersed to three distances from the Waipaoa River mouth at the end of the extreme storm scenario. The distances correspond to the mouth of Poverty Bay, the shelf core MD972122, and the edge of the model domain.

Appendix 4-A: Explanation of Model Visualizations

The supplemental DVD contains three visualizations of the model results are. The first, "April-May_storm.gif" illustrates the 28 April through 9 May, 2006 discharge pulse and the subsequent wave resuspension event. The second, "October_storm.gif" shows the extreme storm in 2005. Finally, "Paleo.gif" highlights the modern, modern pre-anthropogenic (PA) sediment discharge, 2 kya, and 7 kya model runs. Explanations of these visualizations are given in the following sections.

Visualizations can be viewed with numerous video players. Apple QuickTime and Imagen are both freely downloadable and allow for the advance of the visualization 1 frame at a time. This can be beneficial when examining a short time.

A.1 April-May_storm.gif

This visualization contains 4 main panels showing the currents, sediment-transport, and waves overtop a satellite photograph from World Wind of Poverty Bay and the Waipaoa River flood plain. These panels, from left to right, have the bathymetry contoured every 5 meters from 5 to 45 m and show the:

1) Surface salinity (colors) and surface currents (arrows): The white arrow to the left of the panel is a scale arrow for the currents. This panel also contains the location and travel paths for lagrangian floats initialized every 2 days in the surface waters of Poverty Bay.

2) Fluvial sediment deposition (colors) and bottom currents (arrows): The white arrow to the left of the panel is a scale arrow for the currents. Sediment deposition is shown on a $\log_{10}$ scale in units of kg m^{-2}, with 0, 1, and 2 contoured in grey. When a porosity of ~65% is assumed, these units are equivalent to millimeters of thickness. This panel also contains the location and travel paths for lagrangian floats initialized every 2 days in the bottom waters of Poverty Bay.

3) Depth-integrated fluvial suspended sediment within the water column (colors) and the depth-integrated sediment-transport direction (arrows): The depth-integrated suspended sediment is shown on a $\log_{10}$ scale with 1, 2, and 3 contoured in grey, and is the amount of sediment that would be deposited on the seabed if all the sediment within the water column immediately settled out, with the same units as panel 2. The depth-integrated sediment transport was deemed negligible and the arrows not shown when it was less than 0.04 kg m^{-1} s^{-1}. The dashed line represents the transect across the mouth of the bay highlighted below in a profile of the sediment transport.

4) Significant wave height: The locations of three current vertical profiles explained below are shown with the stars.

Other features of the visualization are the:

- **Waipaoa River discharge:** A time-series of the freshwater discharge was provided in the top left corner of the visualization. A red star on this progresses

with time. Discharge data was from the Kanakanaia Bridge about 48 km from the river mouth.

- **Time-stamp:** The date and time are provided in the upper right corner

- **Vertical profile of sediment transport:** The sediment transport through a transect across the mouth of Poverty Bay, shown in main panel 3, is shown on the bottom left. The positive direction (red) represents transport out of Poverty Bay, while the negative direction (blue) represents transport into Poverty Bay. Zero transport is contoured in black to highlight the directional changes.

- **Current vertical profiles:** Overtop Poverty Bay in their approximate locations are three vertical profiles of modeled currents, with the length of the arrows proportional to the current speed and comparable between all three plots. The exact locations of these profiles are the stars in main panel 4.

- **Winds:** To the right of the current profiles is the wind speed and direction. The arrow points in the direction toward which the wind blew and scales with the wind speed, which is also provided in the text to the right of the circle.

The storm dynamics presented in Chapters 2 and 3 can easily be seen in the visualization. Specifically, the shoreward winds and coastal trapped river plume transitioning to seaward winds and plume spreading is from 2 sec to 5 sec. The direct current flow from the Waipaoa River mouth to the mouth of Poverty Bay occurs throughout the flood. Also, the 15-18 May, 2006 swell resuspension event occurs from 18 sec to 22 sec.

A.2 October_storm.gif

The panels on this visualization are exactly the same as the previous visualization, except the floats are not presented. Here, the extreme storm from 21-26 October, 2005 occurs from 2 sec to 4 sec. In the visualization, it is evident the river plume quickly breaks free of the shoreward trapped plume state, and progresses down-slope across Poverty Bay and the continental shelf.

A.3 Paleo.gif

This visualization highlights the extreme storm that occurred from 21-26 October, 2005 for all 4 model configurations from Chapter 4. Water depth is contoured in black every 10 m from 10 to 40 m.

- The top row shows the bottom currents (arrows) and sediment deposition (colors) for the modern (left panels), modern PA (middle left panels), 2 kya (middle right panels), and 7 kya (right panels) Poverty Bay configurations. The scale arrow for the currents is located above the third panel from the left. Sediment deposition is shown in centimeters on a $\log_{10}$ scale with an assumed sediment porosity of ~65%. 0.1, 1, and 10 cm are contoured in grey.

- The bottom row shows the significant wave height in meters.

- A time-series of the freshwater discharge was provided in the top left corner of the visualization. A red dot on this progresses with time. Discharge data was from the Kanakanaia Bridge about 48 km from the river mouth.

- The date and time are provided in the upper right corner.

Appendix 4-B: Source Code and Input Files

This appendix documents the necessity for two small modifications made to the official ROMS and SWAN source code and presents an abbreviated description of these modifications. An explanation of the naming conventions used for the source code and input files on the supplemental DVD is also included below.

A.1. Source Code Modification

The SWAN model did not estimate wave characteristics well in a few grid cells immediately behind a peninsula or obstruction, in this case Young Nick's Head (Fig. A1). The underestimation of the waves in the grid cells immediately behind the headland was an inherent limitation of this model (Pers. Comm. Mauro Sclavo (CNR-ISMAR), 2010). The waves in the cells adjacent to those that were underestimated are travelling in a direction that does not directly input energy into the underestimated grid cells. Also, the waves can only turn so far in one spatial step, so it is generally the second grid cell after an obstruction that begins to estimate more realistic waves. When the waves at this location were used to estimate current velocities in ROMS using the nearshore calculations, unrealistic velocities were generated that lead to model instability. No modification of the model grid or bathymetry could be found that would allow the model to be run for the desired length of time and yet still accurately represent that portion of Poverty Bay. As such, the source code was modified to limit the magnitude of the nearshore calculations.

The ROMS/SWAN source code was slightly modified by adding a C preprocessor definition, MAX_STOKES. The MAX_STOKES definition modified the file

radiation_stress.F and limited the absolute magnitude of the u and v Stokes velocities to 0.75 m s^{-1}. The value of 0.75 m s^{-1} was chosen through downward iterations starting at 1 m s^{-1} until the model ran for the required length of time. This value had little to no effect on the areas away from the problem, because the calculated velocities were not that fast.

The SWAN model also underestimated the significant wave height and orbital velocity during the calm conditions for which data was available. This was solved by setting the wave height and bottom orbital velocity to specified values. This was not performed on the 7 kya Poverty Bay model runs. The WAVE_CORR definition modified the waves as specified in Chapter 3, increasing the minimum wave height and bottom orbital velocity to better match the observations before ROMS used them in calculations.

A.2. Source Code and Naming Conventions

Both the modified ROMS/SWAN source code and input files are included on the supplementary DVD. The ROMS/SWAN source code is in the directory "/SRC/". The netcdf input files are in the "/INPUT_FILES/" directory. Here, three subdirectories exist for the modern, "/MODERN/", 7 kya, "/PALEO/", and SWAN, "SWAN", input files.

The netcdf input files were named to specify what data they contain. For the initialization files, the 2005 refers to the model starting before the October, 2005 storm. For SWAN, the ".grd" files are the input grid files, the ".bot" files are the bathymetry, and the ".wav" files are the open boundary condition files. The files for the modern and 7 kya Poverty Bays are specified with "modern" and "paleo" names, respectively.

Figure A1. Time-averaged significant wave height (colors) and direction (arrows) for the April through September, 2006 simulation. Note the minimum wave height, 0.4 m, immediately behind the headland. Bathymetry is contoured in meters.
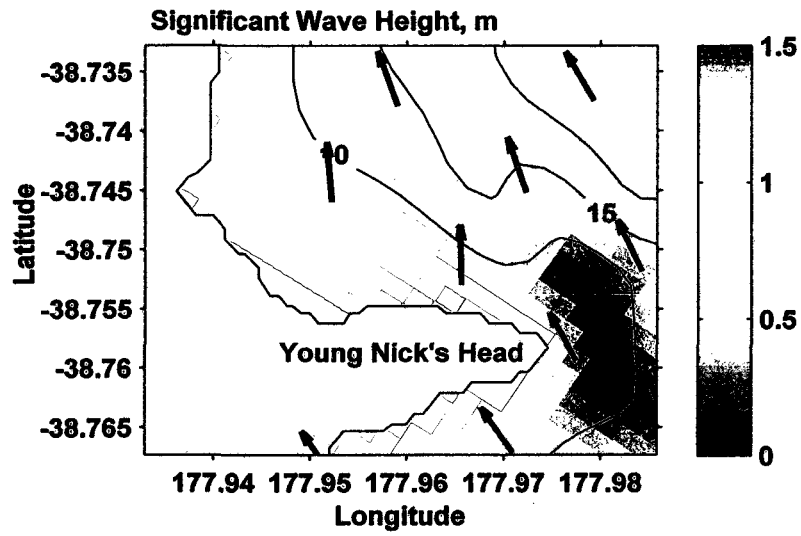
Chapter 5: Conclusions

This dissertation contributed to source-to-sink sedimentary studies through showing that; 1) Significant amounts of sediment can be deposited in shallow water offshore of small mountainous rivers during energetic time-periods. 2) Processes within the relatively small Poverty Bay significantly modulate the fluvial sedimentary signal from the Waipaoa River as it travels from the fluvial source to depositional sinks on the continental shelf and beyond. 3) Physical processes in the nearshore act to segregate the fine from the coarse sediment, with silt and clay preferentially transported to deeper water and the sand moved shoreward. 4) The evolution of Poverty Bay from an elongated embayment 7 kya to today's crescent-shaped beach modified wave exposure and increased current speeds within the bay, which combined with a shorter transit time to the continental shelf to impact sediment retention there and offshore export. 5) The processes controlling marine and nearshore sediment dispersal impact the sedimentary record that accumulates on continental shelves and slopes. These points are summarized below.

1. Significant amounts of sediment can be deposited in shallow water offshore of small mountainous rivers during energetic time-periods.

Wheatcroft (2000) put forth the idea of "oceanic" floods, where river flooding coincides with energetic oceanic conditions, and a direct sediment-transport pathway is formed that quickly transports sediment away from river mouths (see Chapter 2). Results from Poverty Bay showed that this oversimplifies processes within the WSS. In particular, the coastal ocean offshore of this small mountainous river has at least two

dominant sediment-transport pathways that operate at different times relative to flood peaks. Both the observation and modeling results from Chapters 2 and 3 showed that significant quantities of sediment were deposited within 7 km of the river mouth in 10 to 20 m water depth. This was somewhat surprising because the Waipaoa River tends to deliver sediment during oceanic floods, with elevated discharge coinciding with energetic waves and fast currents. Because of the timing of the waves relative to the elevated river discharge, the embayed nature of the coastline, and the tremendous suspended loads carried by the river, however, significant Waipaoa River sediment was deposited close to the river mouth. This sediment was later resuspended and exported from Poverty Bay to the continental shelf during times of energetic swell waves not associated with the original storm. In this way, at least two different sediment-transport pulses from Poverty Bay can be associated with each discharge pulse, one during river flooding and one or more subsequent pulses during swell waves.

2. *Processes within the relatively small Poverty Bay significantly modulate the fluvial sedimentary signal from the Waipaoa River as it travels from the fluvial source to depositional sinks on the continental shelf and beyond.*

The occurrence of two sediment-transport mechanisms, one associated with the flood and subsequent ones triggered by energetic waves, likely influences the timing of sediment export to the continental shelf and the grain size of the sediment supplied to the shelf (Chapters 3 and 4). Extreme floods, such as the October, 2005 Labor Day storm, likely supply relatively more of the coarsest sediment (sand) to the continental shelf than moderate discharge events, because the gravity driven current component quickly and

efficiently exports sediment from Poverty Bay (Chapters 3 and 4). Although sand is transported seaward during such extreme events, the average grain size exported from poverty Bay was relatively fine and mainly composed of a mixture of the suspended sediment classes; in this way the modeled extreme storm was similar to the moderate events. Wave resuspension of nearshore deposits, however, created a pulse of relatively coarser sediment from Poverty Bay, because little of the finest sediment class modeled remained in Poverty Bay after the periods of elevated discharge. This differentiation of grain sizes exported by extreme floods, moderate elevated discharge pulses, and subsequent resuspension events might lead to correlations between grain size distributions and the forcing conditions that supply sediment to the continental shelf (Chapters 3 and 4).

The fact that sediment delivered by the same discharge pulse may carry different terrestrial, fluvial, and oceanic markers, and be subjected to different grain size sorting complicates the identification of flood layers and the evaluation of sediment-transport pathways from sedimentological observations. This demonstrates that fluvial sedimentary signals may undergo transformations before reaching ultimate locations of sediment accumulation. For example, because 10-15% of the fluvial export from Poverty Bay was driven by wave resuspension events occurring well after a flood pulse, the sedimentary signal supplied to the continental shelf offshore of the Waipaoa River may be sensitive to wave climate, along with the fluvial discharge signal itself.

3. *Physical processes in the nearshore of Poverty Bay act to segregate the fine from the coarse sediment, with silt and clay preferentially transported to deeper water and the sand moved shoreward.*

This study found that nearshore processes and potential divergences in currents seaward of the Waipaoa River mouth may segregate coarse sand from the finer silt and clay, and identified the mechanisms behind the preservation of coarse sediment near the shoreline and the seaward export of the fine sediment (Chapter 2). The observations found a divergence in the currents offshore of the Waipaoa River. Currents close to shore (about 10 m water depth) were directed shoreward, while further offshore (15 m) they were directed seaward. Sand would be contained near the seabed and carried as bedload or as near-bed suspended load and be retained within the nearshore. Relatively finer sediment will be suspended more often than sand, be carried higher in the water column, and be mobilized in deeper water, all of which enhance its likelihood of being exported from Poverty Bay.

4. *The evolution of Poverty Bay from an elongated embayment 7 kya to today's crescent-shaped embayment modified wave exposure and current speeds within the bay, which combined with a shorter transit time to the continental shelf to impact sediment retention there and offshore export.*

The wave height and orbital velocity was reduced over much of the 7 kya Poverty Bay compared to the modern bay, because of the sheltering effect of the geometry of the embayment. The wave energy at the coastline and near the river mouth increased as the shoreline prograded toward the open continental shelf, increasing the frequency of

sediment resuspension (Chapter 4). Additionally, currents were estimated to be faster

within the modern and 2 kya configurations than that representing 7 kya. Export from

Poverty Bay increased as the sediment was more often resuspended, leading to more

sediment sequestration in the 7 kya bay and more sediment export from the modern bay.

The sequestration of fine sediment within the 7kya embayment contributed to an

enhanced rate of shoreline progradation compared to more modern times (Chapter 4).

As the shoreline prograded toward the continental shelf, the distance sediment had

to travel before leaving Poverty Bay increased from ~18 km 7 kya to ~5 km today.

Sediment could have traveled the same distance from the river mouth during river

flooding 7 kya as today, but much more sediment would be directly supplied to the

continental shelf in the modern setting (Chapter 4). This increased sediment export from

the modern bay again reduces the shoreline progradation rate compared to that 7 kya.

5. *The processes controlling marine and nearshore sediment dispersal impact the*

sedimentary record that accumulates on continental shelves and slopes.

Through the use of seasonal processes-based marine-dispersal numerical models,

this study explored the degree to which changes to bay geometry, river mouth location,

and sediment load have influenced shoreline progradation rates and preserved grain size

trends that developed within the WSS over a 7000 year time-frame (Chapter 4). The

model recreated the trends evident within shoreline progradation and grain size, although

it neglected climatic changes or climatically-driven sediment supply changes. This

demonstrated the role that coastal dispersal processes that occur over time-scales as short

as a storm or a season play in framing the sedimentary record preserved over much

longer time-frames. Interpretations of the offshore sedimentary record should consider

marine dispersal processes and the degree to which changes to basin geometry or

shoreline location may have on the sediment-transport.

This study showed that dispersal basin geometry and even river mouth orientation

can impact the sediment-transport dynamics of a system. As such, knowledge of their

evolution are useful for upscaling model simulations to longer time-frames. Chapter 4

demonstrated that seasonal process-based models can provide insights into explaining

long-term trends.

Future Directions for Research

The combined use of seasonal time-scale observational data and storm- to

seasonal-time-scale process oriented numerical models to investigate sediment dispersal

within the shallow (less than 30 m) marine portion of the WSS afforded the insights

described above. Future efforts should build upon this by addressing lingering questions:

1. Did the model accurately represent the system behavior during the extreme storm?

   To this end, more measurements are needed on a river dominated margin during a

   storm in which the river nears or exceeds hyperpycnal flow. None are available

   for the Waipaoa River, and few are available worldwide (i.e. Warrick et al., 2008).

2. Could the sediment settling velocity, critical shear stress, or erosion rate

   parameter have been further modified to improve the model results? The

   measurement of these parameters offshore of the Waipaoa River would shed light

   on their values in this system, and allow for better calibration of the model. Also,

   the inclusion a flocculation routine in the numerical model may have improved

the model's timing of sediment deposition. But without data to constrain the rates of particle aggregation and disaggregation, flocculation within the model would also have to have been set through comparisons with the data from Chapter 2.

3. How has climate and land use changes modified the freshwater discharge and sediment grain size distributions of the Waipaoa and other rivers? Studies examining this question could possibly help validate the explanation presented in Chapter 4 for the drastic sediment fining at the top of long cores on the continental shelf. Changes to the Waipaoa River discharges will also be important for expanding the modeling time-frame beyond ~7 kya or for attempting to recreate the observed shoreline progradation rate.

4. Does short-term deposition in 10 to 20 m water depth occur offshore of other small mountainous rivers that empty directly into the ocean, or is the deposition near the Waipaoa River mouth during energetic conditions dependent on the presence of the embayment? Targeted studies in the nearshore of other small mountainous river systems would shed light on this relatively unstudied portion of the sedimentary dispersal system.

References:

Warrick, J.A., Xu, J., Noble, M.A., Lee, H.J. 2008. Rapid formation of hyperpycnal sediment gravity currents offshore of a semi-arid California river. Cont. Shelf Res. 28: 991-1009.

Wheatcroft, R.A., 2000. Oceanic flood sedimentation: a new perspective. Cont. Shelf Res., 20: 2059-2066.

VITA

Aaron John Bever

Born in Mt. Vernon, Washington on 7 April, 1981 to Roy and Teresa Bever. Graduated

from Sedro-Woolley High School in 1999. Earned a Bachelor of Science in

Oceanography from the University of Washington, Seattle, in 2003. Earned a Master of

Science in Marine Science from the College of William & Mary, School of Marine

Science, in 2006. Entered the Ph.D. program at the College of William & Mary, School

of Marine Science, August 2006. Defended Ph.D. dissertation in September, 2010.